Investigation of Carbon Fluxes in Central Metabolic Pathways of *Corynebacterium glutamicum*

by

Sung Min Park

B.S. Chemical Engineering & Biology
California Institute of Technology
(1986)

Submitted to the Department of Chemical Engineering in Partial Fulfillment of the Requirement for the Degree of

DOCTOR OF PHILOSOPHY
IN CHEMICAL ENGINEERING

at the

MASSACHUSETTS INSTITUTE OF TECHNOLOGY
June, 1996

Signature of Author_____
Department of Chemical Engineering
March 18, 1996

Certified by_____
Gregory N. Stephanopoulos
Professor of Chemical Engineering
Thesis Supervisor

_____
Anthony J. Sinskey
Professor of Biology
Thesis Supervisor

Accepted by_____
Robert E. Cohen
Professor of Chemical Engineering
Chairman, Committee on Graduate Students

Investigation of Carbon Fluxes in Central Metabolic Pathways of *Corynebacterium glutamicum*

by

Sung Min Park

Submitted to the Department of Chemical Engineering on January 19, 1996 in partial fulfillment for the Degree of Doctor of Philosophy in Chemical Engineering

Abstract

The primary goal of this thesis is to determine how carbon flows through the central metabolic pathway of *Corynebacterium glutamicum* with the ultimate goal of understanding how such flows affect amino acid production. Specific deletion mutants deficient in the phosphoenolpyruvate carboxylase (PPC) and pyruvate kinase (PK) genes were constructed via a gene disruption technique and characterized in batch fermentations in order to assess the impact of the introduced perturbations on the overall performance of L-lysine production. In addition to obtaining fermentation yields and rates, intracellular carbon flux distributions and carbon partitioning at the key metabolic branchpoints were obtained by using the methodology of metabolic flux analysis. The results can be summarized as follows: (1) There is a significant built-up of intermediate metabolites along the glycolytic pathway in the PK- deficient mutants as evidenced by secretion of dihydroxyacetone and glyceraldehye. This causes an overflow via the pentose phosphate pathway (PPP) as a mechanism of dissimilating large amount of built-up intermediates in the form of CO_2. (3) The high activity through the PPP causes an overproduction of reducing power in the form of NADPH. In order to accommodate this overproduction of reducing power as well as to compensate the shortage of production of NADH via the tricarboxylic acid cycle, an increased activity of the transhydrogenase enzyme is necessary which catalyzes the reversible reaction $NADPH + NAD^+ \leftrightarrow NADP^+ + NADH$. Experimentally, the presence of active transhydrogenase was confirmed directly by the enzymatic assays. (3) Specific glucose uptake rates declined during the course of fermentation and this decline was more pronounced in the case of PPC PK-deficient mutant. (4) PPC is dispensable for cell growth and glucose assimilation in *C. glutamicum*.

The fermentation study with the PPC-deficient mutant provided a groundwork for deducing the existence of a second anaplerotic pathway in *C. glutamicum*. In a series of ^{13}C labeling substrate experiments, ^{13}C distribution in secreted lysine was followed by ^{13}C nuclear magnetic resonance (^{13}C NMR) spectroscopy and gas-chromatography mass-spectrometry (GC-MS). These studies led to the conclusive evidence that the previously undetected anaplerotic reaction is the carboxylation of pyruvate. Furthermore, the pyruvate carboxylating pathway was shown to operate simultaneously with PPC, with the

latter enzyme contributing approximately ten percent of the total oxaloacetate formation in *C. glutamicum*.

Indispensable for the application of carbon substrate labeling study is the ability to deal with ^{13}C label scrambling through multiple turns in the cyclic pathways such as the tricarboxylic acid cycle and the PPP. This problem was solved based on formulating mass conservation balances for all possible isotopomer species and solving simultaneously these sets linear algebraic equations under steady state conditions. This approach provides a rational basis for applying ^{13}C NMR and GC-MS for a wide range of applications from studying the fundamental aspects of metabolism to developing diagnostic methods for the detection of metabolic disease using the isotopic substrates. The developed methodology was verified by comparing theoretical predictions with experimental data reported in the literature. Previously not taking into account for the label redistribution due to the multiple turns via the metabolic cycles has led to erroneous claims, both qualitatively and quantitatively. Examples of these types of errors include: (1) the claim of a non-operating glyoxylate shunt pathway in *Pseudomonas* AM1 strain; (2) the claim of operation of propionate carboxylating pathway in *Escherichia coli*; (3) controversy over acetone utilization pathways in mammals involving "lactate/methylglyoxal" and "acetate" pathways; (4) controversy about the operating mode of the PPP in liver between classical and "L-type"; and (5) the claims about the existence of futile cycling in various tissues.

Thesis Supervisors: Dr. Gregory N. Stephanopoulos (Professor of ChemicalEngineering)
Dr. Anthony J. Sinskey (Professor of Biology)

Acknowledgments

Looking upon my past years at MIT, I need to thank many people for getting me through.

First and foremost, I would like to thank my advisors, Professors Gregory Stephanopoulos and Anthony Sinskey for providing the right combination of freedom, guidance, support, patience and pressure for the completion of this thesis. I also would like to thank the members of my committee, Professors Charles Cooney, Karen Gleason, Daniel Wang and Dr. Max Folliette for serving on my thesis committee and offering helpful advice.

I also would like to thank the members of the Stephanopoulos and Sinskey groups: Cathryn Shaw for collaborating with me on the ^{13}C NMR work and the pentose phosphate pathway modeling work, and encouraging me at many stressed periods; John Chung for providing many helpful critiques and keeping each other motivated; Joe Vallino for initially educating me in the central carbon metabolism of *Corynebacterium* and providing many valuable insights despite having left Boston; Aristos Aristidou for discussion on the flux analysis and proofreading several manuscripts; Grace Colön for discussion on the metabolic engineering of *Corynebacterium*; Martin Reinicke and Mattheos Koffas for helpful suggestions.

Thanks also goes to Marcel Gubler in the Sinskey group for teaching me skills in molecular biology and how to get organized. Thanks to UROP and REU students Chris Chong and Robert Bond for the development of the transconjugation method, and Nancy Ho and Keki Patel for assisting in fermentation.

I also would like to thank all the Korean Chem-E lunchmates in the past and present-Chonghoon Han, Jaesung Han, Shinkyu Kang, Chunhyuk Lee, Dohyun Kim, Taeshin Park, Heeyop Chae, Yongpil Han, Seokwon Lee, Sangjoon Sim-for always making lunch conversation interesting and keeping me interested in Korean culture and politics.

Much thanks go to my parents, sister, brother and in-laws for providing me support and encouragement, especially near the end.

Most important thanks must go to my wife, Linda, for her support, love, and encouragement, and to my daughters, Andrea and newly born Stephanie, who have been the happy reminders that I need to graduate.

Finally, financial support from the National Science Foundation through the MIT Biotechnology Process Engineering Center and from the National Health Institute through the Training Fellowship are acknowledged.

Table of Contents

List of Figures

List of Tables

Chapter 1: Introduction

1.1 Motivation

Optimization of microbial fermentation processes generally proceeds by developing microbial strains that are to be altered in order to achieve the most effective substrate utilization and product synthesis. This often necessitates the modification of cellular metabolic structure. Traditionally, this has been achieved by random mutagenesis followed by a variety of novel selection procedures. Though successful, this procedure is tedious and does not provide much information about the structure and regulation within metabolic network which makes the subsequent improvement as difficult and laborious. More precise manipulations can be applied by contemporary recombinant DNA techniques which is the central theme of metabolic engineering. Some examples of recent metabolic engineering efforts includes [Bailey, 1991; Cameron and Tong, 1992]: (1) improved production of metabolites already produced by the host organisms; (2) utilization of a wide range of substrates for growth and product formation; (3) introduction of new catalytic activities for degradation of toxic chemicals; (4) production of chemicals new to the host organism; and (5) modification of cell properties.

The abilities to introduce new enzymatic reactions and to manipulate the existing metabolic pathway have endowed researchers with many possibilities for innovative strain constructions. Yet, there has been no systematic approach to select the rational targets for this purpose from a wide range of choices available. In order to minimize trial-and-error procedures, it is critical that the introduced metabolic manipulations are characterized as completely as possible. It is imperative to utilize the experimental and theoretical techniques such as mass balancing for intracellular flux determination, ^{13}C labeling, analysis of genetic mutants, and traditional enzymology that are available now for studying metabolic pathways. The combined applications of theses techniques can provide a basis for fundamental understanding of metabolic pathway structures and lead to better targets for next modification for improvement.

In this thesis, the L-lysine overproduction by *Corynebacterium glutamicum* is used as a model system to develop metabolic engineering tools and methodologies. *C. glutamicum* is an ideal candidate because of its industrial significance and fairly well-established biochemistry. Several genetic tools such as cloning vectors, plasmid transformation by electroporation and transconjugation techniques have been developed which allow easy manipulation of pathways. Furthermore, from an engineering standpoint, process yield and productivity for this fermentation process as well as other amino acids and nucleotides fermentations with the genera *Corynebacterium* and its close relative *Brevibacterium* are critical measures of performance and economic success.

1.2 Objectives

Motivated by the ultimate goals of improving the amino acid production with *Corynebacterium*, the main objectives of this thesis are:

1. Understand how perturbations in the central carbon metabolic pathway affect the overall cell growth and L-lysine production in *C. glutamicm.*

    - Develop a genetic technique to introduce specific mutations
    - Construct *C. glutamicum* mutants deficient in phosphoenolpyruvate carboxylase (PPC; EC 2.7.9.2; *ppc* gene) and/or pyruvate kinase (PK; EC 2.7.1.40; *pyk* gene).

2. Develop a ^{13}C labeling methodology and apply it to *C. glutamicum* in order to determine intracellular carbon flux partitioning at the key metabolic branchpoints and to elucidate an unknown enzymatic reaction step in the anaplerotic sequences can be unraveled.

3. Develop a thermodynamic criteria to be used to assess whether or not certain sets of biochemical reactions are feasible.

1.3 Method of Approach and Scope of Thesis

To meet the above objectives, the investigative approach outlined in Figure 1.1 was followed. In addressing objective 1, a gene-disruption technique based on the conjugal plasmid transfer between gram-negative *Escherichia coli* and gram-positive *Corynebacterium* was first developed. Since the construction of mutants based on this

technique requires the gene sequences and *ppc* and *pyk* genes were available in the Prof. Sinskey laboratory, the three mutants deficient in PPC and/or PK were constructed.

The next step was the characterization of these mutants under the identical fermentation conditions in order to assess the impact of the introduced perturbation on the overall performance of L-lysine production and to provide rational targets for future strain improvements. The metabolic flux analysis developed by Vallino [1991] was applied to estimate intracellular carbon fluxes and carbon partitioning at the key metabolic branchpoints during different phases of fermentation.

Objective 2 was achieved by addressing a specific problem. One of the significant findings from the fermentation studies was that the PPC-deficient mutant behaves almost identical as the wild type with glucose as sole carbon source. These finding indicate that PPC is dispensable for cell growth in *C. glutamicum* and that there exists additional anaplerotic pathway(s) in *C. glutamicum* by which oxaloacetate (OAA) can be replenished. In lieu of enzymatic or genetic evidence, the nature of this unknown pathway was elucidated by applying ^{13}C nuclear magnetic resonance (^{13}C NMR) spectroscopy and gas-chromatography mass-spectrometry (GC-MS). ^{13}C distribution in secreted lysine by *C. glutamicum* cultivated with the ^{13}C labeled carbohydrates was followed by ^{13}C NMR and GC-MS which led to the conclusive evidence that the previously undetected anaplerotic reaction of OAA synthesis is the cataltysis of carboxylation of pyruvate.

Of critical importance in applying ^{13}C labeling was the ability to predict ^{13}C label scrambling via the metabolic cycles such as the tricarboxylic acid (TCA) cycle and the pentose phosphate pathway (PPP). This problem was solved by developing mathematical models that account for all possible ^{13}C label transfer through individual enzymatic reactions in a metabolic pathway. The methodology yielded analytical relationships between key pathway fluxes from ^{13}C label distribution in intermediates or secreted metabolites. Furthermore, this methodology provided a rational basis to select the properly labeled substrate. The validity of the models was checked by comparing the theoretical predictions with the experimental data reported in the literature. The models were extended to resolve controversies stemming from the models that did not account for the label redistribution through the multiple turns via the metabolic cycles.

Objective 3 was a theoretical modeling effort to predict whether or not certain sets of biochemical reactions are feasible. The problem was formulated in the context of linear networks with constraints based on the thermodynamic criteria and limits on the intracellular metabolite concentrations. Utility of this method was tested by investigating three well characterized metabolic processes: (1) glycolysis; (2) anaplerotic reactions; (3) gluconeogenesis.

1.4 Thesis Organization

In the following chapters these concepts are further advanced. Chapter 2 serves as a general introduction to the metabolic engineering, amino acids production, taxonomic classification of *Corynebacterium*, and genetic tools for *Corynebacterium*. Chapter 3 describes the materials and methods used throughout this work. Chapter 4 describes development of transconjugation method and its subsequent use for the construction of specific deletion mutants. Chapters 5, 6 and 7 are theoretical chapters describing the methodology and results of modeling the carbon isotope label scrambling via the TCA cycle and the PPP. Chapter 8 summarizes experimental works using the ^{13}C NMR spectroscopy and GC-MS based on the theoretical framework provided in Chapter 5. Chapter 9 provides the detailed analysis of fermentation results with specific deletion mutants constructed in Chapter 4. Chapter 10 summarizes the development of thermodynamic criteria to assess the feasibility of certain sets of biochemical enzymatic reactions. Finally, overall summary, conclusions and recommendations are given in Chapter 11.

1.5 References

Bailey, J.E. (1991). Toward a science of metabolic engineering. *Science* **252:** 1668-1675.

Cameron, D.C., Tong, I.-T. (1993). Cellular and metabolic engineering: An overview. *Appl. Biochem. Biotechnol.* **38:** 105-140.

Vallino, J.J. (1991). Identification of branch-point restrictions in microbial metabolism through metabolic flux analysis and local network perturbations. Ph.D. thesis. Massachusetts Institute of Technology.

Investigative Approach

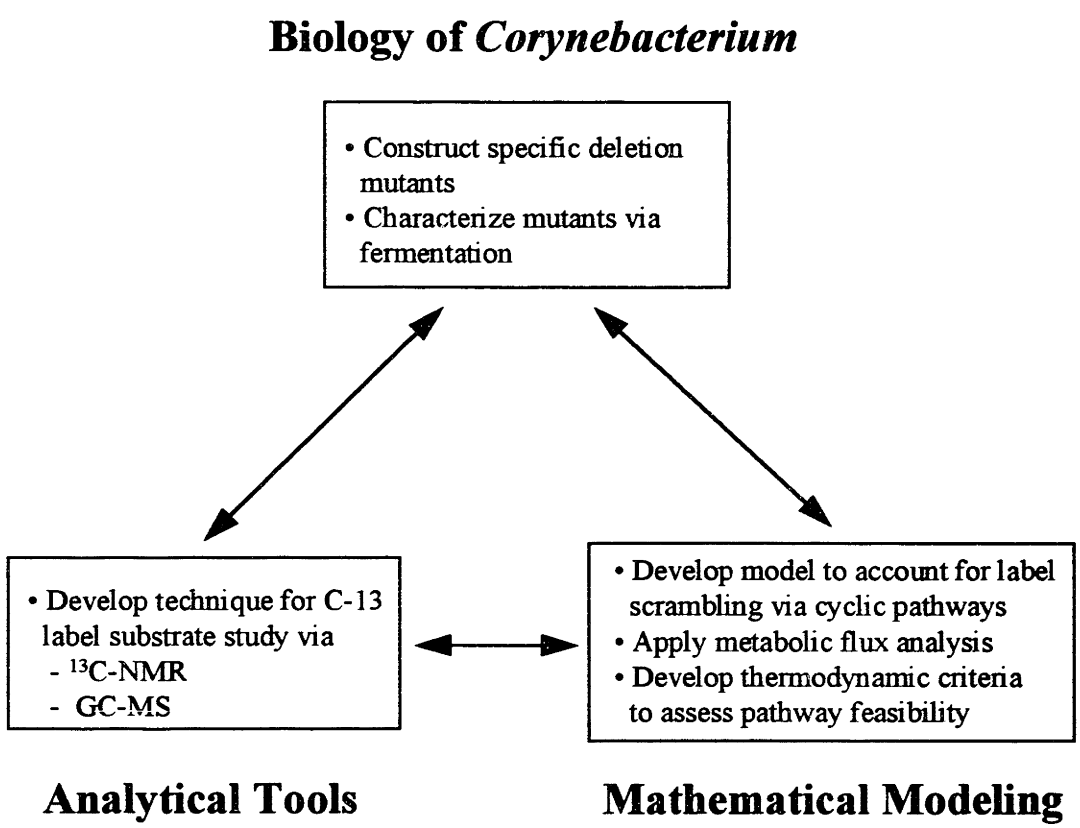

Figure 1.1 Thesis method of approach.

Chapter 2: Background

This chapter provides a brief introduction to the amino acid industry, the taxonomic classification of *Corynebacterium* and the metabolic engineering of *Corynebacterium*. However, this chapter is not intended to be a complete treatment of these topics, but rather is intended to provide the reader with basis that will be relevant for the studies described in subsequent chapters which contain their own introductions and backgrounds.

2.1 Amino Acid Industry

The origin of amino acids in food applications can be attributed to Japanese who first identified essentially L-glutamic acid as a food flavor enhancer and subsequently developed microbial fermentation processes for the various amino acids [Kiss, 1991]. In nature, there are twenty amino acids, eight of which are essential for the growth of most mammals. Amino acids are important not only as nutrients (predominantly animal feed additives) but also as flavors, seasonings, and raw material for the synthesis of cosmetics, toothpaste, shampoo and detergents [Martin *et al.*, 1987].

Amino acids may be prepared by isolation from natural materials, by microbial or enzymatic processes, or by chemical synthesis [Soda *et al.*, 1983]. The chemical synthesis method gives the racemic mixtures which requires an additional purification to obtain optically active amino acid. The microbial production of amino acids was initiated by Kinoshita *et al.* [1957] who first demonstrated the L-glutamate fermentation using *Micrococcus glutamicus* (later named as *C. glutamicum*). Table 2.1 summarizes various organisms employed for the fermentation production of amino acids. Only several organisms are used for the microbial production of amino acids: *Escherichia coli* due to well characterized and well understood biochemistry and genetic as well as well developed gene manipulation techniques, *Serratia marcescens*, several *Bacillus*, and still predominantly bacteria belonging to the *Brevibacterium* and *Corynebacterium* genera. Industrial enzymatic processes for the amino acid production are listed in Table 2.2. The

enzymatic procedure is preferred over the microbial process in some cases for it takes less time, is more efficient, and does not produce complex byproducts which simplify the downstream processing.

2.2 Taxonomic Classification of *Corynebacterium*

Collins and Cummins [1986] describes the genus *Corynebacterium* as the facultatively aerobic coryneform bacteria which contain *meso*-diaminopimelate, arabinose and galactose in the cell wall, a DNA base composition with G+C content in the range of 51-63% and C_{22}-C_{36} corynomycolic acids. *Corynebacterium* can be differentiated from the other coryneform taxa based on the following criteria: major peptidoglycan diamino acid, peptidoglycan type, N-glycolyl glycan moiety of cell wall, mol% of G+C, presence of mycolic acid, fatty acid type, major menaquinone isoprenologue(s), and phosphatidylinositol and phosphatidylinositol mannoside(s). Yet there is a strong similarity between *Corynebacterium* and other actinomyces including *Caseobacter*, *Mycobacterium*, *Nocardia* and *Rhodococcus* which makes the differentiation very difficult. However, the clear distinction can be made between *Corynebacterium* and other genera of *Brevibacterium*, *Arthrobacter*, *Agromyces*, *Cellulomonas*, *Curtobacterium*, and *Microbacterium* which all lack mycolic acids. Most members of the *Corynebacterium* genus requires one or more vitamins, amino acids, purines and pyrimidines. The range of temperature for the growth of most corynebacteria is between 30-37°C.

There are at least sixteen species belonging to this genus which can be differentiated based on the phenotypic characteristics of acid production from various sugar and hydrolysis of protein extracts. These are *C. diphtheriae*, *C. pseudotuberculosis*, *C. xerosis*, *C. pseudodiphtheriticum*, *C. kutscheri*, *C. minutissimum*, *C. striatum*, *C. renale*, *C. cystitidis*, *C. pilosum*, *C. mycetoides*, *C. matruchotii*, *C. flavescens*, *C. vitariumen*, *C. glutamicum*, *C. callunae*, *C. bovis* and *C. paurometabolum*. Based on the chemotaxonomic studies, *B. lactofermentum*, *B. flavum* and *B. divacarium* and *C. lilium* which are also known as amino acid producers are believed to be identical to *C. glutamicum* [Liebl *et al.*, 1991]. Also Riegel *et al.* [1992] reported a new

Corynebacterium group (CGD2), *C. urealyticum*, which produces urease and is similar to other *Corynebacterium* species based on the phenotypic tests.

2.3 Metabolic Engineering of *Corynebacterium*

The content of this section is mainly drawn from a review published by Jetten and Sinskey [1995] which summarized recent findings covering the physiology, biochemistry, and molecular biology of *C. glutamicum* and its closely related organisms.

The most fundamental prerequisites for the metabolic engineering of *Corynebacterium* are the availability of vectors and DNA transformation system that would allow cloning, gene expression and gene disruption. So far five cryptic plasmids were identified in various *Corynebacterium* strains (Table 2.3) with pSR1 [Archer and Sinskey, 1993] and pNG2 [Serwold-Davis *et al.*, 1987] having the broad host range.

For the purpose of DNA transformation, several methods such as protoplast transformation [Katsumata *et al.*, 1985; Santamaria *et al.*, 1985; Yoshihara *et al.*, 1985], transduction [Trautwetter *et al.*, 1987], electroporation [Hyanes and Britz, 1990], and transconjugation [Schafer *et al.*, 1990] are available. Electroporation is by far most convenient and most efficient method of DNA transformation in *Corynebacterium.* Transformants generally appear within 48 h with the efficiency of 5×10^7 per microgram of plasmid DNA whereas the protoplast transformation gives about 10^5 transformants per milligram of plasmid DNA with the regeneration time of one to two weeks. Transconjugation is useful for gene disruption or gene replacement and is discussed in details in Chapter 4.

With the availability of the efficient transformation systems, many genes involved in intermediate metabolism as well as several amino acid biosynthetic pathways have been cloned (Table 2.4). Three common strategies were used to clone these genes; homologous complementation, heterologous complementation, and screening based on the conserved motif found in other organisms or peptide sequences of purified proteins. Obviously, cloned genes are of great value in engineering strains with better performance by raising the activity of the rate-limiting enzymes or deregulating the feedback regulation of the critical enzymes.

It should be noted that besides producing amino acids, members of *Corynebacterium* are utilized in other biotechnological processes [Wohlleben *et al.*, 1993] such as production of nucleotides [Ogata *et al.*, 1976], production of antibiotics [Suzuki *et al.*, 1972], production of surfactants [Zajic *et al.*, 1977], production of Vitamin C precursors [Anderson *et al.*, 1985], cheese ripening [Lee *et al.*, 1985], bioconversion of steroids [Constantinides, 1980], terpenoid oxidation [Yamada *et al.*, 1985] and degradation of carbohydrates [Cardini and Jurtshuk, 1970].

2.4 References

Anderson, S., Marks, C.B., Lazarus, R., Miller, J., Stafford, K., Seymour, S., Light, D., Rastetter, W., Estell, D. (1985). Production of 2-keto-L-gluconate, an intermediate in L-ascorbate synthesis by a genetically modified *Erwinia herbicola*. *Science* **230**: 144-149.

Archer, J.A.C., Sinskey, A.J. (1993). The DNA sequence and minimal replicon of the *Corynebacterium glutamicum* plasmid pSR1: Evidence of a common ancestry with plasmids from *C. diphtheriae*. *J. Gen. Microbiol.* **139**: 1753-1759.

Bigelis, R. (1988). Industrial Products of Biotechnology: Application of Gene Technology. pp. 229-258 In: *Biotechnology*. Rehm, H.-I., Reed, G. (eds.), Verlag Chemie, Weinheim, Germany.

Cardini, G., Jurtshuk, P. (1970). The enzymatic hydroxylation of n-octane by *Corynebacterium* sp. strain 7EC1C. *J. Biol. Chem.* **245**: 2789-2796.

Collins, M.D., Cummins, C.S. (1986). Genus *Corynebacterium* Lehmann and Neumann 1896, 350^{AL}. pp. 1266-1276 In: *Bergey's Manual of Systematic Bacteriology*. Sneath, P.H.A.,Mair, N.S.,Sharpe, M.E., Holt, J.G. (eds.), Williams & Wilkins, Baltimore, DE.

Constantinides, S. (1980). Steroid transformations at high substrate concentration using immobilized *Corynebacterium simplex* cells. *Biotechnol. Bioeng.* **22**: 119-136.

Haynes, J.A., Britz, M.L. (1990). The effect of growth conditions of *Corynebacterium glutamicum* on the transformation frequency obtained by electroporation. *J. Gen. Microbiol.* **136**: 255-263.

Jetten, M.S., Sinskey, A.J. (1995). Recent advances in the physiology and genetics of amino acid-producing bacteria. *Crit. Rev. Biotechnol.* **15**: 73-103.

Kinoshita, S., Nakayama, K. (1978). Amino Acids. pp. 209-261 In: *Primary Products of Metabolism*. Rose, A.H. (ed.), Academic Press, London.

Kinoshita, S., Udaka, S., Shimono, M. (1957). Studies on the amino acid fermentation. Part I. Production of L-glutamic acid by various organisms. *J. Gen. Appl. Microbiol.* **3**: 193-205.

Kiss, B. (1991). *Metabolic activity control of the L-lysine fermentation by restrained growth fed-batch strategies*, Ph. D. thesis, Massachusetts Institute of Technology, Cambridge, MA.

Lee, C.W., Lucas, S., Desomazeaud, M.J. (1985). Phenylalanine and tyrosine catabolism in some cheese coryneform bacteria. *FEMS Microbiol. Lett.* **26**: 201-205.

Liebl, W., Ehrmann, M., Ludwig, W., Schleifer, K.H. (1991). Transfer of*Brevibacterium divaricatum* DSM-20297T, *Brevibacterium flavum* DSM-20411, *Brevibacterium lactofermentum* DSM-20412 and DSM-1412, and *Corynebacterium lilium* DSM-20137T to *Corynebacterium glutamicum* and their distinction by ribosomal RNA gene restriction patterns. *Int. J. Syst. Bacteriol.* **41**: 255-260.

Martin, J.F., Snatamaria, R., Sandoval, H., del Real, G., Mateos, L.M., Gil, J.A., Aguilar, A. (1987). Cloning systems in amino acid-producing corynebacteria. *Bio/Technol.* **5**: 137.

Ogata, K., Kinoshita, S., Tsunnoda, T., Aida, T. (1976). *Microbial Productions of Nucleic Acid Related Substances*, Wiley, New York.

Riegel, P., Grimont, P.A.D., Debriel, D., Ageron, E., Jehl, F., Pelegrin, M., Monteil, H., Minck, R. (1992). *Corynebacterium* group-D2 ("*Corynebacterium urealyticum*") constitutes a new genomic species. *Res. Microbiol.* **143**: 307-313.

Serwold-Davis, T.M., Groman, N., Rabin, M. (1987). Transformation of *Corynebacterium diphtheriae*, *Corynebacterium ulcerans*, *Corynebacterium glutamicum*, and *Escherichia coli* with the *C. diphtheriae* plasmid pNG2. *Proc. Natl. Acad. Sci. USA* **84**: 4964-4968.

Soda, K., Tanaka, H., Esaki, N. (1983). Amino Acids. pp. 467-478 In: *Biotechnology*. Rehm, H.-J., Reed, G. (eds.), Verlag Chemie, Weinheim, Germany.

Suzuki, T., Honda, H., Katsumata, R. (1972). Production of antibacterial compounds analogous to chlroamplenicol by n-paraffin-grown bacteria. *Agric. Biol. Chem.* **36**: 2223-2228.

Trautwetter, A., Blanco, C., Bonnassie, S. (1987). Characterization of the corynebacteriophage CG33. *J. Gen. Microbiol.* **133**: 2945-2952.

Vallino, J.J. (1991). *Identification of branch-point restrictions in microbial metabolism through metabolic flux analysis and local network perturbations*, Ph. D. thesis, Massachusetts Institute of Technology, Cambridge, MA.

Wohlleben, W., Muth, G., Kalinowski, J. (1993). Genetic Engineering of Gram Positive Bacteria. pp. 477-505 In: *Biotechnology: Genetics and Fundamentals of Genetic Engineering*. Rehm, H.J., Reed, G., Puehler, A., Sahm, H. (eds.), VCH Publishers, Weinheim, Germany.

Yamada, K., Kinoshita, S., Tsunoda, T., Aida, K. (1972). *The Microbial Production of Amino Acids*, Wiley, New York.

Yamada, Y., Won Seo, C., Okada, H. (1985). Oxidation of acyclic terpenoids by *Corynebacterium* sp.. *Appl. Environ. Microbiol.* **49**: 960-963.

Yoshihama, M., Walker, G.C., Sinskey, A.J., Shanabruch, W.G., Rao, E.A., Follettie, M.T., Akedo, M., Higashiro, K. (1985). Cloning vector System for *Corynebacterium glutamicum*. *J. Bacteriol.* **162**: 591-597.

Zarjic, J.E., Guignard, H., Gerson, D.F. (1977). Emulsifying and surface active agents from *Corynebacterium hydrocarboclastum*. *Biotechnol. Bioeng.* **19**: 1295-1301.

Table 2.1 Fermentative processes of industrial amino acid production (adopted from Bigelis, 1988).

Amino Acid	Organisms	Maximum Reported Yield (g/L)
L-Arginine	*Corynebacterium glutamicum*	25
	Brevibacterium flavum	35
	Bacillus subtilis	28
	Serratia marcescens	100
L-Glutamate	*Corynebacterium* spp.	100
	Brevibacterium spp.	80
	Arthrobacter paraffineus	62
L-Glutamine	*Corynebacterium glutamicum*	37
	Flavobacterium ringense	25
L-Histidine	*Corynebacterium glutamicum*	15
	Brevibacterium flavum	10
	Serratia marcescens	23
L-Isoleucine	*Corynebacterium glutamicum*	10
	Brevibacterium flavum	30
	Serratia marcescens	25
L-Leucine	*Brevibacterium lactofermentum*	30
	Serratia marcescens	15
L-Lysine	*Corynebacterium glutamicum*	42
	Brevibacterium flavum	34
	Brevibacterium lactofermentum	70
L-Phenylalanine	*Corynebacterium glutamicum*	9.5
	Brevibacterium lactofermentum	25
	Bacillus subtilis	6
L-Proline	*Corynebacterium glutamicum*	15
	Brevibacterium flavum	35
	Serratia marcescens	22
L-Serine	*Corynebacterium glycinophilum*	14
	Pseudomonas sp.	12
	Hyphomicrobium methylovorum	24
L-Threonine	*Corynebacterium glutamicum*	14
	Brevibacterium flavum	17.5
	Serratia marcescens	25
	Escherichia coli	6
L-Tryptophan	*Corynebacterium glutamicum*	12
	Brevibacterium flavum	20
L-Valine	*Corynebacterium glutamicum*	30
	Brevibacterium lactofermentum	31
	Serratia marcescens	10

Table 2.2 Enzymatic processes of industrial amino acid production (adopted from Bigelis, 1988).

Amino Acid	Enzymes	Process
L-Alanine	*Escherichia coli* aspartase and *Pseudomonas* L-aspartate β-decarboxylase	Coversion of ammonium fumarate to L-aspartate and then to L-alanine sequentially by immobilized cells
L-Aspartate	*Escherichia coli* aspartase	Coversion of ammonium fumarate to L-aspartate by immobilized cells
L-Lysine	*Cryptococcus laurentii* L-amino-caprolactam hydrolase and *Achromobacter obae* aminocaprolactam racemase	Conversion of synthetic DL-α-amino-ε-caprolactam to L-lysine by two enzymes
L-Methionine	*Aspergillus oryzae* aminoacylase	Conversion of synthetic DL-methionine to N-acetyl derivative and then asymmetric hydrolysis by immobilized aminoacylase
L-Phenylalanine	*Rhodotorula rubra* phenylalanine ammonia lyase	Conversion of *trans*-cinnamic acid to L-phenylalanine by immobilzed cells in presence of ammonia

Table 2.3 Endogenous Corynebacterial plasmids (adopted from Wohlleben *et al.* [1993]).

Plasmid	Source	Size (kb)	Marker
pHM1519	*C. glutamicum*	3.055	cryptic
pBL1	*B. lactofermentum*	4.45	cryptic
pCC1	*C. callunae*	4.2	cryptic
pCL1	*C. lilium*	4.1	cryptic
pBY503	*B. stationis*	15	cryptic
pAG3	*C. melassecola*	4.5	cryptic
pXZ10145	*C. glutamicum*	5.3	Cm
pGA1	*C. glutamicum*	4.9	cryptic
pNG2	*C. diphtheriae*	14.4	Em
pCG2	*C. glutamicum*	6.8	cryptic
pAG1	*C. melassecola*	20.4	Tc
pTP10	*C. xerosis*	50	Tc, Cm, Em, Km
pCG4	*C. glutamicum*	26	Spc, Str

Abbreviations: Cm, chlorophenicol resistance; Em, erythromycin resistance; Km, kanamycin resistance; Spc, spectinomycin resistance; Str, streptomycin resistance; Tc, tetracycline resistance; *C*, *Corynebacterium*; *B. Brevibacterium.*

Chapter 3. Materials and Methods

3.1 Bacterial Strains and Plasmids

All bacterial strains and plasmids used in this thesis are listed in Table 3.1 and Table 3.2. *Corynebacterium glutamicum* ATCC 21253 (U.S. Patents 3,708,395) serves as the parent type strain for the construction of other mutants. This strain requires biotin, L-homoserine (or L-methionine and L-threonine), and L-leucine for growth. Via random mutagenesis with UV light, this strain was derived from ATCC 13287 (U.S. Patents 2,979,439), a L-homoserine auxotroph and L-lysine overproducer, which was in turn derived from ATCC 13032 (U.S. Patents 3,002,889), a L-glutamate overproducer first isolated from the sewage by researchers at Kyowa Hakko Kogyo Company in Japan [Kinoshita *et al.*, 1957].

3.2 Media

3.2.1 Storage and Cultivation Media

Luria-Bertani (LB) medium [Davis *et al.*, 1986] which contains 10 g/l Tryptone, 5 g/l Yeast Extract, and 10g/l NaCl was used for routine growth and strain maintenance of both *C. glutamicum* and *E. coli*. This medium was also used for initial seed cultures for fermentations. All strains were stored at -80°C in LB medium containing 20% (v/v) glycerol. LB5G medium which is LB medium supplemented with 5 g/l glucose was used for transformation of *C. glutamicum*. M9 medium containing 4 g/l glucose and 50 mg/l L-arginine was used as minimal growth medium for *E. coli* strain XH11 [Sambrook *et al.*, 1989]. Ampicillin (100 mg/l), kanamycin (25 mg/l), chloramphenicol (10 mg/l), nalidixic acid (25 mg/l), spectinomycin (100 mg/l), and IPTG (isopropyl-β-D-thiogalactopyranoside, 0.01-5 mM) were supplemented when appropriate. Agar was added at 17 g/l for plates.

The ^{13}C labeling studies with *C. glutamicum* strains were conducted in a volume of 20 ml with minimal medium (PMB2) listed in Table 3.3. The small volume was used in order to minimize the amount of ^{13}C labeling substrates required. The shake flask

experiments were conducted in a 100-ml triple-baffled Erlenmeyer flask. PMB2 medium is almost identical to the PMB medium designed by Vallino [1991] except that glucose (20 g/l) is replaced by gluconate (10 g/l) plus pyruvate (10 g/l) and citrate (1.14 g/l) is replaced by catecol. Catecol essentially fulfills the role of citrate in the minimal medium which is to facilitate the transport of iron by *C. glutamicum* [von der Osten *et al.*, 1989]. For the ^{13}C labeling studies, high level of citrate in the medium is not desirable since citrate can be utilized as a carbon source. This means that potentially useful metabolites of interest could be derived from this unlabeled citrate instead of ^{13}C labeled substrate. In the shake flask studies, $CaCO_3$ was also necessary as a buffer to maintain pH around 6.5 so that cells continue to secrete lysine. In order to avoid precipitation of salts, PMB2 (also PMB) medium was autoclaved in three separate portions as indicated in Table 3.3 and combined aseptically after cooling. Catecol was added separately after filter sterilization using a 0.22 μm Millex®-GV filter unit (Millipore, Bedford, MA).

[U-^{13}C]gluconate was enzymatically synthesized from [U-^{13}C]glucose using glucose oxidase (EC 1.1.3.4) purchased from Sigma Chemical Co. (St. Louis, MO) based on the following reaction:

$$\text{D-Glucose} + O_2 + H_2O \xrightarrow{\text{glucose oxidase}} \text{D-Gluconate} + H_2O_2$$

Although the manufacturer suggested the use of 50 mM Na·acetate pH 5.1 for the maximum activity of glucose oxidase, this buffer was not employed for the preparation of gluconate because it would require additional purification steps to remove the potential carbon source, Na·acetate, from the reaction mixture. Instead, the reaction was done in 10 mM Tris·HCl pH 7.5. Typically, 1 g of [U-^{13}C]glucose was dissolved in 10 ml of 10 mM Tris·HCl pH 7.5, mixed with 1000 units of glucose oxidase (1,000 units/ml prepared in 10 mM Tris·HCl pH 7.5), and incubated at 37°C and 50 rpm in a 100-ml beaker for 2 h. This gave a greater than 99% conversion. In order to deactivate the enzyme and other impurities, the reaction mixture was heated at 55°C for 1 h, sterilized by filtering through a 0.22 μm Millex®-GV filter and stored at -20°C until use. Conversion of glucose to gluconate was determined by high pressure liquid chromatography (HPLC) with a Bio-Rad Aminex HPX-87C column (details in Section 3.4.1).

[1-^{13}C]pyruvate, [2-^{13}C]pyruvate, [3-^{13}C]pyruvate and [U-^{13}C]glucose were purchased from Cambridge Isotope Laboratories, Inc. (Woburn, MA).

3.2.2 Benchtop Fermentation Media

Fermentation medium for 10-lilter batch fermentation was identical to the FM4 medium (Table 3.4) described by Vallino [1991]. After the addition of a 1-liter innoculum prepared in the PMB medium, this medium produced 10 liter medium and supported the cell growth to 17-20 g DCW/l. Fermentation was prepared in two portions. Portion A was sterilized at 121°C in the fermentor for 40 min. Portion B was autoclaved separately at 121°C for 30 min in a 4-liter shake flask and added aseptically to the fermentor after cooling.

3.3 DNA Techniques

3.3.1 Isolation of Plasmid DNA and Transformations

Plasmid DNA from *E. coli* was purified as described by Birnboim and Doly [1979]. For high purity plasmid purification from large volumes (50-1000 ml) of *E. coli* cultures, the QIAGEN procedure (QIAGEN Inc., Studio City, CA) was used. Plasmid DNA from *C. glutamicum* was purified according to the procedure developed by Yoshihama *et al.* [1985]. *E. coli* were transformed using the $CaCl_2$-method developed by Mandel and Higa [1970]. *E. coli* plasmid DNA was introduced into the wild-type *C. glutamicum* strains via *C. glutamicum* E12, a restriction negative but modification positive variant of *C. glutamicum* ASO19 using the electroporation method [Haynes and Britz, 1990]. For transformation by electroporation, *C. glutamicum* was grown in 1 liter of LB5G at 30°C and 250 rpm. Cells were harvested by centrifugation at 4,000 *g* and 4°C (J2-21 centrifuge, Beckman, Palo Alto, CA) for 10 min when OD_{660} reached between 0.6 and 0.8. Cells were washed three times by resuspending the cell pellets in 50 ml of ice-cold wash buffer (milliQ H_2O containing 15% (v/v) pure glycerol) and centrifugation at 4,000 *g* and 4°C for 10 min. Finally, cells were resuspended in 1 ml of wash buffer and stored at -80°C until further use. After thawing in ice, the concentrated cells (40 µl) were mixed with

1 μg of plasmid DNA in a cold 1.5 ml polypropylene Eppendorf tube. Cells were transferred to 0.2 cm cuvettes (Bio-Rad Laboratories, Richmond, CA) and exposed to a single pulse (2.5 kV, 25 μF, 200Ω) using the Gene Pulser apparatus (Bio-Rad Laboratories, Richmond, CA). This typically gave a pulse length (τ) of 4-5 ms. Immediately following the pulse, 1 ml of LB5G was added and the culture was incubated at 30°C and 50 rpm for 1-1.5 h before dilution and plating on selective media.

3.3.2 Transconjugation of Plasmid from *E. coli* to *Corynebacterium*

Mobilization of plasmids from *E. coli* to *Corynebacterium* strains was done as described by Schäfer *et al.* [1990]. *E. coli* donor and *C. glutamicum* recipient strains were grown in 50 ml LB to an OD of 1.0, harvested and washed once with 0.9% NaCl solution by centrifugation at 4,000 *g* for 15 min, and resuspended in 5 ml of the same buffer. Donor and recipient cells were mixed in an Eppendorf tube (ratio 1:1 or 1:5 v/v) after heat-treating recipient cells at the desired temperature (optimum at 48-50°C for 10 min). The mixture was centrifuged for 30 sec and carefully resuspended in 100 μl LB and spread onto a 0.2 mm nitrocellulose filter on a prewarmed LB plate. After incubation at 30°C for 16-24 h, cells were scraped from the filter into 1 ml LB and the mixture was plated on selective plates containing appropriate antibiotics after dilution (typically 100 μl per plate) at 30°C for 1-2 days.

3.3.3 Random Mutagenesis

Mutations were introduced via random mutagenesis by N-methyl-N'-nitro-N-nitrosoguanidine (NTG; obtained from Aldrich Chemical Co., St. Louis, MO) treatment as follows. *C. glutamicum* 253SM1 was grown to an OD of 1.0 in 50 ml LB and was harvested by centrifugation at 4,000 *g* and 4°C for 15 min. Cells were washed once with 0.1 M Na-citrate pH 6.0 and resuspended to a final volume of 25 ml in the same buffer. 1 ml was saved for the comparison of survivals before and after NTG treatment. To the 24 ml tube, 1 ml of 2 mg/ml NTG stock solution (dissolved in water, filter-sterilized through a 0.22 μm filter and stored at -20°C until use) was added. After incubation at room

temperature (under the hood) for 30 min, 25 ml LB was added to absorb residual NTG and centrifuged at 4,000 *g* and 4°C for 15 min. Cells were washed three times with 25 ml LB and resuspended to a final volume of 24 ml with LB. Cell counts before and after NTG treatment gave a survival rate of about 50%. 16 ml of 50% glycerol stock were added and aliquoted in 1ml for long-term storage of NTG treated cells at -80°C. Extreme care must be taken handling all materials and liquids exposed to NTG which should be first decomposed by soaking in 5 N NaOH and neutralized with concentrated HCl before draining.

3.3.4 Isolation of *C. glutamicum* Chromosomal DNA

Chromosomal DNA from *Corynebacterium* strains was isolated using the modified method of Tomioka *et al.* [1981]. Fresh cultures of *Corynebacterium* strains were grown in 100 ml LB at 30°C and 250 rpm overnight. Cells were harvested by centrifugation at 4,000 *g* and 4°C for 10 min and washed once with 50 ml of TE (10 mM Tris·HCl pH 8.0, 1 mM EDTA). Cells were resuspended in 5 ml of TE plus 2.5 ml of 1 M sorbitol with 100 mg of lysozyme and lysed by adding 0.5 ml of 10% sodium dodecyl sulfate, followed by incubation at 37°C for 1 h. $NaClO_4$ was added to a final concentration of 1 M in the lysate and mixed gently until completely dissolved. Equal volume of phenol/chloroform (50:50 mixture) was added and gently mixed for 30 min. The viscous supernatant of the lysate was isolated by centrifugation at 8,000 *g* and 4°C for 30 min and extracted once with chloroform. RNase A was added to a final concentration of 50 μg/ml, and the lysate was incubated at 37°C for 1 h. After extracting the lysate with phenol/chloroform once and with chloroform twice, two volumes of pure ethanal were added and Na·acetate was added to a final concentration of 0.3 M. Chromosomal DNA was spooled using 1 ml-pipette and washed twice with 70% ethanol. After a brief air-dry (5-10 min), chromosomal DNA was redissolved in 1 ml of TE and kept at 4°C until completely redissolved for storage.

3.3.5 DNA Manipulations

DNA fragments were fractionated by agarose gel electrophoresis and purified using the GeneClean® Kit (BIO 101 Inc., La Jolla, CA). For Southern blot analysis, DNA was electrophoretically separated in agarose gels, denatured and transferred to nitrocellulose filters as described by Sambrook *et al.* [1989]. The probe for the Southern blot was labeled with digoxigenin-11-dUTP (Boehringer, Mannheim, Germany) in a random primed DNA labeling reaction as described by the manufacturer. Hybridization, washing, and colorimetric detection for the Southern blot was performed using the Genius-System (Boehringer, Mannheim, Germany).

All restriction enzymes, and other related enzymes and reagents for DNA manipulations were purchased from New England Biolabs, Bethesda Research Laboratories, or Boehringer Mannheim and used as described by the instructions of the manufacturer.

3.4 Analytical Techniques

3.4.1 Organic Acid Detection

For the analysis of organic acids, an HPLC system, consisting of a Waters (Bedford, MA) 501 pump, 680 pump controller, WISP 710 automatic injector, R401 differential refractometer, a Shimadzu (Columbia, MD) C-R3A Chromatopac integrating recorder, and a Bio-Rad Aminex HPX-87H or HPX-87C column, was used to determine the concentration of several metabolites in the fermentation broth samples that were filtered through a 0.22 μm Millex®-GV filter unit and stored at -20°C until analysis.

A Bio-Rad Aminex HPX-87H reverse phase column was used to measure glucose, acetate, lactate, trehalose, propionate, glyceraldehyde and dihydroxyacetone. The column was run in an isocratic mode at a flow rate of 0.6 ml/min with a mobile phase consisting of 0.005 N H_2SO_4, temperature of 45°C, injection volume of 15-200 μl (typically 30 μl), and a refractometer attenuation of 32X. The mobile phase was prepared by mixing 0.27 ml of concentrated H_2SO_4 (96%) per 1 liter of HPLC-grade H_2O, filtered through a 0.45 μm Millipore HVLP filter, and stored at room temperature until use.

A Bio-Rad Aminex HPX-87C reverse phase column was used to measure

gluconate, pyruvate, and glucose. The column was run in an isocratic mode at a flow rate of 1 ml/min with a mobile phase consisting of 5 mM $CaSO_4$, temperature of 85°C, injection volume of 15-200 µl (typically 30 µl), and a refractometer attenuation of 16X or 32X. The mobile phase was prepared as described above and stored at room temperature until use. This column was especially useful in monitoring the enzymatic conversion of glucose to gluconate and in monitoring gluconate and pyruvate in the ^{13}C labeling shake flask studies. It must be noted that pyruvate and glucose cannot be quantified simultaneously with this column due to the similar retention times of pyruvate and glucose.

3.4.2 Amino Acid Detection

Amino acids were analyzed as *ortho*-phthalaldehyde derivatives [Jones and Gilligan, 1983] separated by an AminoQuant (Hewlett Packard, Waldronn, Germany) 2.1-mm bore reversed phase column with a Hewlett Packard 1050 HPLC system which allowed full automation of derivatization, chromatography, data acquisition, and data evaluation. Detection was done by UV absorbance at 338 nm and the column was run at 40°C in a gradient mode at the flow rate of 0.45 ml/min consisting of two buffers: Buffer A contained 20 mM Na·acetate (prepared in HPLC-grade H_2O and filtered through a 0.45 µm Millipore HVLP filter), 50 mM tetrahydrofuran (HPLC-grade, Fluka Chemical Corp., Ronkonkoma, NY) and 2 mM triethylamine (HPLC-grade, Fluka Chemical Corp.) at pH 7.2. Buffer B contained 20 mM Na·acetate pH 7.2 (filtered through a 0.45 µm filter), methanol (HPLC-grade, Mallincroft Corp.), and acetonitrile (HPLC-grade, Mallincroft Corp.) at a volumetric ratio of 20:40:40.

3.5 Intracellular Enzyme Activity Measurements

3.5.1 Preparation of Cell-Free Crude Extracts

For determination of enzyme activities, cells grown in various media and phases were harvested by centrifugation at 4,000 *g* and 4°C for 15 min and the cell pellets were kept frozen at -20°C until use. The cell pellets were thawed in ice and washed twice with

cold buffer (100 mM Tris·HCl pH 7.5, 20 mM KCl, 5 mM $MnSO_4$, 10 mM $MgCl_2$, and 1 mM dithiothreitol (DTT)). The cell pellets were resuspended in the same buffer to a final cell concentration between 20 to 50 g DCW/l. Cells were disrupted either by ultrasonication in ice at 40 W output power (XL2020 sonicator, Heat Systems, Farmingdale, NY) for 10 x 30 s with alternating cooling periods of 30 s or by homogenizing with glass beads (200-300 μm, Sigma Chemical Co.) in 5100 Bead Mill (SPEX Industries, Edison, NJ) for 5 min. The cell debris was removed by centrifugation at 47,000 *g* and 4°C for 1 h. The supernatant was used for the enzyme measurements. Both methods produced typically 5 to 10 mg of protein per ml of supernatant. The protein concentrations were determined by the method of Bradford [1976] using a bovine serum albumin as a standard.

3.5.2 Enzyme Assays

Enzyme assays were performed in methylacrylate cuvettes (2.9 or 4 ml volume with 1 cm light path; Fisher Scientific Co., Pittsburgh, PA) in a Kontron (Everett, MA) Uvikon® 810 spectrometer at room temperature. Most reactions were carried out in small voumes (1-2 ml) and activity was calculated typically in nmol/min/mg of protein using the following expression:

$$\text{Activity [nmol/min/mg of protein]} = \frac{1000V}{\varepsilon LPY}\frac{dA}{dt} \qquad \textbf{(Eq. 3.1)}$$

where V is the volume (in ml) of the assay mixture, L is the path length of cuvette (1 cm), P is the protein concentration of the cell-free extract (in mg/ml), Y is the volume of cell-free extract added (in ml), and $\frac{dA}{dt}$ is the rate change of absorbance at the desired wavelength (in ΔOD/min). The extinction coefficients (ε) used were 6.22 $mM^{-1}cm^{-1}$ for NADPH and NADH at 340 nm, 14.12 $mM^{-1}cm^{-1}$ for thiophenolate at 412 nm, 17.4 $mM^{-1}cm^{-1}$ for glyoxylic acid phenylhydrozine at 324 nm, 9.02 $mM^{-1}cm^{-1}$ for 3-acetylpyridine adenine dinucleotide (AcPyADH) at 375 nm, and 1.65 $mM^{-1}cm^{-1}$ for NADPH at 375 nm. The extinction coefficients for the last two pyridine nucleotides were determined in a volume of 1 ml by correlating absorbance with concentration (Figure 3.1).

Most enzymes discussed in this thesis were measured with a pyridine nucleotide

system. NADH and NADPH as well as their oxidized forms NAD^+ and $NADP^+$, respectively, have proven to be useful for analytical purposes because of their unusual properties [Lowry and Passonneau, 1972]. They participate in many enzyme reactions as the natural oxidizing and reducing agents. Only the reduced forms, namely NADH and NADPH, absorb at 340 nm, therefore changes in oxidation and reduction can be measured spectrophotometerically. The reduced forms can be completely destroyed in acid without affecting the oxidized forms. Likewise, the oxidized forms can be completely destroyed in base without affecting the reduced forms. This property is extremely useful in the cases requiring more subsequent treatments involving these nucleotides.

All enzymes and reagents used in the enzyme assays were purchased from Sigma Chemical Co. Assays were performed without any purification unless otherwise noted.

3.5.2.1 Pyruvate Kinase (PK: EC 2.7.1.40)

$$\text{PEP} + \text{ADP} \xrightarrow{\text{PK}} \text{Pyruvate} + \text{ATP}$$

$$\text{Pyruvate} + \text{NADH} \xrightarrow{\text{lactate dehydrogenase}} \text{Lactate} + \text{NAD}^+$$

The assay is based on the above coupled reactions [Ozaki and Shiio, 1983]. The activity was determined by the decrease in absorbance at 340 nm due to the oxidation of NADH in a reaction mixture containing 100 mM Tris·HCl pH 7.5, 10 mM $MgCl_2$, 10 mM PEP, 2 mM ADP, 0.4 mM NADH, 20 units of lactate dehydrogenase, and 250-500 μg crude extract in a volume of 1 ml. Background activity due to other enzymes performing NADH oxidation reaction was accounted for by running a blank run without the addition of lactate dehydrogenase.

3.5.2.2 Phosphoenolpyruvate Carboxylase (PPC: EC 4.1.1.31)

Two different protocols were used to measure the activity of PPC: one coupled with malate dehydrogenase and another coupled with citrate synthase. Since the same end product, OAA was produced by PPC, PPCK, PPCTP and PC, the almost identical assay protocols described in this Section could be used to determine the activity of these enzymes with only minor modifications. The first protocol [Tosaka *et al.*, 1979] was based

on the following reactions:

$$PEP + CO_2 \xrightarrow{PPC} OAA + ATP$$

$$OAA + NADH \xrightarrow{\text{malate dehydrogenase}} Malate + NAD^+$$

The activity was determined by the decrease in absorbance at 340 nm due to the oxidation of NADH in a reaction mixture containing 100 mM Tris·HCl pH 7.5, 10 mM $MgCl_2$, 10 mM PEP, 50 mM $KHCO_3$, 0.2 mM acetyl-CoA, 0.4 mM NADH, 10 units of malate dehydrogenase, and 250-500 μg crude extract in a volume of 1 ml. Two blanks were run, one without acetyl-CoA, an activator of PPC, and the other without PEP.

The second protocol was based on the determination of absorbance increase at 412 nm due to the formation of thiophenolate using 5,5′ dithio-bis(-2nitrobenzoic acid) (DNTB, Ellman's reagent) based on the following reactions:

$$PEP + CO_2 \xrightarrow{PPC} OAA + ATP$$

$$OAA + Acetyl\text{-}CoA \xrightarrow{\text{citrate synthase}} Citrate + HSCoA$$

$$HSCoA + DNTB \longrightarrow Thiophenolate$$

The reaction mixture contained in a volume of 1 ml: 100 mM Tris·HCl pH 7.5, 10 mM $MgCl_2$, 10 mM PEP, 50 mM $KHCO_3$, 0.2 mM acetyl-CoA, 10 units of citrate synthase, 0.1 mg of DNTB (from 10 mg/ml stock solution prepared in ethanol), and 250-500 μg crude extract. A blank without acetyl-CoA was run. The second protocol is more specific and sensitive than the first one since the background activity of NADH oxidation reactions does not interfere with the measurement. However, with the second protocol, the effect of acetyl-CoA can not be measured.

3.5.2.3 Phosphoenolpyruvate Carboxykinase (PPCK: EC 4.1.1.32)

$$PEP + CO_2 + GDP \xrightarrow{PPCK} OAA + GTP$$

The almost identical assay protocols described in the Section 3.5.2.1 were used to determine the activity of PPCK, except the addition of 2 mM IDP. It was determined that IDP could replace GDP as the phosphate acceptor in the above reaction.

3.5.2.4 Phosphoenolpyruvate Carboxytransphosphorylase (PPCTP: EC 4.1.1.38)

$$PEP + CO_2 + P_i \xrightarrow{PPCTP} OAA + PP_i$$

The almost identical assay protocols described in the Section 3.5.2.1 were used to determine the activity of PPCTP, except the addition of 1 mM potassium phosphate pH 6.5. No activity of PPCTP was detected in any of *Corynebacterium* strains. With these protocols, it could not be conclusively established that PPCTP does not exist in *Corynebacterium* species since no positive control was used for the measurement of the activity of PPCTP which has been detected only in *Propionibacterium shermanii* [Siu *et al.*, 1961] and *Entamoeba histolytica* [Reeves, 1970].

3.5.2.5 Pyruvate Carboxylase (PC: EC 6.4.1.1)

$$Pyruvate + CO_2 + ATP \xrightarrow{PC} OAA + ADP$$

The almost identical assay protocols described in the Section 3.5.2.1 were used to determine the activity of PC, except the replacement of 10 mM PEP by 10 mM Na-pyruvate and the addition of 5 mM ATP. Contrary to the report by Tosaka et al. [1979], no activity of PC was detected in any of *Corynebacterium* strains though activity of 25 nmol/min/mg of protein was detected in *Pseudomonas citronellolis*, used as a positive control.

3.5.2.6 Transcarboxylase (TC: EC 2.1.3.1)

$$Pyruvate + (S)\text{-}Methylmalonyl\text{-}CoA \xrightarrow{TC} OAA + Propionyl\text{-}CoA$$

The almost identical assay protocols described in the Section 3.5.2.1 were used to determine the activity of TC, except the addition of 0.2 mM methylmalonyl-CoA. No activity of TC was detected in any of *Corynebacterium* strains. With these protocols, it could not be conclusively established that TC does not exist in *Corynebacterium* species since no positive control organism such as *Propionibacterium shermanii* was used for the measurement of the activity of TC.

3.5.2.7 Malic Enzyme (ME: EC 1.1.1.40)

$$\text{Pyruvate} + CO_2 + \text{NADPH (NADH)} \xleftrightarrow{\text{ME}} \text{Malate} + NADP^+ (NAD^+)$$

The activity of ME can be measured by measuring the increase (decarboxylating direction) or decrease (carboxylating) in absorbance at 340 nm [Mori and Shiio, 1987]. For assay in the decarboxylating direction, the reaction mixture contained in a volume of 1ml: 100 mM Triethanolamine pH 7.4, 10 mM $MnCl_2$, 0.5 mM $NADP^+$ (or NAD^+), 10 mM L-malate pH 7.0, and 250-500 µg crude extract. For assay in the decarboxylating direction, the reaction mixture contained in a volume of 1ml: 100 mM Tris·HCl pH 7.5, 10 mM $MnCl_2$, 30 mM KCl, 15 mM $KHCO_3$, 0.5 mM NADPH (or NADH), 15 mM Na·pyruvate, and 250-500 µg crude extract.

3.5.2.8 Malate Synthase (MS: EC 4.1.3.2)

$$\text{Glyoxylate} + \text{Acetyl-CoA} \xrightarrow{\text{malate synthase}} \text{Malate} + \text{HSCoA}$$

$$\text{HSCoA} + \text{DNTB} \longrightarrow \text{Thiophenolate}$$

The malate synthase enzyme activity was measured by measuring the absorbance increase at 412 nm due to the formation of thiophenolate [Dixon and Kornberg, 1959] in a reaction mixture containing 100 mM Tris·HCl pH 7.5, 5 mM $MgCl_2$, 0.1 mg DNTB, 0.2 mM acetyl-CoA, 10 mM Na·glyoxylate, and and 250-500 µg crude extract in a volume of 1 ml. Background activity was measured by omitting glyoxylate in the reaction mixture.

3.5.2.9 Isocitrate Lyase (ISL: EC 4.1.3.1)

$$\text{Isocitrate} \xrightarrow{\text{isocitrate lyase}} \text{Succinate} + \text{Glyoxylate}$$

$$\text{Glyoxylate} + \text{Phenylhydrazine} \longrightarrow \text{Glyoxylic Acid Phenylhydrozine}$$

The isocitrate lyase enzyme activity was measured by measuring the absorbance increase at 324 nm due to the formation of glyoxylic acid phenylhydrozine [Dixon and Kornberg, 1959] in a reaction mixture containing 100 mM potassium phosphate pH 6.85, 5 mM $MgCl_2$, 3 mM phenylhydrazine·HCl, 2 mM cysteine·HCl, 2 mM isocitrate, and and 250-500 µg crude extract in a volume of 1 ml. Background activity was measured by omitting isocitrate in the reaction mixture.

3.5.2.10 Transhydrogenase (THD: EC 1.6.1.1)

$$NAD^+ + NADPH \xleftrightarrow{\text{Transhydrogenase}} NADH + NADP^+$$

Since the THD reaction results in no net generation or consumption of reduced form of pyridine nucleotide, the activity of THD can not be followed by measuring the increase or decrease in absorbance at 340 nm. The modified method based on Phelps and Hatefi [1981] was utilized to measure the reaction in the direction of NADPH oxidation in which $AcPyAD^+$, an analogue of NAD^+, was used. The reaction mixture initially contained in a volume of 1 ml: 50 mM Tris·HCl pH 7.5, 2 mM $MgCl_2$, 0.5 mM $NADP^+$, and 250-500 μg crude extract. After 60 to 120 sec, $AcPyAD^+$ was added to a final concentration of 1 mM. The extinction coefficient of 7.37 $mM^{-1}cm^{-1}$ which is the difference of extinction coefficient between AcPyADH (9.02 $mM^{-1}cm^{-1}$) and NADPH (1.65 $mM^{-1}cm^{-1}$) was used to calculate the activity. It should be noted that other researchers used a dual-beam (at 375 and 450 nm) system to account for the absorbance decrease due to the consumption of NADPH.

In order to validate the above protocol in the detection of THD activity, three *E. coli* strains obtained from Dr. P.D. Bragg (Department of Biochemistry, University of British Columbia, Vancouver, Canada) were used as positive and negative controls: (1) AB1450 *pnt*::Tn5, a THD deficient strain of *E. coli* AB1450 used as a negative control; (2) AB1450 *pnt*::Tn5 pDC11, a THD over-expressing strain of *E. coli* AB1450 used as a positive control; and (3) AB1450 used also as a positive control. Figure 3.2 presents the actual raw data showing the reduction of $AcPyAD^+$ by the three *E. coli* strains. Clearly, no activity (4 nmol/min/mg protein) was found in AB1450 *pnt*::Tn5, and activities of 109 and 321 nmol/min/mg protein were found in AB1450 and AB1450 *pnt*::Tn5 pDC11, respectively. This clearly indicates that the assay is functional. Since the cell-free extract of C. glutamicum contained high levels of NADPH, the extract was passed through Sephadex G-25 (PD10 prepacked column, Pharmacia Biotech Inc., Alameda, CA) to remove small metabolites. With the above assay, the activity of THD in *C. glutamicum* strains was detected. This is in direct contrast to the report of Vallino [1991] who

reported no THD activity in *C. glutamicum* strains. However, Vallino used an assay based on the absorbance change at 340 nm which would not occur even under high THD activity because of the same values of ε for NADH and NADPH at 340 nm.

3.6 Benchtop Fermentation Operation

The equipment configuration and computer monitoring system for a 10-liter bacth fermentation was exactly identical to the setup described in the theses of Vallino [1991] and Kiss [1992] and is shown schematically in Figure 3.3. A 15-liter MBR Laboratory Bioreactor (MBR Bio Reactor AG, Wetzikon, Switzerland) with a working volume of 10 liters was used. The fermentor has five 19 mm and eight 12 mm ports in the headplate which can be used for inlet air, outlet air, pressure gauge, overpressure safety valve, base and acid, antifoam, inoculum, and feed. Four side ports were used for pH probe (F-600-B130-A06BC, Broadley-James, Santa Ana, CA), temperature probe supplied by MBR, dissolved oxygen probe (polarographic electrode, Ingold, Wilmington, MA), and a sampling port. The fermentor was interfaced to a MBR MCS 10 controller for the monitoring and control of temperature, dissolved oxygen, pH, load cell, and impeller agitation and was sterilized *in situ*. Air flow was controlled with a Brooks (Hatfield, PA) 5850E mass flow control valve (0-20 slpm N_2 range) and a Brooks 5878 controller. Inlet was passed through a sterilized 0.2 μm Mini Capsule Filter (Gelman Sciences, Ann Arbor, MI). Exhuast air was passed through a filter assembly containing glass wool before passed to the mass spectrometer. The inlet gas and exhaust gas contents were analyzed on-line by a Dycor quadrupole mass spectrometer (Ametek, Pittsburgh, PA). On-line data were communicated to an IBM PC clone (1400-02 pc$^+$, Wyse, San Jose, CA) via a Data Translation (Marlboro, MA) DT2801 analog and digital input/output board using the program developed by Kiss [1992]. Oxygen uptake rate (OUR) and carbon dioxide evolution rate (CER) in mol/l/h were calculated from the inlet and exhuast gas composition by the following equations:

$$OUR = \frac{F_{AIR}}{V}\left(y^{i}_{O_2} - \frac{y^{i}_{N_2}}{y^{e}_{N_2}} y^{e}_{O_2} \right) \qquad \textbf{(Eq. 3.2)}$$

$$CER = \frac{F_{AIR}}{V}\left(\frac{y^{i}_{N_2}}{y^{e}_{N_2}} y^{e}_{CO_2} - y^{i}_{CO_2}\right) \quad \textbf{(Eq. 3.3)}$$

where F_{AIR} is the air flow rate of inlet air (mmol/h), V is the fermentor broth volume (liter), and the y's are the gas phase mole fractions of O_2, CO_2, and N_2 in the inlet (i) and exhuast (e) gas streams.

The inoculation was begun by transferring a loopful of colonies from a LB plate to a 250 ml baffled shake flask containing 50 ml LB. The shake flask was incubated for 8-10 h at 30°C and 200-250 rpm. The LB shake flask contents were aseptically poured into a 4 liter baffled shake flask containing 1 liter of PMB medium and a sterile syphon tube connected to a 8 mm MBR hypodermic needle and incubate at the same conditions for 8-10 h. The PMB shake flask contents were transferred into the main fermentor containing 9 liter of FM4 medium using a peristaltic pump (Cole Parmer, Chicago, IL). All fermentations were conducted at 30°C, pH 7.0 with (~30% (w/w) NH_3) NH_4OH and air flow rate of 1 VVM. Agitation rate and back pressure were manually controlled to maintain the dissolved oxygen above 10% of saturation.

3.7 ^{13}C Nuclear Magnetic Resonance

^{13}C labelling studies were conducted in 100 ml baffled flasks containing 20 ml PMB2 medium. After 10 to 15 hours, approximately 1 to 2 g/l of lysine was accumulated in the culture broths. The broth was collected and cell-free supernatant was prepared by centrifugation at 5,000 *g* and 4°C for 15 min followed by filtration through a 0.45 μm nitrocellulose filter (Nalge, Rochester, NY, USA). The supernatants were evaporated to dryness at -40°C under vacuum using the Freezer Dryer 4.5 (Labconco, Kansas City, MO, USA). The lyophilized samples were resuspended in 2 to 4 ml 50% D_2O for NMR analysis. This typically resulted in a five to ten fold increase in the concentration of lysine to a final concentration of 10 g/l.

Fourier-transformed NMR were performed on an Analogic® spectrometer operating at a frequency of 400.07 Mhz using a 5mm probe at the Shriners Burns Institute (Mass General Hospital, Cambridge, MA). Proton-decoupled ^{13}C NMR spectra were

obtained by locking on D_2O in the following spectrometer conditions: 90° pulses, 25-kHz spectral width, 20-sec repetition time, and 800-2,000 accumulations. Spectral peaks were quantified by using 3-(trimethylsilyl)-1-propane-sulfonic acid (TSP) as an internal standard. Figure 3.4 shows a typical ^{13}C-NMR spectrum obtained with 60 g/l lysine·HCl indicating six lysine carbon resonances: C-1 at 176.5 ppm, C-2 at 55.4 ppm, C-3 at 27.3 ppm, C-4 at 22.5 ppm, C-5 at 30.8 ppm, and C-6 at 40.1 ppm. Figure 3.5 shows a ^{13}C-NMR spectrum obtained with 10 g/l [U-^{13}C]lysine·HCl. Each peak consists of a multiplet due to ^{13}C-^{13}C coupling between adjacent carbon atoms: a doublet at C-1, a quartet at C-2, a triplet at C-3, a triplet at C-4, a triplet at C-5, and a doublet at C-6. From the multiplet structure of peaks, the ^{13}C-^{13}C spin coupling constants can be calculated: $J_{1-2} = 0.558$ ppm, $J_{2-3} = 0.3855$ ppm, $J_{3-4} = 0.374$ ppm, $J_{4-5} = 0.382$ ppm, and $J_{5-6} = 0.390$ ppm. The signal area was obtained by multiplying peak height by the width of the peak at half height. ^{13}C enrichments at each carbon position were calculated according to the following equation:

$$^{13}\text{C enrichment at position i} = \left(\frac{A_S^i}{C_S}\right) \Big/ \left(\frac{A_C^i}{C_C}\right) \qquad \textbf{(Eq. 3.4)}$$

where the A^i's are the integrated areas of sample (S) and calibration (C) at the carbon position i and the C's are the corresponding concentration.

3.8 Gas-Chromatography Mass-Spectrometry

To determine the distribution of lysine isotopomers following the ^{13}C labeling studies, 100 µl filtered supernatants from shake flasks were sent to Metabolic Solutions, Inc. (Merrimack, NH) for the analysis by gas chromatography-mass spectrometry (GC-MS). GC-MS was performed on a Hewlett Packard 5971 GC/MS. The mass spectrometer was operated under the chemical ionization mode (CI) with methane as reactant gas. The dry samples were derivatized to *N,O*-trifluroacetyl[^{13}C]lysine-n-methylester following the method of Inbar and Lapidot [1987]. The derivatized lysine samples were injected into a 30 m x 0.25mm column. The separation conditions were: injection mode splitless injection for 0.25 min, injection temperature 250°C, temperature program 50°C isothermal for 1

min, then 50-200°C at rate 15 °C/min. Ions of m/e of 353 to 359 corresponding to lysine with zero to six atoms of ^{13}C were monitored and quantified in terms of molar fractions.

Figure 3.6 shows sample calibration data for quantitation of lysine isotopomers with this method. The method is not dependent on the concentration of samples and standard deviations at each peak is less than 5%. Isotopomer distributions due to natural abundance of ^{13}C (1.1%) and ^{15}N (0.37%) and impurity of labeling substrate (usually 98% pure) were corrected by using the algorithm described in the Appendix A of chapter 8 (8.10).

3.9 References

Birnboim, H.C., Doly, J. (1979). A rapid alkaline extraction procedure for screening recombinant plasmid DNA. *Nucleic Acids Res.* **7**: 1513-1523.

Bradford, M.M. (1976). A rapid and sensitive method for the quantification of microgram quantities of protein utilizing the principle of protein-dye binding. *Anal. Biochem.* **72**: 248-254.

Clarke, D.M., Bragg, P.D. (1986). Expression of the cloned subunits of *Escherichia coli* transhydrogenase from separate replicons. *FEBS Lett.* **200**: 23-26.

Cremer, J., Eggeling, L., Sahm, H. (1991). Control of the lysine biosynthesis sequence in *Corynebacterium glutamicum* as analyzed by overexpression of the individual corresponding genes. *App. Environ. Microbiol.* **57**: 1746-1752.

Davis, L.G., Dibner, M.D., Battey, J.F. (1986). *Basic Methods in Molecular Biology*, Elsevier Science Publishers, New York, NY.

Dixon, G.H., Kornberg, H.L. (1959). Assay methods for key enzymes of the glyoxylate cycle. *Biochem. J.* **72**: 3P.

Eikmanns, B.J., Follettie, M.T., Griot, M.U., Sinskey, A.J. (1989). The phosphoenolpyruvate carboxylase gene of *Corynebacterium glutamicum*: Molecular cloning, nucleotide sequence, and expression. *Mol. Gen. Genet.* **218**: 330-339.

Fellay, R., Frey, J., Krisch, H. (1987). Interposon mutagenesis of soil and water bacteria: a family of DNA fragments designed for in vitro insertional mutagenesis of gram-negative bacteria. *Gene* **52**: 147-154.

Follettie, M.T., Peoples, O.P., Agoropoulou, C., Sinskey, A.J. (1993). Gene structure and expression of the *Corynebacterium flavum* N-13 *ask asd* operon. *J. Bacteriol.* **175**: 4096-4103.

Gubler, M., Jetten, M., Lee, S.H., Sinskey, A.J. (1994b). Cloning of the pyruvate kinase gene (*pyk*) of *Corynebacterium glutamicum* and site-specific inactivation of *pyk* in a lysine producing *Corynebacterium lactofermentum* strain. *Appl. Microbiol. Biotechnol.* **60**: 2494-2500.

Hanahan, D. (1983). Studies on transformation of *Escherichia coli* with plasmids. *J. Mol. Biol.* **166**: 557-580.

Haynes, J.A., Britz, M.L. (1991). The effect of growth conditions of *Corynebacterium glutamicum* on the transformation frequency obtained by electroporation. *J. Gen. Microbiol.* **136**: 255-263.

Hudspeth, R.L., Grula, J.W. (1989). Structure and expression of the maize gene encoding the phosphoenolpyruvate carboxylase isozyme involved in C_4 photosynthesis. *Plant Mol. Biol.* **12**: 579-589.

Inbar, L., Lapidot, A. (1987). ^{13}C-NMR, ^{1}H-NMR and gas-chromatography mass-spectrometry studies of the biosynthesis of ^{13}C enriched L-lysine by *Brevibacterium flavum*. *Eur. J. Biochem.* **162**: 621-633.

Jones, B.N., Gilligan, J.P. (1983). *o*-Phthalaldehyde precolumn derivatization and reversed-phase high-performance liquid chromatography of polypeptide hydrolysates and physiological fluids. *J. Chromatogr.* **266**: 471-482.

Kinoshita, S., Udaka, S., Shimono, M. (1957). Studies on the amino acid fermentation. Part I. Production of L-glutamic acid by various microorganisms. *J. Gen. Appl. Microbiol.* **3**: 193-205.

Kiss, R.D., Stephanopoulos, G. (1992). Metabolic characterization of a L-lysine producing strain by continuous culture. *Biotechnol. Bioeng.* **39**: 565-584.

Lowry, O.H., Passonneau, J.V. (1972). *A Flexible System of Enzymatic Analysis*, Academic Press, New York, Ny.

Mandel, M., Higa, A. (1970). Calcium dependent bacteriophage DNA infection. *J. Mol. Biol.* **53**: 154.

Mori, M., Shiio, I. (1987). Pyruvate formation and sugar metabolism in an amino acid-producing bacterium, *Brevibacterium flavum*. *Agric. Biol. Chem.* **51**: 129-138.

Mountain, A., Mann, N.H., Munton, R.N., Baumberg, S. (1984). Cloning of a *Bacillus subtilis* restriction fragment complementing auxitropic mutants of eight *Escherichia coli* genes of arginine biosynthesis. *Mol. Gen. Genet.* **197**: 82-89.

Ozaki, H., Shiio, I. (1983). Production of lysine by pyruvate kinase mutants of *Brevibacterium flavum*. *Agric. Biol. Chem.* **47**: 1569-1576.

Phelps, D.C., Hatefi, Y. (1981). Inhibition of the mitochondrial nicotinamide nucleotide transhydrogenase by dicyclohexylcarbodiimide and diethylpyrocarbonate. *J. Biol. Chem.* **256**: 8217-8221.

Sambrook, J., Fritsch, E.F., Maniatis, T. (1989). *Molecular Cloning-A Laboratory Manual*, 2nd Ed. Cold Spring Harbor Laboratory Press, Cold Spring Harbor, N.Y.

Schafer, A., Kalinowski, J., Simon, R., Seep-Feldhaus, A.-H., Puhler, A. (1990). High-frequency conjugal plasmid transfer from gram-negative *Escherichia coli* to various gram-positive coryneform bacteria. *J. Bacteriol.* **172**: 1663-1666.

Siu, P.M.L., Wood, H.G., Stjernholm, R.L. (1961). *J. Biol. Chem.* **236**: PC21.

Tomioka, N., Shinozaki, K., Sugiura, M. (1981). Molecular cloning and characterization of ribosomal RNA genes from a blue-green alga, *Anacystis nidulans*. *Mol. Gen. Genet.* **184**: 359-363.

Tosaka, O., Morioka, H., Takinami, K. (1979). The role of biotin-dependent pyruvate carboxylase in L-lysine production. *Agric. Biol. Chem.* **43**: 1513-1519.

Vallino, J.J. (1991). *Identification of branch-point restrictions in microbial metabolism through metabolic flux analysis and local network perturbations*, Ph.D. thesis, Massachusetts Institute of Technology, Cambridge, MA.

von der Osten, C.H., Gioannetti, C., Sinskey, A.J. (1989). Design of a defined medium for growth of *Corynebacterium glutamicum* in which citrate facilitates iron uptake. *Biotechnol. Lett.* **11**: 11-16.

Wood, H.G., Jacobson, B., Gerwin, B.I., Northrop, D.B. Oxaloacetate transcarboxylase from *Propionibacterium*. 215-230.

Yoshihama, M., Higashiro, K., Rao, E.A., Akedo, M., Shanabruch, W.G., Follettie, M.T., Walker, G.C., Sinskey, A.J. (1985). Cloning vector system for *Corynebacterium glutamicum*. *J. Bacteriol.* **162**: 591-597.

Table 3.1 Strains used in this study. Abbreviations are: Rif, rifampicin; St, streptomycin; Sp, spectinomycin; Km, kanamycin; Ap, ampicillin; Cm, chloramphenicol; Tet, tetracycline; ATCC, American Type Culture Collection (Rockville, Md., USA).

Strain	Relevant Characteristics	Source or Reference
Escherichia coli		
S17-1	*thi, pro, hsdRM*$^+$, *recA*$^-$, *tra* from RP4-2 integrated in chromosome	Schäfer *et al.*, 1990
XH11	F$^-$ ΔMN42(*ppc- argECBH*), *rpoB*, *nalA*, λ^-, λ^s, *hsd R*$^-$	Mountain *et al.*, 1984
DH5α	*lacZDM15, hsdR*$^-$, *recA*$^-$	Hanahan, 1983
AB1450	*thi-1 ilvD16 argH1 metB1 hisG1 lac malA1 mtl-2 xyl-7 ara-13 gal-6 rpsL* tonA2 tsx-7 supE44 gltB13	Clarke and Bragg, 1986
AB1450 *pnt*::Tn5	AB1450 containing Tn5 in *pnt* locus (lacking transhydrogenase)	Clarke and Bragg, 1986
AB1450 *pnt*::Tn5 pDC11	AB1450 *pnt*::Tn5 harboring plasmid pDC11 encoding *thd* gene	Clarke and Bragg, 1986
C. glutamicum		
AS019	Spontaneous Rif^r derivative of ATCC 13059	Yoshihama *et al.*, 1985
ASM1	*ppc*$^-$ derivative of AS019, Cm^r	This work
21253	L-Lysine producing strain, *hom*$^-$, *leu*$^-$	ATCC
253SM1	*ppc*$^-$ derivative of ATCC 21253, Cm^r	This work
SM575	*pyk*$^-$ derivative of ATCC 21253, St^r/Sp^r	This work
SM607	*ppc*$^-$ *pyk*$^-$ derivative of ATCC 21253, Cm^r, St^r/Sp^r	This work
SM0301	Putative *ppc*$^-$ *pc*$^-$ derivative of 253SM1, Cm^r	This work
SM1001-4	*ppc*$^-$ *malsyn*$^-$ derivative of 253SM1, Cm^r, Km^r	This work
B. lactofermentum		
21799	L-Lysine producing strain, *leu,* AEC^r	ATCC
799SM1	*ppc*$^-$ derivative of ATCC 21799, Cm^r	This work
P. citronellolis		
13674	Wild type	ATCC

Table 3.2 Plasmids used in this study.

Plasmid	Relevant Characteristics	Source or Reference
pUC4-KIXX	pUC4 derivative, Ap^r, Km^r (*neo* from Tn5)	PL Pharmacia
pCM1	pBR322 derivative, Ap^r, promoterless Cm^r gene	PL Pharmacia
pTrc99a	Ap^r, *lacI*^{q}, *tac*	PL Pharmacia
pSUP301	pACYC177 derivative, *mob*, Ap^r, Km^r	Schäfer *et al.*, 1990
pHP45Ω	Ω interposon derivative, Ap^r, St^r/Sp^r	Fellay *et al.*, 1987
pαppc	pSR1 derivative, Km^r, *ppc* of *C. glutamicum* AS019	Eikmanns *et al.*, 1989
pMT1	*E. coli* (Ap^r)-*C. glutamicum* (Km^r) shuttle vector	Follettie *et al.*, 1993
pMF1014α	pSR1 derivative, Km^r	Follettie, 1989
pPEPC4	pBR322 derivative, Ap^r, Tet^r, *ppc* of *Zea mays*	Hudspeth and Grula, 1989
pCXZAna	pMT1 derivative, *fda::ppc* of *Anacystis nidulans*	Follettie (unpublished result)
pMG107	pMT1 derivative, *mob*	This work
pMG108	pMT1 derivative, Km^r, Ap^r, *lacI*^{q}, *tac*	Gubler (unpublished result)
pMG124	pSUP301 derivative, Km^r, 1.1 kb *pyk* fragment, *mob*	Gubler *et al.*, 1994
pMG110	pUC4 derivative, Ap^r, Cm^r gene under promoter control of Km^r from Tn5	This work
pSMD1	pSR1 derivative, Km^r, *ppc* inactivated by insertion of Cm^r cassette from pMG110	This work
pSME7	pSUP301 derivative, Km^r, *mob*, *ppc::cat* (Cm^r)	This work
pSMF10	pMG110 derivative, *tac::ppc* of *C. glutamicum*	This work
pSMG1	pTrc99a derivative, *trc::ppc* of *Z. mays*	This work
pSMH1	pMG110 derivative, *trc::ppc* of *Z. mays*	This work
pSML10	pMG124 derivative, St^r/Sp^r gene inserted within *pyk* fragment, *mob*	This work
pSL20	pSUP301 derivative, *mob*, *aceB* of *C. glutamicum* inactivated by insertion of Km^r gene	Lee (unpublished result)

Table 3.3 *Corynebacterium glutamicum* minimal media.

Component	Concentration in PMB2	Concentration in PMB
Portion A:		
D-Glucose		20 g/L
Citrate·Na_3·$2H_2O$		1.14 g/L
$CaCl_2$·$2H_2O$	55 mg/L	55 mg/L
$MgSO_4$·$7H_2O$	200 mg/L	200 mg/L
$FeSO_4$·$7H_2O$	20 mg/L	20 mg/L
NaCl	1 g/L	1 g/L
100x Mineral Salts	10 mL/L	10 mL/L
Gluconate·Na	10 g/L	
Pyruvate·Na	10 g/L	
Catecol*	2.2 mg/L	
$CaCO_3$	30 g/L	
Portion B:		
K_2HPO_4	8 g/L	8 g/L
KH_2PO_4	1 g/L	1 g/L
L-Threonine	150 mg/L	150 mg/L
L-Leucine	100 mg/L	100 mg/L
L-Methionine	40 mg/L	40 mg/L
Thiamine·HCl	1 mg/L	1 mg/L
Biotin	1 mg/L	1 mg/L
Portion C:		
$(NH_4)_2SO_4$	5 g/L	5 g/L
100x Mineral Salts:		
$MnSO_4$		200 mg/L
$Na_2B_4O_7$·$10H_2O$		20 mg/L
$(NH_4)_6Mo_7O_{24}$·$4H_2O$		10 mg/L
$FeCl_3$·$6H_2O$		200 mg/L
$ZnSO_4$·$7H_2O$		50 mg/L
$CuCl_2$·$2H_2O$		20 mg/L
Adjust pH to 2 with HCl		

*Catecol in PMB2 is added separately after filter sterilization using a 0.22 μm Millex®-GV filter unit (Millipore, Bedford, MA).

Table 3.4 Medium FM4 for a 10-L batch fermentation.

Component	Amount
Portion A:	
D-Glucose	1500 g
Citrate·Na_3·$2H_2O$	1 g
$CaCl_2$·$2H_2O$	20 g
$MgSO_4$·$7H_2O$	6 g
$FeSO_4$·$7H_2O$	500 mg
NaCl	20 g
100x Mineral Salts	200 mL
poly(propylene glycol) MW 2000	10 mL
Volume	7 L
Portion B:	
K_2HPO_4	40 g
KH_2PO_4	20 g
L-Threonine	7.33 g
L-Leucine	15 g
L-Methionine	6 g
Thiamine·HCl	20 mg
Biotin	10 mg
$(NH_4)_2SO_4$	400 g
Volume	2 L
100x Mineral Salts:	
$MnSO_4$	200 mg/L
$Na_2B_4O_7$·$10H_2O$	20 mg/L
$(NH_4)_6Mo_7O_{24}$·$4H_2O$	10 mg/L
$FeCl_3$·$6H_2O$	200 mg/L
$ZnSO_4$·$7H_2O$	50 mg/L
$CuCl_2$·$2H_2O$	20 mg/L
Adjust pH to 2 with HCl	

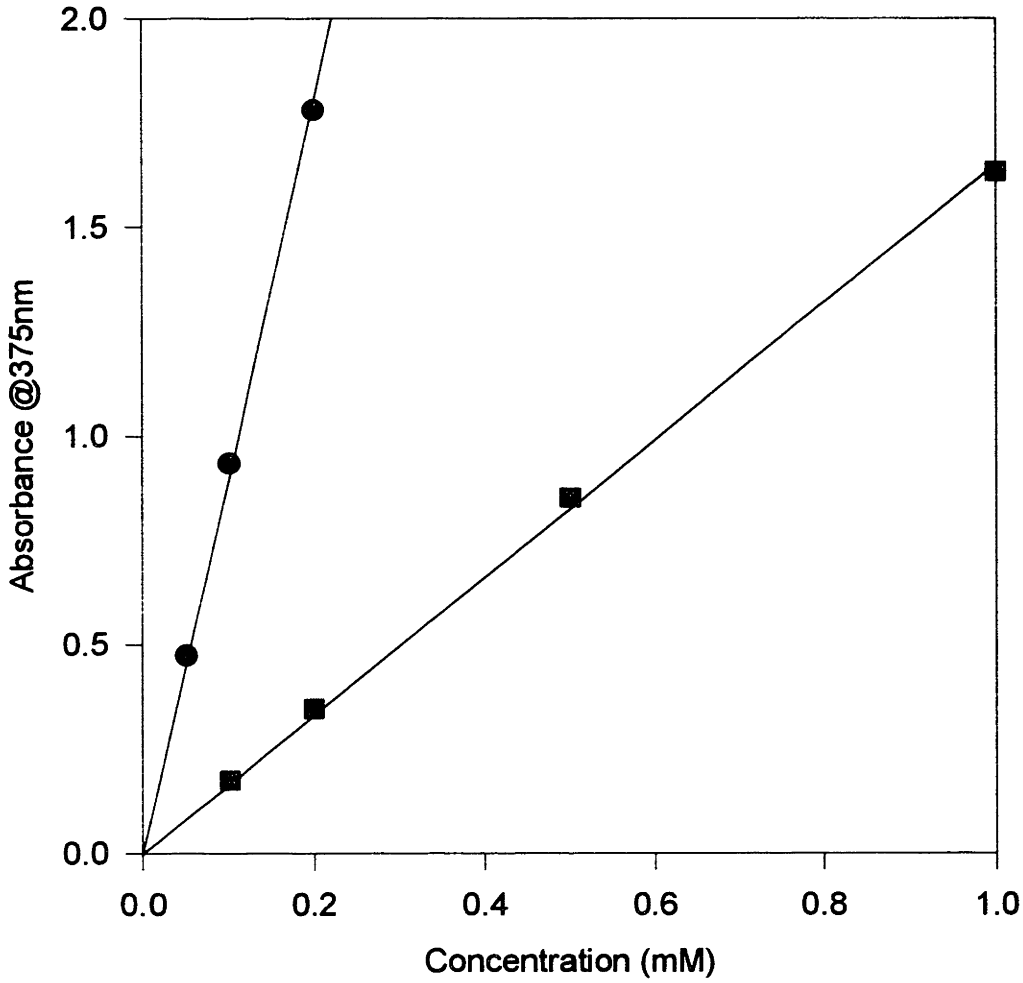

Figure 3.1 Determination of extinction coefficients for AcPyADH and NADPH at 375 nm in a volume of 1 ml: ▲, AcPyADH (ε = 9.02 $mM^{-1}cm^{-1}$); ■, NADPH (ε = 1.65 $mM^{-1}cm^{-1}$). Extinction coefficient (ε) is given by the following relationship: $\varepsilon = \frac{A}{LC}$ where A is the absorbance, L is the cuvette path length (1 cm), and C is the concentration of nucleotide (mM).

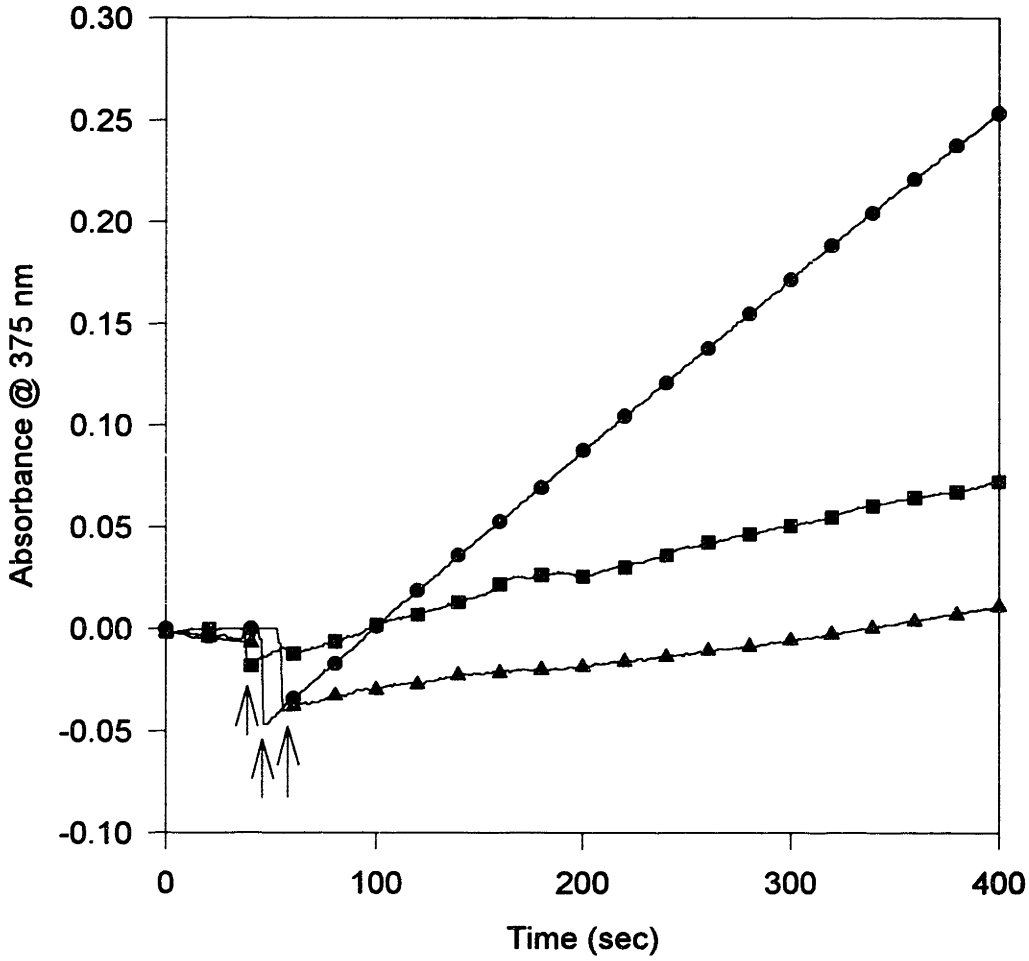

Figure 3.2 Reduction of $AcPyAD^+$ by NADPH via activity of transhydrogenase (THD) by three *E. coli* strains in a reaction volume of 1 ml (see Section 3.5.2.10): ▲, 344 µg of cell-free extract of AB1450 *pnt*::Tn5 (THD deficient); ■, 21 µg of cell-free extract of AB1450 (normal THD expressor); ●, 26 µg of cell-free extract of AB1450 *pnt*::Tn5 pDC11 (THD overexpressor). After monitoring the reaction without $AcPyAD^+$ at 375nm for 60 to 120 sec, 100 µl of 10 mM $AcPyAD^+$ were added as indicated by arrows. Note that 15 times more crude extract was added in the negative control, AB1450 *pnt*::Tn5 compared to the other two positive controls.

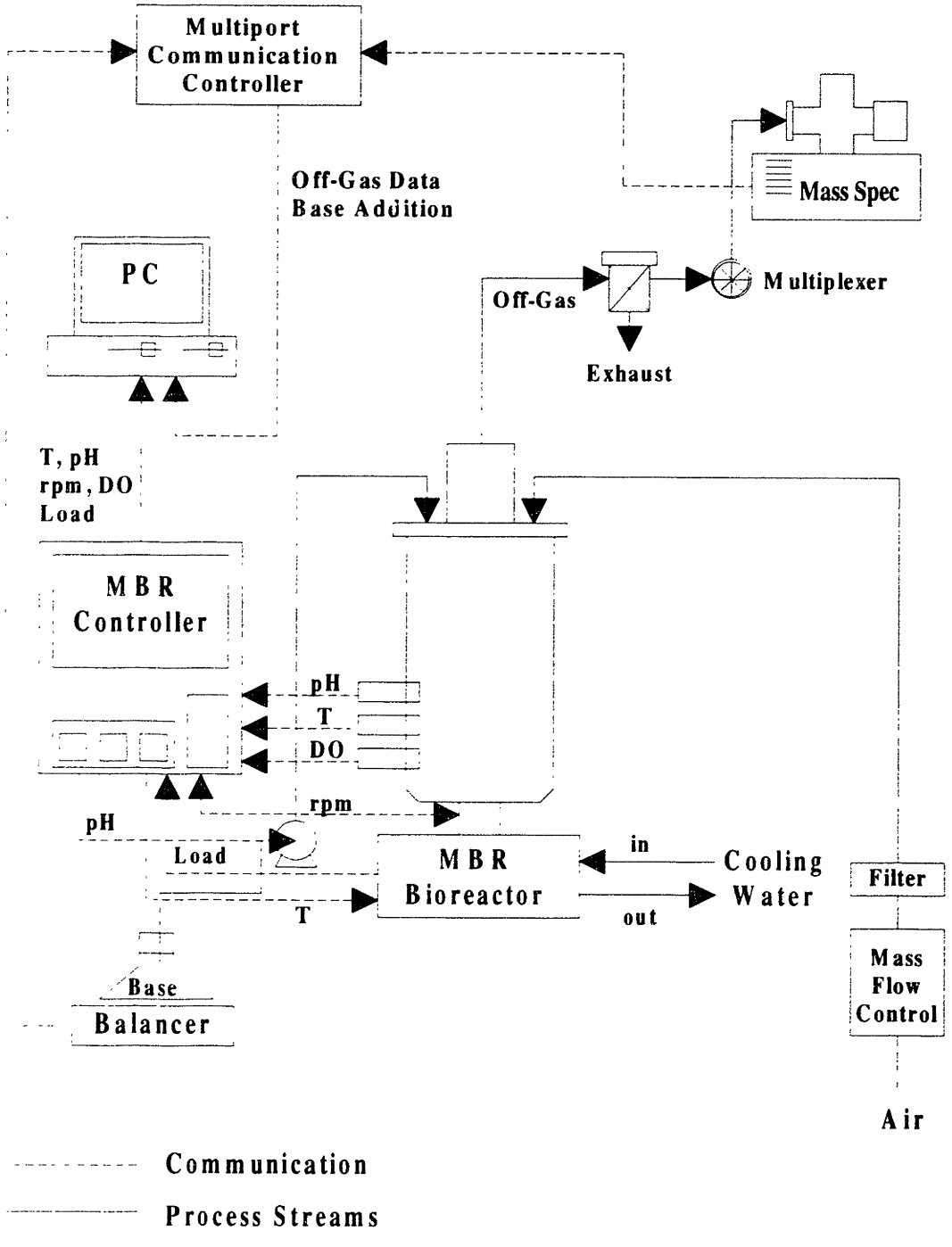

Figure 3.3 Schematic illustration of fermentation equipment and data acquisition.

Figure 3.4 Typical ^{13}C NMR spectrum with 60 g/l natural lysine.

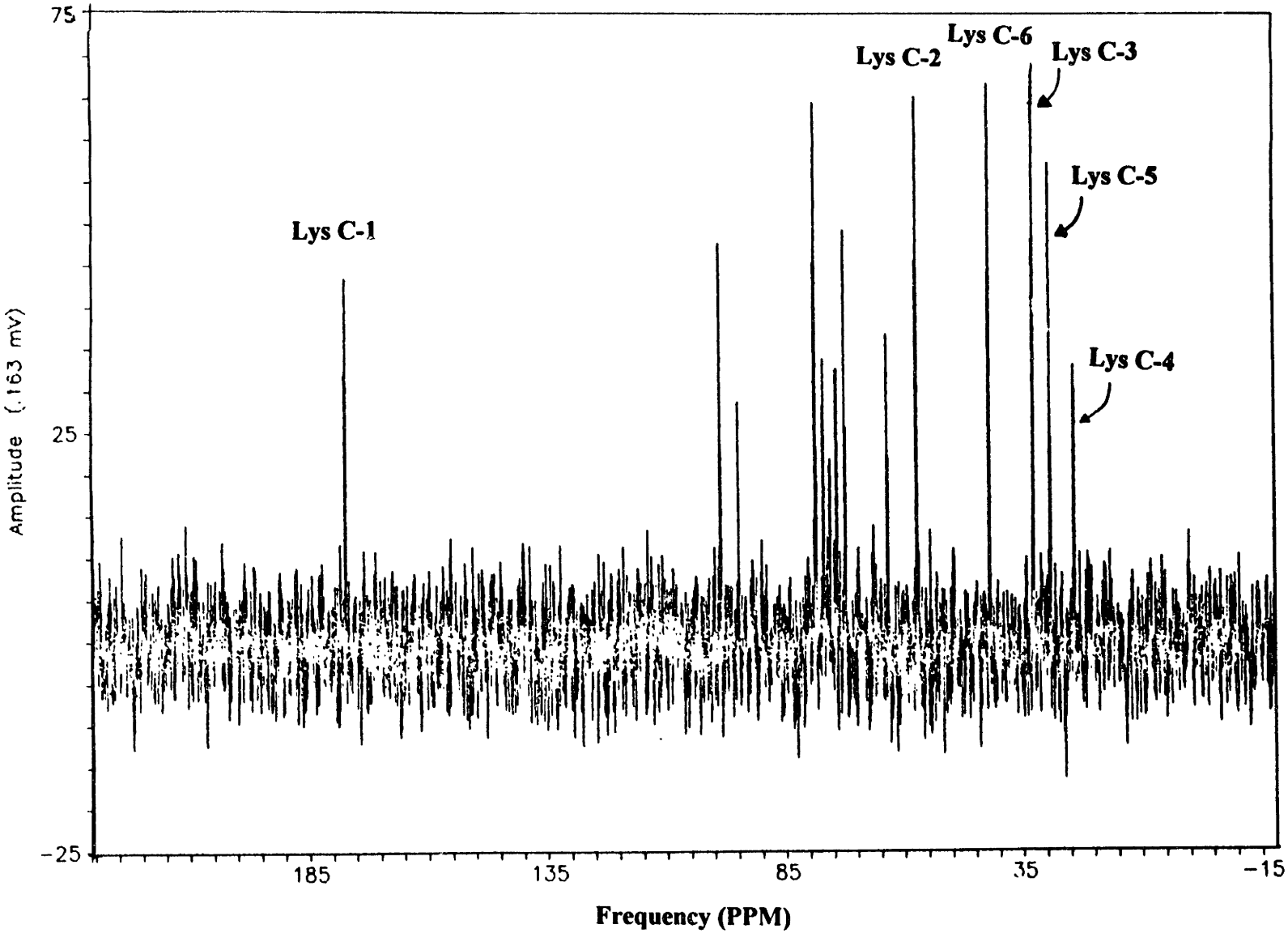

Figure 3.5 ^{13}C NMR spectrum with 10 g/l [U-^{13}C]lysine.

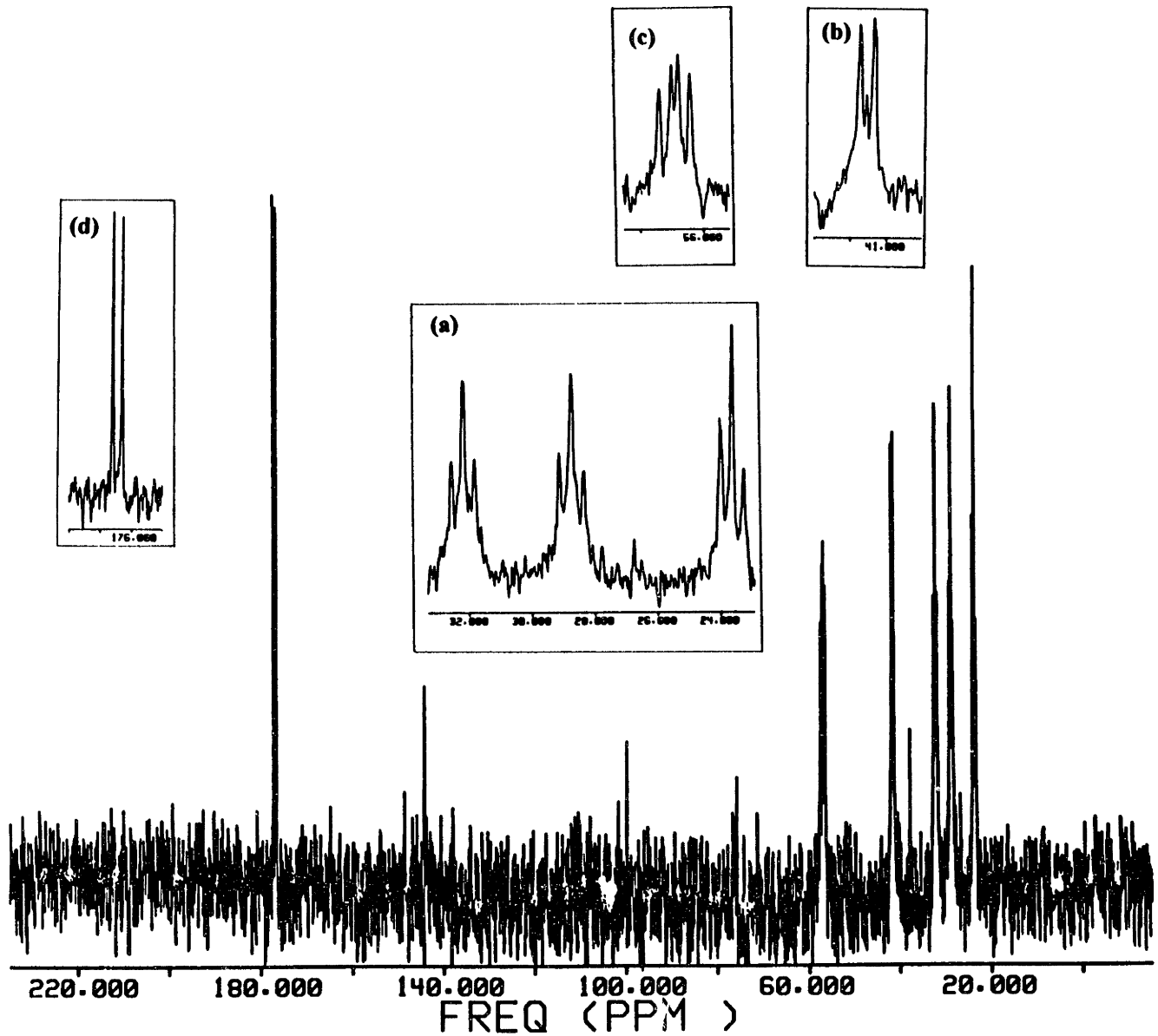

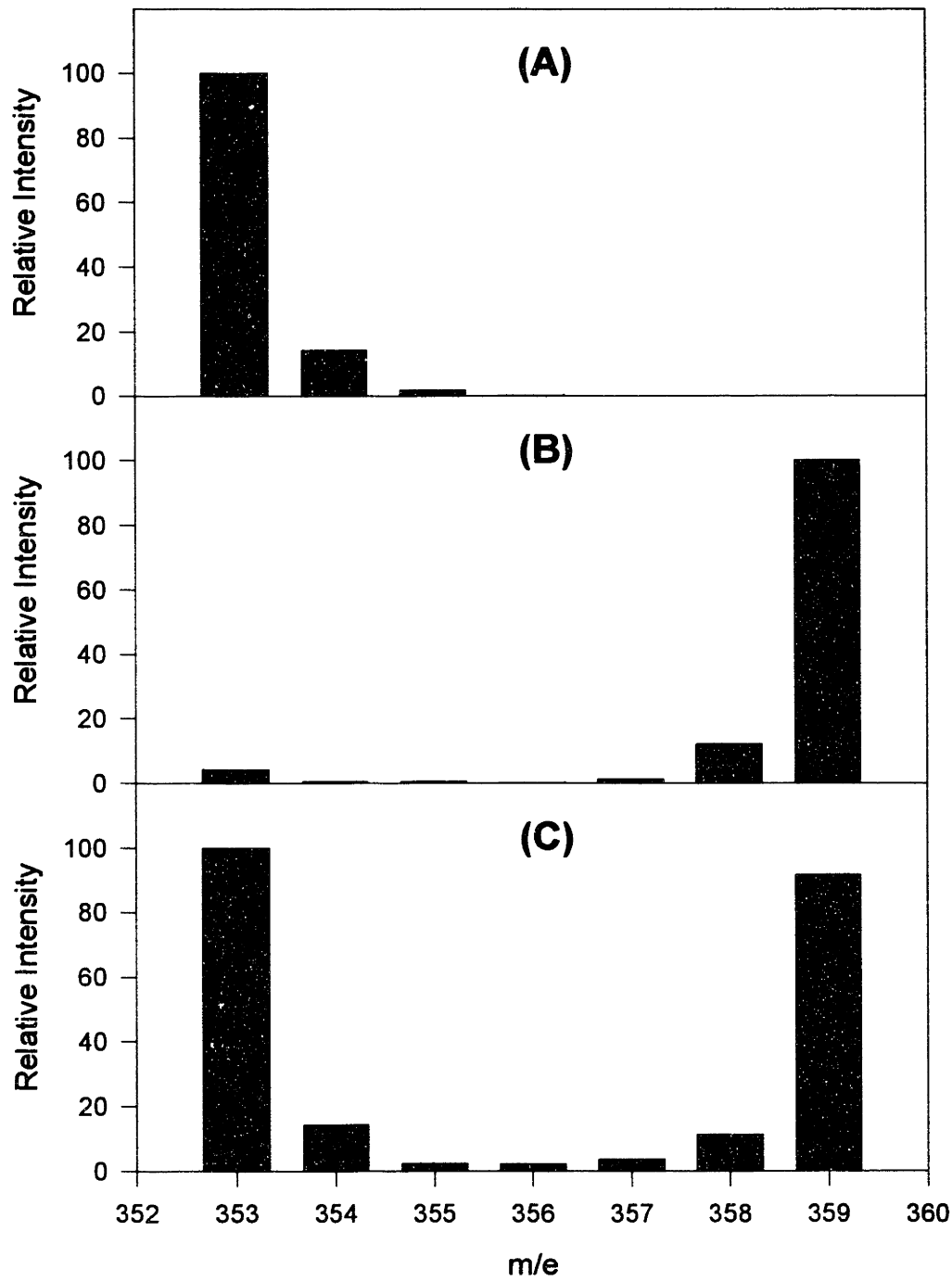

Figure 3.6 Chemical ionization mass spectra of *N,O*-trifluoroacetyl-[^{13}C]lysine-n-methyl-ester with standards: (A) natural abundance lysine; (B) [U-^{13}C]lysine; (C) 50:50 mixture of natural abundance lysine and [U-^{13}C]lysine. Ions of m/e from 353 to 359 were monitored and quantified in terms of relative peak heights.

Chapter 4: Conjugal Plasmid Transfer and Construction of Mutants

4.1 Development of Conjugal Plasmid Transfer

Figure 4.1 shows the principle of vector transfer from gram-negative *Escherichia coli* into gram-positive bacterial recipients. Two things are critical for efficient vector mobilization: (1) the mobilizing donor strains, and (2) vector plasmids capable of being mobilized by the donor strains into recipient strains. Typically, the donor *E. coli* carries the transfer functions RP4 which are used to build the conjugation bridges to allow the transfer of plasmid into the recipient strains. The useful *E. coli* donor strain is S17-1 which is a *rec*A-deficient derivative of E. coli 294 (*thi*, *pro*, *hsd*R$^-$) [Simon *et al.*, 1986].

The vectors that are mobilized by S17-1 usually contain the genetic locus, the *mob* site, that are recognized by the RP4 functions. The exact physical mechanism of vector plasmid transfer is not established yet. Transconjugation of vector plasmid from *E. coli* to several bacterial recipients such as *Rhizobium leguminosarum*, *R. meliloti*, *R. trifolii*, *R. phaseoli*, *Agrobacterium tumefaciens*, *Alcaligenes eutrophus* and *Rhodopseudomonas capsulata* have been reported [Simon *et al.*, 1983]. The possibility of transconjugation between *E. coli* and various gram-positive corynebacteria such as *Arthrobacter albidus*, *Brevibacterium divaricatum*, *B. lactofermentum*, *B. roseum*, *B. ammoniagenes*, *B. flavum*, *B. stationis*, *B. imperiale*, *B. linens*, *B. luteum*, *B. ketoglutamicum*, *B. pusillum*, *Corynebacterium callunae*, *C. glutamicum*, *C. herculis*, *C. acetoacidophilum*, *C. ilicis*, *C. lilium*, *C. pilosum*, *C. fascians*, *C. melassecola*, *C. flaccumfaciens*, *C. xerosis*, *Clavibacter michiganense* and *Clavibacter nebraskense* has been reported [Schäfer *et al.*, 1990].

Figure 4.2 illustrates the construction of mobilizable shuttle vector pMG107. Plasmid pMT1 is a *E. coli-C. glutamicum* shuttle vector based on *C. glutamicum* replicon pHM1519 [Follettie *et al.*, 1993]. It was digested by *Sca* I into two fragments. One 6.0 kb fragment contained the origin of replication and kanamycin (Km) resistance gene. Plasmid pSUP301 is an *E. coli* vector containing the RP4 mobilization fragment (*mob* site) of size 1.2 kb. pSUP301 was digested with *Bst* EII and *Sca* I, and blunt-ended by the

Klenow fragment of DNA Polymerase I. A 1.8 kb fragment was ligated to the 6.0 kb fragment of pMT1 to yield pMG107 which is a mobilizable vector that can replicate in both *E. coli* and *C. glutamicum*.

For efficient mobilization, the restriction system of the recipient cells needs to be deactivated temporarily. This is critical to provide sufficient time for the transferred vector DNA to be modified such that it can either replicate or integrate into the chromosome. This is usually achieved by heating the recipients prior to the mating. Figure 4.3 shows the effect of temperature on transconjugation efficiency on the three recipient strains with *E. coli* S17-1::pMG107 as the donor strain: *C. glutamicum* AS019, *C. glutamicum* ATCC 21253, and *B. lactofermentum* ATCC 21799. Transconjugants were identified by selecting strains resistant to nalidixic acid and kanamycin. Nalidixic acid selection is required to distinguish between the *E. coli* donor and the *Corynebacterium* recipients (all three recipients are naturally resistant to nalidixic acid). Kanamycin selection differentiates among the recipients with and without plasmid pMG107. The optimal temperature for the efficient blockage of restriction system was 50°C with a frequency of 7×10^{-5} in *C. glutamicum* 21253, 1.2×10^{-3} in *C. glutamicum* AS019 and 5.7×10^{-3} in *B. lactofermentum*. Heat treatment below 50°C led to lower frequencies, probably due to the recipient's active restriction system, whereas heat treatment above 50°C is lower, probably due to lower viability. Transconjugation frequencies are calculated as the ratio of the final number of transconjugants per initial number of recipient cells before mating.

4.2 Construction of PPC-Deficient Mutants

The use of the mobilizable *E. coli* vector system was investigated as a mutagenic agent similar to transposon mutagenesis used in many other systems. Clearly, transposon mutagenesis has many advantages over classical mutagenesis based on mutagens [Simon *et al.*, 1986]: (1) Insertion of a transposon into a gene leads to complete loss of its functions. (2) A specific phenotype can be easily identifiable, reducing the number of cells to screen. (3) The antibiotic marker carried by the transposon allows the specific physical location of the disrupted gene. The idea is based on the homologous recombination between the gene

on the vector plasmid and the gene in the chromosome. It is critical that the mobilizing plasmid for this purpose does not replicate in the recipient cells so that only those transconjugants that have integrated the plasmid can be identified by the resistance to the antibiotic marker on the mobilizing plasmid. *C. glutamicum* mutants deficient in *ppc* or *pyk* gene were constructed based on this technique as stated in Chapter 1.

Figure 4.4 shows the construction of a mobilizable plasmid pSME7 used in the disruption of the *ppc* gene for the three recipient strains. A promoterless chloramphenicol acetyl transferase (Cm; *cat*) gene from Tn9 in plasmid pCM1 was excised as a 0.8-kb *Sal*I fragment and was inserted between *Bgl*II and *Sal*I sites of pUC4-KIXX to fuse it to the neomycin/kanamycin resistance gene (*neo*). The junction between *Bgl*II and *Sal*I sites were established by filling in the 5' protruding ends at the *Bgl*II site with DNA polymerase I (Klenow) and dGTP and dATP. The remaining open gap of two nucleotides were allowed to be repaired *in vivo* after ligation and transformation. This resulted in transcriptional fusion of the *cat* gene to the *neo* promoter from Tn5 (pMG110). Fusions to this promoter have been shown to lead to efficient gene expression in *Corynebacterium* [Jäger *et al.*, 1992].

The *cat* cartridge was then used to substitute for a central 0.6-kb DNA fragment of the cloned *C. glutamicum ppc* gene in plasmid pαppc. The *cat* cartridge from plasmid pMG110 was cut as a 1.1-kb *Xho*I-*Sal*I fragment and replaced a 0.6-kb *ppc* internal fragment in pαppc after partial cleavage with *Xho*I. The disrupted *ppc* gene was then transferred as a 3.8-kb *Sal*I fragment from plasmid pSMD1 to the mobilizable plasmid pSUP301. The fragment was inserted into the *Sca*I site of pSUP301 after the addition of *Sal*I linkers, which resulted in the final plasmid pSME7.

Plasmid pSME7 carries a nonfunctional *C. glutamicum ppc* gene and can be mobilized *from E. coli* S17-1 to various *Corynebacterium* strains. Three recipient strains were again used to construct *ppc* mutants via transconjugation. In theory, there exists two possibilities for recombination (Figure 4.5). A single cross-over would result in the integration of the whole vector into the genome whereas a double cross-over would result in the exchange at the homologous regions. These two possibilities can be distinguished by the antibiotic markers on the mobilizable plasmid pSME7. Genotype from the single

cross-over would be Cm^r Km^r ppc^+ whereas genotype from the double cross-over would be Cm^r Km^s ppc^-. Therefore, the selection based on the resistance against kanamycin allows distinction between the single cross-over and double cross-over transconjugants. Three *ppc* mutants ASM1, 253SM1 and 799SM1 were derived from AS019, 21253 and 21799, respectively and assayed for the enzymatic activities of PPC (Table 4.1).

The disruption of the *ppc* gene was also confirmed by Southern blot analysis (Figure 4.6) of genomic DNA from the mutant strains ASM1, 253SM1 and 799SM1 as well as their corresponding parent strains. Genomic DNA were digested with *Sal*I, subjected to agarose gel electrophoresis, blotted onto a nitrocellulose filter and hybridized with a labeled *ppc*-specific DNA probe. Plasmid pαppc and pSMD1 were also cleaved with *Sal*I and used as a control for non-disrupted *ppc* of 3.3 kb in length and for disrupted *ppc* of 3.8 kb in length, respectively. This indicates that the *ppc* genes were disrupted by the insertion of the *cat* gene. Furthermore, the Southern blot analysis demonstrates the close relationship between *C. glutamicum* and *B. lactofermentum* since there is no polymorphism in the *Sal*I restriction pattern of the *ppc* loci of these two strains.

4.3 Construction of PK-Deficient Mutants

C. glutamicum pyk mutants were constructed in a similar procedure to the *ppc* mutants construction. In order to construct *pyk* mutants, the mobilizable plasmid pSML10 was constructed (Figure 4.7). Plasmid pMG124 is a mobilization plasmid containing a partial *pyk* gene, the *mob* site and kanamycin resistance gene [Gubler *et al.*, 1994]. However, only single cross-over mutants can be constructed with this plasmid which may cause long-term stability problems because the homologous *pyk* gene fragment in the chromosome may recombine to excise the integrated plasmid and resulted in reversion to the pyk^+ genotype (Figure 4.8). The plasmid pSML10 was constructed to make stable *pyk* mutants based on the double cross-over recombination. The entire fragment of pMG124 was partially digested with *Hind*III and ligated to a 2-kb fragment containing a streptomycin/spectinomycin resistance gene isolated from pHP45Ω digested with *Hind*III.

C. glutamicum ATCC 21253 and 253SM1 were transconjugated with the *E. coli* S17-1::pSML10. Double cross-over mutants were identified by selection based on the resistance to streptomycin/spectinomycin and the sensitivity to kanamycin. SM575 and SM607 were constructed from 21253 and 253SM1, respectively, yielding the genotype *pyk*⁻ and *ppc*⁻ *pyk*⁻. The ratio of double cross-over to single cross-over transconjugants was about 1:50. SM575 and SM607 were first tested for the enzyme activities of PK which showed negligible levels (Table 4.1) and for the growth on the selective minimal media plates containing either glucose, gluconate or ribose as sole carbon source. Both *pyk* mutants grew well in the glucose medium because of the operation of the PEP:PTS system which compensates the lack of PK. However, in both gluconate and ribose which are imported via the kinase system, the *pyk* mutants did not grow well, supporting that PK is indeed disrupted.

4.4 Construction of Putative PPC PC-Deficient Mutant

A mutant deficient in the anaplerotic sequence of OAA synthesis was isolated via random mutagenesis with NTG. This mutant is of particular interest because it can be used as a host in the complementation strategy of cloning the PPC-compensating enzyme in *C. glutamicum*. The selection of mutants via random mutagenesis is especially problematic if there are multiple enzymes or isozymes that lead to the synthesis of same metabolite. Furthermore, in the case of *C. glutamicum*, the PPC-compensating enzyme has not been characterized which makes the isolation of the mutants difficult.

For the sake of simplicity, in this section it will be assumed that the unknown enzyme is pyruvate carboxylase (PC). The selection strategy is as follows. First, 253SM1 which is deficient in PPC was treated with NTG. Treated cells were first plated on a glucose minimal media plate and then replicated on the glucose plus citrate plates. Out of about 2,000 clones tested, only seven strains were able to grow on the glucose plus citrate plates. This selection step ensures that only the mutants that are unable to synthesize citrate are screened. Only very few mutations such as pyruvate dehydrogenase, citrate synthase and PC can lead to this phenotype. These seven auxotrophs were then transformed with plasmid pαppc and checked for growth on the glucose minimal media

plates. Only one (SM0301:: pαppc) had the phenotype glucose$^+$. The strain SM0301 is probably deficient in both PPC and PC enzymes. The other six clones were probably deficient in other enzymes such that the restoration of PPC did not make a difference.

4.5 References

Follettie, M.T., Peoples, O.P., Agoropoulou, C., Sinskey, A.J. (1993). Gene structure and expression of the *Corynebacterium flavum* N-13 *ask asd* operon. *J. Bacteriol.* **175**: 4096-4103.

Gubler, M., Jetten, M., Lee, S.H., Sinskey, A.J. (1994). Cloning of the pyruvate kinase gene (*pyk*) of *Corynebacterium glutamicum* and site-specific inactivation of *pyk* in a lysine producing *Corynebacterium lactofermentum* strain. *Appl. Microbiol. Biotechnol.* **60**: 2494-2500.

Jager, W., Schäfer, A., Pühler, A., Labes, G., Wohleben, W. (1992). Expression of the *Bacillus subtilis sac*B gene leads to sucrose sensitivity in the Gram-positive bacterium *Corynebacterium glutamicum* but not in *Streptomyces lividans*. *J. Bacteriol.* **174**: 5462-5465.

Schäfer, A., Kalinowski, J., Simon, R., Seep-Feldhaus, A.-H., Pühler, A. (1990). High-frequency conjugal plasmid transfer from gram-negative *Escherichia coli* to various gram-positive coryneform bacteria. *J. Bacteriol.* **172**: 1663-1666.

Simon, R., O'Connell, M., Labes, M., Pühler, A. (1986). Plasmid vectors for the genetic analysis and manipulation of Rhizobia and other gram-negative bacteria. *Methods Enzymol.* **118**: 640.

Simon, R., Priefer, U., Puhler, A. (1983). A broad host range mobilization system for in vivo genetic engineering: transposon mutagenesis in gram negative bacteria. *Bio/Technol.* 784-791.

Table 4.1 Enzyme activities of PPC and PK and growth on various carbon sources for various *C. glutamicum* and *B. lactofermentum* strains. Abbreviations: PPC (*ppc* gene), phosphoenolpyruvate carboxylase; PK (*pyk* gene), pyruvate kinase; wt, wild type; +, growth; +/-, weak growth; -, no growth; ND, not detected. Enzyme activities are given in nmol/min per mg protein. Blank spaces indicate no experiments.

Strain	Genotype	Enzyme Activities		Cell Growth on		
		PPC	PK	Glucose	Gluconate	Ribose
AS019	wt	196		+		
ASM1	*ppc*⁻	ND		+		
21253	wt	344	822	+	+	+
253SM1	*ppc*⁻	ND	677	+	+	+
21799	wt	155		+		
799SM1	*ppc*⁻	ND		+		
SM575	*pyk*⁻	279	ND	+	+/-	-
SM607	*ppc*⁻ *pyk*⁻	ND	ND	+	+/-	-

Figure 4.1 Principle of plasmid mobilization. The transfer functions encoded by the Tra genes of the integrated RP4 derivative in the mobilizing *Escherichia coli* donor strain recognize the mob site and perform the conjugative transfer of the vector into a recipient strain.

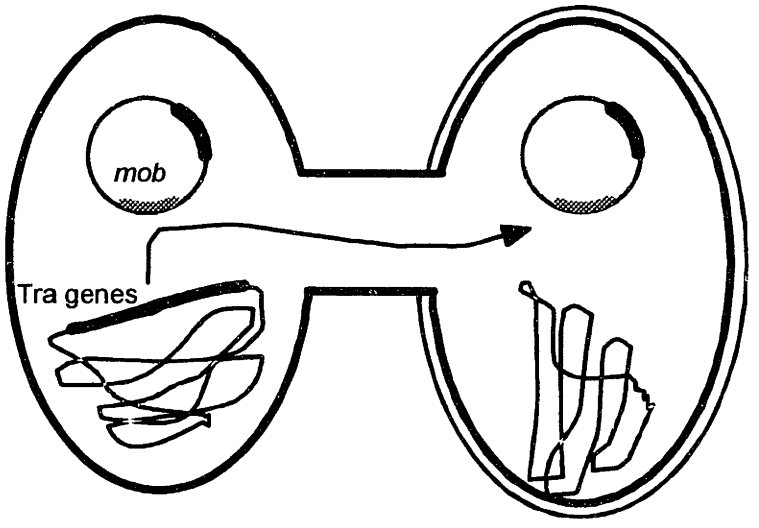

E. coli
Donor Strain

Gram-positive
Recipient Strain

Figure 4.2 Construction of mobilizable shuttle vector pMG107. Abbreviations: Sc, *Sca*I; Bs, *Bst*EII; kb, kilobases; Km, kanamycin resistance determinant; Ap, ampicillin resistance determinant; *mob*, RP4 mobilization fragment. Drawings are not to scale.

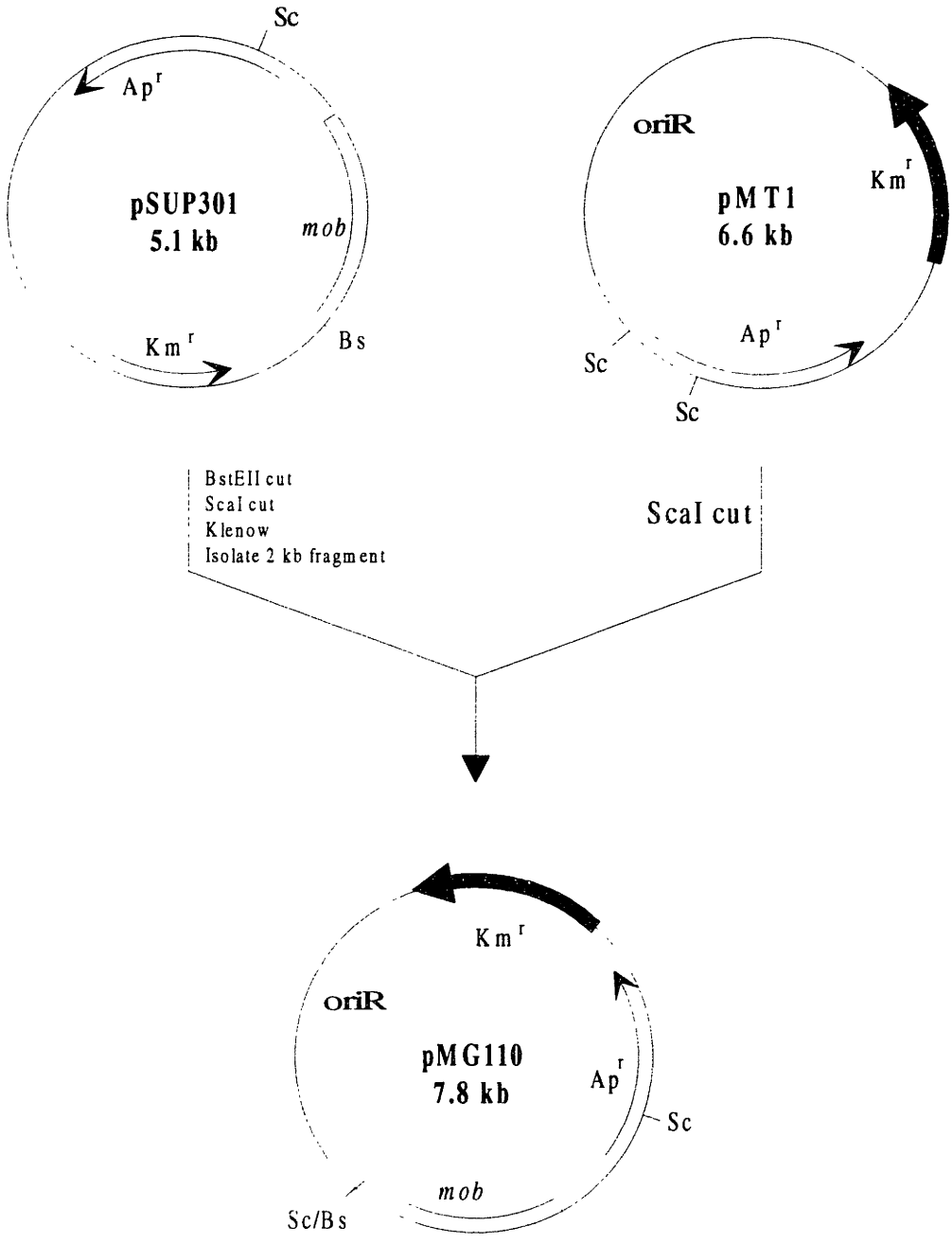

Figure 4.3 Effect of temperature on conjugal plasmid transfer frequency. Heat treatment of recipient *Corynebacterium* and *Brevibacterium* species was performed for 10 min at various temperatures before mating with the *E. coli* donor strain S17-1::pMG107. Top, *B. lactofermentum* ATCC 21799; middle, *C. glutamicum* ASO19; bottom, *C. glutamicum* ATCC 21253.

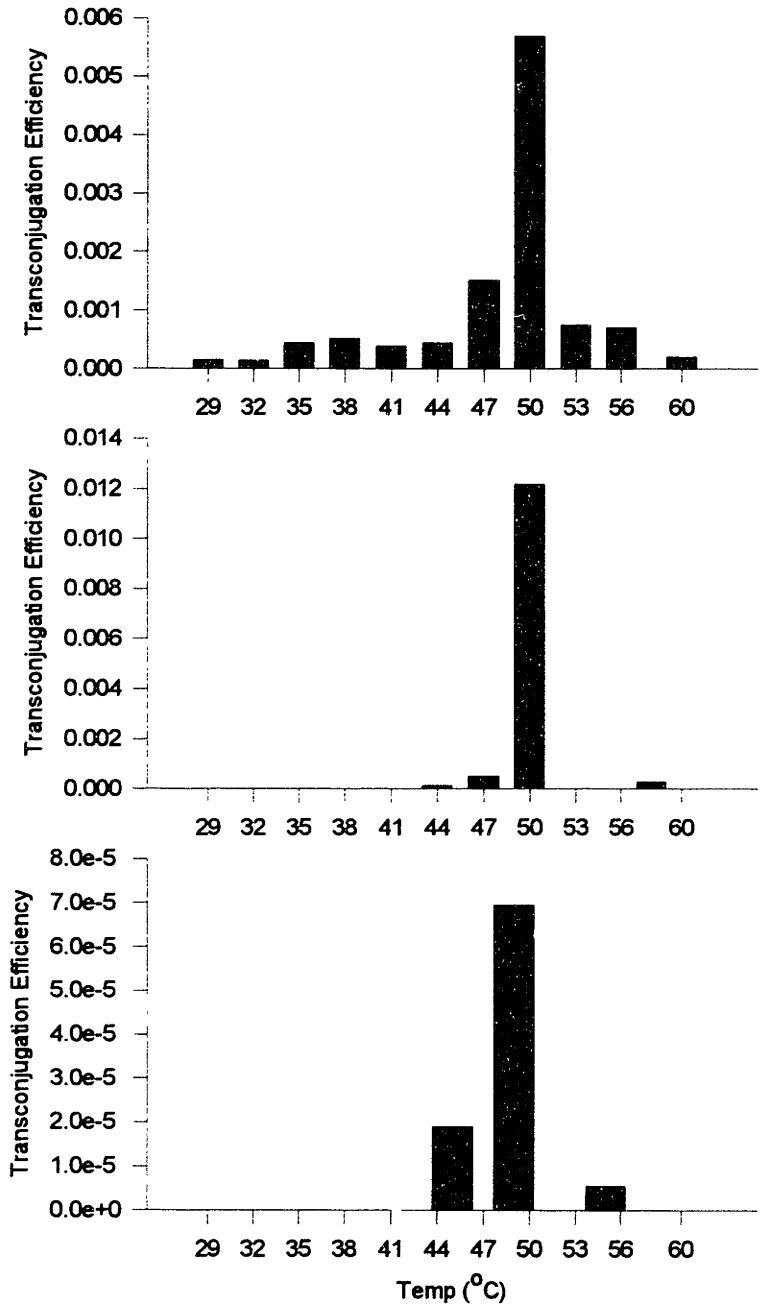

Figure 4.4 Construction of mobilizable vector pSME7 for marker exchange mutagenesis of phosphoenolpyruvate carboxylase (*ppc*) gene. Abbreviations: B, *Bgl*II; S, *Sal*I; X, *Xho*I; Sc, *Sca*I; Bs, *Bst*EII; *aph*, aminoglycoside phosphotransferase from Tn903 (kanamycin resistance determinant); *neo*, aminoglycoside phosphotransferase from Tn5 (kanamycin resistance determinant); *bla*, β-lactamase (ampicillin resistance determinant); *cat*, chloramphenicol acetyltransferase (chloramphenicol resistance determinant).

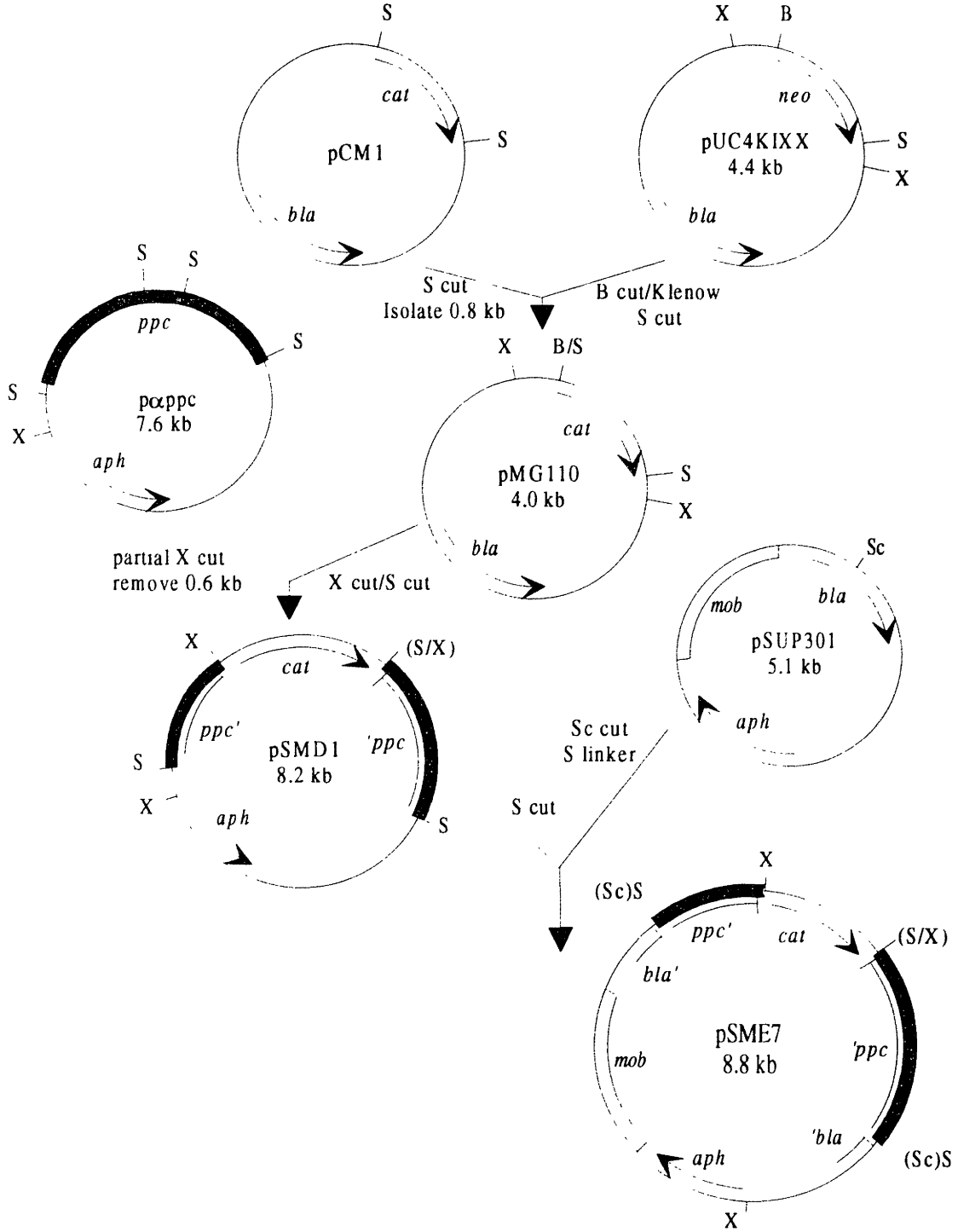

Figure 4.5 Schematic illustration of the recombination event leading to the disruption of *ppc* gene. A single cross-over between the plasmid and the genome results in integration of the entire plasmid and yields mutants which are resistant against kanamycin as well as chloramphenicol. A double cross-over generates mutants which are sensitive to kanamycin but resistant to chloramphenicol. Therefore, the two types of mutants can be differentiated based on resistance against kanamycin. Drawings are not to scale.

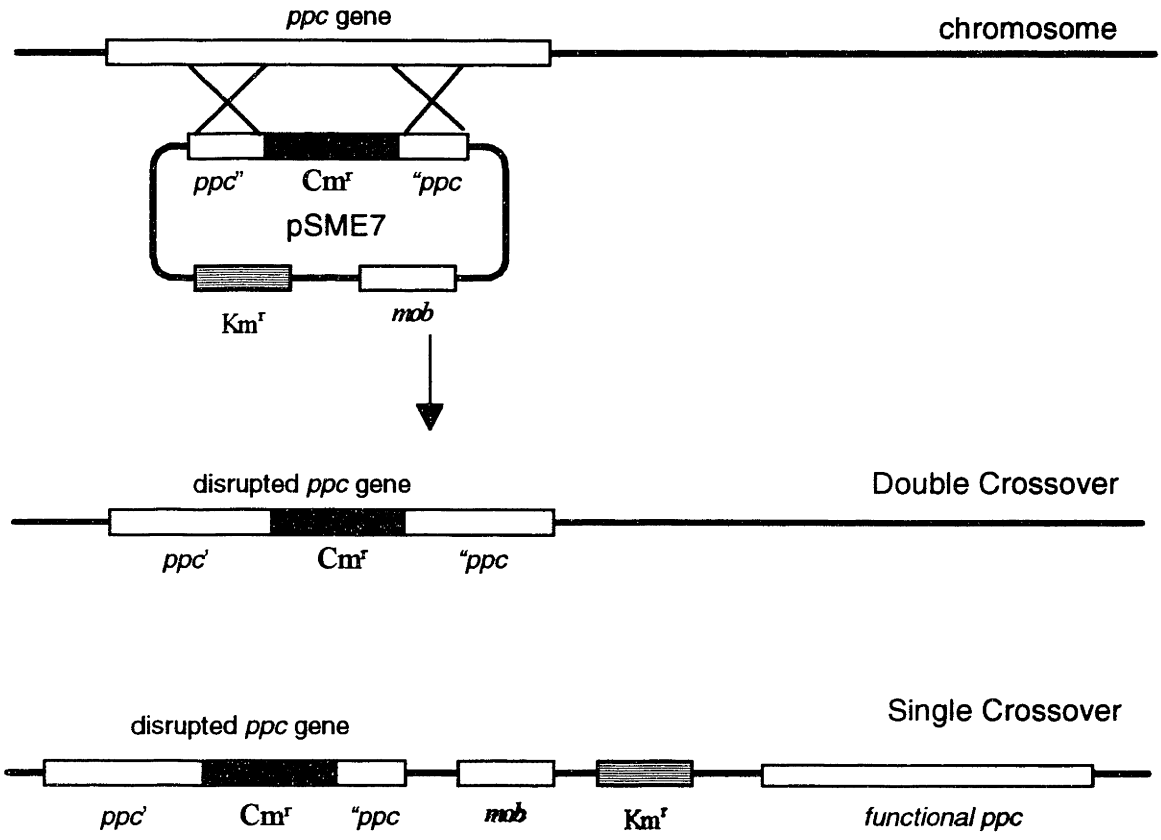

Figure 4.6 Southern blot analysis of the *ppc* mutants. Genomic DNA from the parental strains (ASO19, 21253 and 21799) and from the *ppc* mutants (ASM1, 253SM1 and 799SM1) were cleaved with *Sal*I, subjected to agarose gel electrophoresis, blotted onto a nitrocellulose filter and hybridized with a labeled *ppc*-specific DNA probe. Plasmid pαppc and pSMD1 were also cleaved with *Sal*I and used as a control for non-disrupted *ppc* of 3.3 kb in length and for disrupted *ppc* of 3.8 kb in length, respectively. As a size marker, *Hind*III digested λ DNA fragments are indicated on the left.

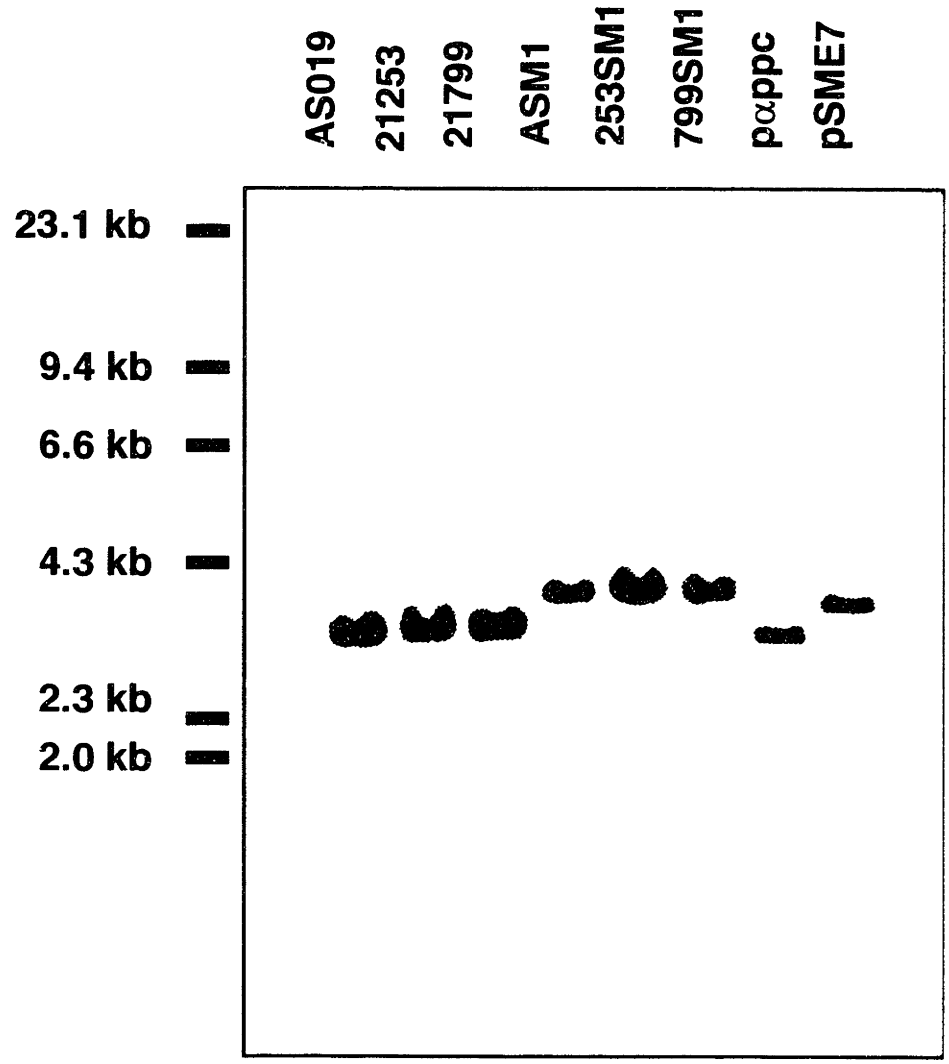

Figure 4.7 Construction of mobilizable vector pSML10 for marker exchange mutagenesis of *pyk* gene. Abbreviations: E, *Eco*RI; S, *Sal*I; X, *Xho*I; Bs, *Bss*HII; H, *Hind*III; B, *Bam*HI; Sm, *Sma*I; P, *Pst*I; *pyk*, pyruvate kinase gene; Km, kanamycin resistance determinant; St, streptomycin resistance determinant; Sp, spectinocymcin resistance determinant; Ap, ampicillin resistance determinant; *mob*, RP4 mobilization fragment. Drawings are not to scale.

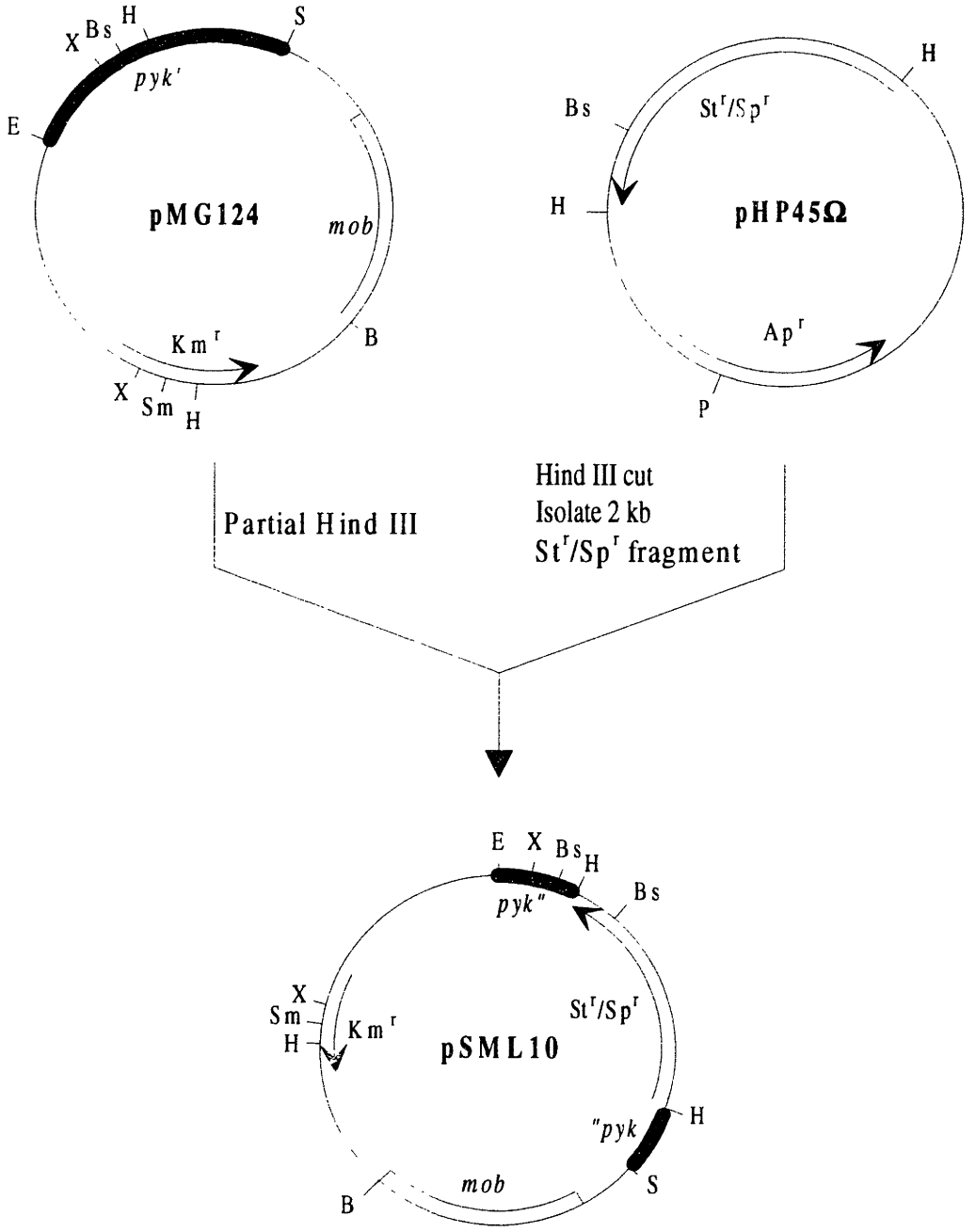

Figure 4.8 Schematic illustration of the recombination event leading to the disruption of *pyk* gene. A single cross-over between the plasmid and the genome results in integration of the entire plasmid and yields mutants which are resistant against kanamycin as well as spectinomycin and streptomycin. A double cross-over generates mutants which are sensitive to kanamycin but resistant to spectinomycin and streptomycin. Therefore, the two types of mutants can be differentiated based on resistance against kanamycin. Drawings are not to scale.

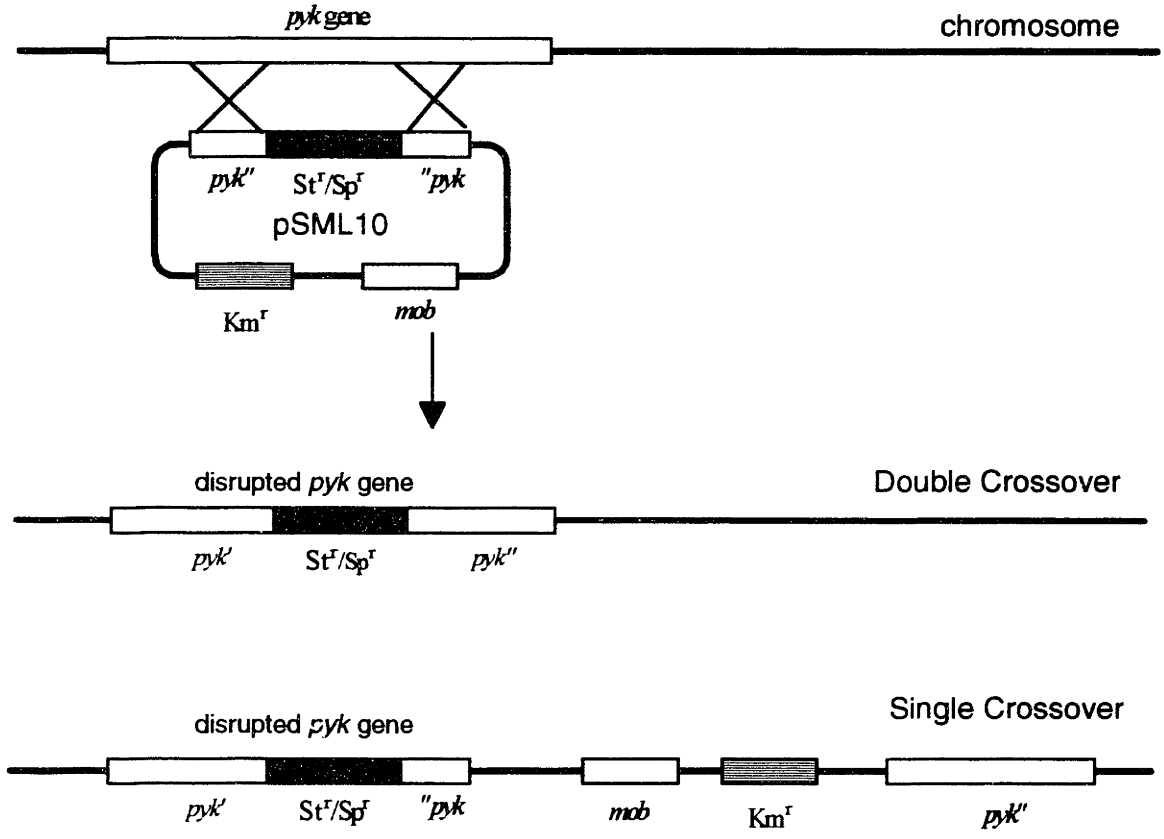

Chapter 5: Effect of The Tricarboxylic Acid Cycle on Metabolite Labeling. I. Theory

5.1 Summary

Proper analysis of label distributions in the intermediates of metabolic pathways is critical for correct interpretation of experimental and strategic experimental design. While, for example, ^{13}C nuclear magnetic resonance (NMR) spectroscopy is usually limited to the measurement of degrees of ^{13}C enrichment, significantly more information about metabolic fluxes can be extracted from the fine structure of NMR spectra or molecular weight distributions of isotopomers of metabolic intermediates (measured by gas chromatography-mass spectrometry). For this purpose, rigorous accounting for the contribution of all pathways to label distribution is required, especially contributions resulting from multiple turns of metabolic cycles. In this paper we present a mathematical model developed to analyze isotopomer distributions of tricarboxylic acid cycle (TCA) intermediates following the administration of ^{13}C (or ^{14}C) labeled substrates. The theory presented provides the basis to analyze ^{13}C NMR spectra and molecular weight distributions of metabolites. In a companion paper (Chapter 6) the theory is applied to the analysis of nine cases of biological significance.

5.2 Introduction

Applications of stable isotopes in metabolic research have increased in the past decade. Experiments with isotopically labeled substrates have provided a vast amount of information about complex metabolic networks. The following examples are just a few ways in which stable isotopes have been used in metabolic research. The stable isotope ^{13}C has been used as a tracer to determine substrate oxidation rates and to develop clinical tests for rapid discrimination of digestive and metabolic disorders in glycolytic and gluconeogenic pathways. Breath tests in which samples of exhaled air are collected and analyzed following oral and parenteral administration of ^{13}C or ^{14}C labeled substrate have proven effective for measuring glucose utilization [Lacroix *et al.*, 1973], fat absorption [Hofmann and Lauterburg, 1977; Watkins *et al.*, 1982; Turner *et al.*, 1987], for assessing

liver [Schneider *et al.*, 1982; Kurumaya *et al.*, 1988] and pancreatic function [Solomons *et al.*, 1977; Watkins *et al.*, 1977; Hiele *et al.*, 1989], and for diagnosing *Helicobacter pyrori* infection [Marshall and Surveyor, 1988; Graham *et al.*, 1988; Ormand *et al.*, 1990; Novis *et al.*, 1991] which is associated with gastric and peptic ulcer disease.

More recently, several other proposals have appeared in the literature for monitoring the metabolic intermediates excreted from the body or in the blood following the administration of labeled substrates in order to detect metabolic diseases. Kassel *et al.* [1989] proposed the measurement of [U-^{13}C]glucose conversion into other metabolites as a diagnostic tool of differentiating enzyme defects associated with congenital lactic acidosis. Kalderon *et al.* [1989a, 1989b] and Gopher *et al.* [1990] suggested the administration of labeled glucose or fructose followed by analysis of plasma glucose using a combination of gas chromatography mass spectrometry (GC-MS) and ^{13}C nuclear magnetic resonance spectroscopy (^{13}C NMR) as a simple noninvasive diagnostic for detecting glycolytic and gluconeogenic disease such as glycogen storage disease type I and type III, and fructose intolerance. Magnusson *et al.* [1991] proposed the use of [3-^{14}C]lactate in conjunction with phenylacetate as a means of following non-invasively the metabolism of the tricarboxylic acid (TCA) cycle in humans by analyzing the labeling pattern of phenylacetylglutamine in urine. Di Donato *et al.* [1993] modified the idea by administering [3-^{13}C]lactate followed by an analysis with GC-MS and ^{13}C NMR.

The "chemical biopsy" [Di Donato *et al.*, 1993] technique utilizing stable isotopic labeling has emerged as a safe, noninvasive diagnostic tool for tracing metabolic pathways as well as for detecting enzymatic disorders. Unfortunately, the lack of a rigorous mathematical method to calculate label distributions in metabolic networks has often necessitated the introduction of simplified reaction schematics yielding erroneous conclusions. The lack of appropriate analytical tools is especially problematic in the studies involving cyclic pathways such as the pentose phosphate pathway (PPP) and the TCA cycle where intermediates can reenter the cycle and produce different labeling patterns.

This paper is an attempt to properly account for all reactions involving the TCA cycle contributing to carbon isotope labeling. In an accompanying paper (Chapter 7), the

carbon label scrambling via the PPP will be presented. The objective of this paper is to present a general method for calculating isotopomer distributions and enrichment patterns in metabolic intermediates of the TCA cycle and glucose via the gluconeogenic pathway. In a companion paper (Chapter 6), the validity of our developed model is assessed by comparing theoretical predictions with experimental data reported in the literature. Furthermore, the types of error associated with improperly accounting for the label redistribution through multiple turns via the TCA cycle are fully discussed.

5.3 Previous Modeling Works

The first analysis of label distribution through the TCA cycle and gluconeogenesis was made by Weinman *et al.* [1957] who studied the conversion of fatty acids to carbohydrate. Using a convergent geometric series, they derived expressions for the distribution of label in individual carbons of glucose and CO_2 resulting from the use of labeled acetate as a function of the relative fluxes via citrate synthase and pyruvate carboxylase. Though correct, the algebra was tedious which makes the application to more complex systems extremely difficult. The idea was extended by Exton and Park [1962] who investigated the label distribution of pyruvate. A more convenient procedure was proposed by Katz and Grunnet [1979] who developed input-output equations for each carbon of intermediary metabolites and applied the methodology to the study of the PPP and TCA cycle intermediates. This method can be extended to other systems with many variables. However, all of these methods calculated only carbon isotope enrichments at specific carbon positions of the metabolites. As such, they did not provide information about isotopomers and the carbon label distribution within molecules of individual metabolites, and consequently failed to explain the multiplet structures observed in the ^{13}C NMR spectra and the molecular weight distribution of metabolites measured by GC-MS.

Chance *et al.* [1983] were the first to realize the importance of label scrambling via the TCA cycle and provided an elegant model for the evolution of ^{13}C enrichment of the TCA cycle intermediates. They developed a transient kinetic model for ^{13}C label enrichment by considering contributions from each isotopomer as distinct, individual

species. This approach requires intensive measurements of metabolite concentrations and kinetic variables which limits its applications to other systems This problem is minimized in the modeling scheme presented here which employs input-output balances for all biochemically feasible isotopomer species instead of individual carbons under the assumption of a metabolic and isotopic steady state. Not only the mathematics is greatly simplified by this method but also fewer measurements are required for obtaining the same type of information. Our work builds on that of Malloy *et al.* [1988] who employed a similar approach involving, however, *all* possible isotopomers. In addition, we provide useful extension of the modeling results that utilize the fine structure of NMR spectra and molecular weight distributions of selected isotopomers.

5.4 Description of Pathways

We will demonstrate our modeling approach in the context of the metabolic pathways associated with two types of gluconeogenic substrates: three-carbon (C_3) metabolites such as pyruvate and lactate and two-carbon (C_2) metabolites such as acetate and ethanol. Each of these substrates is metabolized via different pathways and depending on the extent of the pathway utilized, the resulting pattern of label distribution in the intermediates will be drastically different. Figure 5.1 shows the metabolic scheme of pyruvate utilization via the TCA cycle and gluconeogenic pathway commonly found in eukaryotic systems. We will assume that no phosphoenolpyruvate (PEP) is formed directly from pyruvate via PEP synthetase, but formed rather from oxaloacetate (OAA) via PEP carboxykinase. Pyruvate is converted to OAA by direct carboxylation or it can be converted to acetyl-CoA which then condenses with OAA to form citrate that traverses the TCA cycle and eventually regenerates OAA. Finally, glucose can be formed from PEP via the reverse Embden-Myerhof scheme of glycolysis or gluconeogenic pathway.

Figure 5.2 summarizes three possible models for acetate utilization. Model I shows the metabolic scheme of acetate utilization via the glyoxylate shunt (GS) pathway, active in many bacterial systems. The operation of this pathway is essential for growth on acetate as sole carbon source since it replenishes TCA cycle intermediates drained off for biosynthesis. Bacteria maintain a precise balance of carbon utilization for energetic and

biosynthetic requirements by controlling the carbon flow at the isocitrate branchpoint. Isocitrate, when catalyzed by the action of isocitrate dehydrogenase and subsequently by the enzymes of the TCA cycle, will lead to the production of NADH which is used for energy generation. Alternatively, isocitrate, by the action of isocitrate lyase, can be converted to succinate and glyoxylate, and glyoxylate condenses with acetyl-CoA to produce malate. Thus via the GS pathway, one molecule of OAA is formed from two molecules of acetate.

It has been established that in mammals acetate is utilized solely via oxidation to acetyl-CoA which subsequently passes through the TCA cycle [Figure 5.2, Model II]. However, in order to maintain a balanced steady state flow, a separate anaplerotic source for the synthesis of OAA must exist since some of the intermediates will be drained off the cycle to supply biosynthetic precursors such as glutamate and glutamine or glucose. We will consider two scenarios for the utilization of acetate: Model II is a generally accepted pathway that acetate is utilized only via acetyl-CoA conversion by the reaction of acetyl-CoA synthase. In this case, alternative metabolite sources exist that provide for OAA formation.

Model III is a hypothetical pathway in which OAA is derived directly from acetate. We will assume that lactate or pyruvate, which will eventually become the source for OAA, is derived from acetoacetate via decarboxylation. Acetoacetate in turn is derived from the condensation of two acetyl-CoA molecules. Therefore, OAA entering the TCA cycle will be always labeled if the input acetate is labeled. In fact, this hypothetical pathway is not entirely infeasible because there is evidence for the formation of 3-hydroxybutyrate from acetate in sheep [Annison *et al.*, 1963] and formation of labeled acetoacetate from labeled acetate in rat liver [Desmoulin *et al.*, 1985]. However, the pathway leading to the synthesis of C_3 metabolites such as lactate or pyruvate from acetoacetate is not clearly established. The purpose of including Model III is to test if any of the labeling studies are consistent with Model III. The GS pathway is not found in mammalian systems.

5.5 Model Development

The goal of this analysis is to provide the means for maximizing the amount of information that can be extracted from experiments with ^{13}C and ^{14}C labeled substrates. To this end, one needs, first, to identify the types of isotopomers that arise in a given pathway and labeled substrate, and, second, to obtain expressions for the distributions of these isotopomers. The degree of enrichment at any carbon atom of any metabolite, isotopomer molecular weight distribution and fine structure of NMR spectra can be derived from isotopomer distributions.

5.5.1 Isotopomer Identification via Multiple Turns of TCA Cycle

Figure 5.3 shows the fate of ^{13}C label present in [3-^{13}C]pyruvate after multiple turns through the TCA cycle. Starting with [3-^{13}C]pyruvate, all acetyl-CoA will be labeled at C-2 position via the pyruvate dehydrogenase reaction. OAA derived from the anaplerotic reaction via pyruvate carboxylase will be of the form O_{34}, if the bicarbonate fixed is labeled with $^{13}CO_2$, and O_3 if the bicarbonate fixed is unlabeled. Furthermore, it is assumed that the sequence of reverse reactions from OAA to fumarate is very rapid compared to the reactions of citrate synthase and PEP carboxykinase, and thus result in full symmetrical equilibration of carbon label between C-1 and C-4, and between C-2 and C-3 in OAA, succinate, malate, and fumarate. This assumption results in an equal concentration of O_{34} and O_{12} and of O_3 and O_2.

Following the TCA cycle, O_{34} condensing with Ac_2 will yield in C_{124}, K_{124}, S_{13}, ½ F_{13}+ ½ F_{24}, ½ M_{13}+ ½ M_{24}, and ½ O_{13} + ½ O_{24}. Similarly other input and regenerated OAA species can be followed until no new species are formed. Note that not all combinationally possible isotopomer species are present. For example, there are $2^5 = 32$ α-ketoglutarate species but only six species are present in our model on the basis of the assumed biochemistry.

In a similar manner, the schematics for different-labeled substrates can be obtained: Figure 5.4 for [2-^{13}C]pyruvate, Figure 5.5 for [1-^{13}C]pyruvate, Figure 5.6 for [2-^{13}C]acetate with Model I, Figure 5.7 for [2-^{13}C]acetate with Model II, Figure 5.8 for [2-^{13}C]acetate with Model III, Figure 5.9 for [1-^{13}C]acetate with Model I, Figure 5.10 for [1-^{13}C]acetate with Model II, and Figure 5.11 for [1-^{13}C]acetate with Model III.

Figure 5.12 shows the expected labeling pattern of glucose derived from OAA via the gluconeogenic pathway. It is noted that in deriving the labeling pattern of glucose, the pattern of OAA, not of α-ketoglutarate, should be used. This simple point may seem superfluous but ignoring this simple point leads to a gross misinterpretation as will be discussed later.

5.5.2 Isotopomer Input-Output Balances

Based on the reactions depicted in Figure 5.3, simple material balances can be written for each isotopomer shown. For nine OAA isotopomers, for example, these balances are shown in (Eq. 5.1):

$$\frac{d}{dt}[O_T]\begin{bmatrix} O_3 \\ O_2 \\ O_{34} \\ O_{12} \\ O_{13} \\ O_{24} \\ O_{123} \\ O_{234} \\ O_{23} \end{bmatrix} = V_{KGDH}\begin{bmatrix} 0 \\ 0 \\ 0 \\ 0 \\ \frac{1}{2}K_{24}+\frac{1}{2}K_{124} \\ \frac{1}{2}K_{24}+\frac{1}{2}K_{124} \\ \frac{1}{2}K_{234}+\frac{1}{2}K_{1234} \\ \frac{1}{2}K_{234}+\frac{1}{2}K_{1234} \\ K_{34}+K_{134} \end{bmatrix} + V_{PC}\begin{bmatrix} P_3\left(\frac{1-CO_2^*}{2}\right) \\ P_3\left(\frac{1-CO_2^*}{2}\right) \\ P_3\left(\frac{CO_2^*}{2}\right) \\ P_3\left(\frac{CO_2^*}{2}\right) \\ 0 \\ 0 \\ 0 \\ 0 \\ 0 \end{bmatrix} - V_{CS}\begin{bmatrix} O_3 \\ O_2 \\ O_{34} \\ O_{12} \\ O_{13} \\ O_{24} \\ O_{123} \\ O_{234} \\ O_{23} \end{bmatrix} - V_{PPCK}\begin{bmatrix} O_3 \\ O_2 \\ O_{34} \\ O_{12} \\ O_{13} \\ O_{24} \\ O_{123} \\ O_{234} \\ O_{23} \end{bmatrix}$$

(Eq. 5.1)

In the above equations each isotopomer species is represented in relative population, i.e., its concentration is normalized by the total concentration of the same metabolite (for example, $O_3 = [O_3]/[O_T]$). V is the velocity of the corresponding reaction per subscripts denoted in Figure 5.1 in mmol per unit cell mass per unit time. Assuming metabolic steady state, $V_{MDH} = V_{FDH} = V_{SDH} = V_{KGDH}$. This equation allows the replacement of malate by α-ketoglutarate isotopomers in (Eq. 5.1) while maintaining the labeling pattern indicated in Figure 5.3.

Similar expressions can be written for citrate/isocitrate (indicated by C), (Eq. 5.2), α-ketoglutarate (Eq. 5.3) and the fraction of CO_2 labeled with ^{13}C, CO_2^* (Eq. 5.4):

$$\frac{d}{dt}[C_T]\begin{bmatrix} C_{24} \\ C_{34} \\ C_{124} \\ C_{346} \\ C_{246} \\ C_{134} \\ C_{2346} \\ C_{1234} \\ C_{234} \end{bmatrix} = V_{CS}\begin{bmatrix} O_3 \\ O_2 \\ O_{34} \\ O_{12} \\ O_{13} \\ O_{24} \\ O_{123} \\ O_{234} \\ O_{23} \end{bmatrix} - V_{IDH}\begin{bmatrix} C_{24} \\ C_{34} \\ C_{124} \\ C_{346} \\ C_{246} \\ C_{134} \\ C_{2346} \\ C_{1234} \\ C_{234} \end{bmatrix} \qquad \textbf{(Eq. 5.2)}$$

$$\frac{d}{dt}[K_T]\begin{bmatrix} K_{24} \\ K_{34} \\ K_{124} \\ K_{134} \\ K_{234} \\ K_{1234} \end{bmatrix} = V_{IDH}\begin{bmatrix} C_{24}+C_{246} \\ C_{34}+C_{346} \\ C_{124} \\ C_{134} \\ C_{2346}+C_{234} \\ C_{1234} \end{bmatrix} - V_{KGDH}\begin{bmatrix} K_{24} \\ K_{34} \\ K_{124} \\ K_{134} \\ K_{234} \\ K_{1234} \end{bmatrix} \qquad \textbf{(Eq. 5.3)}$$

$$\begin{aligned} \frac{d}{dt}[CO_{2_T}]\,CO_2^* = {} & \frac{V_{IDH}}{V_{IDH}+V_{KGDH}-V_{PC}+V_{PPCK}}(C_{346}+C_{246}+C_{2346}) \\ & + \frac{V_{KGDH}}{V_{IDH}+V_{KGDH}-V_{PC}+V_{PPCK}}(K_{124}+K_{134}+K_{1234}) \\ & -V_{PC}(CO_2^*) + \frac{V_{PPCK}}{V_{IDH}+V_{KGDH}-V_{PC}+V_{PPCK}}(O_{34}+O_{24}+O_{234}) \end{aligned} \qquad \textbf{(Eq. 5.4)}$$

The reaction velocities of the pyruvate utilization network of Figure 5.1 are related through the following metabolite balances:

$$\frac{d}{dt}[AcCoA] = V_{PDH} - V_{CS}$$

$$\frac{d}{dt}[C] = V_{CS} - V_{ACON}$$

$$\frac{d}{dt}[IC] = V_{ACON} - V_{IDH}$$

$$\frac{d}{dt}[K] = V_{IDH} - V_{KGDH}$$

$$\frac{d}{dt}[S] = V_{KGDH} - V_{SUDH}$$

$$\frac{d}{dt}[F] = V_{SUDH} - V_{FDH}$$

$$\frac{d}{dt}[M] = V_{FDH} - V_{MDH}$$

$$\frac{d}{dt}[O] = V_{MDH} + V_{PC} - V_{CS} - V_{PPCK}$$

$$\frac{d}{dt}[CO_2] = V_{IDH} + V_{KGDH} - V_{PC} + V_{PPCK}$$

$$\frac{d}{dt}[PEP] = V_{PPCK} - V_{GP} \qquad \textbf{(Eq. 5.5)}$$

$$\frac{d}{dt}[P] = V_{IMPORT} - V_{PC} - V_{PDH}$$

Under the steady state assumption, all of the above fluxes can be expressed in terms of V_{CS} and V_{PC}. It is useful to introduce the probability (x) that OAA will exit the TCA cycle via the transaminase (TA) reaction, in which case ($1 - x$) will denote the probability that OAA will enter the TCA cycle via citrate synthase (CS). In terms of x one can write:

$$\frac{x}{1-x} = \frac{V_{TA}}{V_{CS}} = \frac{V_{PC}}{V_{CS}} \qquad \textbf{(Eq. 5.6)}$$

Likewise, we let y be the probability of bicarbonate fixed into pyruvate to be labeled with $^{13}CO_2$. If there is no pathway which generates and consumes CO_2 other than the reactions indicated on this model, y can be expressed exclusively in terms of x as well.

In the case of acetate utilization, we introduce another variable z denoting the probability of isocitrate to be utilized via the GS pathway. Then ($1 - z$) is that via the TCA cycle. Therefore, the ratio of flux via the GS pathway to flux via the TCA cycle can be expressed as

$$\frac{z}{1-z} = \frac{V_{GS}}{V_{TCA}} \qquad \textbf{(Eq. 5.7)}$$

At steady state, (Eq. 5.5) can be solved for the fluxes in terms of the probability x and then substituted into the isotopomer balances of (Eq. 5.1) - (Eq. 5.4) to yield the isotopomer distributions in terms of the two probabilities x and y. For the cases described in section 3 and Figures 5.1 and 5.2, results are summarized in Tables 5.1-5.3. It should be noted that G and K are used interchangeably since the isotopomer distributions of glutamate and α-ketoglutarate are identical.

We close this section with a summary of the assumptions invoked in the derivation of the expressions of Tables 5.1-5.3:

- There is no label recycling due to operation of futile cycles such as the "Pyruvate→OAA→PEP→Pyruvate" and "Malate→Pyruvate→OAA→ Malate" cycles.
- There is no compartmentalization of metabolites and homogenous pools exist which are common to the TCA cycle and other pathways.
- There is no net flux to biosynthesis except in the formation of glucose.
- There is no label scrambling by the operation of the PPP which would redistribute the label of glucose synthesized via the gluconeogenic pathway.
- Metabolic and isotopic steady states are reached.
- Input substrates are isotopically pure. They are either 100% enriched at the designated position and none at the undesignated position.
- Isotopic dilution due to presence of unlabeled endogenous pools is negligible.

5.6 Discussion

Most metabolic NMR experiments are limited to the measurement of ^{13}C label enrichment at specific carbon atoms of various metabolites. The results reported in Tables 5.1-5.3 not only allow the correct interpretation of such label enrichment data, but also extend the amount of information that can be derived from NMR experiments through the analysis of the fine structure of NMR spectra, as well as, the determination of the molecular weight distribution of metabolic isotopomers.

With respect to the interpretation of ^{13}C enrichment data, the degree of enrichment at various carbon atoms can be obtained as the sum of the corresponding isotopomers using the expressions reported in Tables 5.1-5.3. Referring, for example, to the use of [3-^{13}C]pyruvate, the relative degree of enrichment at each carbon position of α-ketoglutarate can be calculated as the sum of all isotopomer species that contain the labeled carbon at that particular position. This is reflected in the following equation:

$$\begin{aligned} C-1 &= K_{124} + K_{134} + K_{1234} \\ C-2 &= K_{24} + K_{124} + K_{234} + K_{1234} \\ C-3 &= K_{34} + K_{134} + K_{234} + K_{1234} \\ C-4 &= K_{24} + K_{34} + K_{124} + K_{134} + K_{234} + K_{1234} = 1 \\ C-5 &= 0 \end{aligned} \qquad \textbf{(Eq. 5.8)}$$

From the isotopomer distributions of Tables 5.1-5.3, the fine structure of NMR peaks at specific carbon atom locations can be further analyzed. Referring again to the results of Table 5.1 for the case of [3-^{13}C]pyruvate labeling, it can be seen that the glutamate C-2 resonance will be split into nine-lines centered at 55.5 ppm. The nine-lines splitting at C-2 will be the sum of a singlet due to G_{24}, a doublet with coupling constant J_{12} due to G_{124}, a doublet with coupling constant J_{23} due to G_{234}, and a quartet due to G_{1234}. Two different doublets occur as a result of the difference in the coupling constants between J_{12} (53.5 Hz) and J_{23} (34.6 Hz). Also the line splitting at C-2 due to G_{1234} is a quartet because of this difference whereas the line splitting at C-3 due to G_{1234} is a triplet with an intensity ratio 1:2:1 due to the similar values of J_{23} and J_{34}. It can be thus seen that the relative amounts of the isotopomers will define the exact nature of the fine structure of the peaks of NMR spectra. Since the relative amounts of isotopomers depend on relative metabolic flux distributions (as represented by the parameters x and z in the expressions shown in Tables 5.1-5.3), it is clear that the NMR spectra fine structure contains useful information about the overall distribution of metabolic fluxes.

The same isotopomer distributions can further be applied to the determination of molecular weight distributions of different isotopomers. For example, the relative amount of glutamate molecules with normal molecular weight M (corresponding to the absence of ^{13}C label from all carbon atoms) can be found from Table 1 to be equal to zero, for all glutamate are expected to carry at least one ^{13}C carbon. Similarly, the relative amount of

isotopomer with molecular weight (M + 1) is also equal to zero. However, the relative amount of isotopomers with molecular weight (M + 2) will be equal to the sum of K_{24} and K_{34}, the relative amount of isotopomers with molecular weight of (M + 3) will be equal to the sum of K_{124}, K_{134} and K_{234}, and, finally, the relative amount of isotopomer with molecular weight of (M + 4) will be equal to the sum of K_{1234}. Such molecular weight distributions can be obtained by gas chromatography-mass spectrometry and can provide further information about the origin of the isotopomers and the corresponding metabolic fluxes.

It is noted that a great deal of redundancy is built into the calculations. For example, isotopomer distributions, molecular weight distributions, and fine structure of NMR spectra depend on the two parameters x and z in the cases considered in Tables 5.1-5.3. Any two of these measurements could be used for the determination of the unknown parameters x and z and the rest of the data could then be employed to test the consistency of the obtained values of x and z. In practice, a better approach may be to fit all measurements to the values of the two unknown parameters x, z and use the residual mean square as a measure of the accuracy of the fit. Low values of the residual mean square will indicate a good fit, while large values will be an indication of the presence of errors either in the measurements or in the assumed biochemical pathways. In the event that inconsistencies are identified, one can try eliminating various measurements one at a time and test the accuracy of the fit obtained with the remaining measurements. If a significant improvement is obtained upon eliminating one measurement, this would make the eliminated measurement suspect of containing gross errors suggesting that it should not be considered in the fit. If none of the measurements are so identified as containing gross errors, then the process can be repeated by altering the biochemical pathways included in the derivation of the corresponding equations, until a satisfactory fit is obtained.

The methodology presented in this paper maintains a focus on the determination of metabolic fluxes instead of concentrations of metabolites. We believe that intracellular fluxes can be very informative about factors controlling the flux of carbon and energy in metabolic networks. Furthermore, the results rely on measurements secreted metabolites

or intracellular metabolites in cell lysates. There is no need for *in situ* NMR measurements and the elaborate arrangements required for this purpose.

The results presented allow one to optimize the selection of the type of labeled substrates. It is clear from Table 5.1 that different enrichments and molecular distributions are obtained from the use of [3-^{13}C]pyruvate, [2-^{13}C]pyruvate, or [1-^{13}C]pyruvate as carbon substrate. Although metabolic pathways should remain unaltered with the use of different labeled substrates, differences in the structure of NMR spectra obtained with different labeled substrates can be extremely elucidating of metabolic fluxes contributing to the utilization of the pyruvate metabolite. Judicious choice of the specific labeled substrate can thus be instrumental in the type of results that will be obtained by ^{13}C NMR experiments.

Clearly, a great deal of information can be extracted from conventional NMR data in light of the analysis presented. The availability of the expressions presented in Tables 5.1-5.3 facilitates greatly the analysis of such measurements. However, analytical solutions for isotopomer distributions cannot be expected in general to be available for any configuration of biochemical pathways analyzed. It is possible that certain network structures will not be amenable to exact analytical solution of the type reported. In such cases, the isotopomer distributions will have to be obtained numerically, although they still contain the same amount and type of information. Suitable computer programs that facilitate the analysis of label transfer and calculation of isotopomer distribution will be invaluable in maximizing the information obtainable from these experiments and providing the best experimental design.

5.8 Nomenclature

Ac	acetyl-CoA
CS	citrate synthase
GS	glyoxylate shunt
Gx	glyoxylate
M	molecular weight of [U-^{12}C]glutamate
OAA	oxaloacetate
PC	pyruvate carboxylase
PEP	phosphoenolpyruvate
PPC	phosphoenolpyruvate carboxylase
TA	transaminase
TCA	tricarboxylic acid cycle
V_i	flux through enzyme i
x	probability of oxaloacetate to exit the TCA cycle
(1 - x)	probability of oxaloacetate to enter the TCA cycle
y	probability of bicarbonate labeled with ^{13}C
(1 - y)	probability of bicarbonate labeled with ^{12}C
z	probability of isocitrate to be utilized via the GS pathway
(1 - z)	probability of isocitrate to be utilized via the TCA cycle

Single letter followed by numbered subscripts (numbers indicate carbon positions labeled)

C	citrate
F	fumarate
K	α-ketoglutarate
M	malate
O	oxaloacetate
P	pyruvate
S	succinate

5.8 References

Annison, E.F., Leng, R.A., Lindsay, D.B., White, R.R. (1963). The metabolism of acetic acid, propionic acid and butyric acid in sheep. *Biochem. J.* **88**: 248-252.

Chance, E.M., Seeholzer, S.H., Kobayashi, K., Williamson, J.R. (1983). Mathematical analysis of isotope labeling in the citric acid cycle with applications to ^{13}C NMR studies in perfused rat hearts. *J. Biol. Chem.* **258**: 13785-13794.

Desmoulin, F., Canioni, P., Cozzone, P.J. (1985). Glutamate-glutamine metabolism in the perfused rat liver: ^{13}C-NMR study using (2-^{13}C)-enriched acetate. *FEBS. Lett.* **185**: 29-32.

Di Donato, L., Des Rosiers, C., Montgomery, J.A., David, F., Garneau, M., Brunengraber, H. Rates of gluconeogenesis and citric acid cycle in perfused livers, assessed from the mass spectrometric assay of the ^{13}C labelling patterns of glutamate. *J. Biol. Chem.* **268**: 4170-4180.

Exton, J.H., Park, C.R. (1967). Control of gluconeogenesis in liver. I. General features of gluconeogenesis in the perfused livers of rats. *J. Biol. Chem.* **242**: 2622-2636.

Gopher, A., Vaisman, N., Mandel, H., Lapidot, A. (1990). Determination of fructose metabolic pathways in normal and fructose-intolerant children - A ^{13}C NMR study using [U-^{13}C]fructose. *Proc. Natl. Acad. Sci. USA* **87**: 5449-5453.

Graham, D.Y., Klein, P.D., Opekun, A.R., Boutton, T.W. (1988). Effect of age on the frequency of active *Campylobacter pylori* infection diagnosed by the [^{13}C]urea breath test in normal subjects and patients with peptic ulcer disease. *J. Infect. Dis.* **157**: 777-780.

Hofmann, A.F., Lauterburg, B.H. (1977). Breath test with isotopes of carbon: progress and potential. *J. Lab. Clin. Med.* **90**: 405-411.

Kalderon, B., Korman, S.H., Gutman, A., Lapidot, A. (1989a). Glucose recycling and production in glycogenosis type-I and type-III: stable isotope technique study. *Am. J. Physiol.* **257**: E346-E353.

Kalderon, B., Korman, S.H., Gutman, A., Lapidot, A. (1989b). Estimation of glucose carbon recycling in children with glycogen storage disease: A ^{13}C NMR-study using [U-^{13}C]glucose. *Proc. Natl. Acad. Sci. USA* **86**: 4690-4694.

Kassel, D.B., Glerum, M., Robinson, B.H., Sweeley, C.C. (1989). Determination of [U-^{13}C]glucose turnover into various metabolite pools for the differential diagnosis of lactic acidemias. *Anal. Biochem.* **176**: 382-389.

Katz, J., Grunnet, N. (1979). Estimation of metabolic pathways in steady state in vitro Rates of tricarboxylic acid and pentose cycles. In: *Techniques in Metabolic Research.* Kornberg, H.L. (eds.), Elsevier/North-Holland Scientific Publushers Ltd., New York, pp. 1-18.

Kurumaya, K., Kajiwara, M., Abel, T., Hirano, S., Kokubun, N. (1988). Synthesis of [^{13}C]phenacetin and its application to the breath test for the diagnosis of liver disease. *Chem. Pharm. Bull.* **36**: 2679-2681.

Lacroix, M., Mosora, F., Pontus, M., Lefebvre, P., Luyckx, A., Lopez-Habib, G. (1979). Glucose naturally labeled with carbon-13: use for metabolic studies in man. *Science* **181**: 445-446.

Magnusson, I., Schumann, W.C., Bartsch, G.E., Chandramouli, V., Kumaran, K., Wahren, J., Landau, B.R. (1991). Noninvasive tracing of Krebs cycle metabolism in liver. *J. Biol. Chem.* **266**: 6975-6984.

Malloy, C.R., Sherry, A.D., Jeffrey, F.M.H. (1988). Evaluation of carbon flux and substrate selection through alternate pathways involving the citric acid cycle of the heart by ^{13}C NMR spectroscopy. *J. Biol. Chem.* **263**: 6964-6971.

Marshall, B.J., Surveyor, I. (1988). Carbon-14 urea breath test for the diagnosis of *Campylobacter pylori* associated gastritis. *Clinical Sciences* **29**: 11-16.

Novis, B.H., Gabay, G., Leichtmann, G., Peri, M., Bernheim, J., Pomeranz, I.S. (1991). Two point analysis 15-minute ^{14}C-urea breath test for diagnosing *Helicobacter pylori* infection. *Digestion* **50**: 16-21.

Ormand, J.E., Talley, N.J., Carpenter, H.A., Shorter, R.G., Conley, C.R., Wilson, W.R., DiMagno, E.P., Zinsmeister, A.R., Phillips, S.F. (1990). [^{14}C]urea breath test for diagnosis of *Helicobacter pylori*. *Digest. Dis. Sci.* **35**: 879-884.

Park, S.M., Sinskey, A.J., Stephanopoulos, G.N. (1996). Effect of the tricarboxylic acid on metabolite labeling. II. Theory. Submitted to *The Journal of Biological Chemistry.*

Schneider, J.F., Schoeller, D.A., Nemchausky, B., Boyer, J.L., Klein, P. (1978). Validation of $^{13}CO_2$ breath analysis as a measurement of demethylation of stable isotope labeled aminopyrine in man. *Clinica Chimica Acta* **84**: 153-162.

Solomons, N.W., Schoeller, D.A., Wagonfeld, J.B., Ott, D., Rosenberg, I.H., Klein, P.D. (1977). Application of a stable isotope (^{13}C)-labeled glycocholate breath test to diagnosis of bacterial overgrowth and ileal function. *J. Lab. Clin. Med.* **90**: 431-439.

Turner, J.M., Lawrence, S., Fellows, I.W., Johnson, I., Hill, P.G., Holmes, G.K.T. (1987). [^{14}C]-triolein absorption: a useful test in the diagnosis of malabsorption. *Gut* **28**: 694-700.

Watkins, J.B., Klein, P.D., Schoeller, D.A., Kirschner, B.S., Park, R., Perman, J.A. (1982). Diagnosis and differentiation of fat malabsorption in children using ^{13}C-labeled lipids: trioctanoin, triolein, and palmitic acid breath tests. *Gastroenterology* **82**: 911-917.

Watkins, J.B., Schoeller, D.A., Klein, P.D., Ott, D.G., Newcomer, A.D., Hofmann, A.F. (1977). ^{13}C-trioctanoin: a nonradioactive breath test to detect fat malabsorption. *J. Lab. Clin. Med.* **90**: 422-430.

Weinman, E.O., Strisower, E.H., Chaikoff, I.L. (1957). Conversion of fatty acids to carbohydrate: Application of isotopes to this problem and role of the Krebs cycle as a synthetic pathway. *Physiol. Rev.* **37**: 252-272.

Table 5.1 Steady state distribution of oxaloacetate (O) and glutamate (G) isotopomers and relative carbon enrichment in glucose and glutamate following the utilization of [1-^{13}C]pyruvate (label diagram in Figure 5.3), [2-^{13}C]pyruvate (Figure 5.4) and [3-^{13}C]pyruvate (Figure 5.5) through the major pathways described in Figure 5.1. y can be obtained exclusively as a function of x: $y=\frac{1-x}{2+x-x^2}$ in [3-^{13}C]pyruvate; $y=\frac{x(3-2x)}{4-3x}$ in [2-^{13}C]pyruvate; $y=\frac{1+x-2x^2}{2+x-x^2}$ in [1-^{13}C]pyruvate. Glutamate (G) and α-ketoglutarate (K) are used interchangeably since the labeling patterns of the two are identical. Glucose synthesized via the gluconeogenic pathway with these substrates has the following enrichment pattern: C-4 = C-3; C-5 = C-2; C-6 = C-1.

	[3-^{13}C]Pyruvate	[2-^{13}C]Pyruvate	[1-^{13}C]Pyruvate
Oxaloacetate Isotopomer Distribution	$O_2 = O_3 = \frac{x(1-y)}{2}$ $O_{12} = O_{34} = \frac{xy}{2}$ $O_{23} = \frac{(1-x)x}{(1+x)}$ $O_{13} = O_{24} = \frac{(1-x)x}{2(1+x)}$ $O_{123} = O_{234} = \frac{(1-x)^2}{2(1+x)}$	$O_2 = O_3 = \frac{x(1-y)}{2}$ $O_{13} = O_{24} = \frac{x(1-x+y+xy)}{2(1+x)}$ $O_{14} = \frac{x(1-x+y+xy)}{2(1+x)}$ $O_1 = O_4 = \frac{(1-x)^2}{2(1+x)}$	$O_1 = O_4 = \frac{x(1-y)}{2}$ $O_{14} = 1-x$ $O = xy$
Glucose Enrichment Pattern	$C-1 = \frac{1}{(1+x)}$ $C-2 = \frac{1}{(1+x)}$ $C-3 = \frac{1-x+xy+x^2y}{2(1+x)}$	$C-1 = \frac{x}{(1+x)}$ $C-2 = \frac{x}{(1+x)}$ $C-3 = \frac{1+x-2x^2+xy+x^2y}{2(1+x)}$	$C-1 = 0$ $C-2 = 0$ $C-3 = \frac{2-x-xy}{2}$
Glutamate Isotopomer Distribution	$K_{24} = \frac{x(2-y-xy)}{2(1+x)}$ $K_{34} = \frac{x}{2}$ $K_{124} = \frac{xy}{2}$ $K_{134} = \frac{x(1-x)}{2(1+x)}$ $K_{234} = \frac{1-x}{2}$ $K_{1234} = \frac{(1-x)^2}{2(1+x)}$	$K_{35} = \frac{x(1-y)}{2}$ $K_{135} = \frac{x(1-x+y+xy)}{2(1+x)}$ $K_{25} = \frac{x}{1+x}$ $K_{15} = \frac{1-x}{2}$ $K_5 = \frac{(1-x)^2}{2(1+x)}$	$K = \frac{2-x-xy}{2}$ $K_1 = \frac{x(1+y)}{2}$

Glutamate Enrichment Pattern	$C-1=\frac{1-x+xy+x^2y}{1+x}$ $C-2=\frac{1}{1+x}$ $C-3=\frac{1}{1+x}$ $C-4=1$ $C-5=0$	$C-1=\frac{1+x-2x^2+xy+x^2y}{2(1+x)}$ $C-2=\frac{x}{1+x}$ $C-3=\frac{x}{1+x}$ $C-4=0$ $C-5=1$	$C-1=\frac{x(1+y)}{2}$ $C-2=0$ $C-3=0$ $C-4=0$ $C-5=0$

Table 5.2 Steady state distribution of oxaloacetate and glutamate isotopomers and relative carbon enrichment in glucose and glutamate following [2-^{13}C]acetate administration through the three different model pathways described in Figure 5.2. In Model II, $y=\frac{(1-x)^2}{2+x-x^2}$ can be obtained exclusively as a function of x.

	[2-^{13}C]Acetate via Model I	[2-^{13}C]Acetate via Model II	[2-^{13}C]Acetate via Model III
Oxaloacetate Isotopomer Distribution	$O_{23}=\frac{3(1-z)}{3-z}$ $O_{123}=O_{234}=\frac{z}{3-z}$	$O=x-xy$ $O_1=O_4=\frac{xy}{2}$ $O_2=O_3=\frac{x(1-x)}{2}$ $O_{23}=\frac{(1-x)^2x}{(1+x)}$ $O_{13}=O_{24}=\frac{(1-x)^2x}{2(1+x)}$ $O_{123}=O_{234}=\frac{(1-x)^3}{2(1+x)}$	$O_{13}=O_{24}=\frac{x(2-y-xy)}{2(1+x)}$ $O_{134}=O_{124}=\frac{xy}{2}$ $O_{23}=\frac{(1-x)x(2-y-xy)}{2(1+x)}$ $O_{123}=O_{234}=\frac{(1-x)(2-2x+xy+x^2y)}{4(1+x)}$
Glucose Enrichment Pattern	$C-1=\frac{3-2z}{3-z}$ $C-2=\frac{3-2z}{3-z}$ $C-3=\frac{z}{3-z}$	$C-1=\frac{1-x}{(1+x)}$ $C-2=\frac{1-x}{(1+x)}$ $C-3=\frac{1-2x+x^2+xy+x^2y}{2(1+x)}$	$C-1=\frac{1}{(1+x)}$ $C-2=\frac{1}{(1+x)}$ $C-3=\frac{2+2x^2+3xy+2x^2y-x^3y}{4(1+x)}$
Glutamate Isotopomer Distribution	$K_{234}=\frac{3-2z}{3-z}$ $K_{1234}=\frac{z}{3-z}$	$K_4=x-\frac{xy}{2}$ $K_{14}=\frac{xy}{2}$ $K_{24}=\frac{x(1-x)}{(1+x)}$ $K_{34}=\frac{(1-x)x}{2}$ $K_{134}=\frac{x(1-x)^2}{2(1+x)}$ $K_{234}=\frac{(1-x)^2}{2}$ $K_{1234}=\frac{(1-x)^3}{2(1+x)}$	$K_{24}=\frac{x(2-y-xy)}{2(1+x)}$ $K_{134}=\frac{x(2-y-xy)}{2(1+x)}$ $K_{124}=\frac{xy}{2}$ $K_{234}=\frac{2-2x+xy+x^2y}{4}$ $K_{1234}=\frac{(1-x)(2-2x+xy+x^2y)}{4(1+x)}$

Glutamate Enrichment Pattern	$C-1=\frac{z}{3-z}$ $C-2=1$ $C-3=1$ $C-4=1$ $C-5=0$	$C-1=\frac{1-2x+x^2+xy+x^2y}{2(1+x)}$ $C-2=\frac{1-x}{1+x}$ $C-3=\frac{i-x}{1+x}$ $C-4=1$ $C-5=0$	$C-1=\frac{2+2x^2+xy-x^3y}{4(1+x)}$ $C-2=\frac{2+xy+x^2y}{2(1+x)}$ $C-3=\frac{1}{1+x}$ $C-4=1$ $C-5=0$

Table 5.3 Steady state distribution of oxaloacetate and glutamate isotopomers and relative carbon enrichment in glucose and glutamate following [1-^{13}C]acetate administration through the three different model pathways described in Figure 5.2. $y=\frac{1-x}{2-x}$ in Model II.

	[1-^{13}C]Acetate via Model I	[1-^{13}C]Acetate via Model II	[1-^{13}C]Acetate via Model III
Oxaloacetate Isotopomer Distribution	$O_{14}=1-z$ $O_1=O_4=\frac{z}{2}$	$O=x-xy$ $O_1=O_4=\frac{1-x+xy}{2}$	$O_2=O_3=\frac{x(1-y)}{2}$ $O_{13}=O_{24}=\frac{x(1-x+y+xy)}{2(1+x)}$ $O_{14}=\frac{x(1-x+y+xy)}{2(1+x)}$ $O_1=O_4=\frac{(1-x)^2}{2(1+x)}$
Glucose Enrichment Pattern	$C-1=0$ $C-2=0$ $C-3=1-\frac{z}{2}$	$C-1=0$ $C-2=0$ $C-3=\frac{1-x+xy}{2}$	$C-1=\frac{x}{(1+x)}$ $C-2=\frac{x}{(1+x)}$ $C-3=\frac{1+x-2x^2+xy+x^2y}{2(1+x)}$
Glutamate Isotopomer Distribution	$K_{15}=1-\frac{z}{2}$ $K_5=\frac{z}{2}$	$K_{15}=\frac{1-x+xy}{2}$ $K_5=\frac{1+x-xy}{2}$	$K_{35}=\frac{x(1-y)}{2}$ $K_{135}=\frac{x(1-x+y+xy)}{2(1+x)}$ $K_{25}=\frac{x}{1+x}$ $K_{15}=\frac{1-x}{2}$ $K_5=\frac{(1-x)^2}{2(1+x)}$
Glutamate Enrichment Pattern	$C-1=1-\frac{z}{2}$ $C-2=0$ $C-3=0$ $C-4=0$ $C-5=1$	$C-1=\frac{1-x+xy}{2}$ $C-2=0$ $C-3=0$ $C-4=0$ $C-5=1$	$C-1=\frac{1+x-2x^2+xy+x^2y}{2(1+x)}$ $C-2=\frac{x}{1+x}$ $C-3=\frac{x}{1+x}$ $C-4=0$ $C-5=1$

Figure 5.1 Pyruvate utilization via the TCA and the gluconeogenic pathway. The abbreviations used in the subscript of the fluxes are: GP, gluconeogenic pathway; PDH, pyruvate dehydrogenase; CS, citrate synthase; ACON, aconitase; KGDH, α-ketoglutarate dehydrogenase; SUDH, succinate dehydrogenase; FUM, fumarase; MDH, malate dehydrogenase; PPCK, phosphoenolpyruvate carboxykinase; PC, pyruvate carboxylase. The abbreviations for metabolites are: PEP, phosphoenolpyruvate; P, pyruvate; AcCoA, acetyl CoA; C, citrate; IC, isocitrate; K, α-ketoglutarate; S, succinate; F, fumarate; M, malate; O, oxaloacetate; CO_2, carbon dioxide; GLU, glucose. The operation of futile cycles such as " PEP $\rightarrow$P $\rightarrow$O$\rightarrow$PEP" is assumed inactive. Other reaction such glutamate-oxaloacetate transaminase and glutamate dehydrogenase for biosynthesis are ignored.

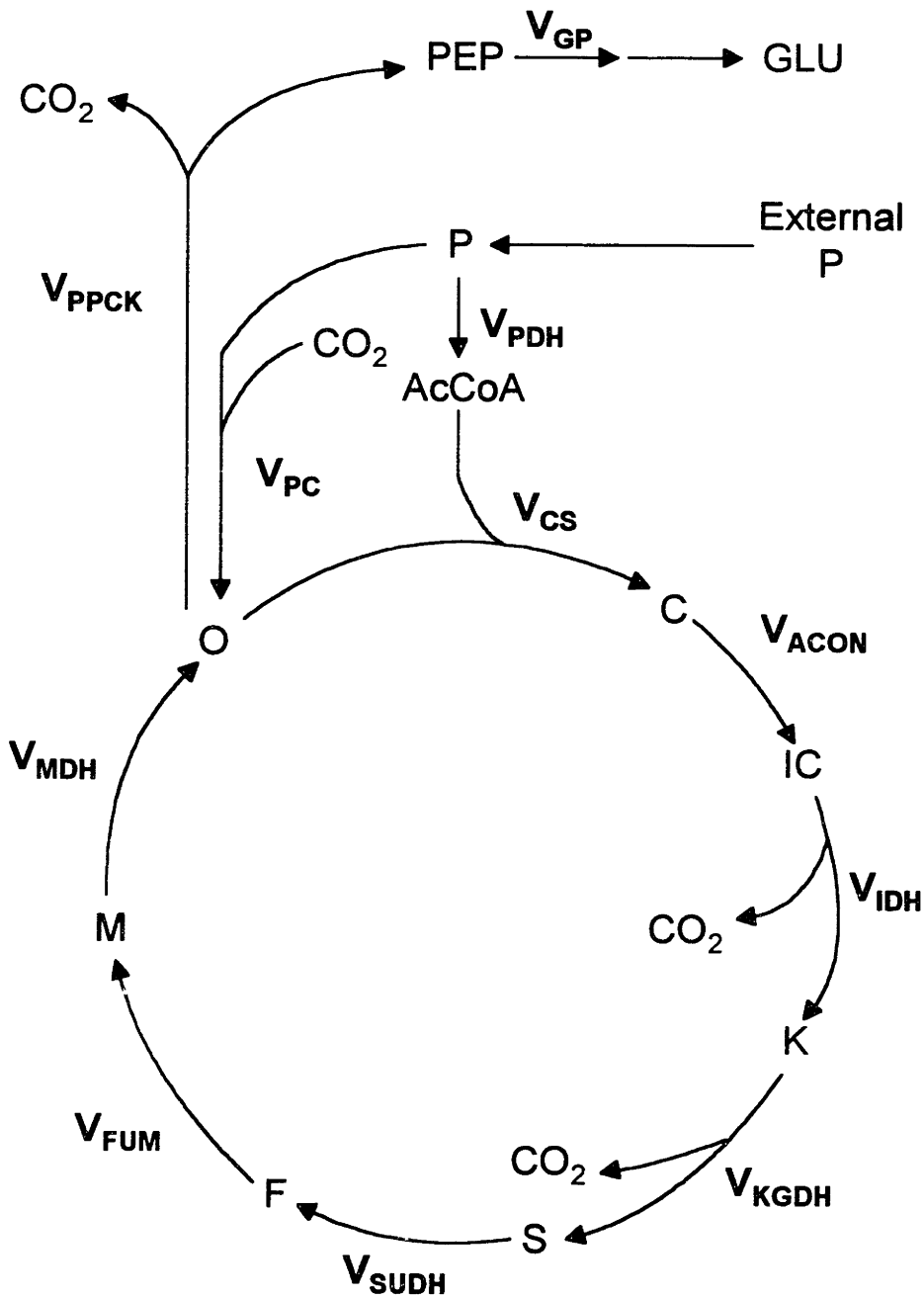

Figure 5.2 Three proposed models for acetate utilization. In Model I, acetate is utilized via the dual pathways: the TCA cycle and the glyoxylate shunt pathway. In Model II, acetate is utilized solely via the conversion to acetyl CoA which traverses the TCA cycle. Oxaloacetate is replenished from the other metabolites endogenously present. In Model III, acetate is converted to acetyl CoA and also becomes the source for oxaloacetate synthesis via the route of acetoacetate to lactate to pyruvate pathway. The operation of the Model III pathway is not clearly established yet.

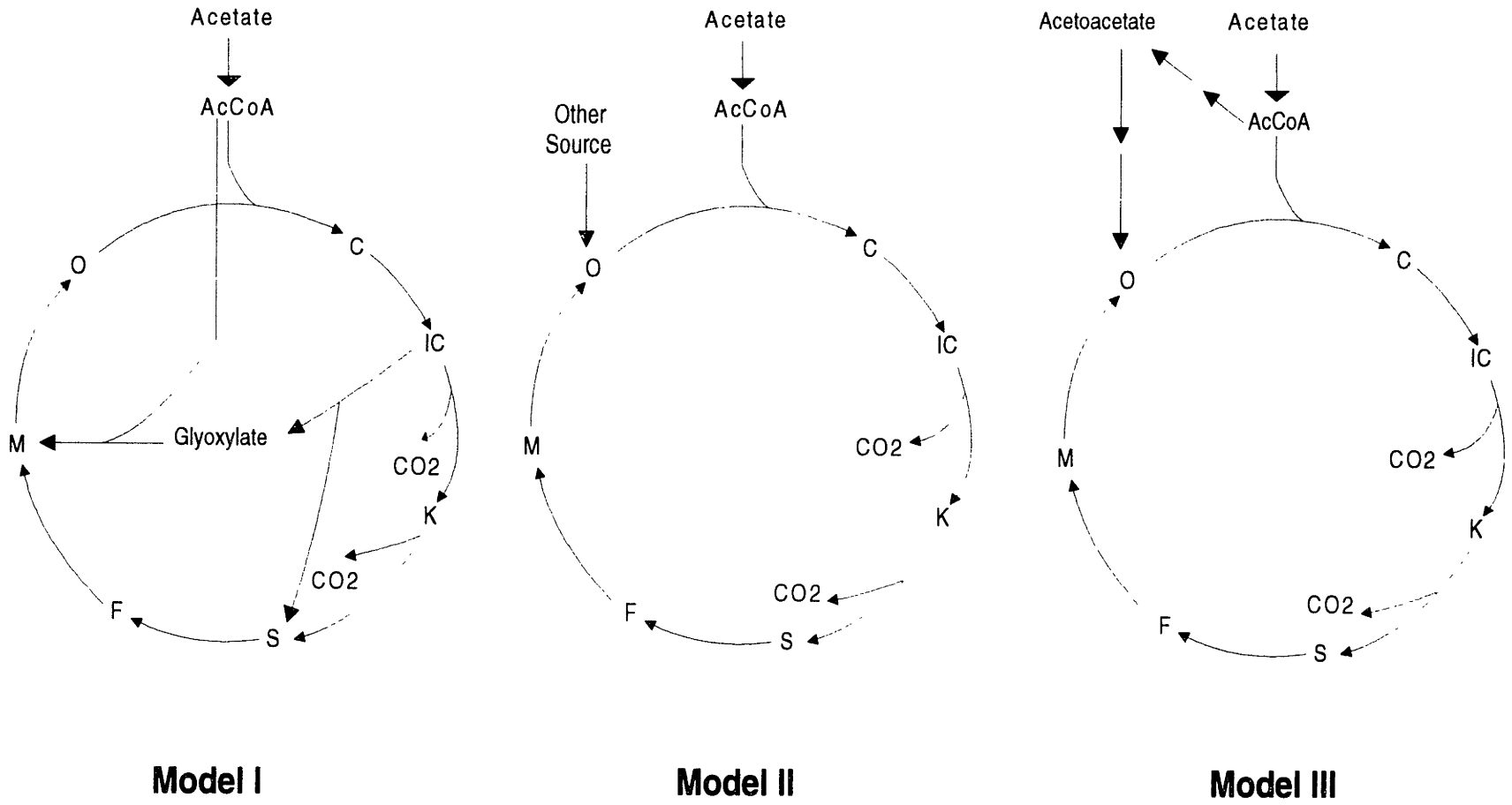

Figure 5.3 Schematic diagram of the sequential labeling of the carbons of intermediates via multiple turns of the TCA cycle using [3-^{13}C]pyruvate. Abbreviations are: Ac, O, C, K, S, and Gx for acetyl CoA, oxaloacetate, citrate, α-ketoglutarate, succinate, and glyoxylate, respectively. The numbers next to the metabolite symbol indicate the carbon position labeled by ^{13}C.

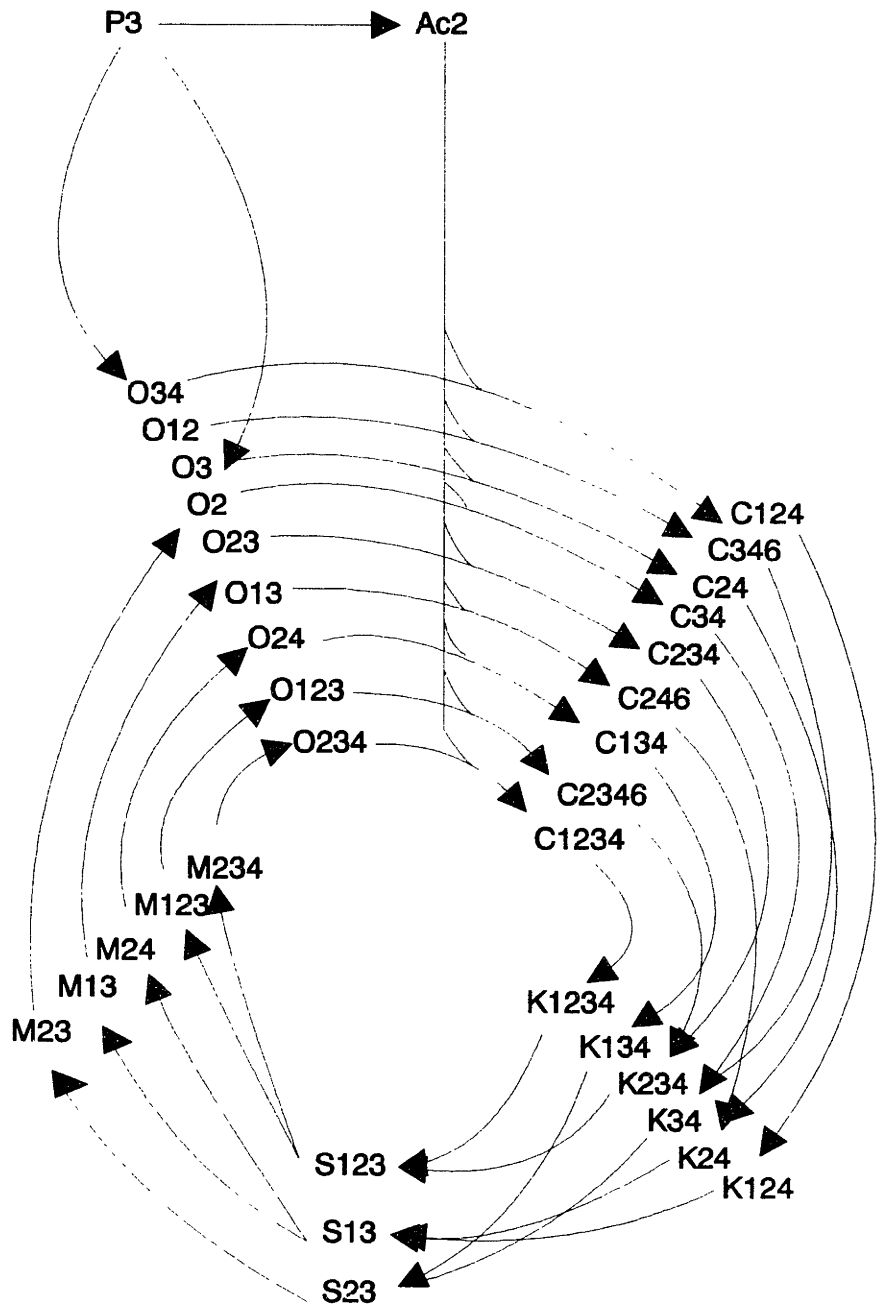

Figure 5.4 Schematic diagram of the sequential labeling of the carbons of intermediates via multiple turns of the TCA cycle using [2-^{13}C]pyruvate.

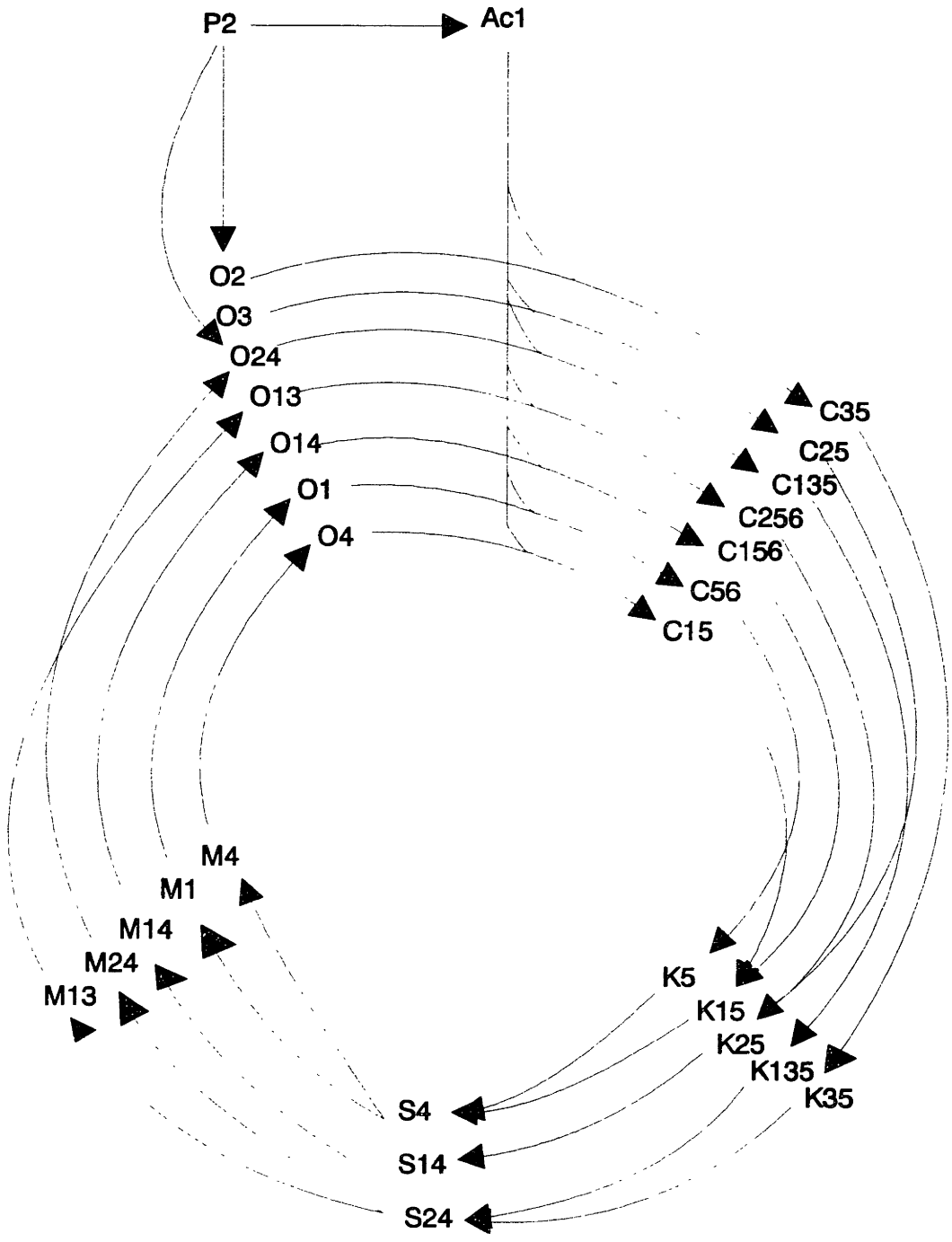

Figure 5.5 Schematic diagram of the sequential labeling of the carbons of intermediates via multiple turns of the TCA cycle using [1-^{13}C]pyruvate.

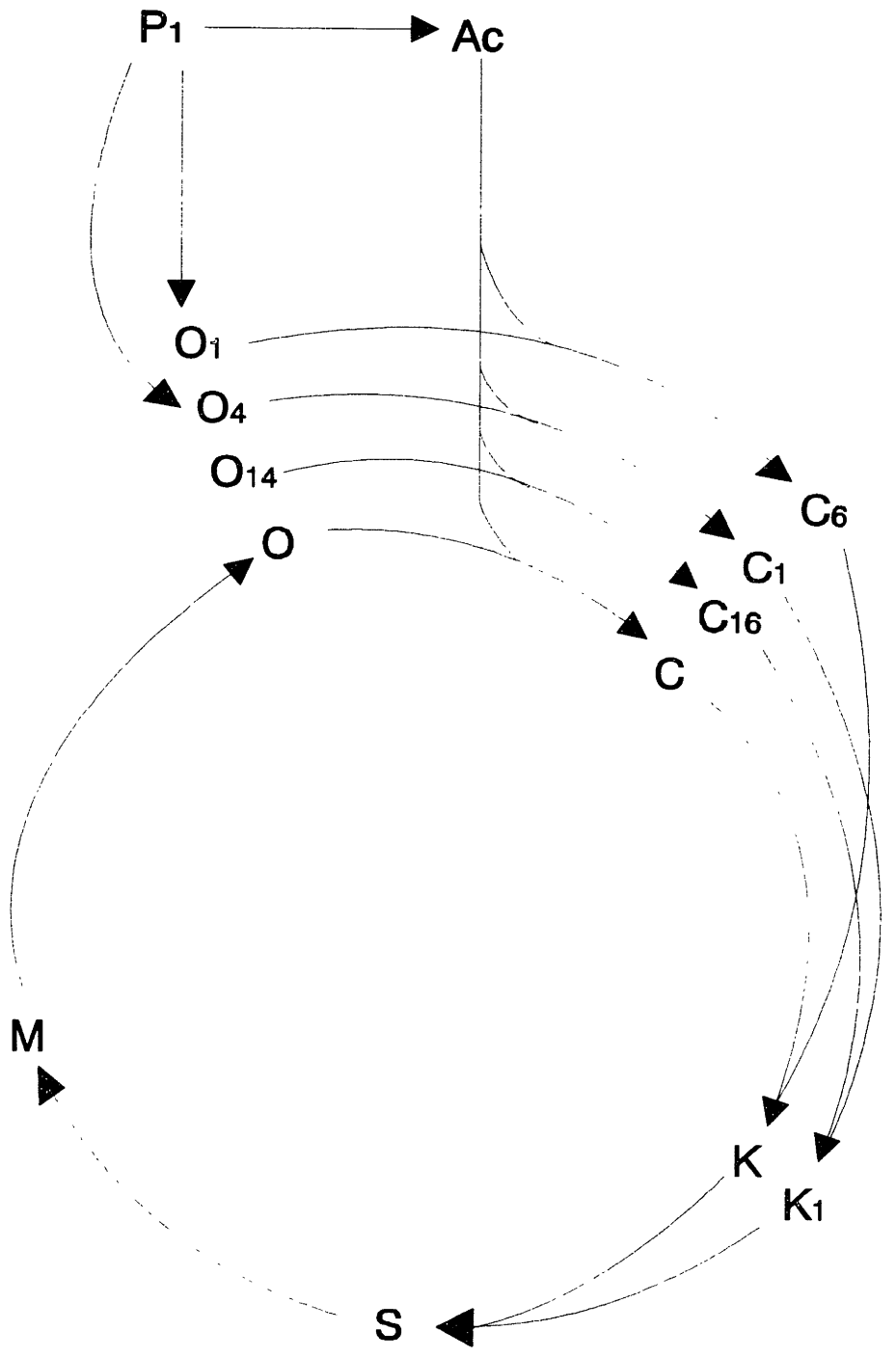

Figure 5.6 Schematic diagram of the sequential labeling of the carbons of intermediates via multiple turns of the TCA cycle and glyoxylate shunt pathway (Model I in Figure 5.2) using [2-^{13}C]acetate.

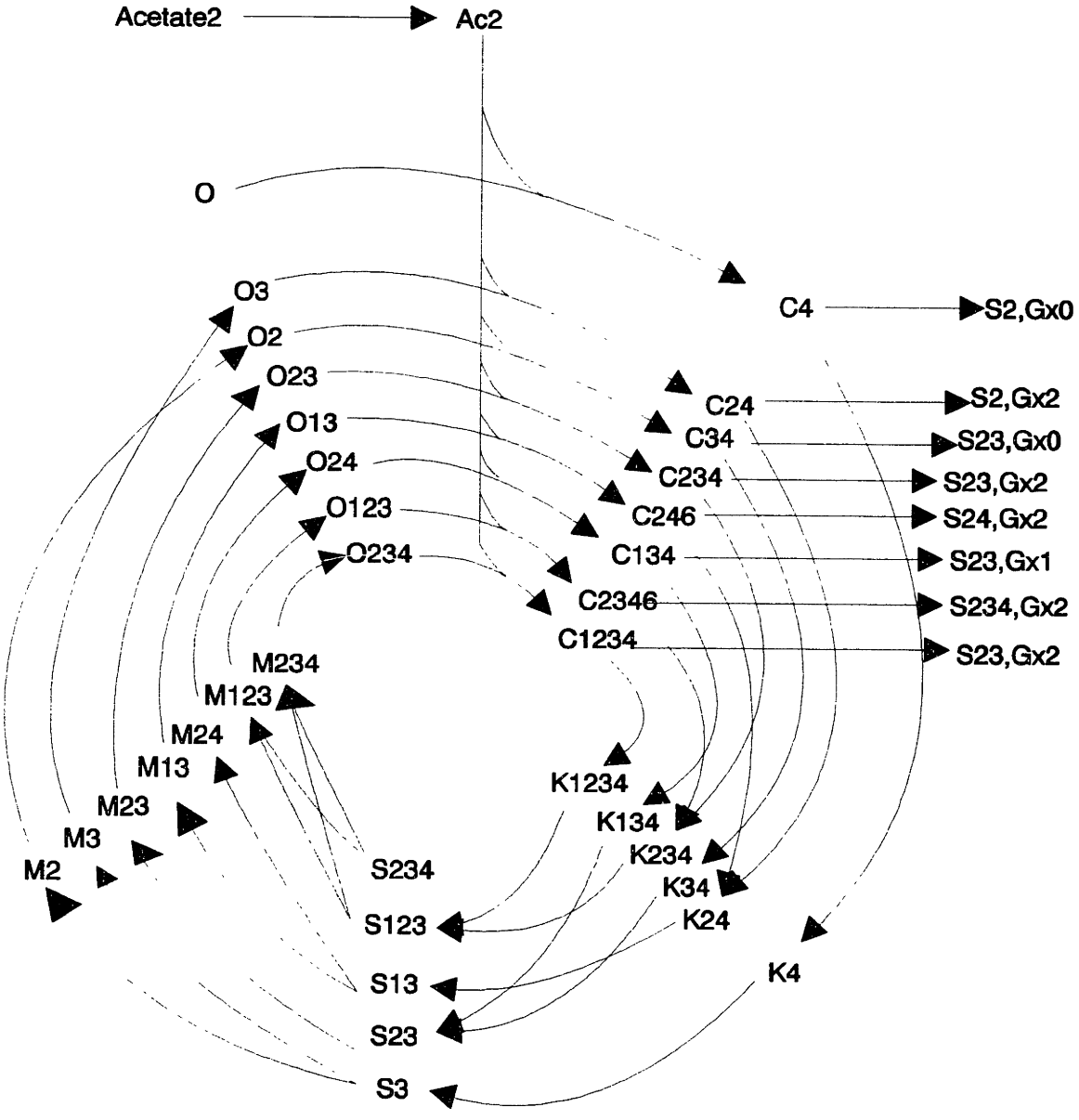

Figure 5.7 Schematic diagram of the sequential labeling of the carbons of intermediates via multiple turns of the TCA cycle and Model II pathway using [2-^{13}C]acetate.

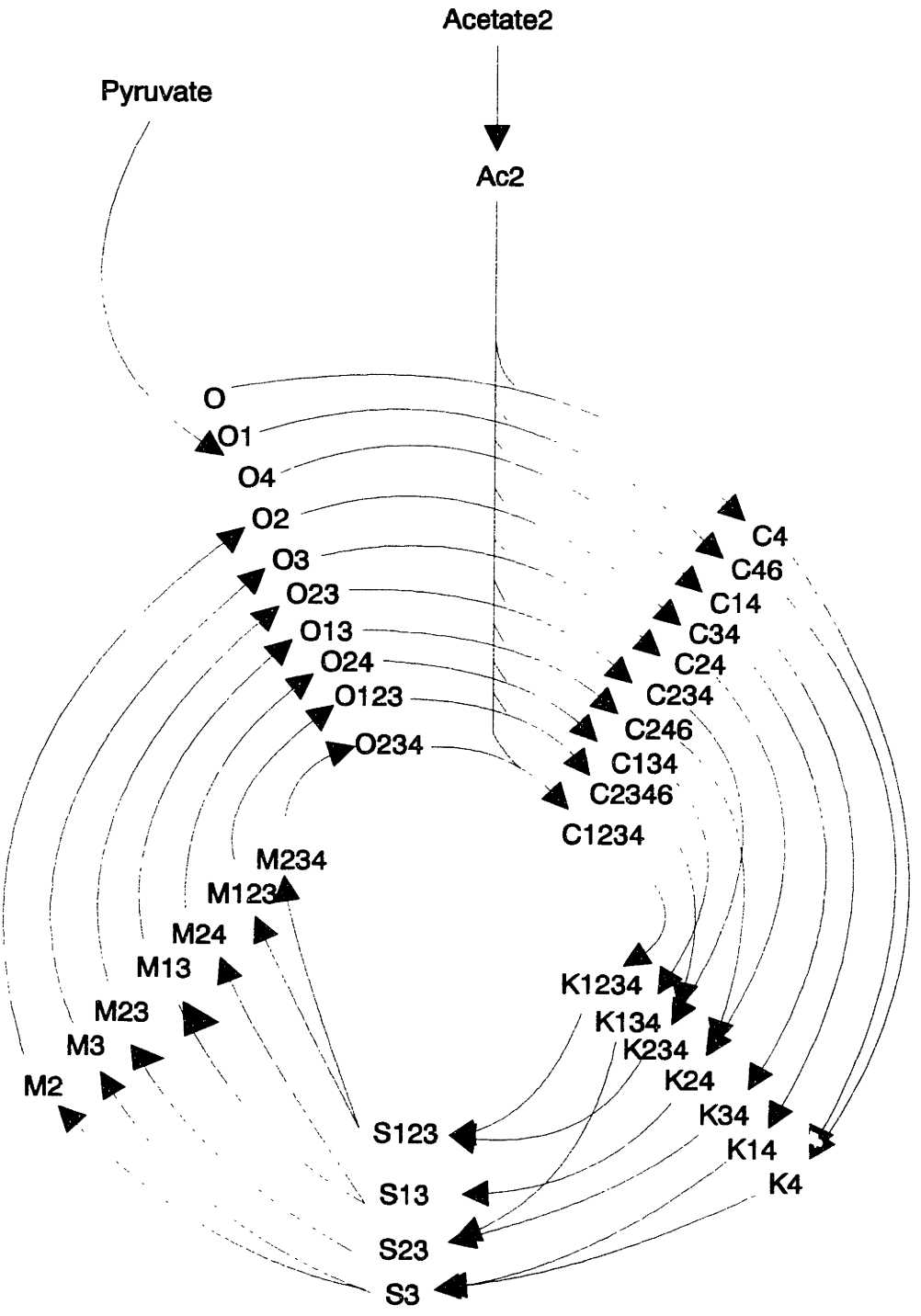

Figure 5.8 Schematic diagram of the sequential labeling of the carbons of intermediates via multiple turns of the TCA cycle and Model III pathway using [2-^{13}C]acetate.

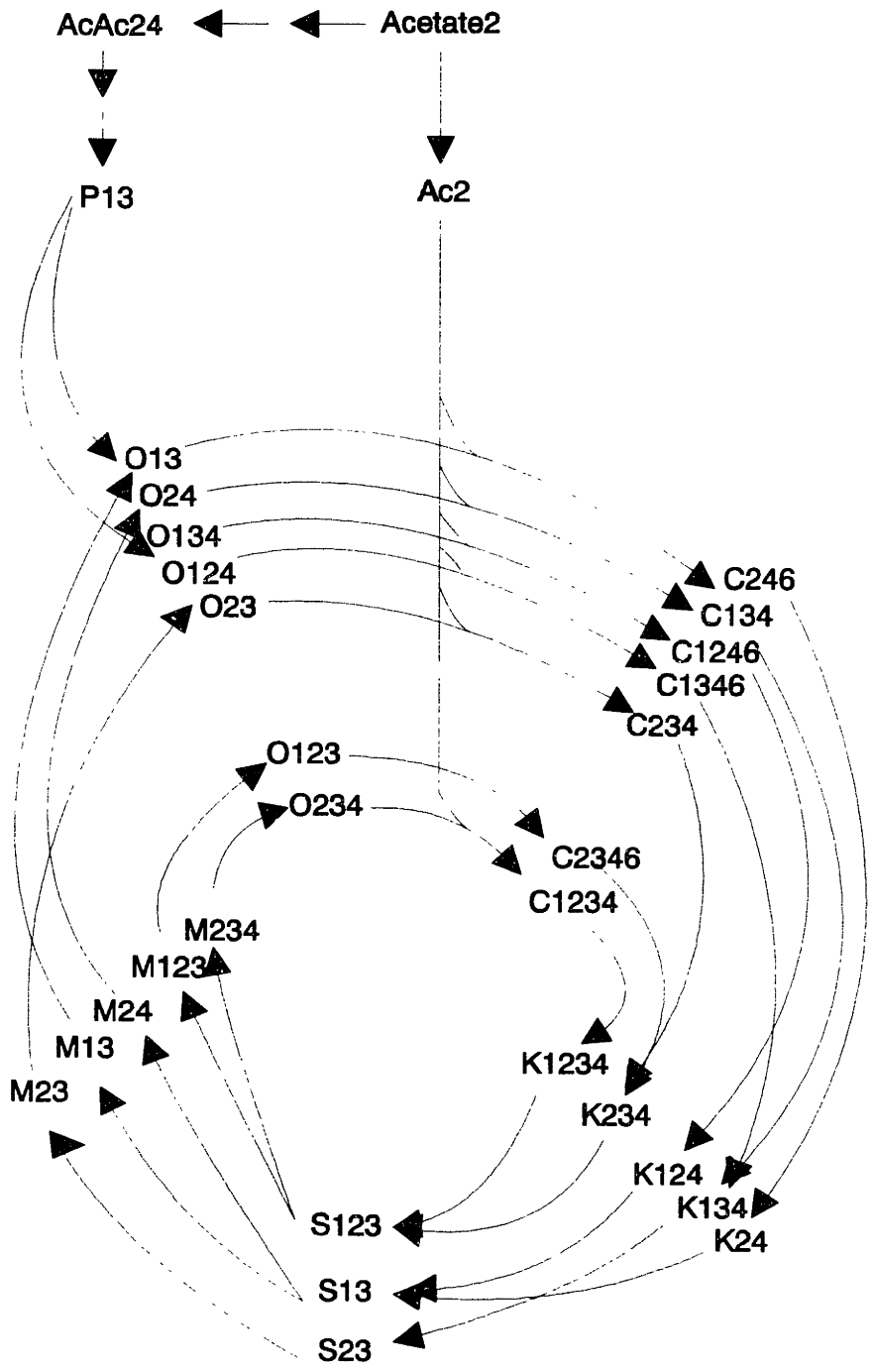

Figure 5.9 Schematic diagram of the sequential labeling of the carbons of intermediates via multiple turns of the TCA cycle and glyoxylate shunt pathway using [1-^{13}C]acetate.

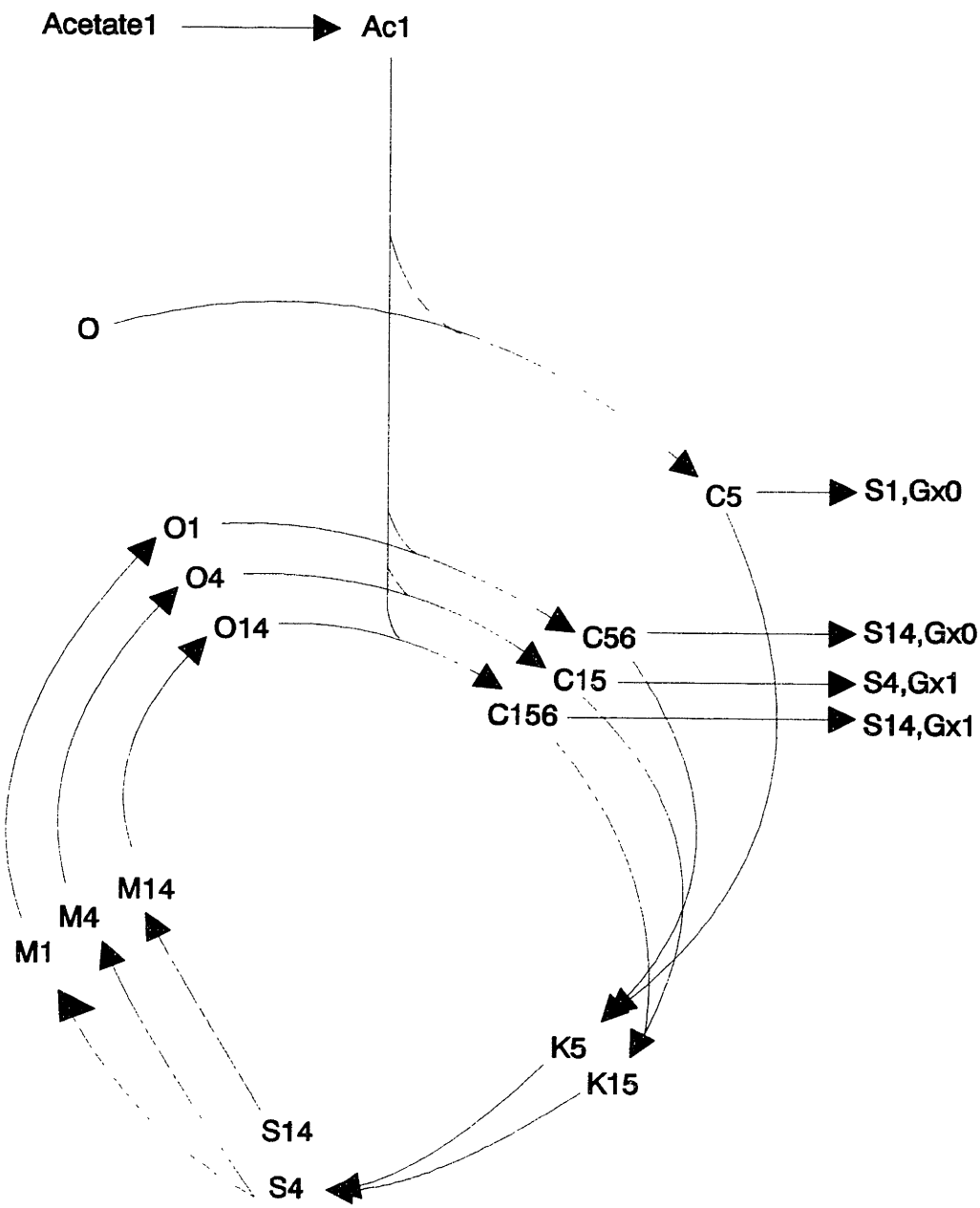

Chapter 6: Effect of The Tricarboxylic Acid Cycle on Metabolite Labeling. II. Applications

6.1 Introduction

In the previous paper (Chapter 5), we presented a rigorous mathematical model for the derivation of isotopomer distributions in specific networks. In particular, the distribution of ^{13}C label was obtained for the isotopomers resulting from pyruvate utilization via the tricarboxylic acid (TCA) cycle and the gluconeogenic pathway. In addition, isotopomer distributions resulting from acetate utilization as a result of three different models of acetate catabolism were presented. It was shown how the results of this modeling approach can be used to extend the amount of information that can be extracted from typical NMR spectroscopy measurements. Specifically, it was noted that, besides the usual carbon enrichment data, isotopomer molecular weight distributions as well as fine structure of NMR data at specific carbon positions can be very informative about metabolic fluxes and the role they play in meeting biosynthetic and energetic requirements.

In this paper we apply the theoretical model to the investigation of nine different examples obtained from the literature. First, we verify our modeling results through comparison with experimental data. Following verification the model is applied to the analysis of several specific cases reported in the literature. Special emphasis is given to the errors associated with the incorrect accounting for possible label scrambling via the TCA cycle

6.2 Model Verification

6.2.1 Pyruvate Utilization in Mammals

The validity of our modeling concept can be tested by comparing our results with experimental data. Chance *et al.* [1983] perfused rat heart tissue with [3-^{13}C]pyruvate and obtained a ^{13}C NMR spectrum which shows resonances and line splittings of the C-2, C-3, and C-4 carbons of glutamate (Figure 6.1). The glutamate C-2 resonance is split into nine-lines (centered at 55.5 ppm), C-4 is split into three-lines (centered at 34.2 ppm), and

C-3 is split into five-lines (centered at 27.8 ppm). The line splittings are caused by ^{13}C-^{13}C spin coupling among carbon atoms. Occurrence of multiple patterns is consistent with our predictions of different isotopomer species as presented in Figure 6.2. The relative distribution of glutamate isotopomer species that determine the line intensity are functions of two variables, x, the proportion of OAA entering the TCA cycle, and y, the proportion of bicarbonate labeled with $^{13}CO_2$. These variables are roughly estimated from Figure 6.2 to be: $x = 0.3$ and $y = 0.3$. The nine-lines splitting at C-2 is the sum of a singlet due to G_{24}, a doublet with coupling constant J_{12} due to G_{124}, a doublet with coupling constant J_{23} due to G_{234}, and a quartet due to G_{1234}. Two different doublets occur as a result of the difference in the coupling constants between J_{12} (53.5 Hz) and J_{23} (34.6 Hz). Also the line splitting at C-2 due to G_{1234} is a quartet because of this difference whereas the line splitting at C-3 due to G_{1234} is a triplet with an intensity ratio 1:2:1 due to the similar values of J_{23} and J_{34}. The intensity of each line is proportional to the isotopomer concentration normalized by the number of lines. Likewise, the line splitting should be five-lines at C-3, three-lines at C-4, three-lines at C-1, and none at C-5. The exact matching with the experimental data strongly supports the validity of our modeling methodology. Similar multiplet patterns in glutamate and glutamine were also obtained in isolated livers of mice perfused with [3-^{13}C]alanine by Hall *et al.* [1988].

6.2.2 Acetate Utilization in *Escherichia coli*

Our modeling result can be verified in another system. Walsh and Koshland [1985] obtained a ^{13}C NMR spectrum of purified glutamate from *E. coli* grown with [2-^{13}C]acetate as the sole carbon source (Figure 6.3). It shows a doublet at C-1, a six-lines at C-2, a triplet at C-3, and a doublet at C-4. This pattern is consistent with the operation of the glyoxylate shunt pathway (Model I) and exactly matches our prediction (Model I of Table 5.2). There is only one variable, z, that essentially determines the relative intensity of each peak and each line within each peak. z is defined as the probability of isocitrate utilized via the glyoxylate shunt pathway which Walsh and Koshland estimated to be 0.2. Even though the labeling diagram (Figure 6.6) shows the presence of up to six α-ketoglutarate isotopomers, under steady state, only two α-ketoglutarate species should be

present: K_{1234} (or G_{1234}) with a relative population $\left(\frac{z}{3-z}\right)$ and K_{234} (or G_{234}) with a relative population $\left(\frac{3-2z}{3-z}\right)$. The multiple pattern can be analyzed in a manner similar to the case of [3-^{13}C]pyruvate. Of particular interest is the pattern at C-2. Here G_{1234} should give rise to a quartet at C-2 with each line intensity $\frac{z}{4(3-z)}$ and G_{234} should give a doublet at C-2 with each line intensity $\frac{3-2z}{2(3-z)}$. Similar labeling patterns were observed in glutamate distribution by *Brevibacterium flavum* [Walker and London, 1987] and proline which also reflects exact labeling pattern of α-ketoglutarate by *E. coli* [Crawford *et al.*, 1987].

Another method of verifying the operation of glyoxylate shunt pathway in bacteria and our model is a similar experiment performed with [1-^{13}C]acetate. The glutamate isotopomer species can be obtained in terms of z. Only two species should be present: G_1 with $\left(\frac{z}{2}\right)$ and G_{15} with $\left(1-\frac{z}{2}\right)$. Therefore, enrichment of glutamate should be C-1 with 1, C-5 with $\left(1-\frac{z}{2}\right)$, and none at C-2, C-3, and C-4. This is exactly what is observed in proline synthesis by *E. coli* [Crawford *et al.*, 1987] and glutamate synthesis by *B. flavum* [Walker and London, 1987].

6.3 Applications

6.3.1 Pathway of Acetate Utilization in *Pseudomonas* AM1

Narbad *et al.* [1987] attempted to establish the absence of the glyoxylate shunt pathway in the methylotropic *Pseudomonas* AM1 strains by examining the distribution of ^{13}C label in trehalose formed from [2-^{13}C]acetate. Based on the labeling pattern of trehalose which should have reflected glucose patterns with C-1:C-2:C-3:C-4:C-5:C-6 = 35.8 : 33.86 : 24.15 : 24.43 : 37.58 : 37.0, they concluded the absence of the glyoxylate shunt pathway. This conclusion appears to be consistent with experimental observation indicating the lack of isocitrate lyase [Dunstan *et al.*; 1972a, 1972b]. However, the label enrichment data presented is consistent with our modeling prediction of simultaneous functioning of the glyoxylate shunt pathway and the TCA cycle as in the case of *E. coli*. From Table 5.2, it can be seen that three OAA isotopomers are formed. From these three

OAA species, two PEP isotopomers are derived: PEP_{23} from O_{23} and O_{234} and PEP_{123} from O_{123}. Finally in the gluconeogenic pathway with PEP as a precursor, four glucose isotopomers can be formed by the combination of two PEP isotopomers: Glu_{12456} and Glu_{12356} with a relative population $\left(\frac{3-2z}{3-z}\right)\left(\frac{z}{3-z}\right)$, Glu_{123456} with a relative population $\left(\frac{3-2z}{3-z}\right)^2$, and G_{1256} with a relative population $\left(\frac{z}{3-z}\right)^2$. Therefore, the relative intensity of C-1:C-2:C-3 = C-4:C-5:C-6 should be 1:1: $\left(\frac{3-2z}{3-z}\right)$ which is exactly what is obtained by Narbad *et al.*. This means that the glyoxylate shunt pathway can not be excluded from this *Pseudomonas* bacterium.

6.3.2 Pathway of Acetate Utilization in Mammals

Many researchers have described acetate metabolism in mammals using labeled acetate under various conditions (Table 6.1). Predominantly monitored substrates are glutamate and/or glucose. Qualitatively, with C-1 labeled acetate, the possibility of the operation of Model III can be distinguished from that of either Model I or Model II by following the carbon enrichments at glutamate or glucose (Table 5.3). With Model III, all six carbons of glucose are expected to be labeled whereas with Model I or Model II, only C-3 of glucose is labeled. Similarly with Model III, four carbons of glutamate, namely C-1, C-2, C-3 and C-5, are labeled whereas with Model I or Model II, only C-1 and C-5 are expected. The data in Table 6.1 excludes the possibility of Model III in mammals. It must be noted that with C-1 labeled C_2 metabolites, the distinction between Model I and Model II can not be made.

The same analysis can be applied with C-2 labeled acetate based on the Table 5.2. Qualitatively, all three models lead to same labeling patterns in the carbons of glutamate and glucose. Quantitatively, Model I can be differentiated from Model II. For example, the relative enrichments at C-2, C-3 and C-4 of glutamate are all equal to 1 with Model I. With Model II, only the enrichment at C-4 of glutamate is equal to 1. According to Model II, C-2 and C-3 of glutamate, and C-1 and C-2 of glucose should be labeled with intensity $\left(\frac{1-x}{1+x}\right)$. The data in the Table 6.1 supports the operation of Model II.

With C-2 labeled acetate, the distinction between Model II and Model III cannot be unequivocally established from either the qualitative or quantitative analysis of the relative enrichment data. However, the multiple pattern structure in the ^{13}C NMR spectrum should be different. If acetate is utilized solely via the acetyl-CoA conversion pathway (Model II), the resulting multiple pattern at glutamate should appear as: three-lines at C-1 consisting of a singlet due to G_{14} and G_{134}, a doublet due to G_{1234}; seven-lines at C-2 consisting of a singlet due to G_{24}, a doublet due to G_{234}, and a quartet due to G_{1234}; five-lines at C-3 consisting of a doublet due to G_{34} and G_{134} and a triplet due to G_{234} and G_{1234}; and three-lines at C-4 consisting of a singlet due to G_4, G_{14}, and G_{24} and a doublet to G_{34}, G_{134}, G_{234}, and G_{1234}. A nearly identical multiple structure is expected in Model III. The major difference is at C-2 which should be a nine-lines peak with an additional doublet due to G_{124}. This additional doublet with coupling constant J_{12} is observed by Chance *et al.* [1983] when the rat heart was perfused with [2-^{13}C]acetate (Figure 6.4). This result raises a possibility that some pathways other than the oxidation via conversion to acetyl-CoA can be involved in acetate utilization in mammals, even though the multiplet structure can be resulted by incorporating the unlabeled carbon substrates endogenously present.

6.3.3 Pathway of Propionate Utilization in *Escherichia coli*

Evans *et al.* [1993] attempted to establish the operation of dual pathways for propionate utilization in *E. coli* using ^{13}C NMR with [2-^{13}C]propionate and [3-^{13}C]propionate as the sole carbon substrate. In *E. coli*, propionate is oxidized to pyruvate which then enters the TCA cycle either as acetyl-CoA via the action of pyruvate dehydrogenase or as OAA via the sequential actions of PEP synthetase and PEP carboxylase. However, in several systems including higher organisms and a number of microorganisms such as *Propionibacterium* [Wood and Stjernholm, 1961], *Ochromonas* [Arstein *et al.*, 1962], and *Rhizobium* [De Hertogh *et al.*, 1964], the major pathway of propionate metabolism is via the propionyl-CoA carboxylation pathway. In such systems, propionate is converted to propionyl-CoA, which is then carboxylated to methylmalonyl-CoA via propionyl-CoA carboxylase, which is finally isomerized to succinyl-CoA via

methylmalonyl-CoA mutase. With [2-^{13}C]propionate, Evans *et al.* obtained a ^{13}C NMR spectrum (Figure 6.5) which shows a singlet at all five carbons of glutamate with relatively high enrichment at C-1 and C-5 positions, and low enrichment at C-4 position. They argued that if [2-^{13}C]propionate is solely utilized via the pyruvate pathway, no C-2 and C-3 of glutamate should be labeled. However, since C-2 and C-3 were also significantly labeled, it was concluded that the propionate carboxylation pathway must be operative in this bacterium. Clearly this is incorrect as the argument is made on the model that describes the label distribution for only a single turn of the TCA cycle. Instead, the labeling pattern is consistent with the sole operation of the pyruvate pathway (Table 5.1). Furthermore, in another experiment with [3-^{13}C]propionate (Figure 6.5), a labeling pattern consistent with a multiple pattern that is associated with the sole operation of the pyruvate pathway was found. Therefore, the operation of the propionate carboxylation pathway in *E. coli* cannot be substantiated with the ^{13}C NMR study.

6.3.4 Pathway of Acetone Utilization in Mammals

The metabolic pathways of acetone utilization in mammals remains unclear despite its presumed importance in diabetic ketoacidosis where large amounts of acetone, along with acetoacetate and 3-hydroxybutyrate, accumulate in the body fluids [Sulway and Malins, 1970; Owen *et al.*, 1982]. Another important question associated with acetone met· olism is how much energy can be derived from acetone during fasting in order to prolong survival. Reichard *et al.* [1979] calculated that up to 11% of the glucose can be derived from acetone during starvation in humans. Previously acetone was considered a non-metabolizable end product of lipid metabolism that accumulates when there are insufficient glycolytic intermediates to effect the complete oxidation of the acetyl-CoA generated in the metabolism of fatty acid. Sakami and Lafaye [1951] proposed two pathways for acetone metabolism in mammalian systems (Figure 6.6). One pathway involves the conversion of acetone to 1,2-propanediol which is then cleaved into acetate (C_2 metabolite) and formate. Acetate is then further oxidized via the pathway in Model II (Figure 5.2). The other pathway allows for acetone conversion into C_3 metabolites,

namely pyruvate, hydroxyacetone, propanediol, hydroxypyruvate, lactaldehyde, lactate or their phosphorylated derivatives as possible intermediates.

To delineate which of the two acetone pathways (Figure 6.6) is active in acetone metabolism, many researchers used [^{14}C]acetone and followed label incorporation in glucose and glutamate. Casazza *et al.* [1984] proposed the conversion of acetone into methylglyoxal and 1,2-propanediol with lactate as an intermediate. Based on findings that there was no carbon label incorporation from [2-^{14}C]acetone into lactate and 3-hydroxybutyrate but significant label incorporation in C-1 of free acetate, Gavino *et al.* [1987] claimed that in perfused rat livers, acetone metabolism proceeds mainly via the "acetate" pathway. Kosugi *et al.* [1986], based on a study with [2-^{14}C]acetone in humans, claimed the simultaneous operation of both "lactate/methylglyoxal" and "acetate" pathways. They also claimed that the extent to which either pathway is utilized is based on the concentration of acetone infused, not the dietary state or the prior exposure to acetone. They found that when trace quantities were administered, only small equal percentages of ^{14}C were found in C-3 and C-4 of glucose and large percentages were distributed equally in C-1, C-2, C-5, and C-6 of glucose. However, upon infusion of large quantities of [2-^{14}C]acetone, the reverse effect was found: large percentages were found in C-3 and C-4 and small percentages were found in C-1, C-2, C-5, and C-6 of glucose. Since the conversion of [2-^{14}C]acetone to [1-^{14}C]acetate will label exclusively C-3 and C-4 of glucose (Table 5.3, Model II) whereas the conversion to [2-^{14}C]lactate will label all six carbons of glucose (Table 5.2), Kosugi *et al.* claimed that at high concentrations the conversion to acetate predominates whereas at low concentrations the conversion to lactate/methylglyoxal predominates. However, their data can be interpreted on the basis of the sole operation of "lactate/methylglyoxal" pathway. As shown in Figure 6.7, at a low value of x which corresponds to high TCA cycle activity, the label incorporation at C-1 and C-2 of glucose should be lower than that of C-3 of glucose, whereas the reverse is true at high value of x. A high TCA cycle activity may be invoked as a detoxification mechanism at high levels of acetone whereas at low concentrations of acetone, a low TCA cycle is needed. However, Kosugi's data clearly eliminate the possibility of the sole utilization of acetone via the "acetate" pathway.

Similar results were obtained by Reichard *et al.* [1986] who perfused small amount of [2-^{14}C]acetone into human with diabetic ketoacidosis. Consistent with Kosugi's result, at low acetone infusion, they found that in six of seven patients, 70% to 90% of ^{14}C resides in C-1, C-2, C-5, and C-6 positions. However, in one patient they found more ^{14}C incorporation in C-3 and C-4 than in C-1, C-2, C-5, and C-6 of glucose. This led them to suggest that other pathways of acetone metabolism may exist among subclasses of diabetic patients. However, it is very likely that the source of variation was the rate of the acetone utilization via the TCA cycle, not that an alternate pathway was involved. This particular patient carried a hypertensive cardiovascular disease which is normally associated with high TCA cycle activity.

Thus, based on the acetone labeling study in mammals, (1) the possibility of acetone utilization solely via the 'acetate" pathway can be eliminated, (2) the possibility that acetone utilization occurs solely via the "lactate/methylglyoxal" pathway is consistent with carbon label experimental data, and (3) the concentration of acetone determines the rate of conversion by effecting different rates of the TCA cycle.

6.3.5 Glyoxylate Shunt Pathway vs. TCA Cycle in Bacteria

The value of z, indicating the fraction of isocitrate converted via the glyoxylate shunt pathway, can be determined by three independent methods involving the use of GC-MS and ^{13}C NMR. First, as done by Walsh and Koshland, the relative enrichment at C-1 of glutamate can be used. This approach requires additional measurement of known standards in order to establish the calibration required for converting the absolute peak intensity into relative enrichment. Secondly, within the C-2 peak, the ratio of quartet (Q) to doublet (D) can be used to find the value of z: $\frac{Q}{D}=\frac{z}{2(3-2z)}$. Thirdly, GC-MS, measuring the fractions of the same metabolite with different molecular weights differentiated by one atomic mass unit, can be used. In the example of Walsh and Koshland, GC-MS should produce two peaks for glutamates, one corresponding to molecular weight (M + 3), and another corresponding to (M + 4), where M represents the molecular weight of glutamate

with all its carbons being ^{12}C. The glutamate species, G_{234}, has a molecular weight of (M + 3) since its C-2, C-3, and C-4 positions are ^{13}C and G_{1234}, has a molecular weight of (M + 4). Therefore the ratio of the (M + 3) to (M + 4) species is $\frac{(M+3)}{(M+4)} = \frac{z}{3-2z}$.

Similarly, in the case of [1-^{13}C]acetate, the value of z can be obtained in two different ways: One from the ^{13}C NMR measurement of relative enrichment at each carbon and the GC-MS measurement of the ratio of (M + 2) to (M + 1).

6.3.6 Determination of Flux of Pyruvate Carboxylase vs. Flux of Citrate Synthase

Cohen [1987] proposed the following formula to estimate the ratio of pyruvate carboxylase (PC) activity to pyruvate dehydrogenase (PDH) activity with a ^{13}C labeled three-carbon substrate:

$$\frac{V_{PC}}{V_{PDH}} = \frac{\text{C-2 of glutamate} + \text{C-3 of glutamate}}{\text{C-4 of glutamate}} \qquad \textbf{(Eq. 6.1)}$$

With a C-2 labeled three-carbon substrate, the formula was modified by Jans and Willem [1989] as:

$$\frac{V_{PC}}{V_{PDH}} = \frac{\text{C-2 of glutamate} + \text{C-3 of glutamate}}{\text{C-5 of glutamate}} \qquad \textbf{(Eq. 6.2)}$$

These formulas were adopted by Jans and Willem [1988, 1989] in studies of rabbit and rat renal cells of proximal convoluted tubules, Jans and Leibfritz [1988] in renal epithelial cell lines, Tran-Dinh *et al.* [1991] in *Saccharomyces cerevisiae*, Brand *et al.* [1992] in rat neuronal and glial tumor and primary cell lines. However, these formulas are based on the assumption that C-2 and C-3 of glutamate can be derived only from the C-2 and C-3 of OAA, and C-4 and C-5 of glutamate can be derived only from C-2 and C-1 of acetyl-CoA. This assumption is true only if all metabolites undergo the TCA cycle once. As can be seen in many of our labeling diagrams, carbon labels can move from C-4 and C-5 of glutamate to C-1, C-2, and C-3 of glutamate.

It should be clear how these relationships should be modified to account for multiple cycle turns following our methodology. We let x to be the proportion of OAA entering the TCA cycle via citrate synthase and $(1-x)$ as the proportion of OAA exiting the TCA cycle. It should be noted that under the steady state assumption, the flux via

citrate synthase is equal to the flux via the pyruvate dehydrogenase, and the flux via the PEP carboxykinase is equal to the flux of pyruvate carboxylase. The above ratio can be represented as:

$$\frac{V_{PC}}{V_{PDH}} = \frac{x}{1-x} \qquad \textbf{(Eq. 6.3)}$$

The expression for x can be obtained exclusively as a function of enrichment. For the C-3 labeled substrate from Table 5.1, this is equal to:

$$\text{C-2 (or C-3) of glutamate} = \frac{1}{1+x} \qquad \textbf{(Eq. 6.4)}$$

Hence,

$$\frac{V_{PC}}{V_{PDH}} = \frac{1-\text{C-2 (or C-3) of glutamate}}{2\times\text{C-2 (or C-3) of glutamate}-1} \qquad \textbf{(Eq. 6.5)}$$

Similarly, for the C-2 labeled substrate, this is related to:

$$\text{C-2 (or C-3) of glutamate} = \frac{x}{1+x} \qquad \textbf{(Eq. 6.6)}$$

$$\frac{V_{PC}}{V_{PDH}} = \frac{\text{C-2 (or C-3) of glutamate}}{1-\text{C-2 (or C-3) of glutamate}} \qquad \textbf{(Eq. 6.7)}$$

Figures 8 (a) and (b) compare the above equations with the predictions based on the Cohen's and our formulas as a function of x for C-2 and C-3 labeled substrates. It can be seen that the two predictions are exactly opposite for C-3 labeled substrates, but are qualitatively similar for C-2 labeled substrates .

The conclusions based on the use of Cohen's formula should be reexamined. For example, Tran-Dinh *et al.* [1991] observed much smaller enrichment in C-2 of glutamate but the same enrichment in C-4 of glutamate when *S. cerevisiae* is incubated with amphotericin B, a polyene fungal antibiotics and [1-^{13}C]glucose which leads to the formation of [3-^{13}C]pyruvate. Based on the use of the Cohen's formula, Tran-Dinh *et al.* concluded that amphotericin B induces a reduction in the pyruvate carboxylase activity in the mitochondria and therefore the effect of amphotericin B should be mitochondrial. However, with our formula, the data can be interpreted as a reduction in either citrate synthase or pyruvate dehydrogenase activity which means that the effect of amphotericin B should be cytosolic. A similar misinterpretation was made by Brand *et al.* [1992] who

observed a higher $\left(\frac{C\text{-}2+C\text{-}3}{C\text{-}4}\right)$ ratio in primary glial cells than neurons and concluded that there was a higher pyruvate carboxylase activity in primary glial cells than neurons. In fact, the exact opposite could be true.

6.3.7 Determination of Labeling Pattern of Glucose via Gluconeogenic Pathway

Schumann *et al.* [1991] followed the fate of carbon label of gluconeogenic substrates in order to assess the intrahepatic metabolic processes during gluconeogenesis in human. One major conclusion was that [2-^{14}C]acetate cannot be used in place of [3-^{14}C]lactate to study the TCA cycle and in relationship to gluconeogenesis. The argument was as follows. If [3-^{14}C]lactate and [2-^{14}C]acetate were metabolized in the same site, the $\left(\frac{C\text{-}1+C\text{-}2}{2\times C\text{-}3}\right)$ ratio obtained by the two substrates would be essentially the same. The observed ratios were markedly different: Magnusson *et al.* [1991] found 5.1-5.7 with [3-^{14}C]lactate and Schumann *et al.* [1991] found 1.5-1.9 with [2-^{14}C]acetate. However, following our results, this difference is expected due to two primary factors: (1) the degree of the probability of bicarbonate to be labeled is higher in the acetate oxidation and (2) lactate can be additionally utilized via the pyruvate carboxylation pathway. In essence, the difference can be attributed to the different rate of oxidation for different metabolites.

The difference in the ratio of $\left(\frac{C\text{-}1+C\text{-}2}{2\times C\text{-}3}\right)$ led Schumann *et al.* [1991] to incorrectly conclude that acetate is metabolized in a site other than a liver. This error was due to the derivation of glucose enrichment pattern from the distribution of α-ketoglutarate (α-KG). They expected

$$\text{C-1 of Glu} = \text{C-2 of Glu} = \frac{1}{2}(\text{C-3 of } \alpha\text{-KG} + \text{C-4 of } \alpha\text{-KG}) \qquad \textbf{(Eq. 6.8)}$$

and

$$\text{C-3 of Glu} = \frac{1}{2}(\text{C-2 of } \alpha\text{-KG} + \text{C-5 of } \alpha\text{-KG}) \qquad \textbf{(Eq. 6.9)}$$

(Eq. 6.8) and (Eq. 6.9) are true only if OAA is derived from α-KG. However, there is always an additional source(s) for OAA synthesis and clearly the above formulations are

always incorrect. In fact, the data of [2-^{14}C]acetate can be explained on the basis of acetate utilization in a single site, the liver and therefore can be used to follow liver metabolism.

6.4 Conclusion

It must be apparent that the ^{13}C or ^{14}C data provides unique information about tissue metabolism in a continuous, noninvasive manner. But this can be realized only if the data is analyzed and interpreted within a proper framework. We have constructed a mathematical model to describe the isotopomer distribution via the TCA cycle and gluconeogenic pathway. Our present modeling approach is similar to the earlier models in that each isotopmer species is treated as distinct, independent variable constrained by the topology of enzymatic reactions. In addition, metabolite labeling resulting from multiple TCA cycle turns has been accounted. Steady state expressions for the distribution of isotopomer species are obtained exclusively in terms of flux variables. Based on the isotopomer analysis, we have illustrated several ways to extract the relevant and useful information from the labeling studies. In the case of monitoring with the ^{13}C NMR, we have shown how our results can be used in interpreting the complex multiplet pattern of peaks that can be only uniquely determined by the ^{13}C NMR. Alternatively, we have shown a rigorous way of determining the flux values from the ^{13}C NMR and GC-MS measurements.

Our modeling results are compared to several published experimental data involving different labeled substrates in order to validate our modeling methodology and shown to fit well with the data. These results were extended to question the validity of conclusions which were built upon the simplified model that does not properly account for all the possible effect of label scrambling via the TCA cycle. These have led us to conclude: (1) there exists the glyoxylate shunt pathway in *Pseudomonas* AM1 strain, (2) there is no evidence of propionate carboxylating pathway in *E. coli*, and (3) acetone utilization in mammals solely via the "lactate/methylglyoxal" pathway is consistent with the labeling data.

6.5 Nomenclature

G	glutamate
Glu	glucose
K, α-KG	α-ketoglutarate
O, OAA	oxaloacetate
PC	pyruvate carboxylase
PDH	pyruvate dehydrogenase
PEP	phosphoenolpyruvate
TCA	tricarboxylic acid cycle
V_i	flux through enzyme i
x	probability of oxaloacetate to exit the TCA cycle
(1 - x)	probability of oxaloacetate to enter the TCA cycle
z	probability of isocitrate to be utilized via the GS pathway
(1 - z)	probability of isocitrate to be utilized via the TCA cycle

6.6 References

Antony, G.J., Landau, B.R. (1968). Relative contribution of α-, β-, and ω-oxidative pathways to in vitro fatty acid oxidation in rat liver. *J. Lipid. Res.* **9**: 267-270.

Arstein, H.R.V., White, A.M. (1962). The function of vitamin B_{12} in the metabolism of propionate by the protozoan *Ochromonas malhamensis*. *Biochem. J.* **83**: 264-270.

Brand, A., Engelmann, J., Leibfritz, D. (1992). A ^{13}C NMR study on fluxes into the TCA cycle of neuronal and glial tumor cell lines and primary cells. *Biochmie* **74**: 941-948.

Casazza, J.P., Felver, M.E., Veech, R.L. (1984). The metabolism of acetone in rat. *J. Biol. Chem.* **259**: 231-236.

Cohen, S.M. (1987). ^{13}C NMR study of effects of fasting and diabetes on the metabolism of pyruvate in the tricarboxylic acid cycle and of the utilization of pyruvate and ethanol in lipogenesis in perfused rat liver. *Biochem.* **26**: 581-589.

Crawford, A., Hunter, B.K., Wood, J.M. (1987). Nuclear magnetic resonance spectroscopy reveals the metabolic origins of proline excreted by an *Escherichia coli* derivative during growth on [^{13}C]acetate. *App. Environ. Microbiol.* **53**: 2445-2451.

De Hertogh, A.A., Mayeux, P.A., Evans, H.J. (1964). The relationship of cobalt requirment to propionate metabolism in *Rhizobium*. *J. Biol. Chem.* **239**: 2446-2453.

Dunstan, P.M., Antony, C., Drabble, W.T. (1972). Microbial metabolism of C_1 and C_2 compounds: The involvement of glycollate in the metabolism of ethanol and of acetate by *Pseudomonas* AM1. *Biochem. J.* **128**: 99-106.

Dunstan, P.M., Antony, C., Drabble, W.T. (1972). Microbial metabolism of C_1 and C_2 compounds: The role of glyoxylate, glycollate and acetate in the growth of *Pseudomonas* AM1 on ethanol and on C_1 compounds. *Biochem. J.* **128**: 107-115.

Evans, C.T., Sumegi, B., Srere, P.A., Sherry, A.D., Malloy, C.R. (1993). [^{13}C]Propionate oxidation in wild type and citrate synthase mutant *Escherichia coli* - evidence for multiple pathways of propionate utilization. *Biochem. J.* **291**: 927-932.

Gavino, V.C., Sommas, J., Philberts, L., David, F., Garneau, M., Belair, J., Brunengraber, H. (1987). Production of acetone and conversion of acetone to acetate in the perfused rat liver. *J. Biol. Chem.* **262**: 6735-6740.

Hall, J.D., Mackenzie, N.E., Mansfield, J.M., McCloskey, D.E., Scotts, A.I. (1988). ^{13}C - NMR analysis of alanine metabolism by isolated perfused livers from C3HeB/FeJ mice infected with African Trypanosomes. *Comp. Biochem. Physiol.* **89B**: 679-685.

Hiele, M., Ghoos, Y., Rutgeerts, P., Vantrappen, G. (1989). Starch digestion in normal subjects and patients with pancreatic disease, using a $^{13}CO_2$ breath test. *Gastroenterology* **96**: 503-509.

Hill, R.J., Hobbs, D.C., Koeppe, R.E. (1958). The incorporation of non-carboxyl carbon into glutamic acid, alanine, and aspartic acid by the rat. *J. Biol. Chem.* **230**: 169-178.

Jans, A.W.H., Leibfritz, D. (1988). A ^{13}C-NMR study on the influxes into the tricarboxylic acid cycle of a renal epithelial cell line, LLC-Pk1/Cl$_4$ - The metabolism of [2-^{13}C]glycine, L-[3-^{13}C]alanine and L-[3-^{13}C]aspartic acid in renal epithelial cells. *Biochim. Biophys. Acta* **970**: 241-250.

Jans, A.W.H., Willem, R. (1988). ^{13}C -NMR study of glycerol metabolism in rabbit renal cells. *Eur. J. Biochem.* **174**: 67-73.

Jans, A.W.H., Willem, R. (1989). A ^{13}C -n.m.r. investigation of the metabolism of amino acids in renal proximal convoluted tubules of normal and streptozotocin-treated rats and rabbits. *Biochem. J.* **263**: 231-241.

Kam, W., Kumaran, K., Landau, B.R. (1978). Contribution of ω-oxidation to fatty acid oxidation by liver of rat and monkey. *J. Lipid. Res.* **19**: 591-600.

Kosugi, K., Chandramouli, V., Kumaran, K., Schumann, W., Landau, B.R. (1986). Determinants in the pathways followed by the carbons of acetone in their conversion to glucose. *J. Biol. Chem.* **261**: 13179-13181.

Narbad, A., Hewlins, M.J.E., Callely, A.G. (1989). ^{13}C -NMR studies of acetate and methanol metabolism by methylotrophic *Pseudomonas* strains. *J. Gen. Microbiol.* **135**: 1469-1477.

Owen, O.E., Trapp, V.E., Skatches, C.L., Mozzoli, M.A., Hoeldtke, R.D., Boden, G., Reichard, G.A. (1982). Acetone metabolism during diabetic ketoacidosis. *Diabetes* **31**: 342-348.

Reichard, G.A., Haff, A.C., Skutches, C.L., Paul, P., Holroyde, C.P., Owen, O.E. (1979). Plasma acetone metabolism in the fasting human. *J. Clin. Invest.* **63**: 619-626.

Reichard, G.A., Skutches, C.L., Hoeldtke, R.D., Owen, O.E. (1986). Acetone metabolism in humans during diabetic ketoacidosis. *Diabetes* **35**: 668-674.

Sakami, W., Lafaye, J.M. (1951). The metabolism of acetone in the intact rat. *J. Biol. Chem.* **193**: 199-203.

Schumann, W.C., Magnusson, I., Chandramouli, V., Kumaran, K., Wahren, J., Landau, B.R. (1991). Metabolism of [2-^{14}C]acetate and its use in assessing hepatic Krebs cycle activity and gluconeogenesis. *J. Biol. Chem.* **266**: 6985-6990.

Sulway, M.J., Malins, J.M. (1970). Acetone in diabetic ketoacidosis. *Lancet* **1**: 736-740.

Tran-Dinh, S., Hervé, M., Lebourguais, O., Jerome, M., Wietzerbin, J. (1991). Effects of amphotericin B on the glucose metabolism in *Saccharomyces cerevisiae* cells - Studies by ^{13}C -, ^{1}H-NMR and biochemical methods. *Eur. J. Biochem.* **197**: 271-279.

Walker, T.E., London, R.E. (1987). Biosynthetic preparation of L-[^{13}C]- and [^{15}N]glutamate by *Brevibacterium flavum*. *App. Environ. Microbiol.* **53**: 92-98.

Walsh, K., Koshland, D.E. (1984). Determination of flux through the branch point of two metabolic cycles-The tricarboxylic acid cycle and the glyoxylate shunt. *J. Biol. Chem.* **259**: 9646-9654.

Wood, H.G., Stjernholm, R. (1961). Transcarboxylase, II. Purification and properties of methylmalonyl-oxaloacetic transcarboxylase. *Proc. Natl. Acad. Sci. USA* **47**: 289-303.

Table 6.1 Distribution of ^{14}C in the carbons of glutamate or glucose with ^{14}C labeled C-2 metabolites.

Substrate	Carbon Position						References
	C-1	C-2	C-3	C-4	C-5	C-6	
[1-^{14}C]Acetate [1]	3	7	48	100	1	1	Antony and Landau, 1968
[1-^{14}C]Acetate [2]	1	2	65	100	2	1	Kam *et al.*, 1978
[1-^{14}C]Ethanol [3]	28.0		0.0		71.8		Schumann *et al.*, 1991
[2-^{14}C]Acetate [4]	57	57	16	23	94	100	Antony and Landau, 1968
[2-^{14}C]Acetate [5]	12.1	21.3	22.7	42.9	1.0		Schumann *et al.*, 1991
[2-^{14}C]Acetate [6]	18.5	18.8	11.4	11.9	19.3	20.4	Schumann *et al.*, 1991
[2-^{14}C]Acetate [7]	11.0	23.6	24.4	37.8	1.9		Hill *et al.*, 1958
[2-^{14}C]Acetate [8]	73.7	68.3	15.3	16	100	92.3	Kam *et al.*, 1978

[1] ^{14}C specific activity in glucose normalized by specific activity in C-4 of glucose from rat liver.

[2] ^{14}C specific activity in glycogen normalized by specific activity in C-4 of glucose from 72-h fasted monkey liver slices

[3] % in carbons of glutamate from urinary phenylacetylglutamine. One sample at time 3-6 h.

[4] ^{14}C specific activity in glucose normalized by specific activity in C-6 of glucose from rat liver.

[5] % in carbons of glutamate from urinary phenylacetylglutamine. Average of four samples at time 4.5-6 h.

[6] % in carbons of glucose in blood. Average of four samples at time 6 h.

[7] % in carbons of glutmate from rat carcuss.

[8] ^{14}C specific activity in glycogen normalized by specific activity in C-4 of glucose from 72-h fasted monkey liver slices. Average of three samples.

Figure 6.1 Observed multiplet pattern of glutamate with [3-13C]pyruvate (adopted from Chance *et al.*,1983). The value of x is estimated to 0.3. The numbers in parenthesis is the total relative enrichment. The intensity of each line within the multiplet should be the relative enrichment normalized by the number of lines.

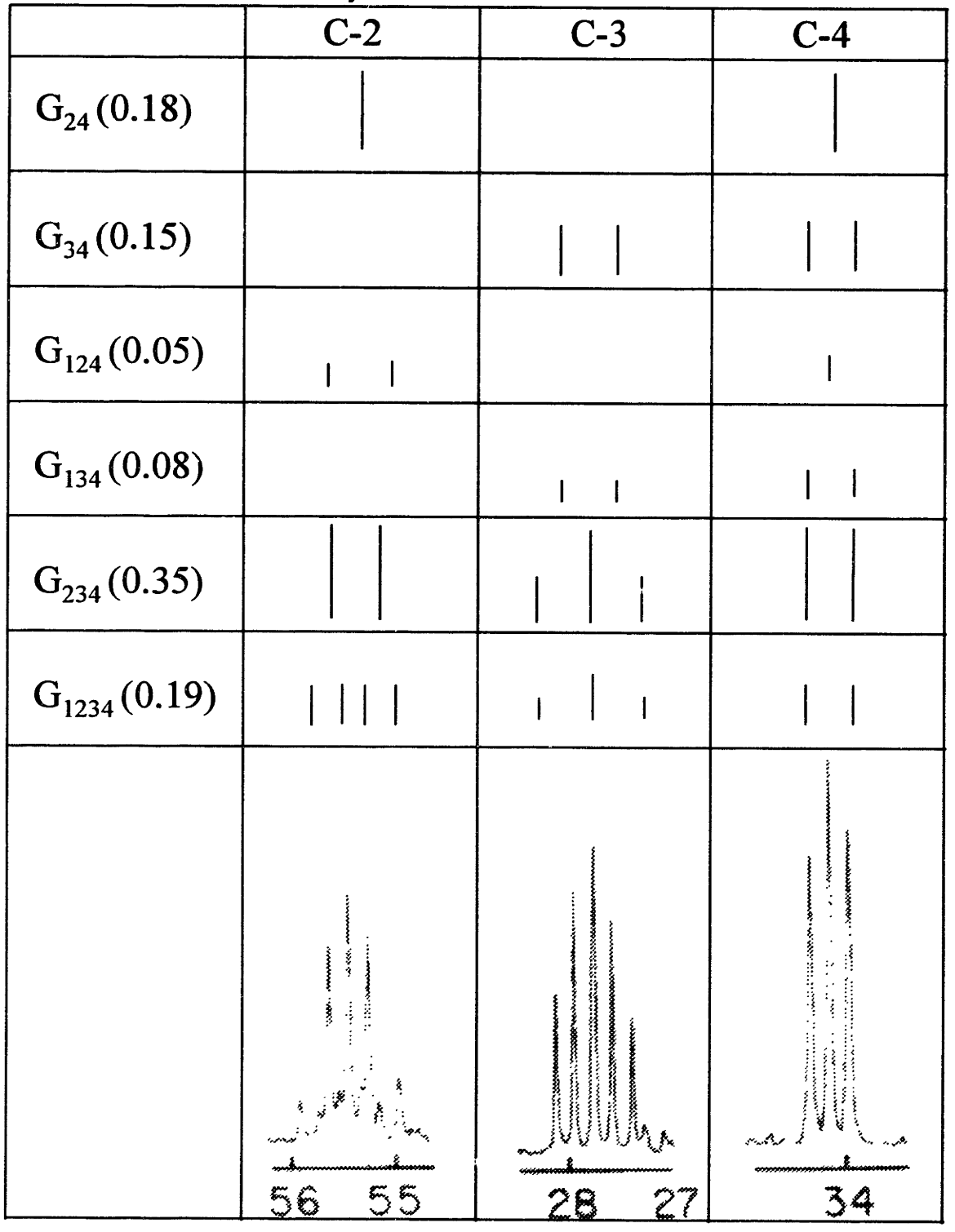

Figure 6.2 Distribution of α-ketoglutarate isotopomers as a function of x for the case of [3-^{13}C]pyruvate. Only six species are present and y is obtained exclusively as a function of x by assuming that there are no other reactions which generate CO_2.

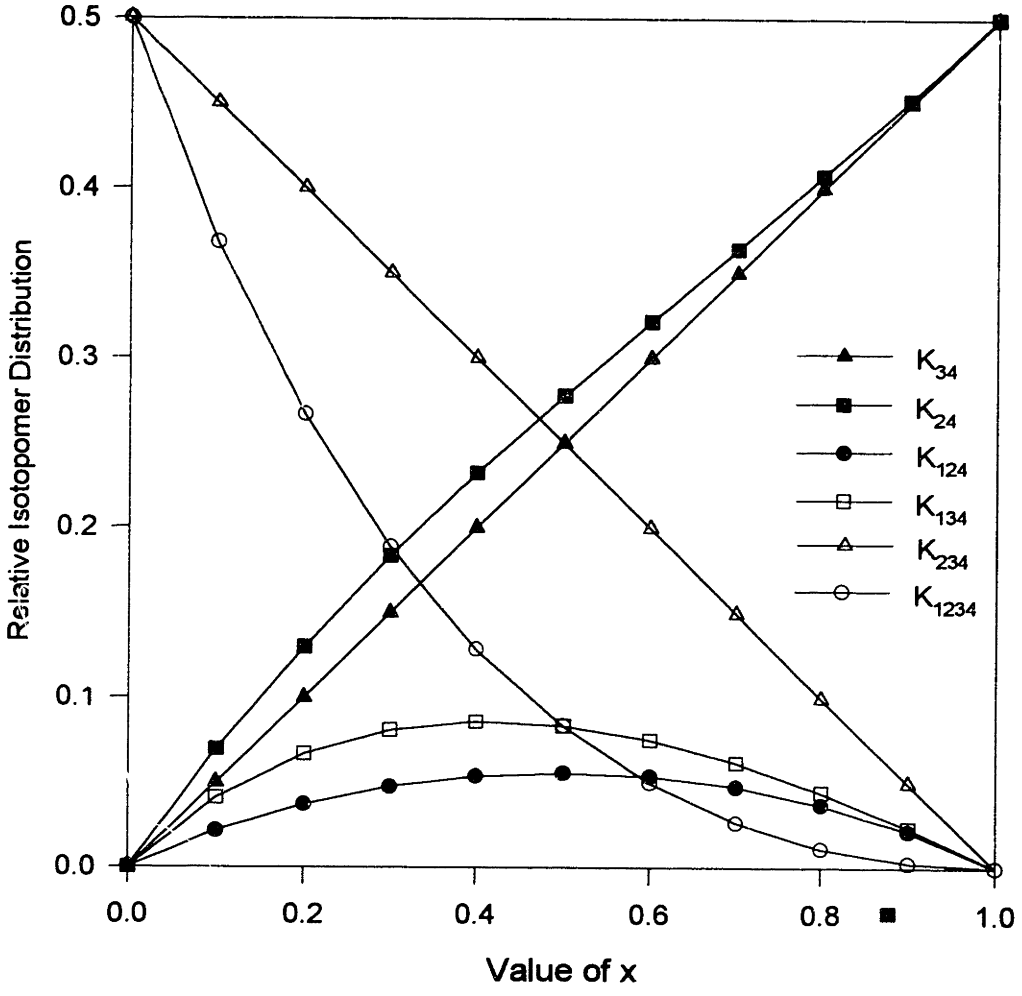

Figure 6.3 Observed glutamate multiplet patterns with [2-^{13}C]acetate (adopted from Walsh and Koshland, 1984). Peak at C-2 is a six-lines consisting of a doublet due to G_{234} with each line intensity 0.4 and a quartet due to G_{1234} with each line intensity 0.05 since the value of z is determined to be 0.2.

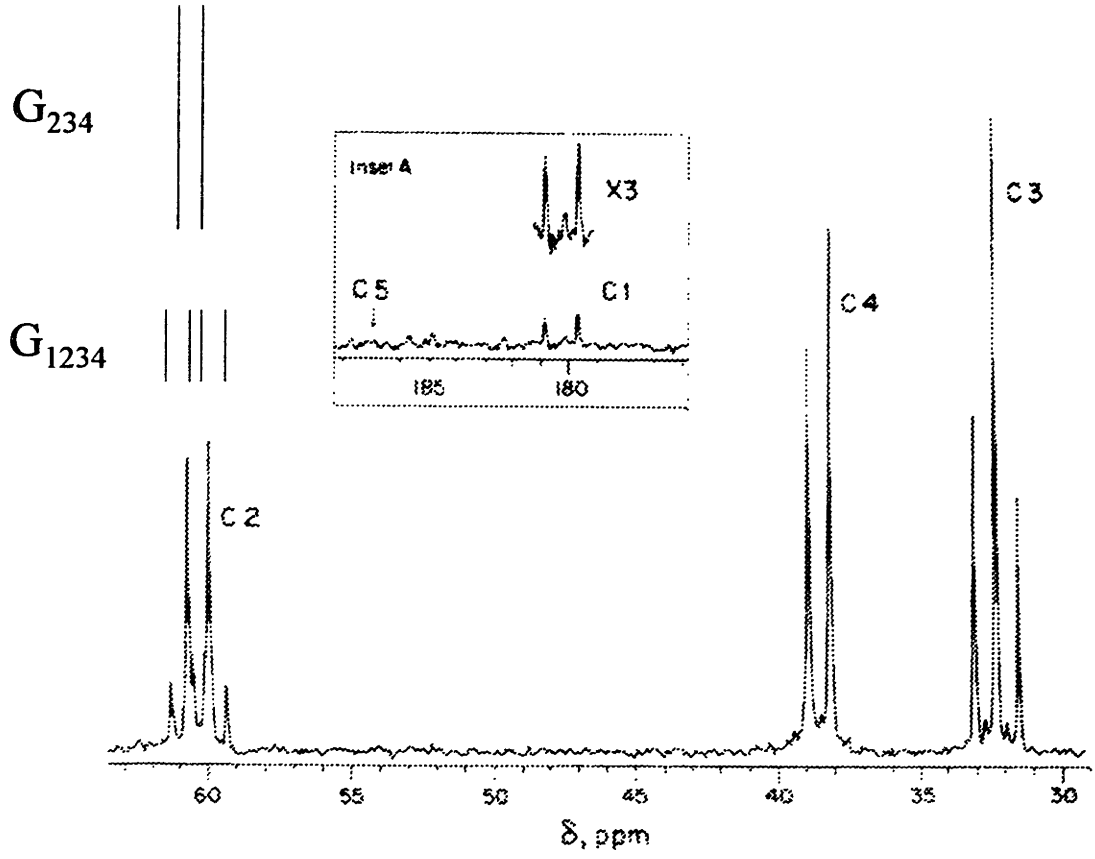

Figure 6.4 Observed multiplet pattern at C-2 of glutamate with [2-^{13}C]acetate (adopted from Chance *et al.*, 1983).

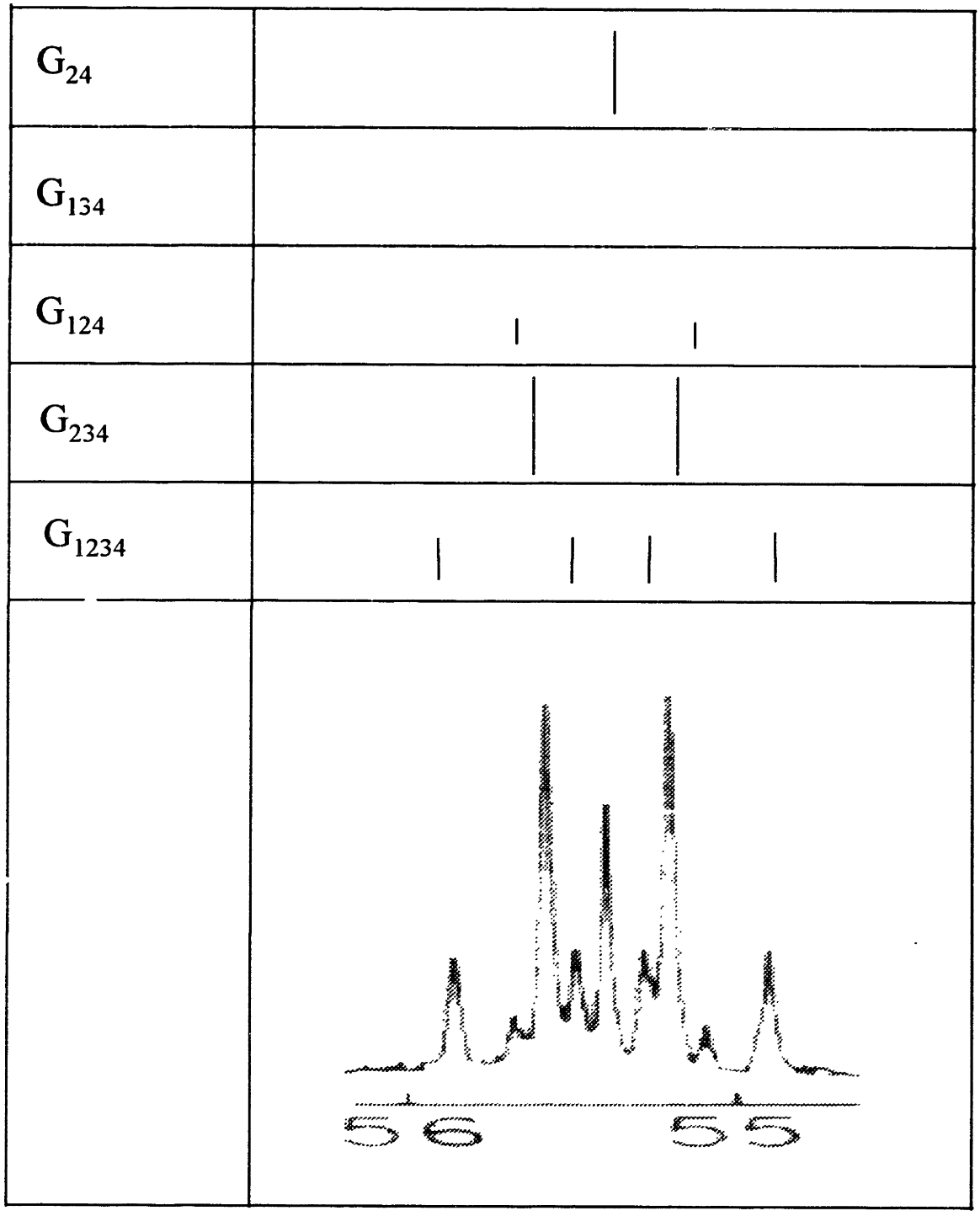

Figure 6.5 Glutamate multiplet pattern observed in *Escherichia coli* with [2-^{13}C]propionate (top) and [3-^{13}C]propionate (bottom) (adopted from Evans *et al.*, 1993).

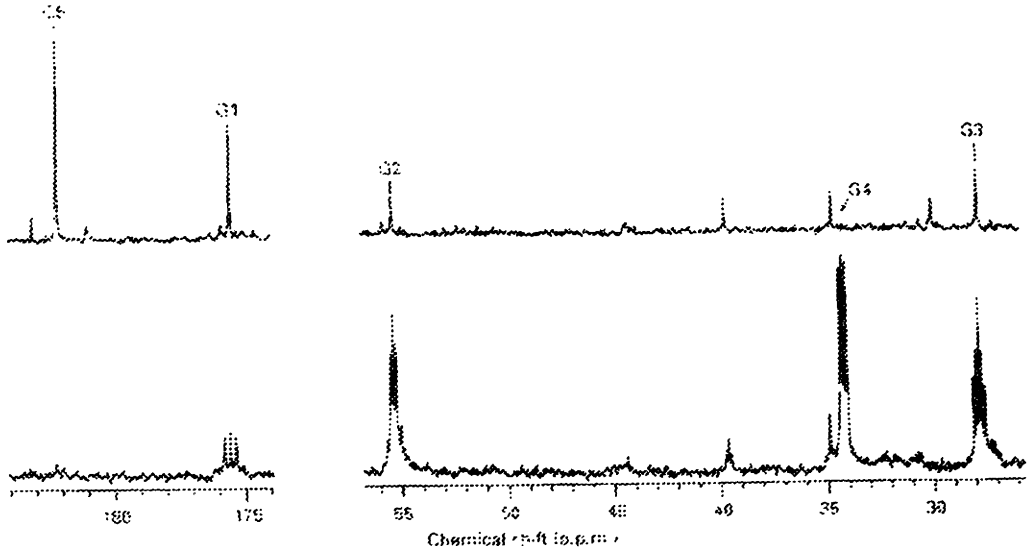

Figure 6.6 Postulated pathways in the conversion of acetone to glucose (adopted from Kosugi *et al.*, 1986): (1) involving C_3 metabolites such as methylglyoxal, D-lactate, L-lactate and L-lactaldehyde, and (2) involving C_2 metabolite, acetate.

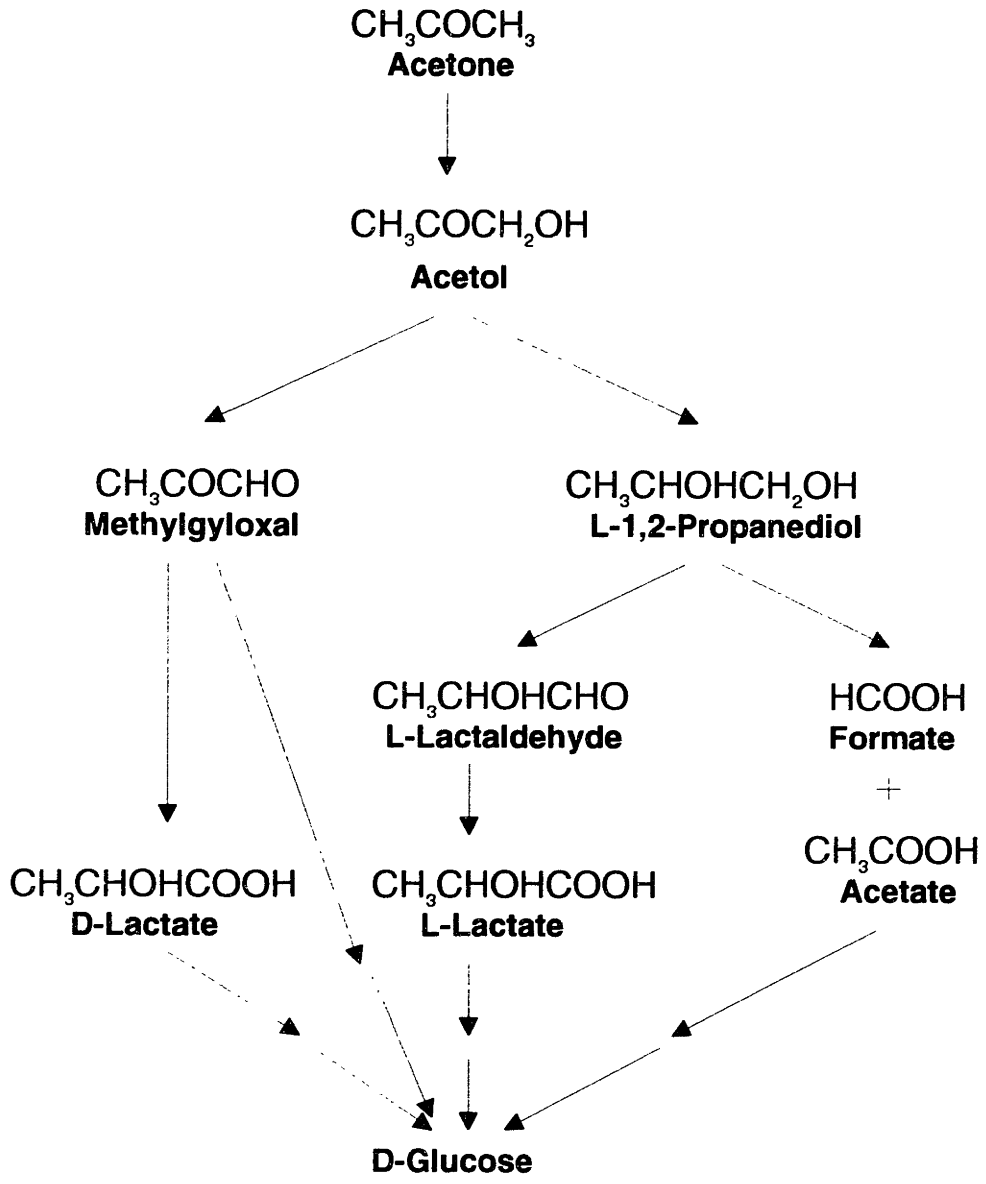

Figure 6.7 Carbon enrichment in glutamate and glucose with [2-^{13}C]pyruvate as a function of x. The enrichments at C-1 and C-2 of glucose and C-2 and C-3 of α-ketoglutarate are same and represented as a solid line. The enrichments at C-3 of glucose and C-1 of α-ketoglutarate are same and represented as a dotted line.

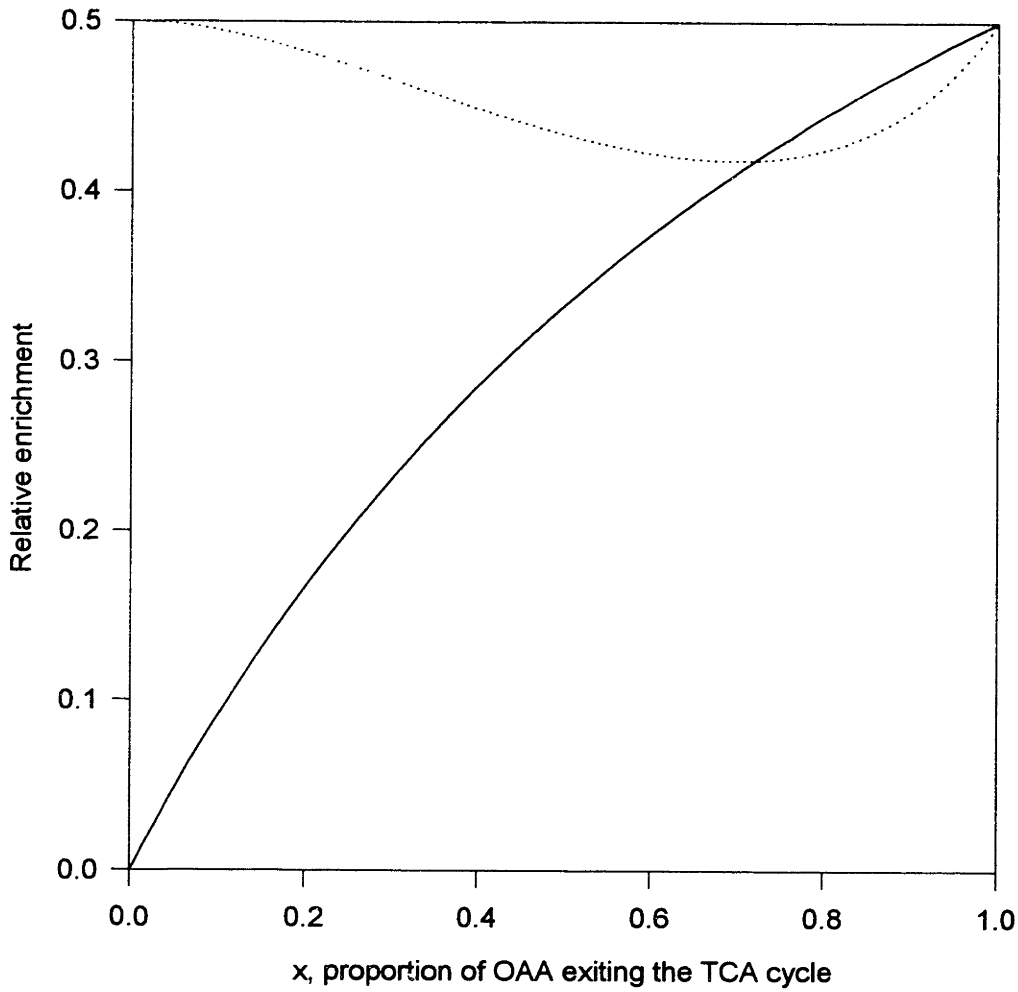

Figure 6.8 Prediction of the ratio of V_{PC}/V_{PDH} as a function of x according to Cohen's and our formulas: (a) [3-^{13}C]pyruvate and (b) [2-^{13}C]pyruvate.

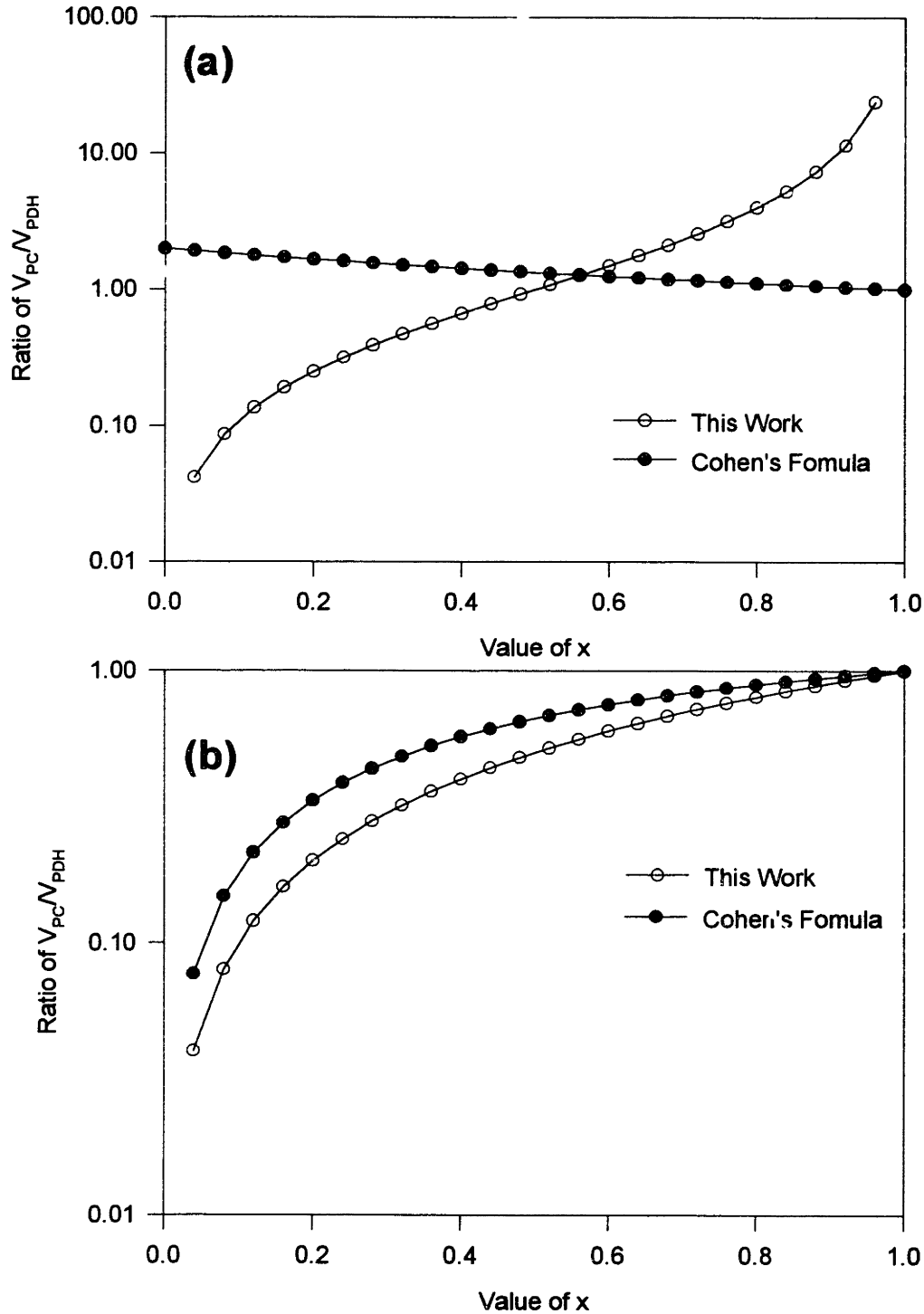

Chapter 7: Effect of Metabolic Cycle on Metabolite Labeling. II: The Pentose Phosphate Pathway

7.1 Summary

The utilization of a mathematical method to determine isotopic label distributions in metabolic pathway intermediates is critical for the implementation of a strategic experimental design. This methodology can be used to select the properly-labeled isotopic substrate that will deliver conclusive results. We have applied a rigorous mathematical model to the analysis of carbon distribution in the pentose phosphate pathway (PPP). A comparison of theoretical labeling patterns provides solidifying evidence to validate the expanded version of the classical mode of PPP operation. In addition, we have used the results of the model (1) to dispel claims of the operation of a glycolytic fructose futile cycle made based solely on the carbon isotope studies and (2) to uphold that the classical PPP is operative in all tissues. In sum, this simple mathematical model proves to be a versatile and robust tool for analyzing isotopic labeling in a variety of experimental systems.

7.2 Introduction

Experiments utilizing isotopically-labeled substrates can provide a vast amount of information about complex metabolic networks. For example, the ability to monitor the distribution of ^{14}C-labeled substrates among metabolic intermediates spurred the elucidation of the tricarboxylic acid cycle, the Calvin photosynthetic pathway, and the pentose phosphate pathway (PPP). The technique of radiolabeling has also been used to calculate reaction flux rates through metabolic pathways [Blum and Stein, 1982]. With the advent of the superconducting magnet, stable isotopic labeling has emerged as a safe, noninvasive diagnostic tool for tracing metabolic pathways as well as for detecting enzymatic disorders in glycolytic and gluconeogenic pathways [Kalderon *et al.*, 1986, 1989, 1990; Gopher *et al.*,1990]. Unfortunately, the lack of a rigorous mathematical method to calculate label distributions in network metabolites has often resulted in misleading conclusions based on intuition or simplified reaction schematics which

invalidate the premise of the undertaken study. The lack of the proper analytical tools has been particularly evident in the case of cyclic pathways where intermediates can reenter the cycle and lead to a number of different labeling patterns.

We have designed a modeling methodology to study label distribution through the simultaneous operation of the cyclic PPP and the glycolytic or gluconeogenic pathways. Previous attempts to study label distributions in the pentose pathway have been based on the simple input-output model proposed by Katz and Wood [1960] and Wood *et al.* [1960] where they assumed no recycle of intermediates to triose-3-phosphate. Subsequently, there have been many inconsistencies between the experimental data and theoretical predictions. These inconsistencies provoked the proposition of alternate pathways in order to reconcile the experimental and theoretical differences. However, as will be demonstrated in this paper, the discrepancies are directly stemming from a use of condensed representation of the PPP and are not due to the incompleteness or inadequacy in the description of the pathway. An analysis following our simple and versatile approach can provide a rational basis for discriminating among the possible modes of operating pathways as well as for selecting properly labeled substrates in a strategic experimental design.

A rigorous application of the modeling methodology will be used to clarify several controversial topics related to the PPP. We will show in this paper that (1) the classical PPP contains the proper biochemistry for a thorough metabolic network analysis, (2) there is no conclusive evidence of futile cycling at fructose-6-phosphate in the glycolytic pathways of organisms discussed in the literature, (3) there is yet no conclusive evidence to prove reversibility of the transaldolase and transketolase reactions *in vivo* and (4) a deterministic mathematical model is a robust design tool that is useful for selecting the proper isotopic substrates and analyzing label distributions in product metabolites when carrying out an isotopic labeling experiment.

7.3 Background: The Classical vs. "L-type" Pentose Phosphate Pathway

The classical PPP and glycolytic pathways are shown in Figure 7.1. The PPP fulfills several major functions in cellular metabolism including (1) the synthesis of ribose-

5-phosphate, which is required to synthesize nucleotide and nucleic acids, and (2) the generation of NADPH reducing equivalents. Other intermediates in the pathway can serve as precursors for cellular constituents. For example, erythrose-4-phosphate is a backbone component of the aromatic amino acids, and sedoheptulose-7-phosphate is required for cell wall synthesis [Wood, 1985].

The classical PPP was illuminated in the early 1950's by using ^{14}C isotopic substrates (see Williams *et al.* [1987] for review of development). However, Williams *et al.* found inconsistencies between several sets of published data and the proposed labeling scheme. Williams and co-workers subsequently proposed the modified "L-type" form of the PPP shown in Figure 7.2. The "L-type" pathway was only partially successful in explaining the inconsistent data. Although both groups employed a series of different labeled substrates to provide supporting evidence [Scofield *et al.*, 1985; Magnusson *et al.*, 1988], neither could conclusively substantiate their claim on the correct pathway. The source of difficulty for both schools is that the analysis was made on the simplified model developed by Katz and Wood which lumps several sets of reactions in the network into a single reaction, as shown in Figure 7.3. Thus, via the PPP, three molecules of hexose-6-phosphate will form two molecules of hexose-6-phosphate (two fructose-6-phosphates in the classical case and one each of glucose-6-phosphate and fructose-6-phosphate in the "L-type" case), one molecule of triose-3-phosphate (glyceraldehyde-3-phosphate in the classical case and dihydroxyacetone phosphate in the "L-type" case) and three molecules of carbon dioxide.

Implicit in the lumping assumption is a strict assignment of carbon isotopic labeling for the newly formed hexose-6-phosphate and triose-3-phosphate metabolites. In the simplified classical pathway shown in Figure 7.3, one of the two hexose-6-phosphate products will have a labeling pattern with C-1, C-2, C-3 positions derived exclusively from carbon C-2, C-3, C-2 positions of glucose-6-phosphate, respectively, and the other will be derived from C-2, C-3, C-3 positions of glucose-6-phosphate C-1, C-2, C-3 positions of triose-3-phosphate will originate from C-4, C-5, C-6 positions of glucose-6-phosphate, respectively. The simplified labeling scheme is summarized in Figure 7.4 for the case of the the "L-type" pathway. In both cases, label distribution due to participation of labeled

intermediates such as pentose-5-phosphates, erythrose-4-phosphate, seduheptulose-7-phosphate, and glyceraldehyde-3-phosphate, is entirely ignored. This simplification has resulted in serious qualitative and quantitative errors in interpreting the labeling data derived from hexose or pentose substrates.

A completely different situation prevails if one considers the realistic case in which all the intermediates shown in Figures 7.1 and 7.2 are accounted for in calculating carbon label redistribution. Varying degrees of isotopic labeling will appear in intermediates due to recycling from a common pool of metabolites. A systematic methodology similar to the one described in Chapter 5 can be used to calculate the degree of label distribution in any intermediate when the substrate labeling pattern is known.

7.4 Model Development

7.4.1 Mathematical Description of Label Distribution Using the Input-Output Method

A general methodology which has been widely used to quantify flux distribution and label distribution in metabolic networks is based on the input-output method which balances the flow of carbon in specific positions of each metabolite under the assumption of metabolic and isotopic steady states. This method can be formalized by setting up two types of mass balance equations. The first set of equations describes metabolite balances:

$$\frac{dM_i}{dt} = \sum_{j=1}^{n_p} \beta_j v_j - \sum_{j=1}^{n_c} \beta_j v_j \qquad ; i = 1,\ldots,n \qquad \textbf{(Eq. 7.1)}$$

where M_i is the concentration of metabolite i (in mol/g cells), β_j is the stoichiometric coefficient of reaction step j, v_j is the reaction rate of step j (in mol/hr/g cells), and n is the number of metabolites in the metabolic network. At a metabolic steady state, (Eq. 7.1) yields a relationship among the fluxes independent of metabolite concentrations, M_i. The summations extend over all reactions producing (n_p) and consuming (n_c) the corresponding metabolite.

The second set of mass balance equations describes the rate change of label enrichment at each carbon of each metabolite. These equations characterize the carbon transfer among the metabolites involved in a reaction. Let $y_i(m)$ denote the specific

activity (if ^{14}C is used) or the fractional enrichment (if ^{13}C is used) of the *m*th carbon of metabolite i. Then

$$\frac{dM_i y_i(m)}{dt} = \sum_{j=1}^{n_p} \beta_j v_j y_i(m) - y_i(m) \sum_{j=1}^{n_c} \beta_j v_j \; ; \; i = 1,\ldots,n \; ; \; m = 1,\ldots, \; m_i \qquad \textbf{(Eq. 7.2)}$$

where m_i is the total number of carbons in metabolite i. Again, with the assumption of isotopic steady state, (Eq. 7.2) reduces to a set of algebraic equations independent of M_i's and describes $y_i(m)$ in terms of v_i's. (Eq. 7.1) and (Eq. 7.2) will be utilized to calculate label distributions in network metabolites when the pentose pathway operates according to one of four models. Model I is the simplified model of the classical PPP with the labeling scheme presented in Figure 7.3. Only three metabolite pools are included in this model. Model II, as illustrated in Figure 7.1, is the expanded version of Model I with five metabolite pools. Model III is the simplified model of the "L-type" PPP whose labeling scheme with three metabolite pools follows Figure 7.4. Model IV is the expanded version of Model III with six metabolite pools as shown in Figure 7.2. The metabolite pools of the expanded "L-type" pathway shown in Figure 7.2 include all five pools of the classical pentose pathway (where arabinose-5-phosphate is included in the X5P pool) in addition to the O8P pool which contains octoluse-8-phosphate and octoluse-1,8-bisphosphate.

Table 7.1 shows metabolite mass balance equations for the four models calculated from (Eq. 7.1). In all four cases, the degree of freedom is two. To remain consistent with previous reports, we arbitrarily choose v_0, the normalized hexose utilization rate and PC, the net fraction of hexose utilized via the PPP, as two independent variables. All other steady state fluxes can be represented in terms of these two variables as shown in Table 7.1. Note that all four models are mathematically equivalent with respect to steady state fluxes, v_i. Only by using the appropriate isotopic labeling strategies can one distinguish between the models.

Carbon balances from Model I, which describes the operation of the simplified classical pentose pathway, are described in Table 7.2 from the expansion of (Eq. 7.2). Label redistribution due to transaldolase and tranketolase reversibility can be captured by decoupling the net flux v_i into the forward flux, v_i^+, and the backward flux, v_i^-, such that

$$v_i = v_i^+ + v_i^- \qquad \textbf{(Eq. 7.3)}$$

Furthermore, the extent of the backward flux relative to the overall hexose utilization rate v_0 can be represented as α_i, where

$$\begin{aligned} v_i^+ &= (PC + \alpha_i)v_0 \\ v_i^- &= \alpha_i v_0 \end{aligned} \qquad \textbf{(Eq. 7.4)}$$

For example, consider the mass and isotopic label balances for the carbons of S7P in Model II. Suppose that there is no backward flux; then, the mass balance for S7P is

$$\frac{d[S7P]}{dt} = v_4^+ - v_5^+ \qquad \textbf{(Eq. 7.5)}$$

The carbon label balance can be calculated by multiplying the fluxes, v_i, by each of the metabolite carbons involved in the reaction. Thus

$$\frac{d}{dt}\begin{bmatrix} S7P(1) \\ S7P(2) \\ S7P(3) \\ S7P(4) \\ S7P(5) \\ S7P(6) \\ S7P(7) \end{bmatrix} = v_4^+ \begin{bmatrix} X5P(1) \\ X5P(2) \\ X5P(1) \\ X5P(2) \\ X5P(3) \\ X5P(4) \\ X5P(5) \end{bmatrix} - v_5^+ \begin{bmatrix} S7P(1) \\ S7P(2) \\ S7P(3) \\ S7P(4) \\ S7P(5) \\ S7P(6) \\ S7P(7) \end{bmatrix} \qquad \textbf{(Eq. 7.6)}$$

The reaction v_4^+ is a S7P-producing step in which carbons of 1-,2- and 1-,2-,3-,4-,5-positions of X5P are transferred into 1-,2-,3-,4-,5-,6-,7-positions of S7P, respectively. Likewise, reaction v_5^+ is a S7P-consuming step. Now suppose that there is a significant reverse reaction, and yet the net flux remains unchanged. Thus

$$\begin{aligned} v_4^+ &= (PC + \alpha_4)v_0, v_4^- = \alpha_4 v_0 \\ v_5^+ &= (PC + \alpha_5)v_0, v_5^- = \alpha_5 v_0 \\ v_6^+ &= (PC + \alpha_6)v_0, v_6^- = \alpha_6 v_0 \end{aligned} \qquad \textbf{(Eq. 7.7)}$$

(Eq. 7.6) can be written

$$\frac{d[S7P]}{dt} = (v_4^+ - v_4^-) - (v_5^+ - v_5^-) \qquad \textbf{(Eq. 7.8)}$$

The corresponding carbon label balance should be rewritten

$$\frac{d}{dt}\begin{bmatrix} S7P(1) \\ S7P(2) \\ S7P(3) \\ S7P(4) \\ S7P(5) \\ S7P(6) \\ S7P(7) \end{bmatrix} = v_4^+ \begin{bmatrix} X5P(1) \\ X5P(2) \\ X5P(1) \\ X5P(2) \\ X5P(3) \\ X5P(4) \\ X5P(5) \end{bmatrix} - v_4^- \begin{bmatrix} S7P(1) \\ S7P(2) \\ S7P(3) \\ S7P(4) \\ S7P(5) \\ S7P(6) \\ S7P(7) \end{bmatrix} - v_5^+ \begin{bmatrix} S7P(1) \\ S7P(2) \\ S7P(3) \\ S7P(4) \\ S7P(5) \\ S7P(6) \\ S7P(7) \end{bmatrix} + v_5^- \begin{bmatrix} H6P(1) \\ H6P(2) \\ H6P(3) \\ E4P(1) \\ E4P(2) \\ E4P(3) \\ E4P(4) \end{bmatrix} \quad \textbf{(Eq. 7.9)}$$

7.4.2 Model Assumptions

The model of the PPP assumes free mixing and homogenous distribution of metabolites. For example, glyceraldehyde-3-phosphate generated by the PPP is in the same metabolite pool as that generated from the glycolytic pathway. The model can be refined if the extent of compartmentalization is known. The second major assumption is that the cellular behavior can be modeled at steady state. Thirdly, any draining from the pathway for the synthesis of cellular constituents has been ignored. Although this type of dilution effect may invalidate quantitative calculations, the model would still hold for qualitative results. Fourth, we assume that there are no unlabeled endogenous metabolites which would dilute the extent of isotopic enrichment in a labeled intermediate. A significant storage of unlabeled metabolites would change our quantifiable results.

Modeled reactions are divided into three types: type I for irreversible reactions, type II for rapidly reversible reactions, and type III for conditionally reversible reactions. Examples of type I reactions are the phosphorylation of glucose to glucose-6-phosphate via hexokinase and the decarboxylation of glucose-6-phosphate to 6-P-gluconolactone via glucose-6-phosphate dehydrogenase. In addition, we assume there is no fructose futile cycling (fructose-6-phosphate $\rightarrow$fructose-1,6-bisphosphate $\rightarrow$fructose-6-phosphate), so the reaction catalyzed by phosphofructokinase is considered a type I irreversible reaction.

Reactions catalyzed by the isomerases and epimerase are assumed to be very rapid and result in complete metabolic and isotopic equilibrium (type II). Thus, in our model the pools of fructose-6-phosphate and glucose-6-phosphate will constitute a single common pool of hexose-6-phosphate (H6P). Likewise, ribose-5-phosphate, ribulose-5-phosphate, and xylulose-5-phosphate constitute the pentose-5-phosphate pool (X5P), and

dihydroxyacetone phosphate and glyceraldehyde-3-phosphate are members of the triose-3-phosphate pool (T3P).

Reactions catalyzed by transaldolase and transketolase in the non-oxidative portion of the PPP are assumed to be conditionally reversible (type III). For example, under the conditions when there is excess NADPH available, the transaldolase and/or ketolase can operate in a reversible manner to meet the cell's demand for ribose. In previous studies, these reactions were assumed to be strictly irreversible and label redistribution due to the backward reaction fluxes were not considered.

7.5 Results

By employing the four biochemical pathway models of the PPP, we can find explicit analytical solutions for the label distribution at specific metabolite carbon positions with the use of software such as Mathematica [Wolfram Research, Inc., Champaign, IL, USA] designed to manipulate symbolic operations. Steady state expressions for the six carbons of hexose-6-phosphate and the three carbons of triose-3-phosphate are given as a function of only one variable, PC, as shown in Table 7.3. For each of the four models, the input substrate is 100% enriched at [1-^{13}C]glucose. These initial results presented in Table 7.3 reflect the assumption that backwards reactions at reversible steps are negligible, i.e., $\alpha_i = 0$. Tables 7.4-7.9 show results for various hexose and pentose substrates.

Figure 7.6(a) graphically illustrates the expected carbon enrichment at C-1 and C-6 of H6P products using [1-^{13}C]hexose as a substrate under the four model cases. Although there are no significant differences among the four models at the first carbon position in the product, note that only Model II can predict the label appearance in C-6 of H6P. Labeling at hexose position C-6 can be atrributed to C-3-labeled triose participating in the transaldolase reaction: [3-^{13}C]G3P + S7P $\rightarrow$ [6-^{13}C]H6P + E4P. The appearance of label at position C-6 of H6P is a direct consequence of the operation of the expanded version of the classical PPP. The graph in Figure 7.6(b) shows that the ratio of C-6/C-1 of H6P varies as a function of PC which becomes significant with active PPP.

If we follow Model II further, Figure 7.7 depicts the isotopic label distribution in H6P and G3P using [2-^{13}C]hexose. Significant labeling is evident in C-4, C-5, and C-6

positions of H6P. As in the case of [1-^{13}C]hexose substrate, Models I, III, and IV cannot predict label distribution at C-4, C-5, and C-6 positions of H6P. Table 7.10 summarizes C-2 labeled hexose study from the literature. Consistent with our prediction, all data reported most significant labeling at C-5 and weak labeling at C-4 and C-6 as well.

Figure 7.8 shows similar result with [3-^{13}C]hexose. Again carbon label from the "top" three positions of H6P will be shuffled to the bottom "three" positions of H6P. However, unlike the case [2-^{13}C]hexose, not all three "top" three carbons are prominent at the low PC value. In fact, C-1 of H6P is insignificant compared to the "bottom" three carbons at the low PC value. Among the "bottom" three carbons, the most significant is at C-6.

Figure 7.9 shows the isotopic label distribution with [1-^{13}C]pentose which is drastically different from [2-^{13}C]hexose. The most prominent labeling should occur at C-1 and then at C-3. However, experimental results summarized in Table 7.11 is inconsistent with this prediction except the case of [1-^{14}C]xylose. It is also plausible that ribose is metabolized via pathways other than the PPP.

With [4-^{13}C], [5-^{13}C], and [6-^{13}C]hexose, no shuffling to other carbon positions are expected. However, the label will be diluted to $\frac{1}{2-PC}$. These examples illustrate the importance of selecting the proper substrate when designing isotopic labeling experiments. For example, if one is interested in measuring the reverse glycolytic flow in conjunction with the PPP, C-2 labeled substrate may not be the best choice since the labeling at the C-5 of H6P which is used as an indicator of the reverse glycolytic pathway can also arise from the PPP. However, if C-3 labeled hexose is used, C-4 of H6P can be used for the detection of the reverse glycolytic pathway whereas C-6 of H6P for the PPP. Our methodology provides a robust technique for discriminating among a wide range of substrate choices.

The effect of the transaldolase and transketolase reverse reactions can be seen in Figures 7.10 and 7.11. Results are shown for the conditions where (a) Model II is assumed to be operative, (b) the input substrate is [1-^{13}C]hexose and (c) PC is fixed either at 0.05 (Figure 7.10) or at 0.5 (Figure 7.11). The three variables α_4, α_5, and α_6 which

indicate the extent of backward flux relative to the overall hexose utilization rate are assumed to be equal to the same value, α (varying from zero to infinity on the x-axis). According to Figure 7.10, once the backward flux of these reactions becomes significant (i.e., within the order of the hexose utilization rate), the label starts to appear at all carbon positions of every intermediate. In the limit $\alpha \to \infty$, H6P(1), H6P(2) and H6P(3) will approach the asymptotic value of $\frac{1}{3}$, while H6P(4), H6P(5) and H6P(6) will approach $\frac{1-PC}{3(2-PC)}$. The same observations are evident with [2-^{13}C]hexose and [3-^{13}C]hexose substrates. However, if the substrate is labeled at C-4, C-5, or C-6 positions (the "bottom" three carbons of hexose), no label will be seen at positions other than the input position. The "bottom" three carbons do not mix with other intermediates. The asymptotic value of the label at the input position is $\frac{1}{2-PC}$ in the limit $\alpha \to \infty$ (Results not shown). These analyses clearly demonstrate the wealth of information that can be obtained by using a rigorous mathematical model for experimental design.

7.6 Discussion

7.6.1 The Classical vs. "L-type" Pentose Phosphate Pathway

A principal motivation for developing this mathematical methodology is to discriminate between the operation of the classical and "L-type" PPP in a number of biological systems. A review summarizing proponents of the classical mode is presented by Scofield *et al.*[1985], while arguments supporting the "L-type" mode are given by Williams *et al.*[1987].

One of the major discrepancies in the literature which led to this controversy is based on data derived from [2-^{14}C]glucose (Table 7.10) or [1-^{14}C]ribose substrates (Table 7.11). Although the incorporation of isotopic label into C-1 and C-3 positions of H6P from [2-^{14}C]glucose can be explained by either the simplified classical Model I or the expanded classical Model II, only Model II predicts label distribution in C-4, C-5 and C-6 positions of H6P. Several researchers [Wajngot *et al.*, 1989; Magnusson *et al.*, 1988]

attempted to explain this unexpected observation of "bottom"-labeled H6P, based on their assumption of the operation of Model I. These explanations included the possibility of reverse reactions of the glycolytic pathway (gluconeogenesis or Cori cycling), transaldolase exchange reactions combining fructose-6-P and glyceraldehyde-3-P and/or fructose futile cycling. Williams' group proposed the "L-type" pathway operation to explain this data qualitatively. Following the labeling scheme proposed by Williams, we have shown rigorously in Models III and IV that only C-2 labeling is expected in hexose products under the "L-type" operation of the pentose pathway when [2-^{14}C]glucose is used as a substrate.

In sum, the label distribution at C-4, C-5, and C-6 positions of H6P products is a direct consequence of the operation of the expanded classical PPP following Model II. Note that if reversibility of the transketolase and transaldolase reactions in the non-oxidative portion of the "L-type" PPP is considered, isotopic labeling would be distributed at other carbons as well. Unfortunately, if reversibility is considered there is no way to distinguish between the classical and "L-type" pathways based on qualitative labeling data.

One way of extending the given mathematical model is to consider the effect of using different atomic substrates to detect unique labeling patterns. For example, the isotopic distribution pattern of tritium in products derived from [2-^{3}H, 2-^{13}C]glucose is distinct from that of carbon-13. The administration of multiply-labeled substrates as well as the coadministration of numerous substrates could lead to more conclusive results in difficult cases.

7.6.2 Dispeling the Hypothesis of Fructose Futile Cycling

Fructose futile cycling occurs under the simultaneous operation of hexose bisphosphatase and phosphofructokinase in the reaction fructose-6-phosphate $\rightarrow$fructose-1,6-bisphosphate $\rightarrow$fructose-6-phosphate. Several researchers have used the detection of isotopic label at the C-6 position of H6P or its metabolic equivalents, such as glycogen or trehalose, as evidence for fructose futile cycling when [1-^{13}C] or [1-^{14}C]hexose is administered as a substrate (Table 7.9).

The rationale for the suggestion of futile cycling is based on the use of Model I. When the substrate is [1-^{13}C]hexose, the entire C-1 label will be lost as $^{13}CO_2$ by the first step in the oxidative PPP; therefore, no label will be distributed via the PPP. Subsequent regeneration of label at C-6 is thought to be a direct consequence of the reverse glycolytic flux or futile cycling. However, as shown in Table 7.1 and Figure 7.6, the operation of the classical PPPs should always result in label appearance at C-6 without the necessity of futile cycling.

There are two important considerations in assessing the presence of fructose futile cycling. First, the hexose substrate employed should be labeled at C-4, C-5 or C-6 positions to avoid interference from the PPP. Recall that these "bottom" three carbons do not shuffle via PPP activity. Magnusson *et al.*[1990] used this strategy to dismiss the notion of fructose futile cycling in humans.

The second consideration in assessing fructose futile cycling is that the metabolite monitored must be a direct indicator of futile cycling. Fructose futile cycling must be monitored by metabolites derived directly from fructose-6-phosphate as shown by the work done by Chamboost and Fraenkel [1980] This group carried out a genetic control and measured glycogen stores in *E. coli* to dismiss the notion of fructose futile cycling. Navas *et al.* [1993] reported similar results by following trehalose labeling in *S. cerevisiae*.

Note that fructose-1,6-biphosphate is not an indicator of futile cycling because it only reflects the extent of the reverse reaction between the aldolase and triose isomerase. Although Ugurbil *et al.* [1978] detected significant amounts of ^{13}C-labeling at C-6 positions of fructose-1,6-biphosphate in *E. coli* when they used [1-^{13}C]glucose as a substrate, the same group did not detect a corresponding label in the C-1 position of fructose-1,6-biphosphate when they used [6-^{13}C]glucose as a substrate [Shulman, 1979]. These results correlate directly with the operation of the classical PPP described by Model II.

7.6.3 Reversibility in the Non-oxidative Portion of the Pentose Phosphate Pathway

As shown by the graphs in Figures 7.10 and 7.11, [1-^{13}C]glucose can be used as substrate to monitor the reversibility of the transaldolase and transketolase in the PPP. If

the extent of reversibility is notable (i.e., greater than 20%), monitored hexose products will be labeled in all six carbon positions. We have monitored the appearance of trehalose labeled in every position when [1-^{13}C]glucose was fed to *Corynebacterium glutamicum* in fermentation culture (Data not shown). Based on these qualitative results, the reversibility of the transaldolase and transketolase reactions appears significant.

Schrader *et al.* [1993] attempted to measure the cycling of metabolites through the non-oxidative portion of PPP in erythrocytes using [2-^{13}C] and [3-^{13}C]glucose. They measured the appearance of ^{13}C-lactate and used the debatable assumption that lactate reflects the distribution of label in fructose-6-phosphate. Labeling at C-1, C-2, and C-3 positions of lactate served as their evidence for the operation of the reverse flux of transaldolase and transketolase. Unfortunately, this claim is not conclusive because the evidence of label at every lactate position would occur as a natural consequence of the classical PPP behaving under Model II when [2-^{13}C] and [3-^{13}C]glucose serve as substrates. Schrader's experience provides another example of how the implementation of our rigorous mathematical model can be effective in experimental design.

7.7 Conclusions

The multitude of data discussed in this paper uneqivocally supports the operation of the expanded classical PPP. The debate between the proponents of the classical versus the "L-type" PPP has been built on simplified models which created inconsistencies between the theoretical and experimental data. Our rigorous mathematical model (Model II) reconciles the experimental data with the operation of the classical pentose pathway shown in Figure 7.1.

The extent of fructose futile cycling is dependent on the relative activity of the PPP and cannot be accurately determined by using a C-1 labeled hexose substrate alone. Controlled experiments carried out with C-4, C-5, and C-6-labeled hexose substrates demonstrate that futile cycling is negligible in *E. coli* and *S. cerevisiae* under the conditions studied. There is no conclusive evidence to suggest that fructose futile cycling exists in any of the organisms reviewed.

Experimental data suggests that there is a considerable reverse flux in the pentose pathway transaldolase and transketolase reactions. In contrast to the investigation of fructose futile cycling, the preferred substrate for analysis of reversibility in the non-oxidative portion of the PPP is C-1-labeled hexose.

All in all, a steady state mathematical analysis can be an invaluable tool for answering a wide range of questions related to the determination of isotopic distributions in labeled products. This predictive technique can be used as a guide for selecting the proper substrates for a rational experimental design. Finally, a rigorous mathematical model is essential for distinguishing among a number of operative modes in a metabolic network of reactions.

7.8 Nomenclature

α_i	extent of backward flux in enzyme i
β_i	stoichiometric coefficient of reaction step i
H6P	hexose 6-phosphate
PC	net fraction of hexose utilized via PPP
PPP	pentose phosphate pathway
T3P	triose 3-phosphate
v_0	flux via hexose import system
v_i	flux through enzyme i

7.9 References

Blum, J.J., Stein, R.B. (1982). On the analysis of metabolic networks. pp. 99-125 In: *Biological regulation and development.* R. F. Goldberger, K. R. Yamamoto (eds.), Plenum Press, New York.

den Hollander, J.A., Bednar, M., Brown, T.R., Redfield, C., Shulman, R.G., Ugurbil, K. (1986). Studies of anaerobic and aerobic glycolysis in *Saccharomyces cerevisiae*. *Biochem.* **25**: 203-211.

Gaudet, G., Forano, E., Dauphin, G., Delort, A.M. (1992). Futile cycling of glycogen in *Fibrobacter succinogenes* as shown by *in situ* ^{1}H-NMR and ^{13}C-NMR investigation. *Eur. J. Biochem.* **207**: 155-162.

Gopher, A., Vaisman, N., Mandel, H., Lapidot, A. (1990). Determination of fructose metabolic pathways in normal and fructose intolerant children: A ^{13}C NMR study using [U-^{13}C]fructose. *Proc. Acad. Natl. Sci.* **87**(14): 5449-5453.

Green, M.E., Landau, B.R. (1965). Contribution of the pentose cycle to glucose metabolism in muscle. *Arch. Biochem. Biophys.* **111**: 569-575.

Hiatt, H.H. (1957). Glycogen formation via the pentose phosphate pathway in mice in vivo. *J. Biol.Chem.*: 851-859.

Horecker, B.L., Domagk, G., Hiatt, H.H. (1958). A comparison of C^{14}-labeling patterns in deoxyribose and ribose in mammalian cells. *Arch. Biochem. Biophys.* **78**: 510-517.

Hostetler, K., Cooperstein, S.J., Landau, B.R., Lazarow, A. (1966). Pathways of glucose metabolism in the isolated islet of the goosefish in vitro. *Am. J. Physiol.* **211**: 1057-1062.

Hostetler, K.Y., Landau, B.R. (1967). Estimation of the pentose cycle contribution to glucose metabolism in tissue *in vivo*. *Biochem.* **6**: 2961-2964.

Hostetler, K.Y., Landau, B.R., White, R.J., Albin, M.S., Yashon, D. (1970). Contribution of the pentose cycle to the metabolism of glucose in the isolated, perfused brain of the monkey. *J. Neurochem.* **17**: 33-39.

Kalderon, B., Gopher, A., Lapidot, A. (1986). Metabolic pathways leading to liver glycogen repletion in vivo, studied by GC-MS and NMR. *FEBS Let.* **204**: 29-32.

Kalderon, B., Korman, S.H., Gutman, A., Lapidot, A. (1989). Estimation of glucose carbon recycling in children with glycogen storage disease - A ^{13}C NMR study using [U-^{13}C]glucose. *Proc. Acad. Natl. Sci.* **86**: 4690-4694.

Kalderon, B., Korman, S.H., Gutman, A., Lapidot, A. (1989). Glucose recycling and production in glycogenosis type I and type III: stable isotope technique study. *Am. J. Physiol.* **257**: E346-E353.

Kats, J., Wood, W.G. (1960). The use of glucose-C^{14} for the evaluation of the pathways of glucose metabolism. *J. Biol.Chem.* **235**: 2165-2177.

Katz, J., Abraham, S., Hill, R., Chaikoff, I.L. (1955). The occurrence and mechamism of the hexose monophosphate shunt in rat liver slices. *J. Biol.Chem.*: 853-868.

Katz, J., Wals, P.A., Lee, W.N.P. (1991). Determination of pathways of glycogen synthesis and the dilution of the three carbon pool with [U-^{13}C]glucose. *Proc. Acad. Natl. Sci.* **88**: 2103-2107.

Landau, B.R., Katz, J. (1964). A quantitative estimation of the pathways of glucose metabolism in rat adipose tissue *in vitro*. *J. Biol.Chem.* **239**: 697-704.

London, R.E., Walker, T.E. (1985). Biosynthesis of trehalose by *Brevibacterium flavum* : Use of long range ^{13}C-^{13}C coupling data to characterize triose phosphate isomerase activity. *Bioscience Reports* **5**: 509-515.

Magnusson, I., Chandramouli, V., Schumann, W.C., Kumaran, K., Wahren, J., Landau, B.R. (1988). Pentose pathway in human liver. *Proc. Acad. Natl. Sci.* **85**: 4682-4685.

Magnusson, I., Wennlund, A., Chandramouli, V., Schumann, W.C., Kumaran, K., Wahren, J., Landau, B.R. (1990). Fructose 6-phosphate cycling and the pentose cycle in hyperthyroidism. *J. Clin. Endocrinol. Metab.* **70**: 461-466.

Merlevede, W., Weaver, G., Landau, B.R. (1963). Effects of thyrotropic hormone on carbohydrate metabolism in thyroid slices. *J. Clin. Invest.* **1963**: 1160-1171.

Mitrakou, A., Jones, R., Okuda, Y., Pena, J., Nurjhan, N., Field, J.B., Gerich, J.E. (1991). Pathway and carbon sources for hepatic glycogen repletion in dogs. *Am. J. Physiol.* **260**: E194-E202.

Rognstad, R., Katz, J. (1976). Effects of hormones and of ethanol on the fructose 6-P-fructose 1,6-p2 futile cycling during gluconeogenesis in the liver. *Arch. Biochem. Biophys.* **177**: 337-345.

Schrader, M.C., Eskey, C.J., Simplaceanu, V., Ho, C. (1993). A carbon-13 nuclear magnetic resonance investigation of the metabolic fluxes associated with glucose metabolism in human erythrocytes. *Biochim. Biophys. ACTA* **1182**: 162-178.

Scofield, R.F., Kosug, K., Schumann, W.C., Kumaran, K., Landau, B.R. (1985). Quantitative estimation of the pathways followed in the conversion to glycogen of glucose administered to the fasted rat. *J. Biol.Chem.* **260**: 8777-8782.

Scofield, R.F., Kosugi, K., Chandramouli, V., Kumaran, K., Schumann, W.C., Landau, B.R. (1985). The nature of the pentose pathway in liver. *J. Biol.Chem.* **260**: 1549-15444.

Siu, P.M.L., Wood, H.G. (1959). Conversion of galactose and glucose to liver glycogen *in vivo*. *J. Biol.Chem.* **234**: 2223-2226.

Susskind, B.M., Warren, L.G., Reeves, R.E. (1982). A pathway for the interconversion of hexose and pentose in the parasitic amoeba *Entamoeba histolytica*. *Biochem. J.* **204**: 191-196.

Ugurbil, K., Brown, T.R., den Hollander, J.A., Glynn, P., Shulman, R.G. (1978). High-resolution ^{13}C nuclear magnetic resonance studies of glucose metabolism in *Escherichia coli*. *Proc. Acad. Natl. Sci.* **75**(8): 3742-3746.

Van Schaftingen, E., Hue, L., Hers, H.G. (1980). Study of the fructose 6-phosphate/fructose 1,6-bi-phosphate cycle in the liver *in vivo*. *Biochem. J.* **192**: 263-271.

Wajngot, A., Chandramouli, V., Schumann, W.C., Kumaran, K., Efendic, S., Landau, B.R. (1989). Testing of the assumption made in estimating the extent of futile cycling. *Am. J. Physiol.* **256**: E668-E675.

Weaver, G., Landau, B.R. (1963). Contribution of the pentose cycle to glucose metabolism by adrenal cortex *in vitro*. *J. Biol.Chem.* **73**: 640-646.

Williams, J.F., Arora, K.K., Longenecker, J.P. (1987). The pentose phosphate pathway: a random harvest [Impediments which oppose acceptance of the classical (F-type) pentose cycle for liver, some neoplasm and photosynthetic tissue. The case for the L-type pentose pathway. *Int. J. Biochem.* **19**: 749-818.

Wood, H.G., Katz, J., Landau, B.R. Estimation of pathways of carbohydrate metabolism. *Biochemische Zeitschrift* **338**: 809-847.

Wood, T. (1985). The Pentose Phosphate. Academic Press, Orlando.

Table 7.1 Flux balances on metabolites and steady stste solutions. To be consistent with other workers, we will let PC be the net fraction of hexose 6-phosphate (either in the form of glucose 6-phosphate or fructose 6-phosphate) utilized via PPP. Steady state fluxes can be represented by two unknowns, v_0 and PC.

Model I and Model III	Model II	Model IV
$\frac{d[\text{H6P}]}{dt} = v_0 - v_1 - v_2 + 2v_4$ $\frac{d[\text{X5P}]}{dt} = v_1 - 2v_4 - v_5$ $\frac{d[\text{G3P}]}{dt} = 2v_2 + v_5 - v_3$ $v_4 = v_5$	$\frac{d[\text{H6P}]}{dt} = v_0 - v_1 - v_2 + v_5 + v_6$ $\frac{d[\text{X5P}]}{dt} = v_1 - 2v_4 - v_6$ $\frac{d[\text{G3P}]}{dt} = 2v_2 + v_4 - v_5 + v_6 - v_3$ $\frac{d[\text{S7P}]}{dt} = v_4 - v_5$ $\frac{d[\text{E4P}]}{dt} = v_5 - v_6$	$\frac{d[\text{H6P}]}{dt} = v_0 - v_1 - v_2 + v_5 + v_6$ $\frac{d[\text{X5P}]}{dt} = v_1 - 2v_4 - v_5$ $\frac{d[\text{T3P}]}{dt} = 2v_2 + v_4 - v_5 + v_6 - v_3$ $\frac{d[\text{S7P}]}{dt} = v_4 - v_6$ $\frac{d[\text{E4P}]}{dt} = v_6 - v_7$ $\frac{d[\text{O8P}]}{dt} = v_5 - v_7$
$v_1 = 3\text{PC}\, v_0$ $v_2 = (1 - \text{PC})\, v_0$ $v_3 = (2 - \text{PC})\, v_0$ $v_4 = v_5 = \text{PC}\, v_0$	$v_1 = 3\text{PC}\, v_0$ $v_2 = (1 - \text{PC})\, v_0$ $v_3 = (2 - \text{PC})\, v_0$ $v_4 = v_5 = v_6 = \text{PC}\, v_0$	$v_1 = 3\text{PC}\, v_0$ $v_2 = (1 - \text{PC})\, v_0$ $v_3 = (2 - \text{PC})\, v_0$ $v_4 = v_5 = v_6 = v_7 = \text{PC}\, v_0$

Table 7.2 Label balances on the individual carbons of metabolites for Model I. Numbers in the parenthesis indicate the carbon position. Hexose(i) represent carbon label enrichment of input hexose substrate. For example, if the unput substrate consists of 50% unlabeled glucose and 50% [1,3-$^{13}C_2$]glucose, Hexose(1) = Hexose(3) = 0.5 and all other Hexose(i) = 0.

$$\frac{d}{dt}\begin{bmatrix}\text{H6P(1)}\\ \text{H6P(2)}\\ \text{H6P(3)}\\ \text{H6P(4)}\\ \text{H6P(5)}\\ \text{H6P(6)}\end{bmatrix} = v_0\begin{bmatrix}\text{Hexose(1)}\\ \text{Hexose(2)}\\ \text{Hexose(3)}\\ \text{Hexose(4)}\\ \text{Hexose(5)}\\ \text{Hexose(6)}\end{bmatrix} - v_1\begin{bmatrix}\text{H6P(1)}\\ \text{H6P(2)}\\ \text{H6P(3)}\\ \text{H6P(4)}\\ \text{H6P(5)}\\ \text{H6P(6)}\end{bmatrix} - v_2\begin{bmatrix}\text{H6P(1)}\\ \text{H6P(2)}\\ \text{H6P(3)}\\ \text{H6P(4)}\\ \text{H6P(5)}\\ \text{H6P(6)}\end{bmatrix} + v_4\begin{bmatrix}\text{H6P(2)}\\ \text{H6P(3)}\\ \text{H6P(3)}\\ \text{H6P(4)}\\ \text{H6P(5)}\\ \text{H6P(6)}\end{bmatrix} + v_4\begin{bmatrix}\text{H6P(2)}\\ \text{H6P(3)}\\ \text{H6P(2)}\\ \text{H6P(4)}\\ \text{H6P(5)}\\ \text{H6P(6)}\end{bmatrix}$$

$$\frac{d}{dt}\begin{bmatrix}\text{X5P(1)}\\ \text{X5P(2)}\\ \text{X5P(3)}\\ \text{X5P(4)}\\ \text{X5P(5)}\end{bmatrix} = v_1\begin{bmatrix}\text{H6P(2)}\\ \text{H6P(3)}\\ \text{H6P(4)}\\ \text{H6P(5)}\\ \text{H6P(6)}\end{bmatrix} - 2v_4\begin{bmatrix}\text{X5P(1)}\\ \text{X5P(2)}\\ \text{X5P(3)}\\ \text{X5P(4)}\\ \text{X5P(5)}\end{bmatrix} - v_5\begin{bmatrix}\text{X5P(1)}\\ \text{X5P(2)}\\ \text{X5P(3)}\\ \text{X5P(4)}\\ \text{X5P(5)}\end{bmatrix}$$

$$\frac{d}{dt}\begin{bmatrix}\text{G3P(1)}\\ \text{G3P(2)}\\ \text{G3P(3)}\end{bmatrix} = v_2\begin{bmatrix}\text{H6P(4)}\\ \text{H6P(5)}\\ \text{H6P(6)}\end{bmatrix} + v_2\begin{bmatrix}\text{H6P(3)}\\ \text{H6P(2)}\\ \text{H6P(1)}\end{bmatrix} + v_5\begin{bmatrix}\text{H6P(4)}\\ \text{H6P(5)}\\ \text{H6P(6)}\end{bmatrix} - v_3\begin{bmatrix}\text{G3P(1)}\\ \text{G3P(2)}\\ \text{G3P(3)}\end{bmatrix}$$

Table 7.3 Steady state solutions of label distribution in hexose 6-phosphate and triose phosphate using [1-^{13}C]glucose as a substrate. PC denotes the net fraction of hexose utilized via PPP. For Model II and Model IV all $\alpha_i = 0$.

Carbon	Model I	Model II	Model III	Model IV
H6P(1)	$\frac{1}{1+2PC}$	$\frac{1}{1+2PC}$	$\frac{1}{1+2PC}$	$\frac{2}{2+3PC+PC^2}$
H6P(2)	0	0	0	0
H6P(3)	0	0	0	0
H6P(4)	0	0	0	0
H6P(5)	0	0	0	0
H6P(6)	0	$\frac{(1-PC)PC}{2+5PC+PC^2-2PC^3}$	0	0
T3P(1)	0	0	0	0
T3P(2)	0	0	0	0
T3P(3)	$\frac{1-PC}{2+3PC-2PC^2}$	$\frac{1-PC}{2+3PC-2PC^2}$	$\frac{1-PC}{2+3PC-2PC^2}$	$\frac{1-PC}{2+3PC+PC^2}$

Table 7.4 Steady state solutions of label distribution in hexose 6-phosphate and triose phosphate using [2-^{13}C]glucose as a substrate.

Carbon	Model I	Model II	Model III	Model IV
H6P(1)	$\frac{2PC(1+PC)}{1+5PC+6PC^2}$	$\frac{2PC(1+PC)}{1+5PC+6PC^2}$	0	$\frac{4PC^2}{4+8PC+7PC^2+4PC^3+PC^4}$
H6P(2)	$\frac{1+PC}{1+3PC}$	$\frac{1+PC}{1+3PC}$	$\frac{1}{1+PC}$	$\frac{2}{2+PC+PC^2}$
H6P(3)	$\frac{PC}{1+3PC}$	$\frac{PC}{1+3PC}$	0	0
H6P(4)	0	$\frac{(1-PC)PC^2}{2+7PC+2PC^2-3PC^3}$	0	0
H6P(5)	0	$\frac{(1-PC)PC}{2+5PC-3PC^2}$	0	0
H6P(6)	0	$\frac{2(1-PC)PC^2}{2+9PC+7PC^2-6PC^3}$	0	0
T3P(1)	$\frac{(1-PC)PC}{2+5PC-3PC^2}$	$\frac{(1-PC)PC}{2+5PC-3PC^2}$	$\frac{PC}{2+PC-PC^2}$	$\frac{PC}{2+PC+PC^2}$
T3P(2)	$\frac{1-PC^2}{2+5PC-3PC^2}$	$\frac{1-PC^2}{2+5PC-3PC^2}$	$\frac{1-PC}{2+PC-PC^2}$	$\frac{1-PC}{2+PC+PC^2}$
T3P(3)	$\frac{2PC(1-PC^2)}{2+9PC+7PC^2-6PC^3}$	$\frac{2PC(1-PC^2)}{2+9PC+7PC^2-6PC^3}$	$\frac{PC}{2+PC-PC^2}$	$\frac{PC(2+5PC-PC^2)}{4+8PC+7PC^2+4PC^3+PC^4}$

Table 7.5 Steady state solutions of label distribution in hexose 6-phosphate and triose phosphate using [3-^{13}C]glucose as a substrate.

Carbon	Model I	Model II	Model III	Model IV
H6P(1)	$\frac{4PC^2}{1+5PC+6PC^2}$	$\frac{4PC^2}{1+5PC+6PC^2}$	0	$\frac{PC(2-PC+PC^3)}{4+8PC+7PC^2+4PC^3+PC^4}$
H6P(2)	$\frac{2PC}{1+3PC}$	$\frac{2PC}{1+3PC}$	0	$\frac{PC^2}{2+PC+PC^2}$
H6P(3)	$\frac{1+2PC}{1+3PC}$	$\frac{1+2PC}{1+3PC}$	1	1
H6P(4)	0	$\frac{PC+PC^2-2PC^3}{2+7PC+2PC^2-3PC^3}$	0	0
H6P(5)	0	$\frac{2(PC-PC^3)}{2+7PC+2PC^2-3PC^3}$	0	0
H6P(6)	0	$\frac{4(PC-PC^4)}{2+11PC+16PC^2+PC^3-6PC^4}$	0	0
T3P(1)	$\frac{1+PC-2PC^2}{2+5PC-3PC^2}$	$\frac{1+PC-2PC^2}{2+5PC-3PC^2}$	$\frac{1-PC}{2-PC}$	$\frac{2-PC}{2(2+PC+PC^2)}$
T3P(2)	$\frac{2(PC-PC^2)}{2+5PC-3PC^2}$	$\frac{2(PC-PC^2)}{2+5PC-3PC^2}$	$\frac{PC}{2-PC}$	$\frac{PC(1+PC)}{2+PC+PC^2}$
T3P(3)	$\frac{4PC^2(1-PC)}{2+9PC+7PC^2-6PC^3}$	$\frac{4PC^2(1-PC)}{2+9PC+7PC^2-6PC^3}$	0	$\frac{PC(2-3PC+3PC^2+4PC^3)}{2(4+8PC+7PC^2+4PC^3+PC^4)}$

Table 7.6 Steady state solutions of label distribution in hexose 6-phosphate and triose phosphate using [4-^{13}C]glucose as a substrate.

Carbon	Model I	Model II	Model III	Model IV
H6P(1)	0	0	$\frac{PC}{1+2PC}$	$\frac{PC^2}{2+3PC+PC^2}$
H6P(2)	0	0	0	0
H6P(3)	0	0	0	0
H6P(4)	1	$\frac{1}{2-PC}$	1	1
H6P(5)	0	0	0	0
H6P(6)	0	0	0	0
T3P(1)	$\frac{1}{2-PC}$	$\frac{1}{2-PC}$	$\frac{1-PC}{2-PC}$	$\frac{1}{2}$
T3P(2)	0	0	0	0
T3P(3)	0	0	$\frac{(1-PC)PC}{2+3PC-2PC^2}$	$\frac{(1-PC)PC}{2(2+3PC+PC^2)}$

Table 7.7 Steady state solutions of label distribution in hexose 6-phosphate and triose phosphate using [5-^{13}C]glucose as a substrate.

Carbon	Model I	Model II	Model III	Model IV
H6P(1)	0	0	0	$\frac{2PC^3}{4+8PC+7PC^2+4PC^3+PC^4}$
H6P(2)	0	0	$\frac{PC}{1+PC}$	$\frac{PC}{2+PC+PC^2}$
H6P(3)	0	0	0	0
H6P(4)	0	0	0	0
H6P(5)	1	$\frac{1}{2-PC}$	1	1
H6P(6)	0	0	0	0
T3P(1)	0	0	$\frac{PC^2}{2+PC-PC^2}$	$\frac{PC^2}{2(2+PC+PC^2)}$
T3P(2)	$\frac{1}{2-PC}$	$\frac{1}{2-PC}$	$\frac{1+PC-2PC^2}{2+PC-PC^2}$	$\frac{1+PC}{2+PC+PC^2}$
T3P(3)	0	0	$\frac{PC^2}{2+PC-PC^2}$	$\frac{PC^2(2+5PC-PC^2)}{2(4+8PC+7PC^2+4PC^3+PC^4)}$

Table 7.8 Steady state solutions of label distribution in hexose 6-phosphate and triose phosphate using [6-^{13}C]glucose as a substrate. PC denotes the net fraction of hexose utilized via PPP.

Carbon	Model I	Model II	Model III	Model IV
H6P(1)	0	0	$\frac{PC}{1+2PC}$	$\frac{PC}{2+3PC+PC^2}$
H6P(2)	0	0	0	$\frac{2PC}{1+3PC}$
H6P(3)	0	0	0	0
H6P(4)	0	0	0	0
H6P(5)	0	0	0	0
H6P(6)	1	$\frac{1}{2-PC}$	1	1
T3P(1)	0	0	0	0
T3P(2)	0	0	0	0
T3P(3)	$\frac{1}{2-PC}$	$\frac{1}{2-PC}$	$\frac{1+2PC-3PC^2}{2+3PC-2PC^2}$	$\frac{1+2PC}{2+3PC+PC^2}$

Table 7.9 Assessment of fructose futile cycling or indirect glycogen synthesis using C-1 and C-6 labeled hexose substrate

System	Substrate Used	Results	Reference
Rat	[1-^{14}C]galactose	C-1/C-6 glucose within 15.3 to 269	Rognstad and Katz, 1976
Escherichia coli	[1-^{13}C]glucose	25% enrichment at C-6 of Fructose-1,6-bisphosphate	Ugurbil *et al.*, 1978
Escherichia coli	[6-^{13}C]glucose	No peak identified at C-1 of Fructose-1,6-bisphosphate	Shulman *et al.*, 1979
Escherichia coli	[6-^{13}C]glucose	86-92% enrichment at C-6 but none at C-1 of glycogen	Chambost and Fraenkel, 1980
Rat	[1-^{13}C]galactose or [1-^{13}C]glucose	0.16 to 2.12% of total ^{14}C label in glucose	van Schaftingen *et al.*, 1980
Brevibacterium flavum	[1-^{13}C]glucose	Significant label at C-6 of α,α-trehalose	London and Walker, 1985
Saccharomyces cerevisiae	[1-^{13}C]glucose [6-^{13}C]glucose	C-1/C-6 trehalose = 0.22 C-6/C-1 trehalose = 0.17	den Hollander *et al.*, 1986
Human	[6-^{14}C]galactose	7.7 to 9.1% found in C-1 of glucose	Magnusson *et al.* 1990
Rat	[1-^{14}C]glucose	C-6/C-1 glycogen = 0.06 to 0.08	Katz *et al.*, 1991
Dog	[1-^{14}C]glucose	C-6/C-1 glycogen = 0.178	Mitrakou *et al.*, 1991
Fibrobacter succinogenes	[1-^{13}C]glucose	Significant label at C-6 of glycogen	Gaudet *et al.* 1992
Saccharomyces cerevisiae	[6-^{13}C]glucose	C-1/C-6 trehalose less than 0.03	Navas *et al.*, 1993

Table 7.10 Assessment of pentose phosphate activity using C-2 labeled hexose. Metabolite monitored is glycogen unless specified otherwise.

System	Carbon Distribution						Reference
	C-1	C-2	C-3	C-4	C-5	C-6	
Rat, Liver Regenerating	35	100	21	32	28	20	Horecker et al, 1958
Rat, Liver Fasted	13.9	100	3.3	2.4	8.4	6.3	Siu and Wood, 1959
Cow, Cortex Adrenal	15.7	100	7.9	1.4	11.0	2.1	Weaver and Landau, 1963
Cow, Cortex Adrenal (w/ ACTH)	17.0	100	9.3	2.2	9.2	2.2	
Cow, Thyroid	6.6	100	5.0	0.9	9.6	1.1	Merlevede et al, 1963
Cow, Thyroid (w/ TSH)	19.3	100	13.5	2.2	10.3	2.1	
Cow, Thyroid (w/ TSH)	8.4	100	5.9	2.0	12.1	1.1	
Rat, Adipose	15.2	100	12.8	1.9	13.9	2.9	Landau and Katz, 1964
Rat, Adipose (w/ Insulin)	30.7	100	17.9	3.5	14.8	5.3	
Mice, Infant Heart Muscle	4.6	100	5.7		28.3*		Green and Landau, 1965
Mice, Adult Heart Muscle	3.4	100	5.2		30.9*		
Mice, Infant Abdominal Muscle	0.6	100	1.9		16.7*		
Mice, Adult Abdominal Muscle	0.1	100	1.2		19.8*		
Mice, Infant Diaphragm Muscle	0.7	100	2.2		19.6*		
Mice, Adult Diaphragm Muscle	1.0	100	1.4		10.2*		
Human, Intestine	13.4	100	10.3	1.7	10.7	1.3	White and Landau, 1965
	8.0	100	6.2	1.6	9.5	4.4	
Goosefish, Islet	11.1	100	8.3	1.3	15.0	1.7	Hostetler et al, 1966
	6.4	100	4.5	1.9	20.2	1.6	
	4.7	100	4.8	0.8	17.7	0.9	
Rat, Liver	5.2	100	3.2	0.7	4.7	2.5	Hostelter and Landau, 1967
Rat, Diaphragm Muscle	1.9	100	3.0	0.8	1.2	0.9	
Rat, Diaphragm Muscle	1.6	100	2.6	0.9	4.0	1.2	
Rat, Diaphragm Muscle	2.1	100	2.9	0.6	2.9	0.4	

Rat, Thyroid	6.1	100	12.4	0.7	4.0	2.4	
Rat, Kidney	7.2	100	8.0	0.8	9.7	2.6	
Rat, Brain	5.4	100	5.5	1.3	5.1	1.9	
Monkey, Brain Stem	10.7	100	3.0	0.6	6.1	2.0	Hostetler et al, 1970
Monkey, Cerebellum	12.8	100	5.7	0.7	6.0	0.9	
Monkey, Hemispheres	10.0	100	4.7	0.7	6.4	1.0	
Monkey, Hypothalamus	11.6	100	3.8	1.0	7.5	1.3	
Rat, Liver	17.2	100	8.3	1.4	9.7	3.2	Scofield et al, 1985
Rat, Liver (w/ phenazine methosulphate)	10.4	100	5.9	4.8	14.2	23.6	
Rat, Liver Regenerating	10.7	100	5.2	1.6	12.1	3.9	
Human, Liver**	4.6	100	3.4	4.8	6.7	9.4	Magnusson et al, 1988
Human, Liver (w/ Diflunisal)***	2.7	100	1.8	1.8	2.6	3.0	
Human, Liver (w/ Acetaminophen)$	2.1	100	1.8	1.4	1.8	3.2	
Human, Normal$$	5.4	100	3.6	1.0	2.4	1.5	Wajngot et al, 1989
Human, Diabetic$$	4.8	100	3.2	0.7	2.7	1.9	
Human, Hyperthyroid$$$	3.5	100	4.9	1.4	7.1	2.4	Magnusson et al, 1990

* Sum of carbons 4,5, and 6

** Glucose from blood in 4.5 hr

*** Glucose in blood in 3.25 hr

$ Glucose in blood in 3hr. Average of three human subjects

$$ Glucose in blood. Average of two human subjects. [2-^{14}C]Galactose infused.

$$$ [2-^{14}C]Galactose infused.

Table 7.11 Assessment of pentose phosphate activity using labeled pentose. Glucose is monitored unless specified otherwise. [1-^{14}C]Ribose is used unless specified otherwise. It should be noted that our model predicts less labeling at C-3 than at C-1 when C-1 labeled pentose is used. However, as summarized in Table 7.21, this seems to be true only with xylose. It is plausible that pathway other than pentose phosphate pathway is involved in metabolizing ribose.

System	Percent Carbon Distribution						
	C-1	C-2	C-3	C-4	C-5	C-6	
Rat, Liver	39.5	4.5	39.0	8.0	4.5	4.5	Katz et al, 1955
Mouse, Liver*	37.3	4.2	45.0	5.2	3.8	4.5	Hiatt, 1957
Mouse, Liver with [1-^{14}C]Xylose*	64.5	6.5	12.5	3.5	3.5	6.0	
Rat, Liver	26.7	4.8	62.1	3.6	0.8	2.1	Scofield et al, 1985
Human	18.3	4.6	71.3	2.8	1.8	1.2	Magnusson et al, 1988
Human (w/ Diflunisal)	26.1	4.6	63.0	2.0	1.8	2.5	
Human (w/ Acetaminophen)	34.8	3.1	55.8	2.6	1.7	2.3	

*With more than one subject tested, average was taken.
*Glycogen monitored.

Figure 7.1 Reaction sequence of the classical pentose phosphate pathway. The enzymes catalyzing the reaction steps are: E, ribulose-5-phosphate 3-epimerase (EC 5.1.2.1); I, ribose 5-phosphate isomerase (EC 5.3.1.6); TA, transaldolase (EC 2.2.1.2); TK, transketolase (EC 2.2.1.1). Abbreviations for metabolites are: G6P, glucose 6-P; X5P, xylulose 5-P; R5P, ribose 5-P; Ru5P, ribulose 5-P; G3P, glyceraldehyde 3-P; S7P, sedoheptulose 7-P; F6P, fructose 6-P; E4P, erythrose 4-P.

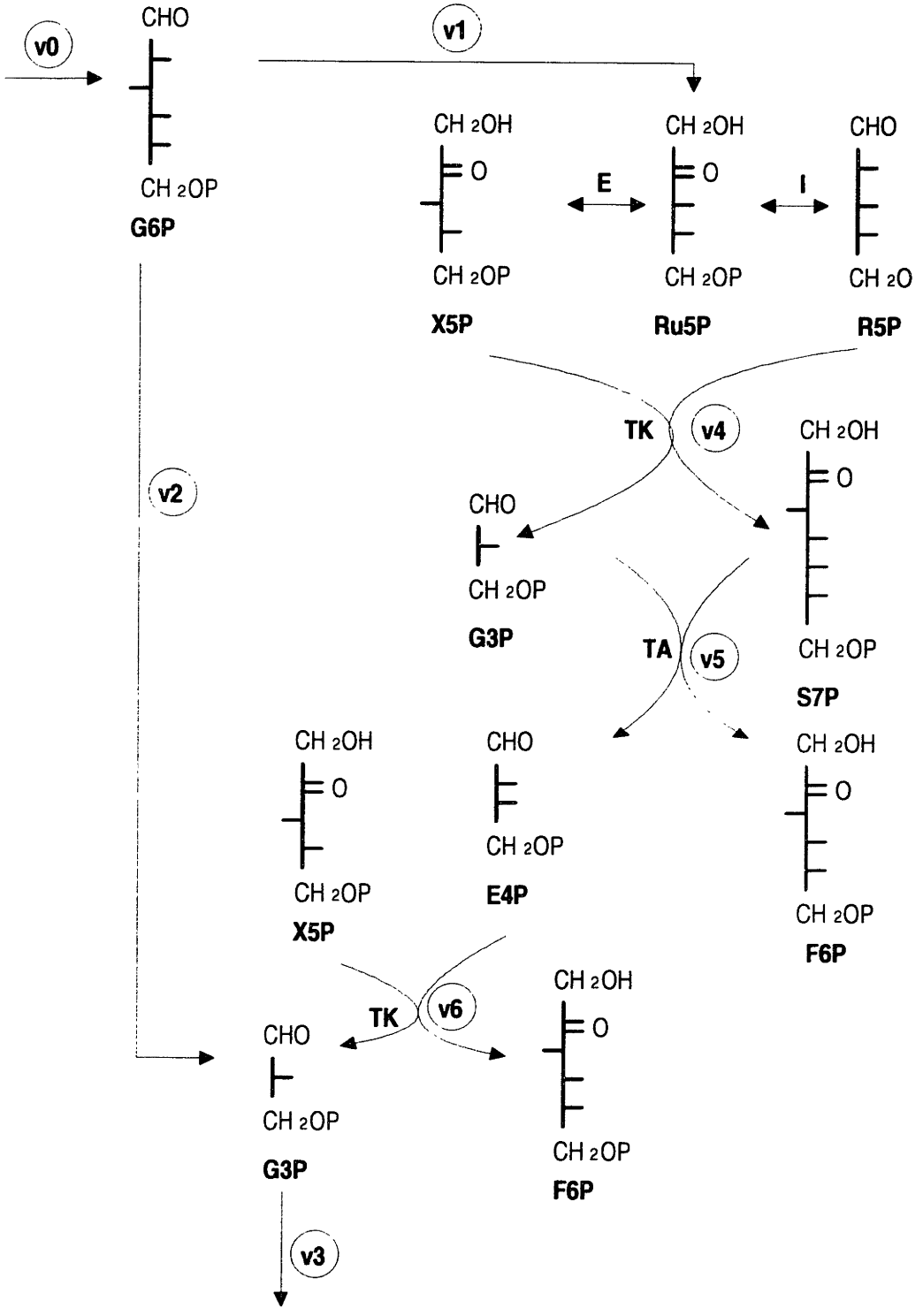

Figure 7.2 Proposed reaction sequence of the "L-type" pentose phosphate pathway. Additional reactions involved are: PE, P-5-P 2'-epimerase catalyzing interconversion between arabinose 5-P and ribose 5-P; PT, phosphotransferase; A, aldolase; TPI, triose isomerase. Additional metabolites involved are: A5P, arabinose 5-P; S17P2, sedoheptulose 1,7-P_2; O8P, octulose 8-P; O18P2, octulose 1,8-P_2; DHAP, dihydroxyacetone P.

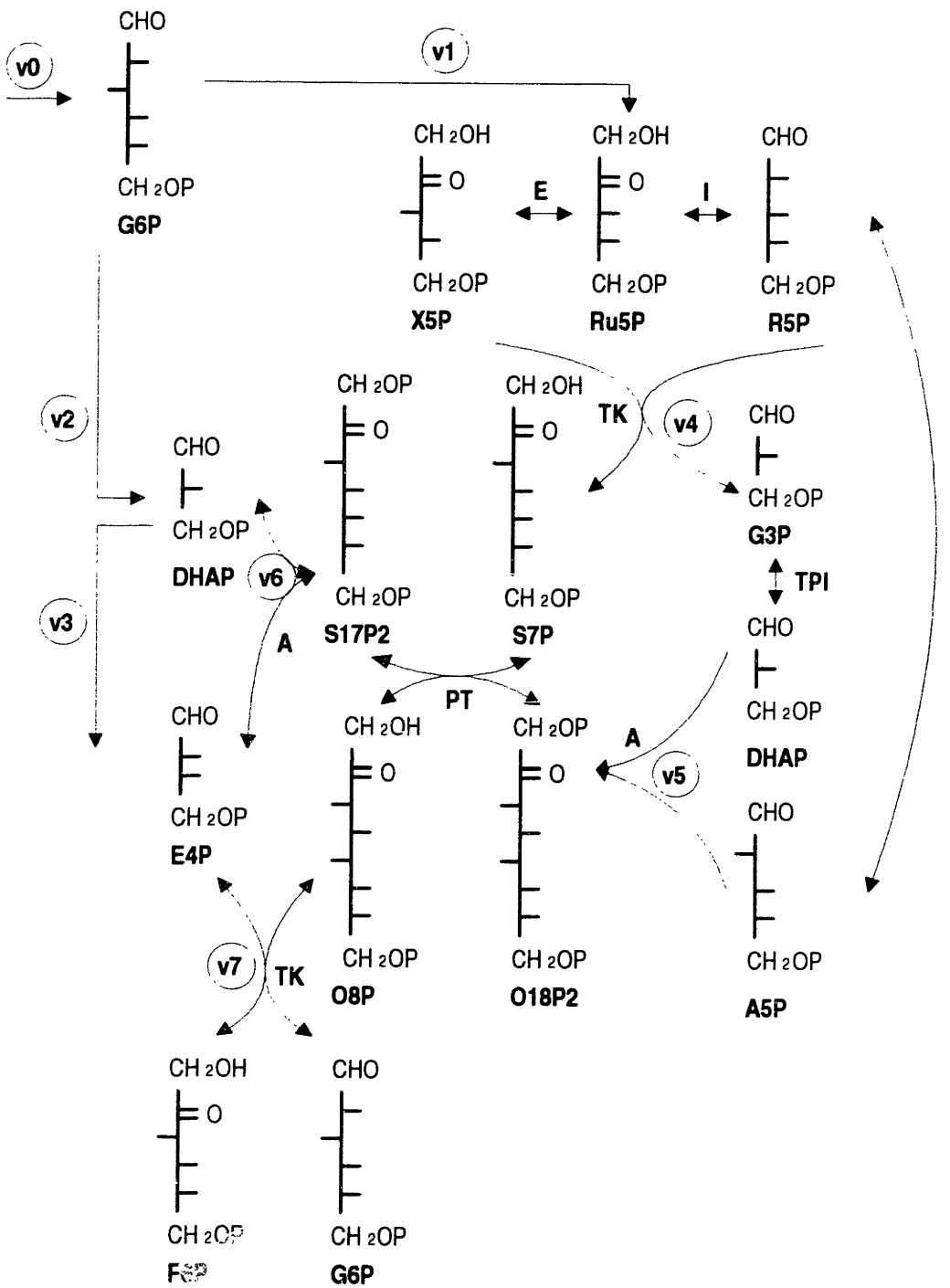

Figure 7.3 Simplified labeling scheme in accordance with the classical pentose phosphate pathway. H denotes hexose and T triose. Origin of carbon source is denoted inside parenthesis.

Via Glycolysis:

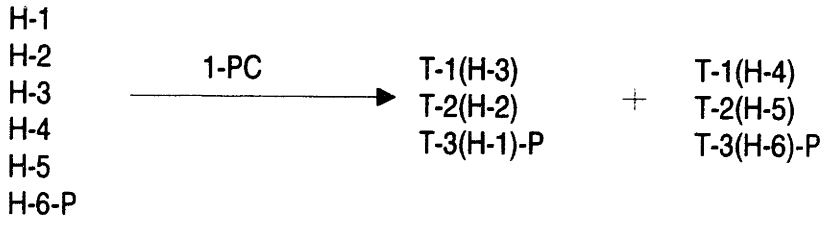

Via Pentose Phosphate Pathway:

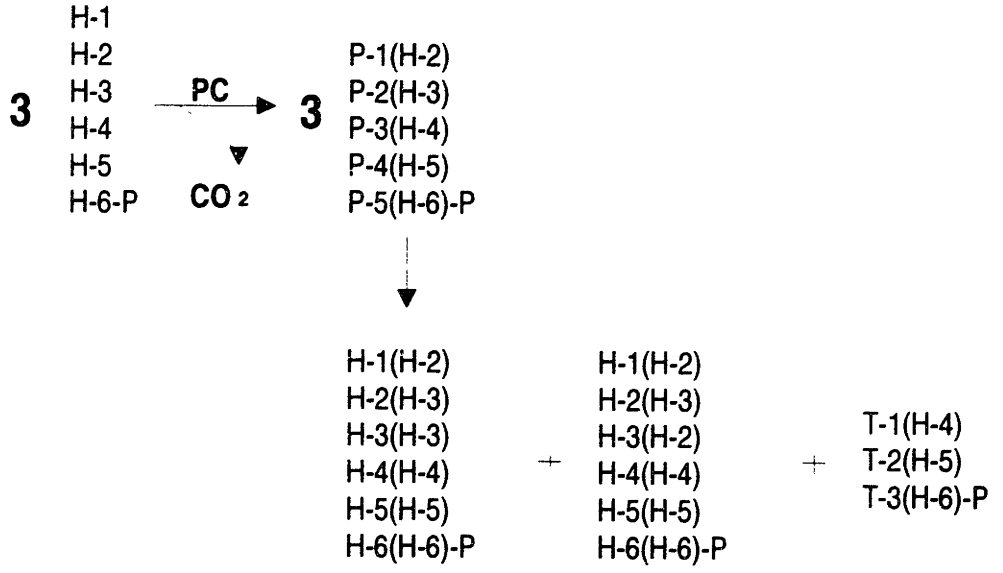

Figure 7.4 Simplified labeling scheme according to the "L-type" pentose phosphate pathway.

Via Glycolysis:

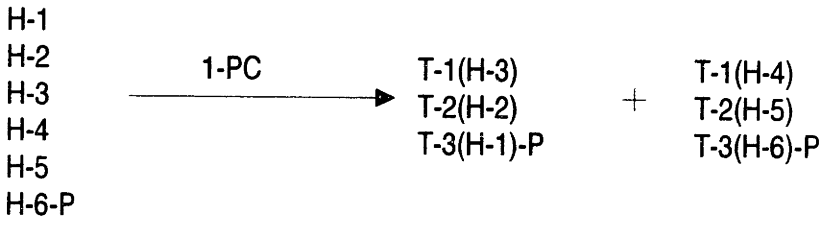

Via Pentose Phosphate Pathway:

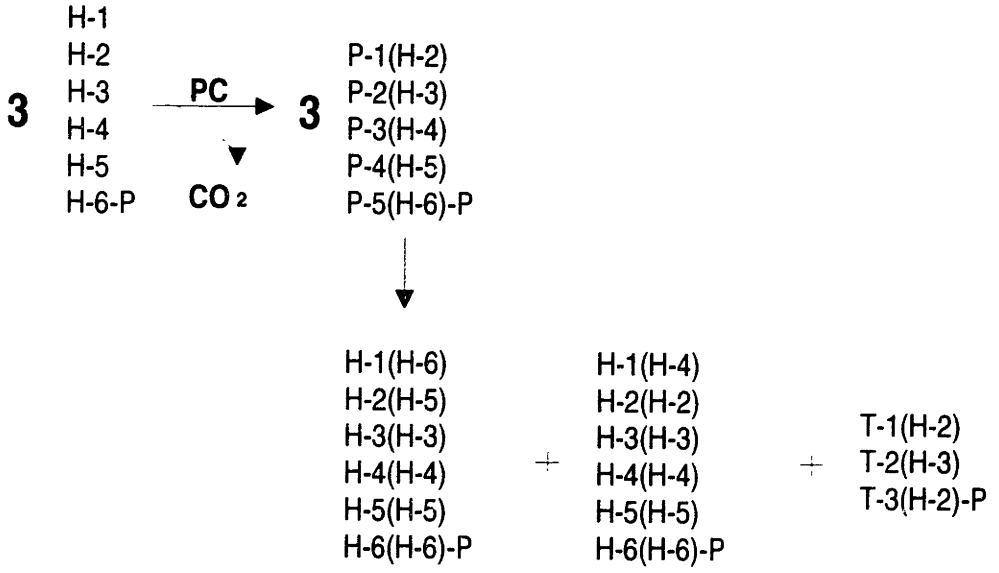

Figure 7.5 Simplified metabolite balance according to the classcial and "L-type" pentose phosphate pathways. Only three pools are assumed to be present; hexose 6-P, pentose 5-P, and triose 3-P pools. Solid thick arrows indicate irreversible reactions. Double arrows indicate rapid reversible reactions. Dotted double arrows indicate slow reversible reactions.

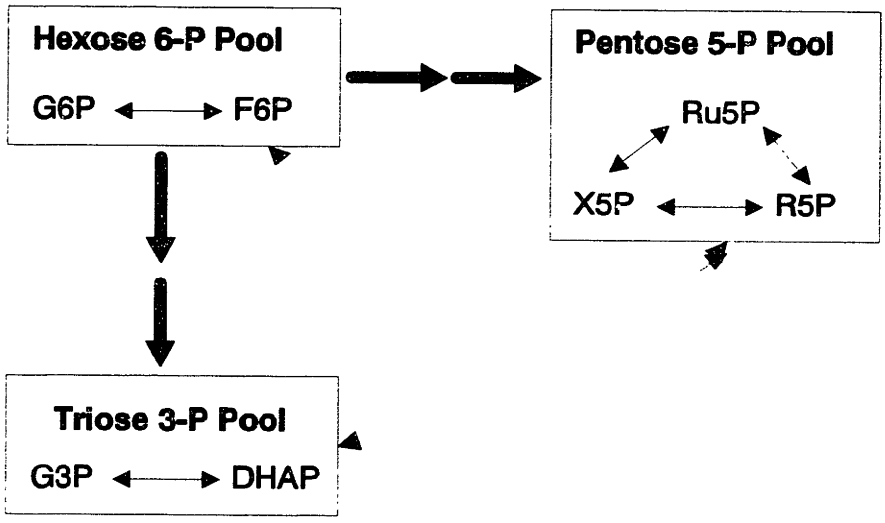

Figure 7.6 Fractional enrichment expected at C-1 and C-6 of hexose 6-P or its metabolic equilivalents with C-1 labeled hexose as substrate. Only Model II predicts label appearance at C-6 (top). Ratio of C-6/C-1 of hexose 6-P predicted by Model II (bottom).

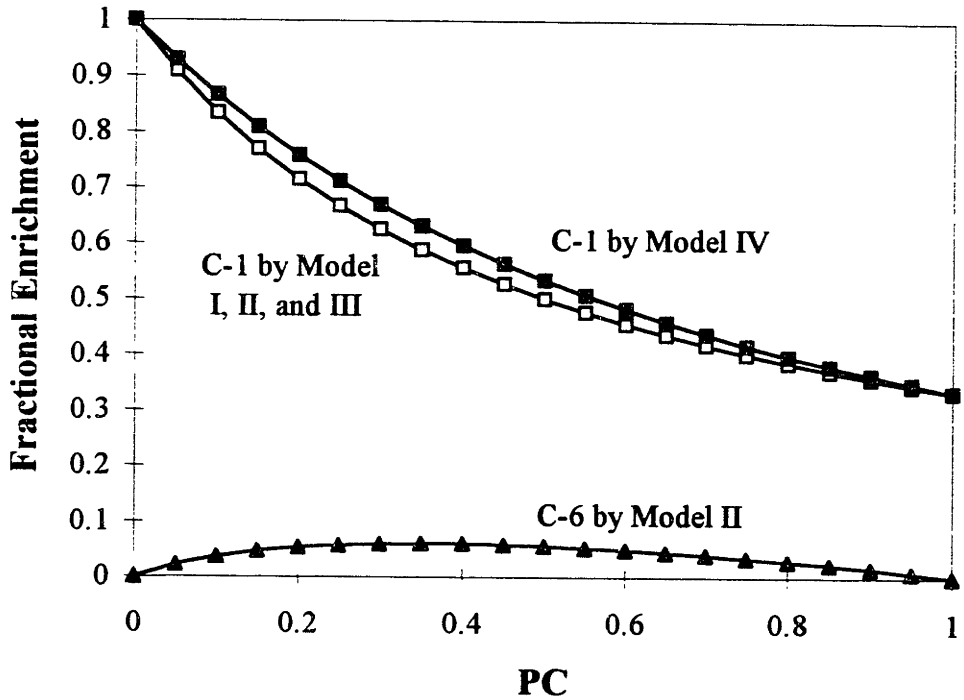

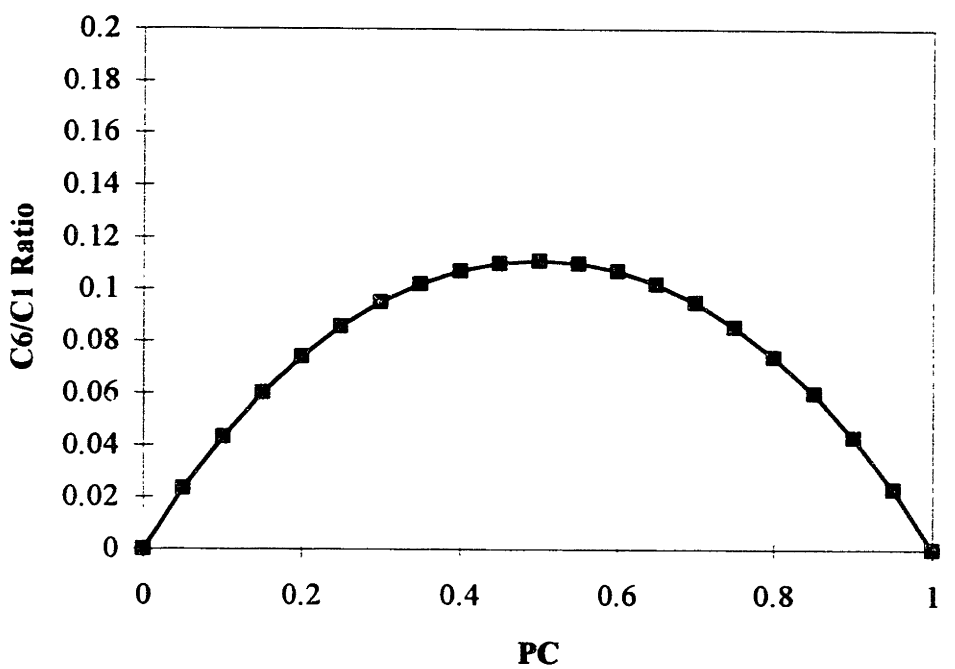

Figure 7.7 Prediction of label appearance in carbons of hexose 6-phosphate and triose 3-phosphate using C-2 labeled hexose as substrate.

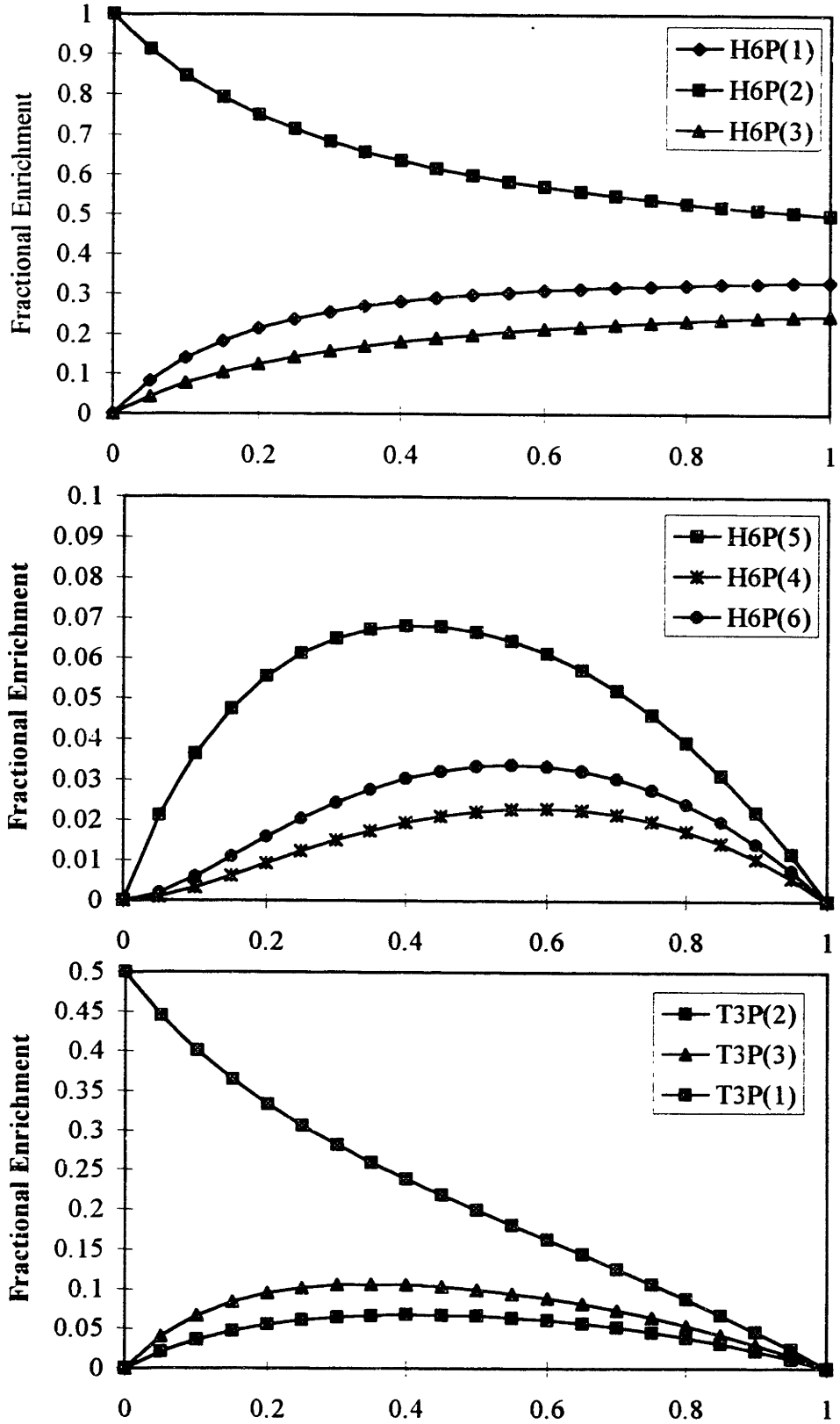

Figure 7.8 Prediction of label appearance in carbons of hexose 6-phosphate and triose 3-phosphate using C-2 labeled hexose as substrate.

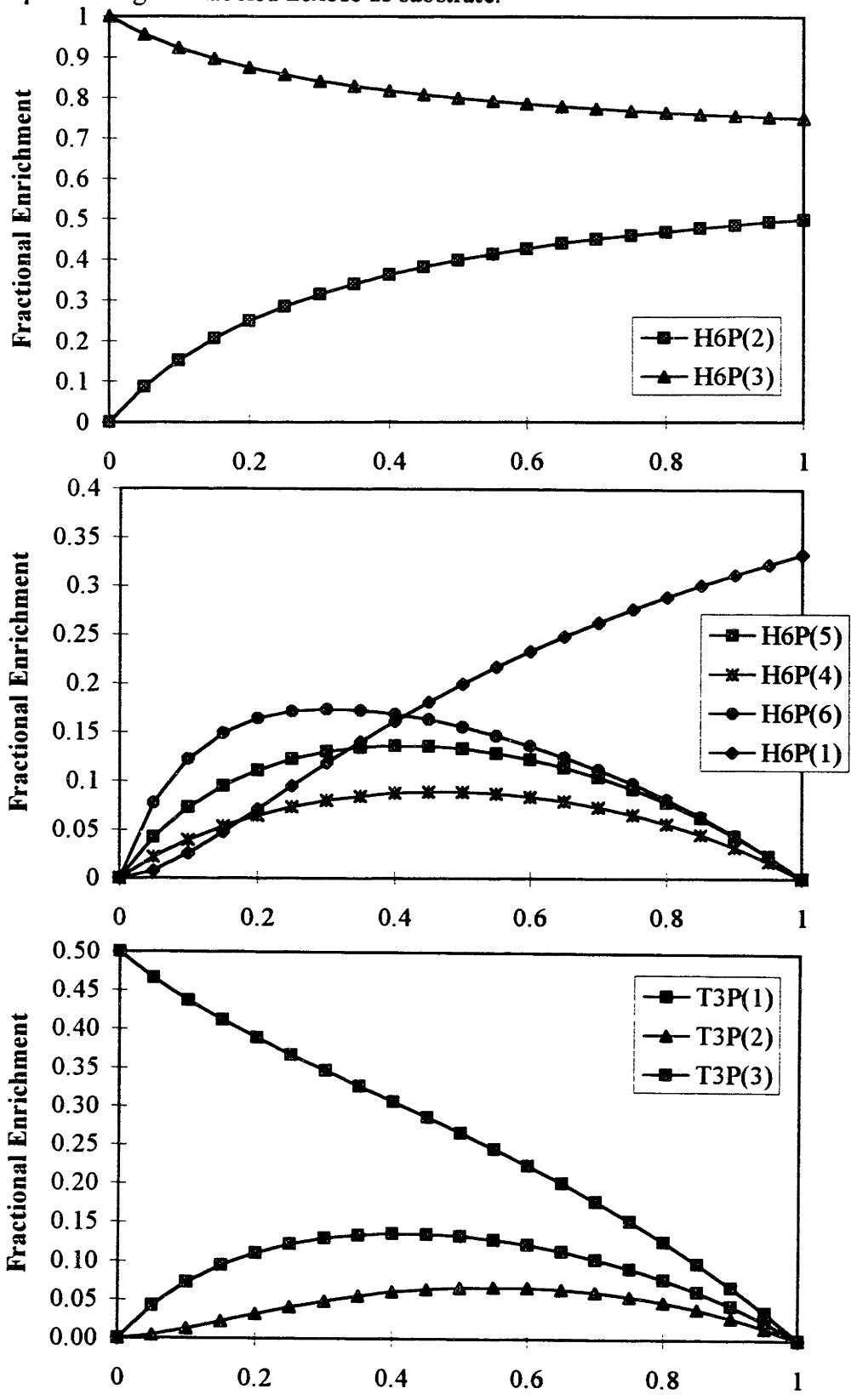

Figure 7.9 Prediction of label appearance in carbons of hexose 6-phosphate using C-1 labeled pentose as substrate.

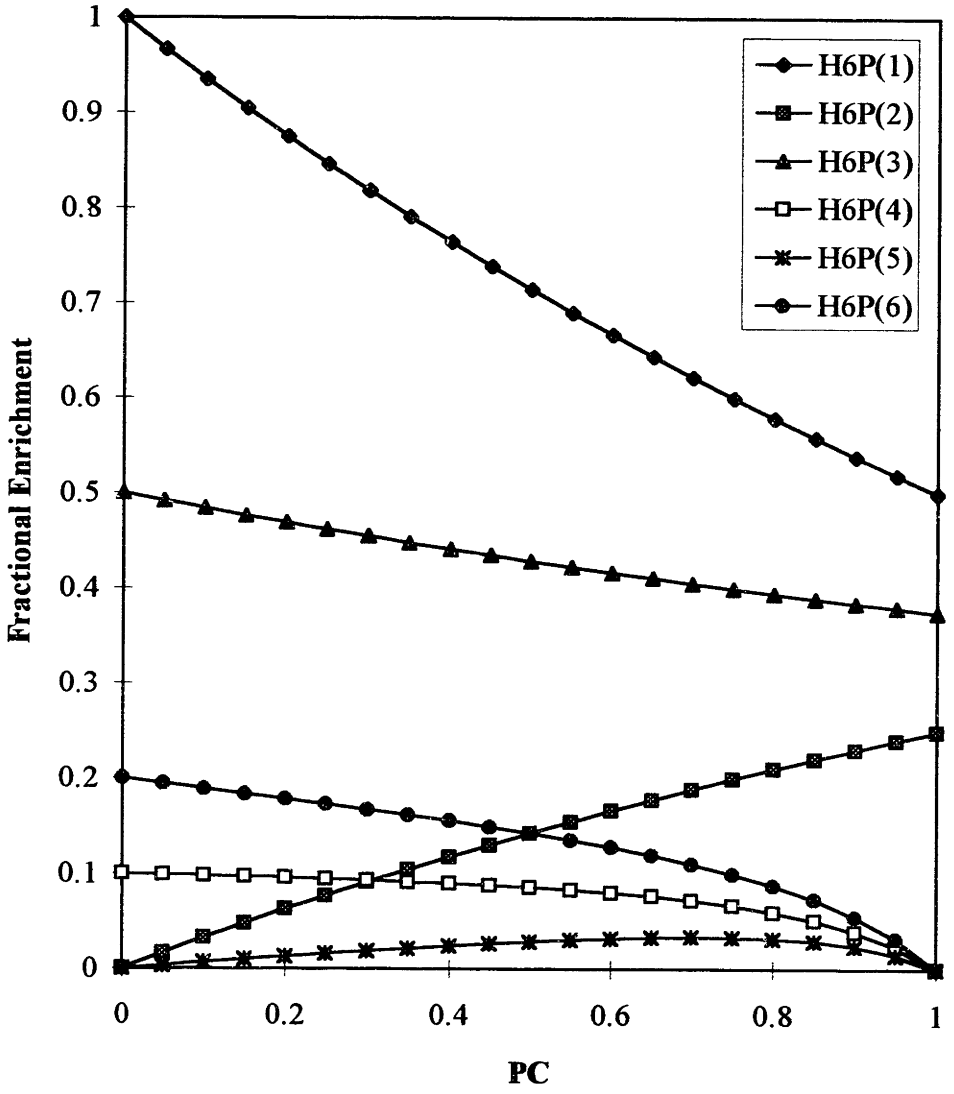

Figure 7.10 Effect of reversible reactions on label redistribution on hexose 6-phosphate: PC = 0.05.

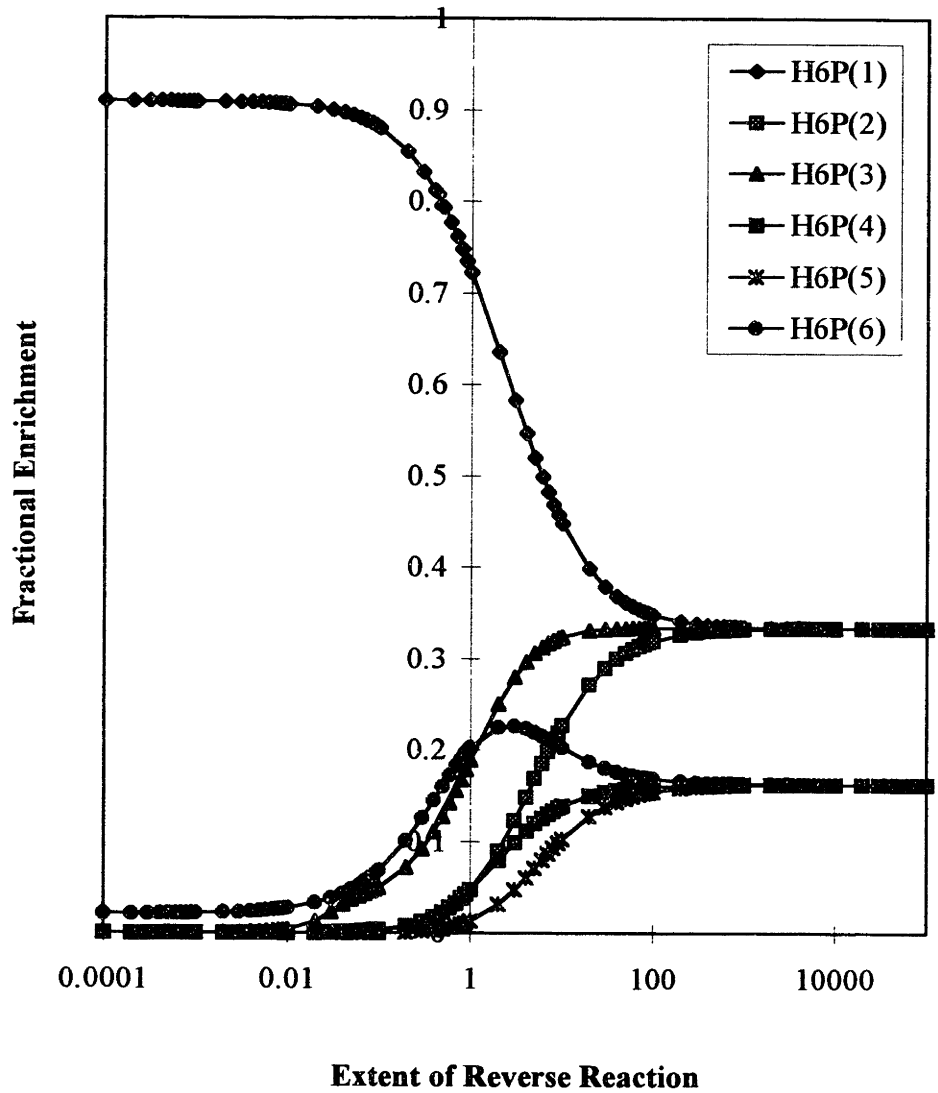

Figure 7.11 Effect of reversible reactions on label redistribution on hexose 6-phosphate: PC = 0.50.

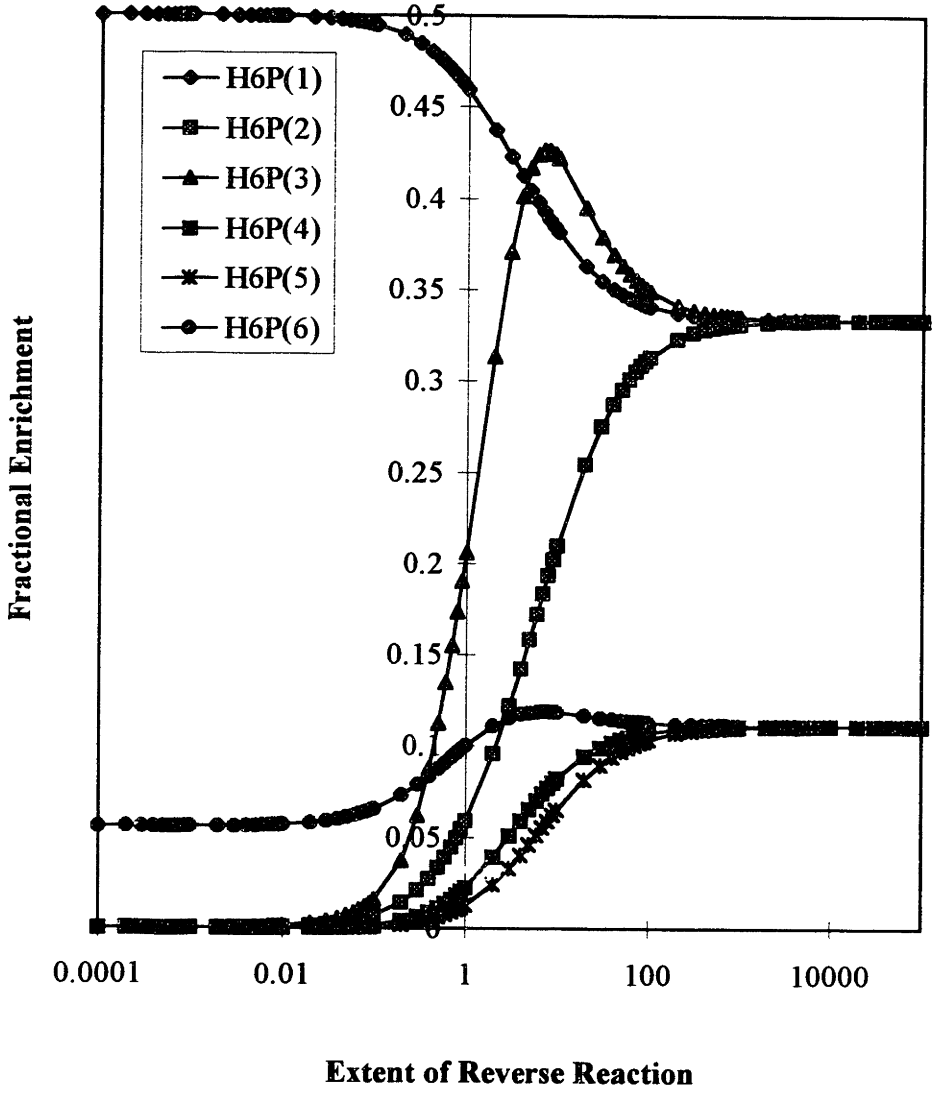

Chapter 8: Elucidation of Anaplerotic Pathways in *Corynebacterium glutamicum* via ^{13}C NMR Spectroscopy and GC-MS

8.1 Summary

We have obtained direct evidence indicating the presence of pyruvate carboxylating activity in *Corynebacterium glutamicum*, a lysine overproducing bacterium. This evidence was obtained through the use of ^{13}C nuclear magnetic resonance (NMR) spectroscopy and gas- chromatography mass-spectrometry (GC-MS) of secreted metabolites in a lysine fermentation. The distribution of ^{13}C label through multiple turns in the tricarboxylic acid cycle was accounted for properly and the resulting ^{13}C metabolite enrichments were employed in the interpretation of ^{13}C NMR and GC-MS data. Of critical importance in arriving at the conclusions was the use of *C. glutamicum* mutants with deletions of the pyruvate kinase (PK) and/or phosphoenolpyruvate carboxylase (PPC) enzymes. Our results demonstrate the presence of pyruvate carboxylating pathway(s) in *C. glutamicum* operating simultaneously with phosphoenolpyruvate carboxylase, with the latter enzyme contributing approximately 10% of the total oxaloacetate (OAA) synthesis during the lysine production phase with pyruvate and gluconate as carbon sources. Additionally, the flux through the TA enzyme converting OAA to aspartate was found to be between 24% and 42% of the total anaplerotic flux, i.e., the synthesis rate of OAA from phosphoenolpyruvate and pyruvate. These results are important for developing strategies to increase the total amount of carbon flux for the biosynthesis of the amino acids of aspartate family through metabolic engineering.

8.2 Introduction

Corynebacterium glutamicum and its related species, *Brevibacterium lactofermentum* and *Brevibacterium flavum*, have been used widely in the fermentation industry for amino acid production. Through genetic modifications via random mutagenesis [Shiio *et al.*, 1990; Yokota and Shiio, 1988] and gene cloning [Schrumpf *et al.*, 1992], these bacteria have been improved to excrete large amounts of amino acids into

the fermentation medium. While the above results were obtained through the manipulation of enzymes catalyzing the last few reactions of the product forming pathway, our interest here focuses primarily on the elucidation of the carbon flow in central carbon metabolism. Specifically, we are interested in identifying the metabolic pathways responsible for the synthesis of oxaloacetate (OAA) which is the immediate precursor of the aspartate family amino acids in these bacteria.

In cells grown on carbohydrate, OAA is a key metabolic branchpoint between energy generation and biosynthesis (Figure 8.1). OAA can condense with acetyl-CoA to enter the tricarboxylic acid (TCA) cycle for energy generation or it can be transaminated to aspartate, thus exiting the TCA cycle for amino acid biosynthesis. OAA and other TCA cycle intermediates used for biosynthesis can be replenished via the anaplerotic reactions which will be discussed in detail in the next section.

Previous research [Vallino and Stephanopoulos, 1993] has indicated that the yield and productivity of the aspartate family amino acids would depend critically on the carbon flux through anaplerotic pathways. Based on metabolite balances, it can be shown that the rate of lysine biosynthesis is always less than or equal to the rate of OAA synthesis via the anaplerotic pathways. Moreover, Gubler *et al.* [1994] and Peters-Wendisch *et al.* [1993] recently provided a surprising result that unlike many other organisms, there exist at least two anaplerotic pathways by which OAA can be replenished in *C. glutamicum* and its close relative, *B. lactofermentum.* In the above two studies, mutants deficient in phosphoenolpyruvate carboxylase (PPC) were constructed via a gene-disruption method and were grown in glucose minimal medium. Both wild type and PPC deficient mutant strains exhibited similar growth and lysine production profiles, establishing that PPC is dispensable for cell growth and lysine overproduction in these bacteria (at least up to the growth and synthesis rates obtained in these studies). Both PEP carboxykinase (PPCK) [Jetten *et al.*, 1994] and pyruvate carboxylase (PC) [Tosaka *et al*, 1979] have been reported to be present in *B. lactofermentum* and these enzymes can provide anaplerotic activity in the absence of PPC. However, previous researchers have failed to provide unequivocal and reproducible evidence for the establishment of either of the two enzymes as the PPC-compensating enzyme. Therefore, the objective of this work is to clarify the

role and activity of unknown anaplerotic pathways in *C. glutamicum*. Although the identification of active anaplerotic pathways is necessary for enhancing the productivity and yield of amino acid production, it is by no means suggestive of the exact type of manipulation that will bring about these results. Flux enhancing modifications can be determined through further examination of the kinetics of competing enzymatic reactions, the level of effector metabolites, and the carbon flux through the overall pathway following the methodologies of metabolic engineering.

In order to achieve the above objective, we have combined ^{13}C nuclear magnetic resonance (NMR) spectroscopy and gas chromatography-mass spectrometry (GC-MS) on one hand with specific genetic constructs and biochemical accounting on the other. ^{13}C NMR spectroscopy alone or in combination with GC-MS has been described in many applications in the literature: glycogen synthesis in rats studied by GC-MS and ^{13}C NMR [Kalderon *et al.*, 1986]; glucose recycling and production in glycogenosis type I and III studied by GC-MS [Kalderon *et al.*, 1989a] and by ^{13}C NMR [Kalderon *et al.*, 1989b]; ^{13}C NMR analysis of gluconeogenesis in primary hepatocytes and mouse liver [Cohen, 1979; Cohen *et al.*, 1987]; acetate utilization in *Sacchromyces cerevisiae* [den Hollander *et al.*, 1981; Dickinson *et al.*, 1983]; L-lysine biosynthesis in *Corynebacterium* species [Walker *et al.*, 1982; Yamaguchi *et al.*, 1986; Inbar *et al.*, 1987; Sonntag *et al.*, 1993]. Although in theory, metabolism can be followed noninvasively via ^{13}C NMR, in practice this application is often limited by the sensitivity of ^{13}C NMR spectroscopy. On the other hand, GC-MS requires very little sample and is much more sensitive than ^{13}C NMR spectroscopy, although the amount of information that can be obtained by this technique is indirect and thus often limited.

The primary result of this work is evidence for the presence of pyruvate carboxylating pathway(s) in *C. glutamicum*. We were able to obtain this result by applying the above analytical techniques to fermentation experiments using specifically constructed genetic mutants of *C. glutamicum*. In the following sections we first review the known anaplerotic reactions interconverting three-carbon and four-carbon metabolites in various organisms. We then summarize the theoretical framework for the interpretation of fractional ^{13}C enrichment at the individual carbon atoms of secreted lysine and

distributions of ^{13}C lysine isotopomers resulting from various labeled substrates. This framework demonstrates how the theoretical analysis can be used to provide a rational basis for the selection of substrates in fermentations with specific deletion mutants of *C. glutamicum*. Fermentation results are analyzed in light of this framework and conclusions regarding the activity of the various possible anaplerotic pathways are presented. Additionally, ^{13}C NMR and GC-MS data are further analyzed to provide an estimate of the relative carbon fluxes through two branchpoints: (1) OAA, the junction between energy generation and biosynthesis; and (2) tetrahydrodipicolinate, the junction between one-step *meso*-diaminopimelate dehydrogenase and four-step succinylase variant pathways in the terminal sequence from aspartate to lysine [Sonntag *et al.*, 1993].

8.3 Review of Anaplerotic Pathways

There are eight possible routes for the formation of OAA from glucose based on known enzymatic reactions reported in the literature (Table 8.1). OAA can be derived from three primary precursors: (1) the carboxylation of PEP (Reactions 1-3); (2) the carboxylation of pyruvate (Reactions 4-7); (3) via the glyoxylate shunt pathway (Reaction 8). Though Reactions 5-7 are correct stoichiometrically, they are extremely unlikely to occur in the proposed direction due to highly unfavorable thermodynamics. In fact, in various organisms studied to date (Table 8.2), only PPC, PC, PPCK, and PEP carboxytransphosphorylase (PPCTP) are known to be capable of replenishing OAA from PEP or pyruvate. For the operation of transcarboxylase (Reaction 5) as an OAA-replenishing reaction, the second enzyme (propionyl-CoA carboxylase) must be also operative in order to maintain the pool of methylmalonyl-CoA. Oxaloacetate decarboxylase (OAADC; Reaction 6) and malic enzyme (ME; Reaction 7) are active generally under the gluconeogenic conditions in which PEP or pyruvate is synthesized from the TCA cycle intermediates. The glyoxylate shunt pathway (Reaction 8) consisting of isocitrate lyase and malate synthase is generally regulated by catabolite repression and therefore remains uninduced when cultivated in glucose or other sugars. The exception occurs in *Arthrobacter pyridinolis* which apparently lacks PC and PPC and utilizes this pathway to synthesize OAA from glucose [Krulwich and Pelliccione, 1979].

Apparently, as indicated in Table 8.2, a remarkable diversity exists in nature for the choice of enzymes involved in OAA generation, as summarized in Table 8.2. Variations can be observed even within similar organisms. For example, three carboxylating enzymes (PPC, PC, and PPCK) are distributed in algae. In most prokaryotes, PPC is the prevalent choice although PC is found in some *Bacillus* and *Pseudomonas* species, and PPCK is found in some anaerobic bacteria. In most eukaryotes, PC is the only enzyme, although PPCK is reported in *Tubifex*, an anaerobic parasite [Hoffmann *et al.*, 1979]. Although plants are known to employ PPC universally, Wurtele and Nikolau [1990] recently reported the detection of PC in higher plants, a finding which suggests diversity in plants as well.

PPCTP has been detected so far in only two organisms: *Propionibacterium shermanii* [Cooper *et al.*, 1968] and the protozoan *Entamoeba histolytica* [Reeves, 1970]. A byproduct of this enzymatic reaction is diphosphate (PP_i) whose balance may be critical to the efficient functioning of this enzyme. Interestingly, in both organisms, several enzymes utilize PP_i instead of ATP to drive enzyme reactions.

PPCK is almost ubiquitous in all organisms and generally fulfills a gluconeogenic function. Organisms that employ PPCK as the anaplerotic enzyme are generally living in the aquatic environment and have to cope with limiting O_2 availability. Under such environmental conditions, it would be beneficial to conserve energy in every possible way and therefore PPCK, which produces ATP contrary to PPC and PC which consume ATP, may have been preferred route.

There are precedents to our finding that *C. glutamicum* contains more than one enzymes to perform the anaplerotic function of regenerating OAA. *Pseudomonas citronellolis* [O'Brien et al., 1977], *Pseudomonas fluorescens* [Higa et al., 1976] and *Azotobacter vinelandii* [Scrutton and Taylor, 1974] contain both PPC and PC. *Zea mays* contain three isozymes of PPC [Toh *et al.*, 1994], and *Saccharomyces cerevisiae* contains two isozymes of PC [Brewster *et al.*, 1992] though each is differentially regulated. Based on this observation, it is conceivable that organisms may contain multiple anaplerotic enzymes.

8.4 Predictions of ^{13}C Label Distribution

Several methods for obtaining quantitative expressions of the fractional ^{13}C enrichment at specific carbon atoms of intermediate metabolites, as well as distributions of ^{13}C isotopomers with different molecular masses, have been presented in the literature [Walker *et al.*, 1983; Chance *et al.*, 1983; Jans and Willem, 1989; Park *et al.*, 1996a]. These distributions depend not only on the type of labeled substrate but also on the metabolic pathways used by the cells. The general methodology of quantifying the ^{13}C distribution involves a detailed accounting of the ^{13}C label transfer through individual enzymatic reactions occurring in a metabolic pathway. The methodology yields analytical relationships for the ^{13}C label distribution in intermediate or secreted metabolites as functions of key pathway fluxes. The following two assumptions are generally applied to all cases considered:

1. There is no label scrambling by the conversion of OAA or malate to pyruvate by the activities of OAADC and ME. Likewise, it is assumed that PEP synthesis from OAA via PPCK, and PEP synthesis from pyruvate via PEP synthetase do not occur. These assumptions should be valid since these enzymes are only known to be active under the gluconeogenic conditions.
2. There is a full equilibration of label exchange from succinate to OAA in the TCA cycle. For example, the label at C-1 position of succinate will appear equally at C-1 and C-4 positions of OAA. Similarly, there is a full equilibration of label exchange between OAA and fumarate via reverse actions of MDH and fumarase. This is based on the assumption that the reactions catalyzed by MDH and fumarase are very rapid compared to reactions of citrate synthase (CS) and transaminase (TA). Likewise, malate formed via the glyoxylate shunt pathway is in full equilibrium with fumarate.

Two different combinations of genetic backgrounds and labeling media were used. The first employed a *C. glutamicum* mutant strain deficient in PK activity with labeled gluconate and unlabeled pyruvate as carbon sources. The use of gluconate bypasses the PEP:PTS system thus eliminating direct formation of pyruvate from glycolysis. Under these conditions, PEP carboxylation is the sole anaplerotic pathway. Thus, if gluconate is

unlabeled, OAA is also unlabeled. Similarly, any label in OAA and downstream metabolites of the TCA cycle and aspartate pathway are derived from gluconate.

The above possibility is illustrated in Figure 8.2 showing gluconate and [2-^{13}C]pyruvate as possible carbon source. Figure 8.2 also shows the second genetic/biochemical combination used in these studies. A double mutant deficient in both PPC and PK activities was used with unlabeled gluconate and labeled pyruvate as carbon sources. Under these conditions, OAA can be derived only from pyruvate via a pyruvate carboxylating pathway. Via the action of pyruvate carboxylating enzyme, P_2 is initially converted to O_2 if the bicarbonate fixed is unlabeled, and O_{24} if ^{13}C labeled bicarbonate is fixed. Ac_1 is formed from P_2 via the pyruvate dehydrogenase reaction. O_2 and Ac_1 condense to form C_{35} which subsequently traverses the TCA cycle in a sequence $K_{35} \rightarrow S_{24} \rightarrow \frac{1}{2} M_{13} + \frac{1}{2} M_{24} \rightarrow \frac{1}{2} O_{13} + \frac{1}{2} O_{24}$. Likewise, O_{24} results in a sequence $C_{135} \rightarrow K_{135} \rightarrow S_{24} \rightarrow \frac{1}{2} M_{13} + \frac{1}{2} M_{24} \rightarrow \frac{1}{2} O_{13} + \frac{1}{2} O_{24}$. For the newly formed OAA species, O_{13}, the same accounting principle is applied which results in the formation of O_{14}. The iterative process continues until there are no new species generated. It must be noted that due to topological constraints imposed by the enzymes, not all theoretically possible isotopomer species are found. For example, theoretically there are $2^4 = 16$ OAA isotopomer species possible, but only 7 species are generated.

Under the assumption of steady state, the relative population of all isotopomers can be obtained exclusively in terms of probabilities also reflecting the fluxes of connecting pathways. At each metabolic branchpoint, a probability is assigned to each competing pathway as measure of the likelihood that the branchpoint metabolite will be depleted by the corresponding reaction. The sum of all such probabilities equals unity. For example, if we assign the probability x to the event that OAA exits the TCA cycle via TA, then the probability of OAA to enter the TCA cycle via CS is $(1-x)$. Under the steady state assumption, the flux via CS is equal to the flux via pyruvate dehydrogenase and the flux via malate dehydrogenase. This implies that flux via TA is equal to the flux via pyruvate carboxylating pathway (PCP). Therefore, the probability, x, can be related to the flux rates as follows:

$$\frac{x}{1-x} = \frac{\text{Flux via TA}}{\text{Flux via CS}} = \frac{\text{Flux via PCP}}{\text{Flux via CS}} \qquad \textbf{(Eq. 8.1)}$$

As another example, we assign *w* to the probability that the bicarbonate is labeled with ^{13}C and *(1-w)* that it is unlabeled. Following a methodology described in Chapter 5, the relative population of OAA isotopomers can be obtained:

$$O_2 = O_3 = \frac{x(1-w)}{2} \qquad \textbf{(Eq. 8.2)}$$

$$O_{13} = O_{24} = O_{14} = \frac{x(1-x+w+xw)}{2(1+x)} \qquad \textbf{(Eq. 8.3)}$$

$$O_1 = O_4 = \frac{(1-x)^2}{2(1+x)} \qquad \textbf{(Eq. 8.4)}$$

$$O_1 + O_2 + O_3 + O_4 + O_{13} + O_{24} + O_{14} = 1 \qquad \textbf{(Eq. 8.5)}$$

Labeling patterns of the lysine from the two building blocks, OAA and pyruvate, can be determined based on the scheme in Figure 8.3 which shows the two different pathways in the terminal sequence [Sonntag *et al.*, 1993]. The four-step succinylase variant pathway contains the enzymes of N-succinyl-2,6-ketopimelate synthase, N-succinyl-aminoketopimelate:glutamate aminotransferase, N-succinyl-diaminopimelate desuccinylase, and diaminopimelate epimerase. The epimerase generates equimolar distributions of two differently labeled lysine isotopomer whereas the one-step pathway via the activity of *meso*-DAP dehydrogenase produces only one form of lysine. Because of the operation of these two pathways, an unequal distribution of lysine isotopomers is expected. One can therefore determine the relative contribution of each of these pathways based on the ^{13}C labeling distribution of lysine isotopomers. Again, we assign probabilities to denote the relative activities of two pathways and let *y* be the probability of lysine formed via the one-step *meso*-DAP pathway. Therefore, the following relationship can be described:

$$\frac{y}{1-y} = \frac{\text{Flux via } meso\text{ - DAP}}{\text{Flux via Succinylase}} \qquad \textbf{(Eq. 8.6)}$$

The relative population of lysine isotopomers can be related to that of OAA as follows. One mole of O_1 condensing with P_2 produces $\frac{(1-y)}{2}$ moles of L_{16} and $\frac{(1-y)}{2}$ moles of L_2 via the succinylase pathway and *y* moles of L_{16} via the *meso*-DAP pathway.

Incorporating the relative concentration of O_1 from (Eq. 4), the relative concentrations of L_{16} and L_2 are

$$L_{16} = \frac{(1-x)^2}{2(1+x)}\frac{(1+y)}{2} \quad \textbf{(Eq. 8.7)}$$

$$L_2 = \frac{(1-x)^2}{2(1+x)}\frac{(1-y)}{2} \quad \textbf{(Eq. 8.8)}$$

Similarly, the relative concentrations for the remaining nine lysine isotopomers can be found:

$$L_{26} = \frac{(1-w)}{2} \quad \textbf{(Eq. 8.9)}$$

$$L_3 = \frac{(1-w)}{2}\frac{(1+y)}{2} \quad \textbf{(Eq. 8.10)}$$

$$L_{15} = \frac{(1-w)}{2}\frac{(1-y)}{2} \quad \textbf{(Eq. 8.11)}$$

$$L_{246} = \frac{x(1-x+w+xw)}{2(1+x)} \quad \textbf{(Eq. 8.12)}$$

$$L_{136} = \frac{x(1-x+w+xw)}{2(1+x)}\frac{(1+y)}{2} \quad \textbf{(Eq. 8.13)}$$

$$L_{25} = \frac{x(1-x+w+xw)}{2(1+x)}\frac{(1-y)}{2} \quad \textbf{(Eq. 8.14)}$$

$$L_{146} = \frac{x(1-x+w+xw)}{2(1+x)}\frac{(1+y)}{2} \quad \textbf{(Eq. 8.15)}$$

$$L_{46} = \frac{(1-x)^2}{2(1+x)}\frac{(1+y)}{2} \quad \textbf{(Eq. 8.16)}$$

$$L_{24} = \frac{x(1-x+w+xw)}{2(1+x)}\frac{(1-y)}{2} + \frac{(1-x)^2}{2(1+x)}\frac{(1-y)}{2} \quad \textbf{(Eq. 8.17)}$$

Expressions for the fractional ^{13}C enrichment of the lysine carbon atoms follows directly from the lysine isotopomer distribution as the sum of isotopomers that contain the ^{13}C label at the specific position. For example, the fractional ^{13}C enrichment at C-1 position of lysine is

$$C\text{-}1 = L_{16} + L_{15} + L_{136} + L_{146} \quad \textbf{(Eq. 8.18)}$$

Contribution from the other seven species are not considered since none of them contain ^{13}C label at C-1 position. Likewise,

$$C\text{-}2 = L_2 + L_{26} + L_{246} + L_{25} + L_{24} \quad \textbf{(Eq. 8.19)}$$

$$C\text{-}3 = L_3 + L_{136} \quad \textbf{(Eq. 8.20)}$$

$$C\text{-}4 = L_{246} + L_{146} + L_{46} + L_{24} \quad \textbf{(Eq. 8.21)}$$

$$C\text{-}5 = L_{15} + L_{25} \quad \textbf{(Eq. 8.22)}$$

$$C\text{-}6 = L_{16} + L_{26} + L_{246} + L_{136} + L_{146} + L_{46} \quad \textbf{(Eq. 8.23)}$$

Expressions for the molecular weight (MW) distribution of lysine isotopomers can be calculated in the similar manner. If M is the MW of natural lysine with all six carbon atoms unlabeled (i.e., equal to ^{12}C), then L_2 and L_3 have a MW equal to (M + 1) since both contain only one ^{13}C atom. Therefore, the relative population of lysine isotopomers with MW equal to (M + 1) is

$$(M + 1) = L_2 + L_3 \quad \textbf{(Eq. 8.24)}$$

Likewise, the isotopomer populations with MW of (M + 2) and (M + 3) can be given by

$$(M + 2) = L_{16} + L_{26} + L_{15} + L_{25} + L_{24} \quad \textbf{(Eq. 8.25)}$$

$$(M + 3) = L_{136} + L_{146} + L_{246} \quad \textbf{(Eq. 8.26)}$$

Following the above methodology, analytical expressions for the fractional ^{13}C enrichment at individual carbon atoms of lysine as well as ^{13}C lysine isotopomer distribution are summarized in Tables 8.3 through 8.5 for the three cases using unlabeled gluconate and [2-^{13}C]pyruvate, [1-^{13}C]pyruvate, [3-^{13}C]pyruvate, respectively, as substrates.

Another possibility is illustrated in Figure 8.4 for the case of a PK-deficient strain and [U-^{13}C]gluconate and unlabeled pyruvate as carbon sources. Table 8.6 summarizes the predicted enrichments and isotopomer distributions in this case where both PEP and pyruvate carboxylation are assumed to operate. Since OAA can be synthesized from two different sources, namely PEP and pyruvate, we have introduced an additional parameter, v, which denotes the probability of OAA to be derived from PEP carboxylation. Thus, $\frac{v}{(1-v)}$ indicates the ratio of the activities of PEP carboxylation versus pyruvate carboxylation pathways.

Although the analysis of ^{13}C label distribution in the metabolites can yield exact analytical expressions, the results of Tables 8.3-8.5 are also useful in a qualitative manner. The analysis of these results provide a rational basis for selecting properly labeled pyruvate in order to discriminate between the three possible pathways. For example, if [1-^{13}C]pyruvate is chosen as the labeled substrate, this will yield an identical labeling pattern in both PEP carboxylating and pyruvate carboxylating pathways (Table 8.7). No distinction between these cases is thus possible on the basis of qualitative presence of ^{13}C label in the six carbons of the lysine molecules, even though the possibility of the operation of glyoxylate shunt pathway can be differentiated. The expected patterns by [2-^{13}C]pyruvate provides a clear distinction between the three possibilities. Under the assumption of the operation of pyruvate carboxylating pathway, we expect ^{13}C enrichment at all six carbons of lysine and lysine isotopomers with MWs of (M + 1), (M + 2), and (M + 3). However, under the assumption of the operation of PEP carboxylating pathway, we expect no ^{13}C enrichment at C-3 and C-5 positions, and also no isotopomers with mass (M + 3). Finally, under the assumption of the operation of glyoxylate shunt pathway, we expect no C-3 and C-5 enrichment but isotopomers with mass (M + 1), (M + 2), and (M + 3). Therefore, the combined measurements of ^{13}C enrichment and isotopomer distribution using the [2-^{13}C]pyruvate should distinguish among the three possibilities.

With [3-^{13}C]pyruvate, no such discrimination can be achieved by ^{13}C NMR since ^{13}C labels are expected at all six positions irrespective of anaplerotic pathways involved. GC-MS allows distinction only in a theoretical sense. With the PEP carboxylation pathway, all four isotopomers with MWs of (M + 1), (M + 2), (M + 3), and (M + 4) are expected whereas with pyruvate carboxylation pathway, three isotopomers with MWs of (M + 2), (M + 3), and (M + 4) are expected and with glyoxylate shunt pathway, only two with (M + 3) and (M + 4) are expected. However, discrimination simply based on the absence of peaks is difficult due to impurity in the labeling and derivatization substrates. This makes [3-^{13}C]pyruvate unsuitable.

8.5 Results

8.5.1 Simultaneous Uptake of Gluconate and Pyruvate

The metabolic profiles of 1-liter batch fermentations on gluconate and pyruvate with the wild type (ATCC 21253), *pyk* mutant (SM575) and *ppc pyk* mutant (SM607) strains are shown in Figure 8.5. Although the three strains exhibit significant differences under usual fermentation conditions, such differences are notably absent under the low concentrations chosen for these experiments. Simultaneous uptake and consumption of gluconate and pyruvate is critical in confirming with the metabolic model dictating that all intermediates leading up to PEP are derived from gluconate and intermediates located below pyruvate are derived from pyruvate. Typically, in approximately 12-15 hours, these strains accumulated about 1.5 g/l of lysine.

8.5.2 ^{13}C Labeling Experiments with [2-^{13}C]Pyruvate, [1-^{13}C]Pyruvate, and [U-^{13}C]Gluconate

A proton-decoupled ^{13}C NMR spectrum of the supernatant taken from *ppc pyk* mutant (SM607) incubated with [2-^{13}C]pyruvate is shown in Figure 8.6 with relative ^{13}C enrichment summarized in Table 8.8. All six peaks, due to the resonances of the corresponding six lysine carbons, can be identified; C-1 at 176.5 ppm, C-2 at 55.4 ppm, C-3 at 27.3 ppm, C-4 at 22.5 ppm, C-5 at 30.8 ppm, and C-6 at 40.1 ppm. Analyzed in the context of Table 8.7, the ^{13}C enrichment pattern eliminates the possibilities of the sole operation of either PEP carboxylation or glyoxylate shunt pathways. GC-MS measurements, summarized in Table 8.9, show a significant fraction of isotopomers with mass (M + 3) as well as (M + 1) and (M + 2). The GC-MS results, taken in conjunction with the ^{13}C enrichments of Table 8.8, eliminate the possibilities that, PEP carboxylation only, or the glyoxylate shunt only, or any combination of PEP carboxylation and glyoxylate shunt are the sole sources of OAA anaplerotic carbon. Taken together, these results support the supposition of the operation of a pyruvate carboxylating pathway.

A proton-decoupled ^{13}C NMR spectrum taken from the *ppc pyk* mutant (SM607) incubated with [1-^{13}C]pyruvate is shown in Figure 8.7. Only two peaks due to resonances of C-1 and C-4 of lysine can be observed at 24.2 ppm and 178.1 ppm, respectively. GC-MS analysis shows isotopomer species with MWs of (M + 0), (M + 1), and (M + 2).

Although they add no new information, these data are consistent with the conclusions derived from the [2-^{13}C]pyruvate experiment.

A proton-decoupled spectrum of the concentrated supernatant sample taken from *pyk* mutant (SM575) incubated with labeled [U-^{13}C]gluconate and unlabeled pyruvate reveals visible peaks at C-1, C-2, C-3, and C-4 positions as shown in Figure 8.8. Peaks corresponding to C-5 and C-6 were not detected, even though the sample is concentrated to 10g/l, suggesting the high activity of *meso*-DAP dehydrogenase activity. The GC-MS data resulted in a distribution of 76.87% at (M + 0), 18.99% at (M + 1), and 3.54% at (M + 2).

8.6 Discussion

8.6.1 Evidence for the Presence of Pyruvate Carboxylating Pathway in *C. glutamicum*

One motivation for our work is the result that PPC is dispensable in *Corynebacterium*. Previously, Tosaka *et al.* [1979] reported the detection of pyruvate carboxylase in *B. lactofermentum*. However, using the identical assay, we have not been able to detect PC activity above background levels in the cell-free extracts of both wild type and PPC-deficient *C. glutamicum* strains. Therefore, another means was sought to establish the presence of a pyruvate carboxylating enzyme *in vivo*. A steady state analysis of the supernatants from the experiments of [1-^{13}C]pyruvate and [2-^{13}C]pyruvate as analyzed by ^{13}C NMR spectroscopy and GC-MS can be best explained by the hypothesis that a pyruvate carboxylating pathway exists in *C. glutamicum*.

Pyruvate carboxylation can be catalyzed by four enzymes as indicated in Table 8.2. Even though the genetic and enzymatic evidence is not yet established, the pyruvate carboxylation enzyme is most likely PC. This is based on experimental data showing that OAA formation by the gluconeogenic enzymes such as OAADC, ME and PPCK is not sufficient to support growth on glucose. For example, a *ppc* mutant of *E. coli* was not able to grow on glucose, even when transformed with a plasmid encoding the gene of PPCK under the control of *tac* promoter system, a modification that removed the expression of PPCK gene from catabolite repression [Chao and Liao, 1994]. Disruption

of both genes of PC in *S. cerevisiae* resulted in inability to grow on glucose despite the enhanced levels of PPCK and ME [Brewster *et al.*, 1992]. Similarly, a PC-deficient strain of *B. subtilis* was unable to grow on glucose even though a high PPCK activity was detected under the normal glycolytic conditions [Diesterhaft and Freese, 1973]. There is no *in vivo* evidence that OAADC and ME can operate in the carboxylation direction, and this scenario is very unlikely due to thermodynamic limitations.

Claims regarding the presence of biochemical enzymatic steps based on isotopic labeling studies must be done with care, especially in the presence of multiple pathways. de los Santos *et al.* [1985] applied ^{13}C NMR to settle the controversy on the nature of the primary CO_2-fixation reaction in the insect parasite *Crithidia fasciculata*. They claimed PPCK as the main CO_2-fixing enzyme despite the fact that other enzymes such as PC and ME are present in *C. fasciculata*. However, this claim is invalid since the model did not account for the possible label scrambling via the TCA cycle. Tosaka *et al.* [1979] suggested the possibility of PC in *B. lactofermentum* with a ^{13}C NMR study. They incubated the cells with lactate and ^{13}C labeled bicarbonate and detected the appearance of ^{13}C label in lysine that would correspond to $^{13}CO_2$-fixation. However, the possibility of $^{13}CO_2$ fixation via the action of PPC, which is also present when cultivated in lactate [Jetten *et al.*, 1994], is not clearly eliminated which would necessitate the use of PPC-deficient strains.

8.6.2 Calculation of Relative Fluxes at Metabolic Network Branchpoints

In addition to providing evidence for the unknown pathway, ^{13}C NMR and GC-MS also contain information about the relative activities at the tetrahydrodipicolinate and OAA branchpoints. Algebraic manipulation of expressions in Tables 8.3-8.6 gives a straightforward way of obtaining these values. In the case of [2-^{13}C]pyruvate, from the expressions of C-2 and C-6, one can obtain

$$y = \frac{C_6 - C_2}{2 - (C_2 + C_6)} \quad \text{and} \quad x = \frac{(C_2 + C_6) - 1}{2 - (C_2 + C_6)} \qquad \textbf{(Eq. 8.27)}$$

Alternatively, from the expressions of C-3 and C-5,

$$y = \frac{C_3 - C_5}{C_3 + C_5} \text{ and } x = \frac{(C_3 + C_5)}{1 - (C_3 + C_5)} \quad \textbf{(Eq. 8.28)}$$

The remaining parameter w, which is the fraction of bicarbonate labeled with ^{13}C, can be calculated by using the expression of C-1 or C-4. From the expression of C-4 one can obtain

$$w = \frac{2x^2 - x - 1}{x(1+x)} + \frac{2C_4}{x} \quad \textbf{(Eq. 8.29)}$$

Alternatively, from the expression of C-1 one can obtain

$$w = \frac{2x^2 - x - 1}{x(1+x)} + \frac{4C_1}{(1+y)} \quad \textbf{(Eq. 8.30)}$$

From the measurements of the ^{13}C enrichments of C-2, C-6, and C-4 in Table 8.8, the following parameters were estimated: $x = 0.24$ which is the fraction of OAA exiting the TCA cycle via TA reaction and $y = 0.51$ which is the fraction of lysine derived via the one-step *meso*-DAP dehydrogenase pathway. Consequently, $w = 0.45$. These values predict isotopomer distributions of 5.7% (M + 1), 60.8% (M + 2), and 33.5% (M + 3). GC-MS indicates a rather significant fraction of lysine isotopomers with mass (M + 1) but the ratio of $\frac{(M+2)}{(M+3)}$ is about 1.9, close to theoretically expected value of 1.8. Alternatively, from the enrichments at C-3, C-5, and C-4, $x = 0.26$, $y = 0.46$, and $w = 0.46$ were obtained. These values predict isotopomer distributions with 5.9% (M + 1), 60.8% (M + 2), and 33.3% (M + 3).

Similar calculations can be performed with [1-^{13}C]pyruvate. Since there are three unknown parameters x, y and w and only two measured values were available from ^{13}C NMR, two additional measurements from GC-MS were provided to calculate the parameters using the nonlinear least square fit. This gave $x = 0.42$, $y = 0.61$, and $w = 0.39$.

The purpose of the [U-^{13}C]gluconate experiment was to estimate the relative activities of the two carboxylation enzymes. The ratio of the activities of PEP carboxylation versus pyruvate carboxylation pathways can be expressed as $\frac{v}{(1-v)}$. v denotes the probability of OAA to be derived from PEP carboxylation and can be

determined from the analytical expressions of Table 8.6. Lysine whose OAA is derived via pyruvate carboxylation would be predominantly in the form of L, L_1, and L_4. The latter two species are essentially due to the fixation of ^{13}C bicarbonate which could be evolved following the oxidation of [U-^{13}C]gluconate. Lysine whose OAA is derived via PEP carboxylation would contain up to four ^{13}C carbons.

Similar to the procedure used in estimating the probability parameters in [1-^{13}C]pyruvate and [2-^{13}C]pyruvate, the measurements of ^{13}C NMR and GC-MS were used to calculate the four unknown parameters: This gave $x = 0.35$, $y = 0.50$, $w = 0.51$, and $v = 0.10$. The value of $v = 0.10$ indicates that the pyruvate carboxylating pathway is about 9 times more active than the PEP carboxylating pathway. This is feasible if there exists no regulation on the activity of pyruvate carboxylating enzyme. In fact, in *P. fluorescens* [Higa, 1976], *A. vinelandii* [Scrutton, 1974], and *P. citronellolis* [Scrutton, 1972], all of which are known to possess two OAA-forming carboxylases, i.e., PPC and PC, PPC is subject to a tight regulation via activation by acetyl-CoA and feedback inhibition by L-aspartate [Shiio *et al.*, 1990] whereas PC is insensitive to such regulation. The probable lack of regulatory control on the pyruvate carboxylating enzyme makes this enzyme an attractive target for amplification in order to increase carbon flow into OAA and hence to increase the productivity and yield of aspartate-amino acids. Our calculated value of y which is in the range of 46 to 61%, is rather large, as compared to those values reported in the literature: 30 to 40% calculated by Yamaguchi *et al.* [1986] and 30% reported by Sonntag *et al.* [1993]. The ratio of anaplerotic pathway to the TCA cycle can be represented as $\frac{x}{(1-x)}$ and calculated as 0.72 in [1-^{13}C]pyruvate, 0.32 in [2-^{13}C]pyruvate, and 0.54 in [U-^{13}C]gluconate. The large deviations could be attributed to the fact that our calculated parameter values represent the cumulative average, and not instantaneous values.

8.7 Conclusions

The ^{13}C labeling studies in the present paper provides strong evidence for the presence of pyruvate carboxylating pathway in *C. glutamicum*. Two factors were critical

in reaching this conclusion. First is the development of mutant strains that allowed minimal ^{13}C label scrambling among intermediates. For example, the possibility of label scrambling between PEP and pyruvate is eliminated by using the PK- deficient *C. glutamicum* strain. This is critical since the labeling pattern of OAA formed by PEP carboxylation is identical to that formed via the combined actions of PK and pyruvate carboxylation. Likewise, the contribution of PEP to OAA via PPC present in the wild type is eliminated by using a strain deficient in PPC. Second, we followed a rigorous modeling methodology which accounts for label scrambling due to the operation of cyclic pathways such as the TCA cycle. This allowed us to predict label distributions under various scenarios and helped to select proper substrate for the ^{13}C labeling studies. We are currently seeking genetic and biochemical evidence for pyruvate carboxylating enzyme in *C. glutamicum*.

8.8 Nomenclature

CS	citrate synthase
M	molecular weight of natural lysine
MDH	malate dehydrogenase
ME	malic enzyme
OAA	oxaloacetate
OAADC	oxaloacetate decarboxylase
PC	pyruvate carboxylase
PCP	pyruvate carboxylating pathway
PDH	pyruvate dehydrogenase
PEP	phosphoenolpyruvate
PK	pyruvate kinase
PPC	phosphoenolpyruvate carboxylase
ppc	gene encoding phosphoenolpyruvate carboxylase
PPCK	phosphoenolpyruvate carboxykinase
PP_i	diphosphate
pyk	gene encoding pyruvate kinase
TA	transaminase
TCA	tricarboxylic acid cycle
x	probability of oxaloacetate to exit the TCA cycle
(1 - x)	probability of oxaloacetate to enter the TCA cycle
y	probability of lysine formed via one-step *meso*-dihydrogenase pathway
(1 - y)	probability of lysine formed via four-step succinylase pathway
w	probability of bicarbonate labeled with ^{13}C
(1 - w)	probability of bicarbonate labeled with ^{12}C
v	probability of OAA formed via PEP carboxylating pathway
(1 - v)	probability of OAA formed via pyruvate carboxylating pathway

8.9 References

Appleby, G., Colbeck, J., Holdsworth, E.S. (1980). β-carboxylation enzymes in marine phytoplankton: Isolation and purification of PEPC from *Amphidinium carterae* (Dinophyceae). *J. Phycol.* **16**: 290-295.

Bercovitz, A., Peleg, Y., Battat, E., Rokem, J.S., Goldberg, I. (1990). Localization of pyruvate carboxylase in organic acid-producing *Aspergillus* strains. *App. Environ. Microbiol.* **56**: 1594-1597.

Brewster, N.K., Val, D.L., Walker, M.E., Wallace, J.C. (1994). Regulation of pyruvate carboxylase Isozyme (*PYC*1, *PYC*2) gene expression in *Saccharomyces cerevisiae* during fermentative and nonfermentative growth. *Arch. Biochem. Biophys.* **311**: 62-71.

Chance, E.M., Seeholzer, S.H., Kobayashi, K., Williamson, J.R. (1983). Mathematical analysis of isotope labeling in the citric acid cycle with applications to ^{13}C NMR studies in perfused rat hearts. *J. Biol. Chem.* **258**: 13785-13794.

Chao, Y.-P., Liao, J.C. (1993). Alteration of growth-yield by overexpression of phosphoenolpyruvate carboxylase and phosphoenolpyruvate carboxykinase in *Escherichia coli*. *App. Environ. Microbiol.* **59**: 4261-4265.

Cohen, S.M. (1987). ^{13}C and ^{31}P NMR studies of hepatic metabolism in two experimental-models of diabetes. *Ann. N.Y. Acad. Sci.* **508**: 109-129.

Cohen, S.M., Ogawa, S., Shulman, R.G. (1979). ^{13}C NMR studies of gluconeogenesis in rat liver cells: Utilization of labeled glycerol by cells from euthyroid and hyperthyroid rats. *Proc. Natl. Acad. Sci. USA* **76**: 1603-1607.

Cooper, T.G., Tchen, T.T., Wood, H.G., Benedict, C.R. (1968). The carboxylation of phosphoenolpyruvate and pyruvate. I. The active species of "CO_2" utilized by phosphoenolpyruvate carboxykinase, carboxytransphosphorylase, and pyruvate carboxylase. *J. Biol. Chem.* **243**: 3857-3863.

de los Santos, C., Buldain, G., Frydman, B., Cannata, J.J.B., Cazzulo, J.J. (1985). Carbon-13 nuclear magnetic resonance analysis of [1-^{13}C] glucose metabolism in *Crithidia fasciculata* - Evidence of CO_2 fixation by phospho*enol*pyruvate carboxykinase. *Eur. J. Biochem.* **149**: 421-429.

den Hollander, J.A., Behar, K.L., Shulman, R.G. (1981). ^{13}C NMR study of transamination during acetate utilization by *Saccharomyces cerevisiae*. *Proc. Natl. Acad. Sci. USA* **78**: 2693-2697.

Descolas-Gros, C., Fontugne, M.R. (1985). Carbon fixation in marine phytoplankton: carboxylase activities and stable carbon-isotope ratios; physiological and paleoclimatological aspects. *Mar. Biol.* **87**: 1-6.

Descolas-Gros, C., Oriol, L. (1992). Variations in carboxylase activity in marine phytoplankton cultures. β–carboxylation in carbon flux studies. *Mar. Ecol. Prog. Ser.* **85**: 163-169.

Dickinson, J.R., Dawes, I.W., Boyd, A.S.F., Baxter, B.L. (1983). ^{13}C NMR studies of acetate metabolism during sporulation of *Saccharomyces cerevisiae*. *Proc. Natl. Acad. Sci. USA* **80**: 5847-5851.

Diesterhaft, M.D., Freese, E. (1973). Role of pyruvate carboxylase, phosphoenolpyruvate carboxykinase, and malic enzyme during growth and sporulation of *Bacillus subtilis*. *J. Biol. Chem.* **248**: 6062-6070.

Gubler, M., Park, S.M., Jetten, M., Stephanopoulos, G., Sinskey, A.J. (1994). Effects of phosphoenol pyruvate carboxylase deficiency on metabolism and lysine production in *Corynebacterium glutamicum*. *Appl. Microbiol. Biotechnol.* **40**: 857-863.

Gupta, S.D., Maheshwari, R. (1985). Is organic acid required for nutrition of thermophilic fungi? *Arch. Microbiol.* **141**: 164-169.

Higa, A.I., Milrad de Forchetti, S.R., Cazzulo, J.J. (1976). CO_2-fixing enzymes in *Pseudomonas fluorescens*. *J. Gen. Microbiol.* **93**: 63-74.

Hoffmann, K.H., Mustafa, T., Jorgensen, J.B. (1979). Role of pyruvate kinase, phosphoenolpyruvate carboxykinase, malic enzyme and lactate dehydrogenase in anaerobic energy metabolism of *Tubifex* spec. *J. Comp. Physiol.* **130**: 337-345.

Holdsworth, E.S., Bruck, K. (1977). Enzymes concerned with β-carboxylation in marine phytoplankter-purification and properties of phosphoenolpyruvate carboxykinase. *Arch. Biochem. Biophys.* **182**: 87-94.

Inbar, L., Lapidot, A. (1987). ^{13}C-NMR, ^{1}H-NMR and gas-chromatography mass-spectrometry studies of the biosynthesis of ^{13}C-enriched L-lysine by *Brevibacterium flavum*. *Eur. J. Biochem.* **162**: 621-633.

Israel, A., Beer, S., Bowes, G. (1991). Photosynthetic carbon acquisition in the red alga *Gracilaria conferta*. *Mar. Biol.* **110**: 195-198.

Jetten, M.S.M., Pitoc, G.A., Follettie, M.T., Sinskey, A.J. (1994). Regulation of phospho(enol)-pyruvate- and oxaloacetate-converting enzymes in *Corynebacterium glutamicum*. *Appl. Microbiol. Biotechnol.* **41**: 47-52.

Jones, B.N., Gilligan, J.P. (1983). *o*-Phthalaldehyde precolumn derivatization and reversed-phase high-performance liquid chromatography of polypeptide hydrolysates and physiological fluids. *J. Chromatogr.* **266**: 471-482.

Kalderon, B., Gopher, A., Lapidot, A. (1986). Metabolic pathways leading to liver glycogen repletion in vivo, studied by GC-MS and NMR. *FEBS Lett.* **204**: 29-32.

Kalderon, B., Korman, S.H., Gutman, A., Lapidot, A. (1989a). Estimation of glucose carbon recycling in children with glycogen-storage disease: A ^{13}C NMR study Using [U-^{13}C]glucose. *Proc. Natl. Acad. Sci. USA* **86**: 4690-4694.

Kalderon, B., Korman, S.H., Gutman, A., Lapidot, A. (1989b). Glucose recycling and production in glycogenosis type I and typeIII: stable isotope technique study. *Am. J. Physiol.* **257**: E346-E353.

Kapke, P.A., Brown, A.T., Lillich, T.T. (1980). Carbon dioxide metabolism by *Capnocytophaga ochracea*: Identification, characterization, and regulation of a phosphoenolpyruvate carboxykinase. *Infect. Immun.* **27**: 756-766.

Katagiri, F., Kodaki, T., Fujita, N., Izui, K., Katsuki, H. (1985). Nucleotide sequence of the phosphoenolpyruvate carboxylase gene of the cyanobacterium *Anacystis nidulans*. *Gene* **38**: 265-269.

Kerby, N.W., Raven, J.A. (1985). Transport and fixation of inorganic carbon by marine algae. *Adv. Bot. Res.* **11**: 71-123.

Krulwich, T.A., Pelliccione, N.J. (1979). Catabolic pathways of coryneforms, nocardias, and mycobacteria. *Ann. Rev. Microbiol.* **33**: 95-111.

Lem, N.W., Penrose, D.M., Glick, B.R. (1986). Partial purification and characterization of phosphoenolpyruvate carboxylase from the cyanobacterium *Anabaena variabilis*. *Biochem. Cell Biol.* **64**: 427-433.

Melville, S.B., Michel, T.A., Macy, J.M. (1988). Pathway and sites for energy conservation in the metabolism of glucose by *Selenomonas ruminantium*. *J. Bacteriol.* **170**: 5298-5304.

O'Brien, R.W., Chuang, D.T., Taylor, B.L., Utter, M.F. (1977). Novel enzymic machinery for the metabolism of oxaloacetate, phosphoenolpyruvate, and pyruvate in *Pseudomonas citronellolis*. *J. Biol. Chem.* **252**: 1257-1263.

Peters-Wendisch, P.G., Eikmanns, B.J., Thierbach, G., Bachmann, B., Sahm, H. (1993). Phosphoenolpyruvate carboxylase in *Corynebacterium glutamicum* is dispensable for growth and lysine production. *FEMS Microbiol. Let.* **112**: 269-274.

Podkovyrov, S.M., Zeikus, J.G. (1993). Purification and characterization of phosphoenolpyruvate carboxykinase, a catabolic CO_2-fixing enzyme, from *Anaerobiospirillum succiniciproducens*. *J. Gen. Microbiol.* **139**: 223-228.

Pönsgen-Schmidt, E., Schneider, T., Hammer, U., Betz, A. (1988). Comparison of phosphoenolpyruvate-carboxykinase from autotrophically and heterotrophically grown Euglena and its role during anaerobiosis. *Plant Physiol.* **86**: 457-462.

Reeves, R.E. (1970). Phosphopyruvate carboxylase from *Entamoeba histolytica*. *Biochim. Biophys. Acta* **220**: 346-349.

Reiskind, J.B., Bowes, G. (1991). The role of phosphoenolpyruvate carboxykinase in a marine macroalga with C_4-like photosynthetic characteristics. *Proc. Natl. Acad. Sci. USA* **88**: 2883-2887.

Schobert, P., Bowien, B. (1984). Unusual C_3 and C_4 metabolism in the chemoautotroph *Alcaligenes eutrophus*. *J. Bacteriol.* **159**: 167-172.

Schöttler, U., Wienhausen, G. (1981). The importance of the phosphoenolpyruvate carboxykinase in the anaerobic metabolism of two marine polychaetes- *In vivo* investigation on *Nereis virens* and *Arenicola marina*. *Comp. Biochem. Physiol.* **68B**: 41-48.

Schrumpf, B., Eggeling, L., Sahm, H. (1992). Isolation and prominent characteristics of a L-lysine hyperproducing strain of *Corynebacterium glutamicum*. *Appl. Microbiol. Biotechnol.* **37**: 566-571.

Schuller, K.A., Plaxton, W.C., Turpin, D.H. (1990). Regulation of phosphoenolpyruvate carboxylase from the green alga *Selenastrum minutum* - Properties associated with replenishment of tricarboxylic acid cycle intermediates during ammonium assimilation. *Plant Physiol.* **93**: 1303-1311.

Scrutton, M.C., Taylor, B.L. (1974). Isolation and characterization of pyruvate carboxylase from *Azotobacter vinelandii* OP. *Arch. Biochem. Biophys.* **164**: 641-654.

Shiio, I., Yoshino, H., Sugimoto, S. (1990). Isolation and properties of lysine-producing mutants with feedback-resistant aspartokinase derived from a *Brevibacterium flavum* strain with citrate synthase- and pyruvate-kinase-defects and feedback-resistant phosphoenol pyruvate carboxylase. *Agric. Biol. Chem.* **54**: 3275-3282.

Sonntag, K., Eggeling, L., de Graaf, A.A., Sahm, H. (1993). Flux partitioning in the split pathway of lysine synthesis in *Corynebacterium glutamicum*-quantification by ^{13}C NMR and ^{1}H-NMR Spectroscopy. *Eur. J. Biochem.* **213**: 1325-1331.

Sundaram, T.K., Cazzulo, J.J., Kornberg, H.L. (1969). Anaplerotic CO_2 fixation in mesophilic and thermophilic bacilli. *Biochim. Biophys. Acta* **192**: 355-357.

Toh, H., Kawamura, T., Izui, K. (1994). Molecular evolution of phosphoenolpyruvate carboxylase. *Plant Cell Environ.* **17**: 31-43.

Tosaka, O., Morioka, H., Takinami, K. (1979). The role of biotin-dependent pyruvate carboxylase in L-lysine production. *Agric. Biol. Chem.* **43**: 1513-1519.

Vallino, J.J., Stephanopoulos, G. (1993). Metabolic flux distributions in *Corynebacterium glutamicum* during growth and lysine overproduction. *Biotechnol. Bioeng.* **41**: 633-646.

Walker, T.E., Han, C.H., Kollman, V.H., London, R.E., Matwiyoff, N.A. (1982). ^{13}C nuclear magnetic resonance studies of the biosynthesis by *Microbacterium ammoniaphilum* of L-glutamate selectively enriched with carbon-13. *J. Biol. Chem.* **257**: 1189-1195.

Willison, J.C. (1988). Pyruvate and acetate metabolism in the photosynthetic bacterium *Rhodobacter capsulatus*. *J. Gen. Microbiol.* **134**: 2429-2439.

Wurtele, E.S., Nikolau, B.J. (1990). Plants contain multiple enzymes: discovery of 3-methylcrotonyl-CoA carboxylase, propionyl-CoA carboxylase and pyruvate carboxylase in the plant kingdom. *Arch. Biochem. Biophys.* **278**: 179-186.

Yamaguchi, K., Ishino, S., Araki, K., Shirahata, K. (1986). ^{13}C-NMR studies of lysine fermentation with a *Corynebacterium glutamicum* mutant. *Agric. Biol. Chem.* **50**: 2453-2459.

Yokota, A., Shiio, I. (1988). Effects of reduced citrate synthase activity and feedback-resistant phosphoenol pyruvate carboxylase on lysine productivities of *Brevibacterium flavum* mutants. *Agric. Biol. Chem.* **52**: 455-463.

Zimba, P.V., Sullivan, M.J. (1990). Carbon fixation in cultured marine benthic diatoms. *J. Phycol.* **26**: 306-311.

8.10 Appendix: GC-MS Correction Algorithm

Our theoretical derivations are based on the use of isotopically pure substrate, i.e., all carbons ^{12}C except those labeled carbons and all nitrogens ^{14}N. Since there exists ^{13}C and ^{15}N in natural abundance which would increase masses of expected isotopomers, it is necessary to correct for dilution of distribution due to these background enrichments. For example, if the unlabeled naturally abundant lysine is analyzed, not all isotopomers have the same m/e with (M + 0). In fact, as shown in Table 8.7, only 90% of isotopomers have m/e equal to (M + 0).

The effect of background labeling due to presence of ^{13}C and ^{15}N in natural abundance can be accounted by the following method similar to the algorithm of Katz, *et al* [1993]. After derivatization, there exists ten carbons and two nitrogens in the lysine-derivatized sample. The probability of all carbons being ^{12}C and nitrogens being ^{14}N will be

$$M+0 = p_C{}^{10} p_N{}^{2} \qquad \textbf{(Eq. 8.31)}$$

where p_C is the natural abundance of ^{12}C (98.9%) and p_N is the natural abundance of ^{15}N (99.63%). Likewise, the probability of finding isotopomers with (M + 1) is

$$M+1 = \binom{10}{1} p_C{}^{9}(1-p_C) p_N{}^{2} + \binom{2}{1} p_C{}^{10}(1-p_N) p_N \qquad \textbf{(Eq. 8.32)}$$

Following this argument, the theoretically expected values can be related to the experimentally measured values by the following equations:

$$\mathbf{C} \cdot \mathbf{T} = \mathbf{M} \qquad \textbf{(Eq. 8.33)}$$

where **C** is a 7x7 matrix representing the correction factors, **T** is a 1x7 matrix representing the theoretically expected values, and **M** is a 1x7 matrix representing the experimentally measured values. **C**, **T**, and **M** are shown as below:

$$\mathbf{C}=\begin{bmatrix} 0.8985 & 00966. & 0.0047 & 0 & 0 & 0 & 0 \\ 0 & 0.9086 & 0.0876 & 0.0038 & 0 & 0 & 0 \\ 0 & 0 & 0.9187 & 0.0783 & 0.0029 & 0 & 0 \\ 0 & 0 & 0 & 0.9289 & 0.0689 & 0.0022 & 0 \\ 0 & 0 & 0 & 0 & 0.9392 & 0.0592 & 0.0016 \\ 0 & 0 & 0 & 0 & 0 & 0.9497 & 0.0493 \\ 0 & 0 & 0 & 0 & 0 & 0 & 0.9602 \end{bmatrix} \quad \textbf{(Eq. 8.34)}$$

$$\mathbf{T}=\begin{bmatrix} (M+0)_T \\ (M+1)_T \\ (M+2)_T \\ (M+3)_T \\ (M+4)_T \\ (M+5)_T \\ (M+6)_T \end{bmatrix} \text{ and } \mathbf{E}=\begin{bmatrix} (M+0)_E \\ (M+1)_E \\ (M+2)_E \\ (M+3)_E \\ (M+4)_E \\ (M+5)_E \\ (M+6)_E \end{bmatrix} \quad \textbf{(Eq. 8.35)}$$

Similarly, the dilution of isotopomer distribution due to the presence of ^{12}C at the ^{13}C labeling position of the substrate can be accounted. Suppose that we expect isotopomer with mass $(M+n)$ where n is the expected number of ^{13}C derived from the labeling substrate. Then the probability of all n carbons are ^{13}C is p_E^n where p_E is the enrichment of ^{13}C in the substrate. For example, in the case of [1-^{13}C]pyruvate, p_E is 0.98, namely that 2% of carbons at C-1 position of pyruvate is ^{12}C. Likewise, the probability of finding isotopomer with mass $(M+n-1)$ is $\binom{n}{1}p_E^{n-1}(1-p_E)$. The correction for this can be represented in the following matrix form:

$$\mathbf{F}=\begin{bmatrix} 1.0 & 0. & 0 & 0 & 0 & 0 & 0 \\ 0.02 & 0.98 & 0 & 0 & 0 & 0 & 0 \\ 0 & 0.0396 & 0.9604 & 0 & 0 & 0 & 0 \\ 0 & 0 & 0.0588 & 0.9411 & 0 & 0 & 0 \\ 0 & 0 & 0 & 0.0776 & 0.9224 & 0 & 0 \\ 0 & 0 & 0 & 0 & 0.0960 & 0.9039 & 0 \\ 0 & 0 & 0 & 0 & 0 & 0.1142 & 0.8858 \end{bmatrix} \quad \textbf{(Eq. 8.36)}$$

Finally, the theoretically expected value can be found from the following relationship:

$$\mathbf{F}\cdot\mathbf{C}\cdot\mathbf{T}=\mathbf{E} \quad \textbf{(Eq. 8.37)}$$

In this manner, the effect of increase in mass due to natural abundance of ^{13}C and ^{15}N as well as decrease in mass due to impurity of ^{13}C labeling substrate can be accounted for.

Table 8.1 Eight possible routes for OAA formation known to occur in cells. It should be mentioned that some metabolites appearing in an individual reaction may not necessarily be the exact form of the molecule involved. For example, in some organisms, CO_2 instead of H_2CO_3 can be the carboxyl donating molecule. GDP in Reaction 2 may not be only viable phosphate acceptor. In Reactions 5, 7 and 8, two enzymatic reactions are required to generate OAA.

Reaction	Enzyme Reaction(s)	Reaction Stoichiometry
1	PEP carboxylase (PPC; EC 4.1.1.31)	$PEP + H_2CO_3 \rightarrow OAA + P_i$
2	PEP carboxykinase (PPCK; EC 4.1.1.32)	$PEP + H_2CO_3 + GDP \rightarrow OAA + P_i + GTP$
3	PEP carboxytransphosphorylase (PPCTP; EC 4.1.1.38)	$PEP + H_2CO_3 + P_i \rightarrow OAA + PP_i$
4	Pyruvate carboxylase (PC; EC 6.4.1.1)	$Pyr + H_2CO_3 + ATP \rightarrow OAA + P_i + ADP$
5	Transcarboxylase (TC; EC 2.1.3.1) Propionyl-CoA carboxylase (PCC; EC 6.4.1.3)	Pyr + Methylmalonyl-CoA → OAA + Propionyl-CoA Propionyl-CoA + H_2CO_3 → Methylmalonyl-CoA
6	OAA decarboxylase (OAADC; EC 4.1.1.2)	$Pyr + H_2CO_3 \rightarrow OAA + H^+$
7	Malic enzyme (ME; EC 1.1.1.38 or 39 or 40) Malate dehydrogenase (MDH; EC 1.1.1.37)	Pyr + H_2CO_3 + NAD(P)H → Malate + NAD(P) Malate + NAD → OAA + NADH
8	Isocitrate lyase (IL; EC 4.1.3.1) Malate synthase (MS; EC 4.1.3.2) Malate dehydrogenase	Isocitrate → Succinate + Glyoxylate Glyoxylate + Acetyl-CoA → Malate Malate + NAD → OAA + NADH

Table 8.2 Examples of the diversity of anaplerotic enzymes found in various organisms.

Enzyme	Organism	Reference or Comments
PPC	bacteria:	
	Escherichia coli	
	Pseudomonas citronellolis	O'Brien *et al.*, 1977
	Pseudomonas fluorescens	Higa *et al.*, 1976
	Azotobacter vinelandii	Scrutton and Taylor, 1979
	plants:	
	Zea mays	
	algae:	
	Gracilaria conferta	Israel *et al.*, 1991
	Selenastrum minutum	Schuller *et al.*, 1990
	Prorocentrum micans	Descolas-Gros and Fontugne, 1985
	Dunaliella marina	Descolas-Gros and Fontugne, 1985
	Bacillariophyceae	Zimba and Sullivan, 1990
	Chlorophyceae	Zimba and Sullivan, 1990
	Anacystis nidulans	Katagiri *et al.*, 1985
	Anabaena variabilis	Lem *et al.*, 1986
PC	bacteria:	
	Bacillus subtilis	Diesterhaft and Freese, 1973
	Bacillus stearothermophilus	Sundaram *et al.*, 1969
	Bacillus licheniformis	Sundaram *et al.*, 1969
	Pseudomonas citronellolis	O'Brien *et al.*, 1977
	Pseudomonas fluorescens	Higa *et al.*, 1976
	Azotobacter vinelandii	Scrutton and Taylor, 1979
	algae:	
	Amphidinum carterae	Appleby *et al.*, 1980
	Scrippsiella trochoidea	Descolas-Gros and Oriol, 1992
	Rhodobacter capsulatus	Willison, 1988
	plants:	
	Daucus carota	Wurtele and Nikolau, 1990
	Zea mays	Wurtele and Nikolau, 1990
	Heliauthus annus	Wurtele and Nikolau, 1990
	Brassica napus	Wurtele and Nikolau, 1990
	fungi:	
	Saccharomyces	Bercovitz *et al.*, 1990
	Aspergillus	Bercovitz *et al.*, 1990
	Candida	Bercovitz *et al.*, 1990
	Leptosphaeria michotii	Tozo *et al.*, 1992

	Thermomyces lanuginosus	Gupta and Maheshwari, 1985
PPCK	bacteria (anaerobic):	
	Anaerobiospirillum succiniciproducens	Podkovyrov and Zeikus, 1993
	Capnocytophaga ochracea	Kapke *et al.*, 1980
	Selenomonas ruminantinum	Melville *et al.*, 1988
	algae:	
	Alcaligenes eutrophus	Schobert and Bowien, 1984
	Udotea flabellum	Reiskind and Bowes, 1991
	Euglena gracilis	Pönsgen-Schmidt *et al.*, 1988
	Phaeodactylum tricornutum	Holdsworth and Bruck, 1977
	Cylindrotheca closterium	Appleby *et al*, 1980
	Thalassiosira pseudonana	Appleby *et al*, 1980
	Phaeophyceae (brown algae)	Kerby and Raven, 1985
	Tubifex (anaerobic annelids)	Hoffmann *et al.*, 1979
	Nereis virens (anaerobic polychaetes)	Schöttler and Wienhausen, 1981
	Arenicola marina (anaerobic polychaetes)	Schöttler and Wienhausen, 1981
PPCTP	*Entamoeba histolytica* (anaerobic protozoa)	Reeves, 1970
	Propionibacterium shermanii	Cooper *et al.*, 1968

Table 8.3 ^{13}C fractional enrichment at individual carbon positions of lysine (top) and distribution of lysine isotopomers (bottom) using unlabeled gluconate and [2-^{13}C]pyruvate as carbon substrates. As the anaplerotic reaction for the synthesis of OAA, Mode 1 assumes the sole operation of PEP, Mode 2 assumes pyruvate carboxylation and Mode 3 assumes glyoxylate shunt pathway. w denotes the probability of bicarbonate to be labeled with ^{13}C which is fixed onto C-4 position of OAA in the cases of Mode 1 and 2. x denotes the probability of OAA to exit the TCA cycle via the reaction of transaminase reaction. Therefore, $(1 - x)$ denotes the probability of OAA to enter the TCA cycle via the action of citrate synthase. y denotes the probability of tetrahydrodipicolinate to be converted to meso-diaminopimelate via the one-step enzymatic reaction of meso-diaminopimelate dehydrogenase. In the operation of Mode 3, z indicates the probability of isocitrate to be catalyzed via the glyoxylate shunt pathway. M denotes the molecular weight of natural lysine, whose six carbons are all ^{12}C.

Position	Mode 1: PPC	Mode 2: PC	Mode 3: GS
C-1	$\frac{(1+y)(x-xw)}{2}$	$\frac{(1+y)(1+x-2x^2+xw+x^2w)}{4(1+x)}$	$\frac{(1+y)(1-z)}{4}$
C-2	$\frac{(1-y)}{2}$	$\frac{1+2x-y}{2(1+x)}$	$\frac{(1-y)}{2}$
C-3	0	$\frac{x(1+y)}{2(1+x)}$	0
C-4	$\frac{1-x+xw}{2}$	$\frac{(1+x-2x^2+xw+x^2w)}{2(1+x)}$	$\frac{(2-z)}{2}$
C-5	0	$\frac{x(1-y)}{2(1+x)}$	0
C-6	$\frac{(1+y)}{2}$	$\frac{1+2x+y}{2(1+x)}$	$\frac{(1+y)}{2}$

MW	Mode 1: PPC	Mode 2: PC	Mode 3: GS
M+1	$\frac{1-xy+xyw}{2}$	$\frac{(1-x)^2(1-y)}{4(1+x)}$	$\frac{(1-y)z}{4}$
M+2	$\frac{1+xy-xyw}{2}$	$\frac{3+x+4x^2+y-5xy+4x^2y-3xw-3x^2w-xyw-x^2yw}{4(1+x)}$	$\frac{2-2y+z+3yz}{4}$
M+3	0	$\frac{x(5-5x+3y-3xy+3w+3xw+yw++xyw)}{4(1+x)}$	$\frac{(1+y)(1-z)}{4}$

Table 8.4 ^{13}C fractional enrichment at individual carbon positions of lysine (top) and distribution of lysine isotopomers (bottom) using unlabeled gluconate and [1-^{13}C]pyruvate as carbon substrates.

Position	Mode 1: PPC	Mode 2: PC	Mode 3: GS
C-1	$\frac{2-2y+xw+xyw}{4}$	$\frac{(2+x-2y+xy+xw+xyw)}{4}$	$\frac{(1-y)}{2}$
C-2	0	0	0
C-3	0	0	0
C-4	$\frac{xw}{2}$	$\frac{x(1+w)}{2}$	0
C-5	0	0	0
C-6	0	0	0

MW	Mode 1: PPC	Mode 2: PC	Mode 3: GS
M+0	$\frac{(1+y)(1-xw)}{2}$	$\frac{(1+y)(1-x)}{2}$	$\frac{(1+y)}{2}$
M+1	$\frac{2-2y+xw+3xyw}{4}$	$\frac{2+x-2y+3xy-3xw-xyw}{4}$	$\frac{(1-y)}{2}$
M+2	$\frac{x(1-y)w}{4}$	$\frac{x(1-y+3w+yw)}{4}$	0

Table 8.5 ^{13}C fractional enrichment at individual carbon positions of lysine (top) and distribution of lysine isotopomers (bottom) using unlabeled gluconate and [3-^{13}C]pyruvate as carbon substrates.

Position	Mode 1: PPC	Mode 2: PC	Mode 3: GS
C-1	$\frac{(1+y)(1-2x+x^2+xw+x^2w)}{4(1+x)}$	$\frac{(1+y)(1-x+xw+x^2w)}{4(1+x)}$	$\frac{(1+y)z}{6-2z}$
C-2	$\frac{(1-x)(1+y)}{2(1+x)}$	$\frac{(1+y)}{2(1+x)}$	$\frac{(1+y)}{2}$
C-3	$\frac{(1+x^2y-xyw-x^2yw)}{(1+x)}$	$\frac{(2+x-xy)}{2(1+x)}$	1
C-4	$\frac{(1-2x+x^2+xw+x^2w)}{2(1+x)}$	$\frac{(1-x+xw+x^2w)}{2(1+x)}$	$\frac{z}{3-z}$
C-5	$\frac{(1-x^2y+xyw+x^2yw)}{(1+x)}$	$\frac{(2+x+xy)}{2(1+x)}$	$\frac{(1-y)}{2}$
C-6	$\frac{(1-x)(1-y)}{2(1+x)}$	$\frac{(1-y)}{2(1+x)}$	1

MW	Mode 1: PPC	Mode 2: PC	Mode 3: GS
M+1	$\frac{x(4-3w-yw)}{4}$	0	0
M+2	$\frac{x(5-2x-3x^2-y+2xy-x^2y+3w+3xw+yw+xyw)}{4(1+x)}$	$\frac{x(5+3x-y+xy-3w-3xw-yw-xyw)}{4(1+x)}$	0
M+3	$\frac{(1-x)^2(1+6x-y+2xy)}{4(1+x)}$	$\frac{(1+5x-6x^2-y+3xy-2x^2y+3xw+3x^2w+xyw+x^2yw)}{4(1+x)}$	$\frac{6-5z-yz}{6-2z}$
M+4	$\frac{(1-x)^3(3+y)}{4(1+x)}$	$\frac{(1-x)^2(3+y)}{4(1+x)}$	$\frac{(3+y)z}{6-2z}$

Table 8.6 ^{13}C fractional enrichment at individual carbon positions of lysine (top) and distribution of lysine isotopomers (bottom) using [U-^{13}C]gluconate and unlabeled pyruvate as carbon substrates. Both PEP and pyruvate carboxylation pathways are assumed to be operative. v denotes the probability of oxaloacetate to be formed via PEP carboxylating pathway. Therefore, $(1-v)$ denotes the probability of OAA to be formed via pyruvate carboxylating pathway.

Position	Fractional Enrichment
C-1	$\frac{x(1+y)(w+xw+3v-vx)}{4(1+x)}$
C-2	$\frac{x(1+y)v}{(1+x)}$
C-3	$\frac{x(1+y)v}{(1+x)}$
C-4	$\frac{x(2w+2xw+5v-3xv+yv+xyv+wv+xyv-ywv-xywv)}{4(1+x)}$
C-5	$\frac{x(1-y)v}{(1+x)}$
C-6	$\frac{x(1-y)v}{(1+x)}$

MW	Isotopomer Distribution
M+0	$\frac{x(1-y)(w+xw+v-2xv+x^2v-wv-xwv)}{4(1+x)}+$ $\frac{(1+x-xw-x^2w-4xv+3x^2v-x^3v+xyv+x^2yv)}{(1+x)}$
M+1	$\frac{x}{4(1+x)}\left[\begin{array}{l}3w+3xw+yw+xyw+8v-14xv+6x^2v-2yv \\ +2x^2yv-3wv-3xwv-ywv-xywv\end{array}\right]$
M+2	$\frac{x(4-3x-xy-w+yw)v}{4}$
M+3	$\frac{x(3+y-w-3yw)v}{4}$
M+4	$\frac{x(1+y)wv}{2}$

Table 8.7 Qualitative comparison of fractional ^{13}C enrichment at individual carbon positions of lysine (top) and distribution of lysine isotopomers (bottom) using [1-^{13}C]pyruvate, [2-^{13}C]pyruvate and [3-^{13}C]pyruvate assuming sole operation of PEP carboxylation pathway (Mode 1), pyruvate carboxylating pathway (Mode 2), and glyoxylate shunt pathway (Mode 3). + indicates the presence of ^{13}C enrichment and isotopomer species.

	[1-^{13}C]pyruvate			[2-^{13}C]pyruvate			[3-^{13}C]pyruvate		
Position	Mode 1	Mode 2	Mode 3	Mode 1	Mode 2	Mode 3	Mode 1	Mode 2	Mode 3
C-1	+	+	+	+	+	+	+	+	+
C-2				+	+	+	+	+	+
C-3					+		+	+	+
C-4	+	+		+	+	+	+	+	+
C-5					+		+	+	+
C-6				+	+	+	+	+	+
MW									
M + 0	+	+	+						
M + 1	+	+	+	+	+	+	+		
M + 2	+	+		+	+	+	+	+	
M + 3					+	+	+	+	+
M + 4							+	+	+

Table 8.8 ^{13}C labeling at the individual carbons of lysine as detected by ^{13}C NMR. Values indicate the fractional ^{13}C enrichment and calculated based on the calibration using natural lysine of 60 g/L as a standard. For [1-^{13}C]pyruvate and [2-^{13}C]pyruvate labeling experiments, *ppc pyk* mutant (SM607) was used. For [U-^{13}C]gluconate experiment, *pyk* mutant (SM575) was used. N.D.≡ not detected.

Sample	C-1	C-2	C-3	C-4	C-5	C-6	Conc. (g/l)
[1-^{13}C]Pyr Exp	0.337	N.D.	N.D.	0.058	N.D.	N.D.	1.5
[2-^{13}C]Pyr Exp.	0.337	0.391	0.150	0.506	0.056	0.802	10.3
[U-^{13}C]Gluc. Exp.	0.057	0.025	0.025	0.109	N.D.	N.D.	10.2

Table 8.9 Distribution of lysine isotopomers as detected by GC-MS. Numbers on top rows indicate experimental values obtained by GC-MS. Values in parenthesis indicates the corrected values using the algorithm described in the Appendix.

Sample	M+0	M+1	M+2	M+3	M+4	M+5	M+6
Natural Lysine	86.90	11.65	1.30	0	0	0	0
	(96.71)	(2.53)	(0.68)	(0.00)	(0.00)	(0.00)	(0.00)
[U-^{13}C]Lysine	0	0	0	0	2.70	13.06	84.28
	(0.00)	(0.00)	(0.00)	(0.00)	(0.00)	(1.79)	(98.25)
[1-^{13}C]Pyr Exp.	58.45	31.59	8.92	1.04	0	0	0
	(64.49)	(28.13)	(6.97)	(0.48)	(0.00)	(0.00)	(0.00)
[2-^{13}C]Pyr Exp.	4.52	20.167	46.15	26.17	2.68	0.30	0
	(4.63)	(20.14)	(48.57)	(25.44)	(0.99)	(0.00)	(0.00)
[U-^{13}C]Gluc Exp.	76.87	18.99	3.54	0.62	0	0	0
	(85.40)	(11.85)	(2.35)	(0.45)	(0.00)	(0.00)	(0.00)

Figure 8.1 Simplified lysine biosynthesis from glucose and schematic illustration of the three possible oxaloacetate-forming pathways: PEP carboxylation (Mode 1), pyruvate carboxylation (Mode 2), and glyoxylate shunt pathway (Mode 3) consisting of isocitrate lyase (3a) and malate synthase (3b).

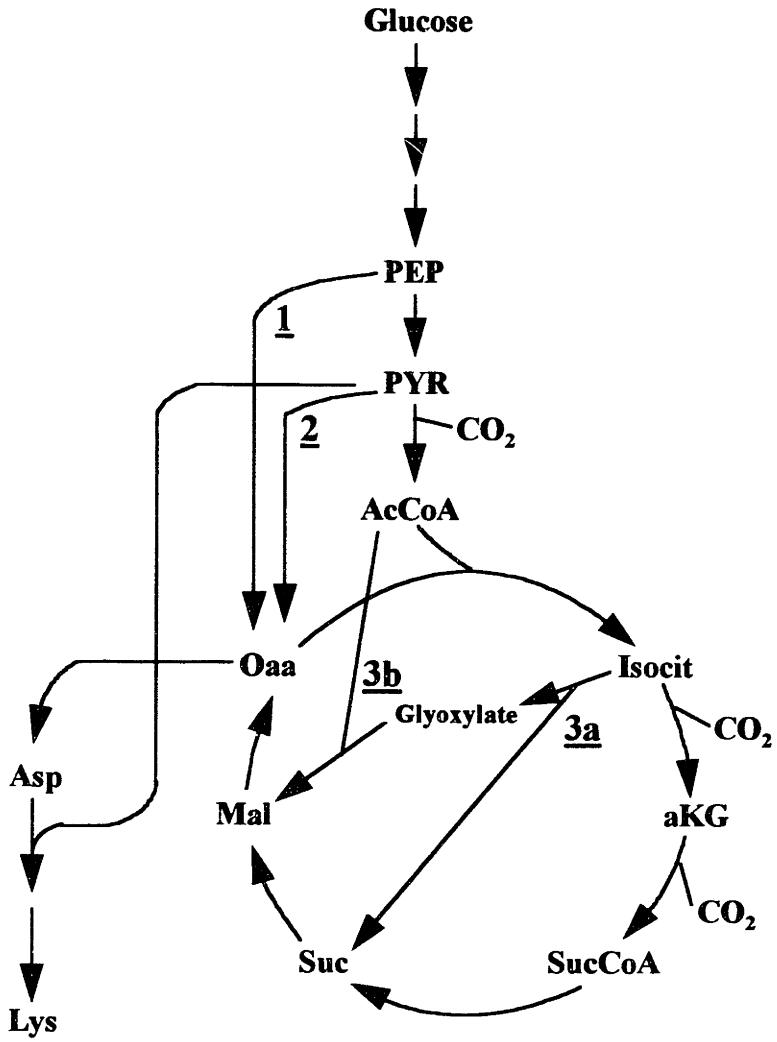

Figure 8.2 Simplified labeling diagram depicting the sequence of ^{13}C labeling in the TCA cycle intermediates and lysine isotopomers resulting from [2-^{13}C]pyruvate, assuming a pyruvate carboxylating pathway is present. The abbreviations O, C, K, S, M, P, Ac and L sumbolize oxaloacetate, citrate, α-ketoglutarate, succinate, malate, pyruvate, acetyl-CoA and lysine, respectively. Subscripts denote the ^{13}C labeling position. **X** indicates the blockage of carbon flow.

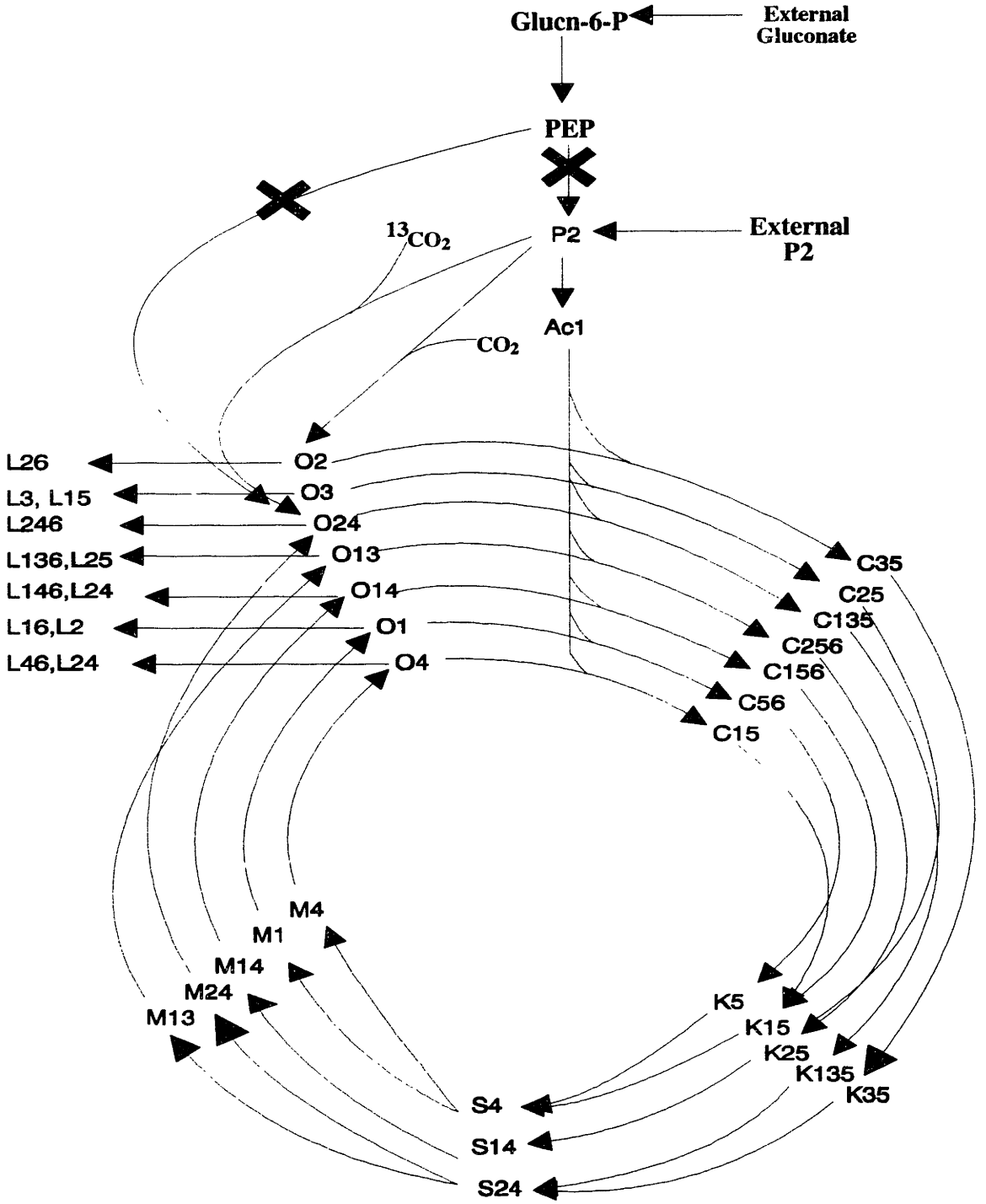

Figure 8.3 Template for lysine labeling from pryuvate and oxaloacetate through the dual pathways. The four-step succinylase pathway (1 - y) contains the enzymatic sequence of N-succinyl-2,6-ketopimelate synthase, N-succinyl-aminoketopimelate:glutamate aminotransferase, N-succinyl-diaminopimelate desuccinylase, and diaminopimelate epimerase. The one-step pathway (y) involves the action of *meso*-DAP dehydrogenase. *y* is the probability of lysine formed via the one-step *meso*-DAP pathway (modified from Sonntag *et al.*, 1993). Subscripts in O and P indicate the original carbon positions.

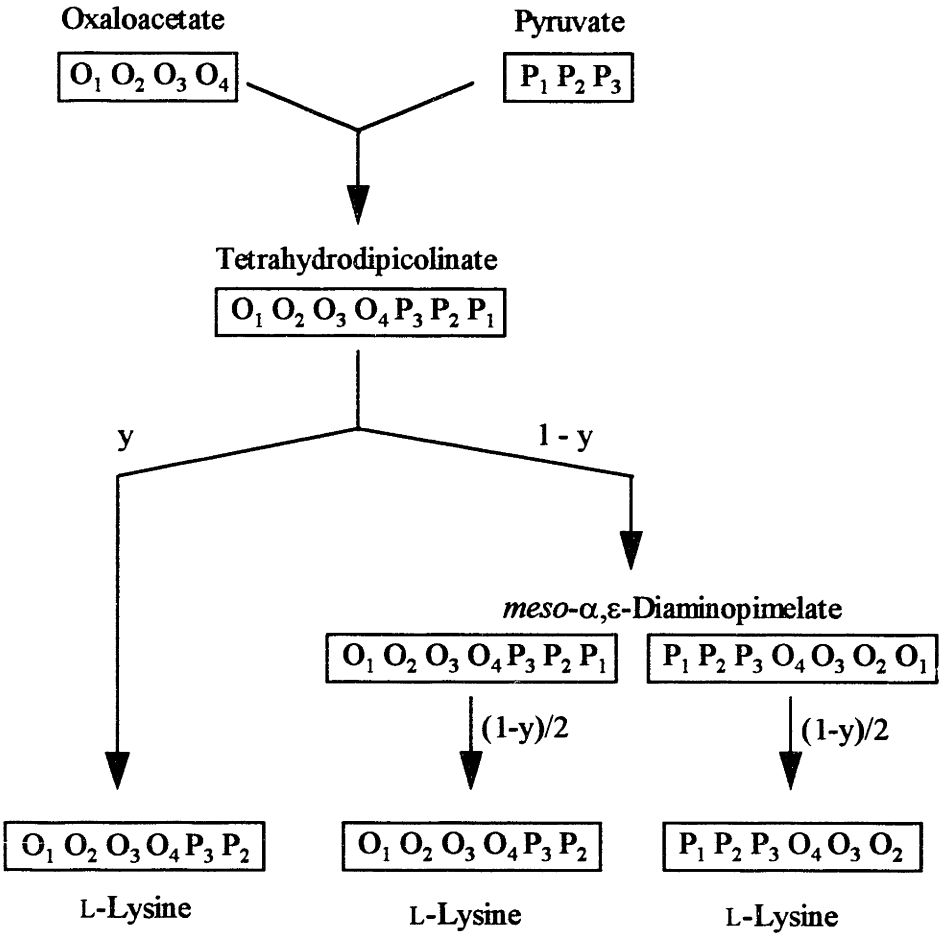

Figure 8.4 Simplified labeling diagram depicting the sequence of ^{13}C labeling in the TCA cycle intermediates and lysine isotopomers resulting from [U-^{13}C]gluconate and unlabeled pyruvate assuming the simultaneous operation of both PEP and pyruvate carboxylating pathways.

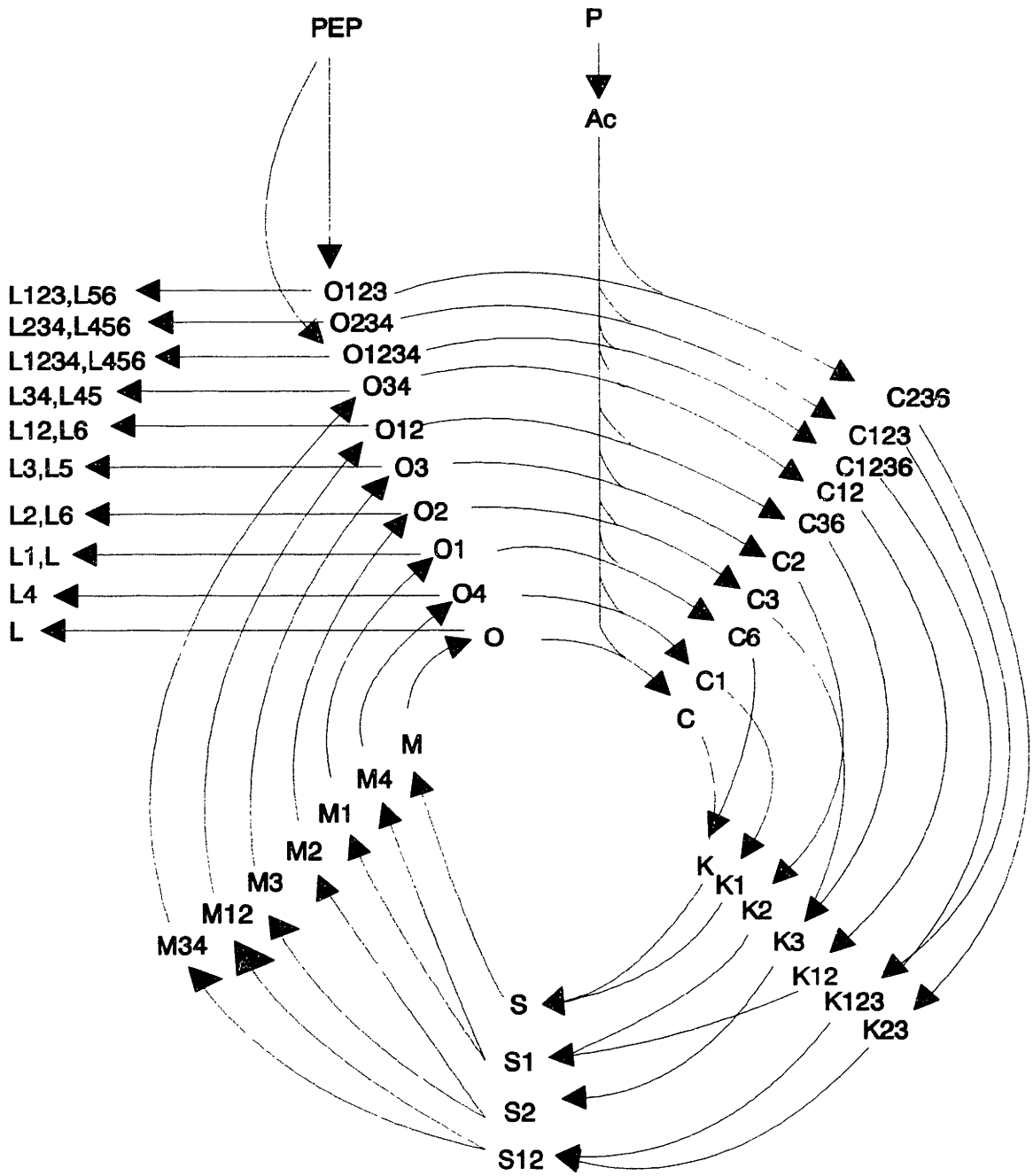

Figure 8.5 Time course of cell growth, gluconate and pyruvate utilization, and lysine production in four strains: ●, wild type (ATCC 21253); ■, *ppc* mutant (253SM1); ○, *pyk* mutant (SM575); □, *ppc pyk* mutant (SM607).

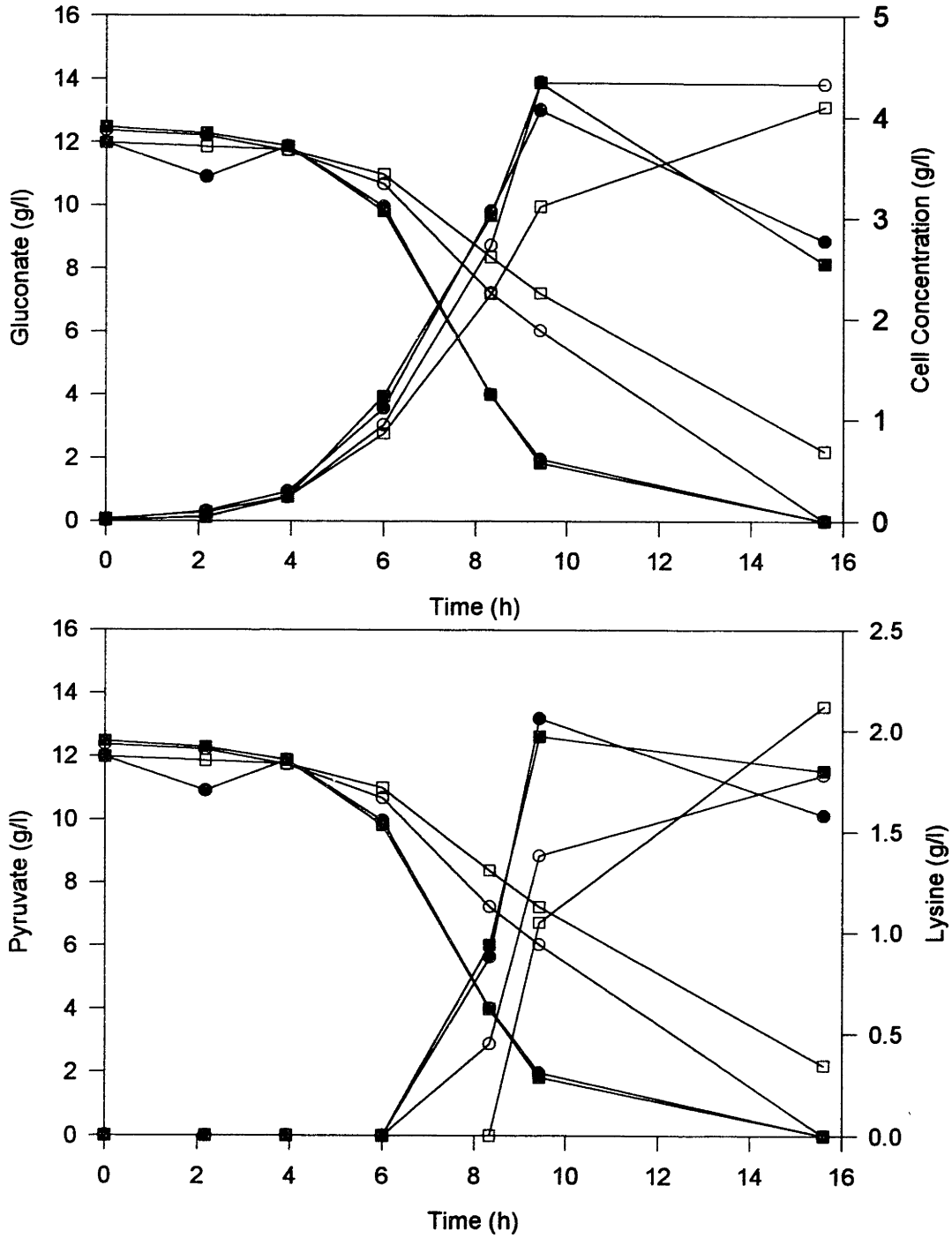

Figure 8.6 A proton-decoupled ^{13}C NMR spectrum from the supernatant of PPC PK-deficient mutant (SM607) incubated with 10 g/l [2-^{13}C]pyruvate and 10g/l unlabeled gluconate (800 accumulation).

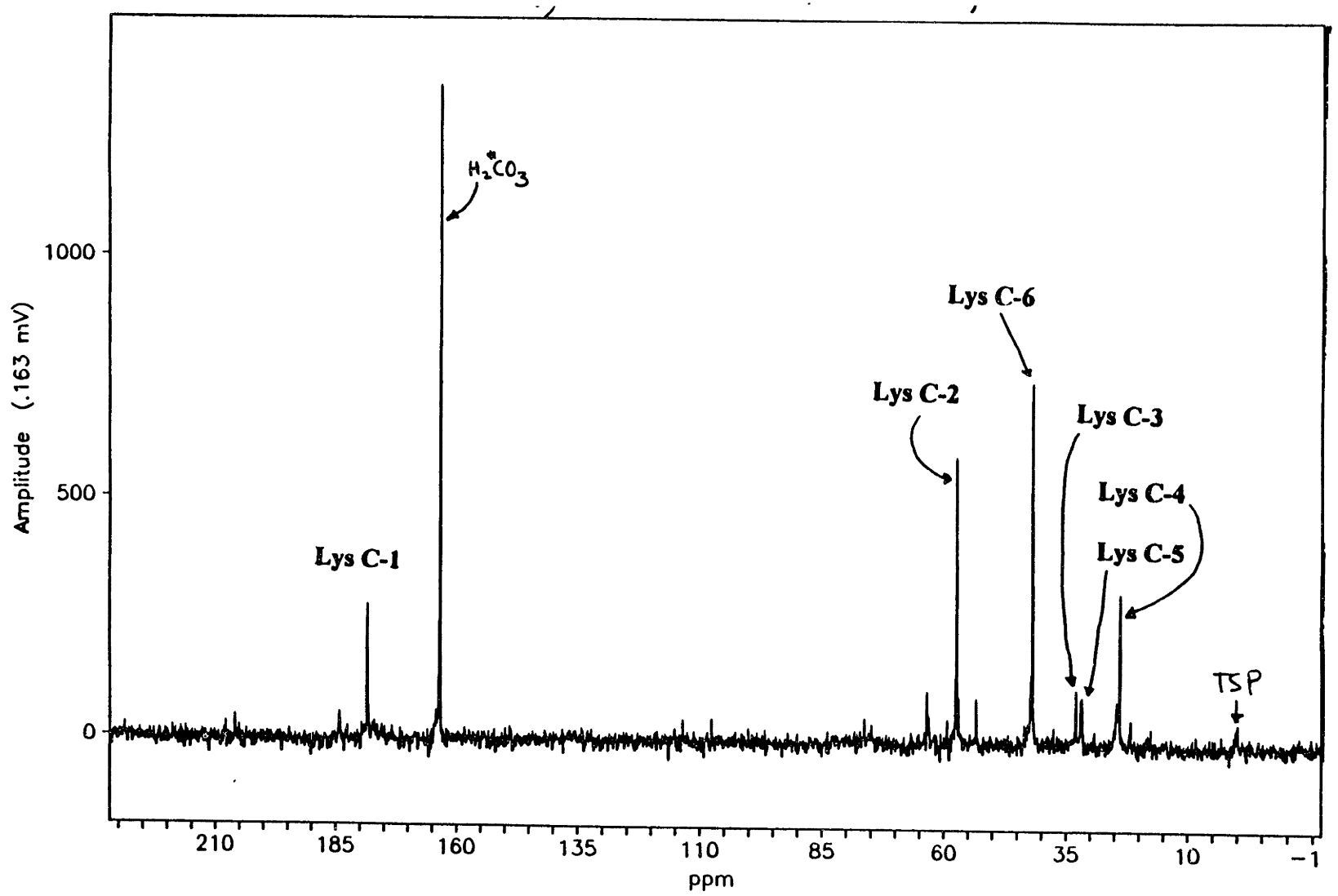

Figure 8.7 A proton-decoupled ^{13}C NMR spectrum from the supernatant of PPC PK-deficient mutant (SM607) incubated with 10 g/l [1-^{13}C]pyruvate and 10g/l unlabeled gluconate (164 accumulation).

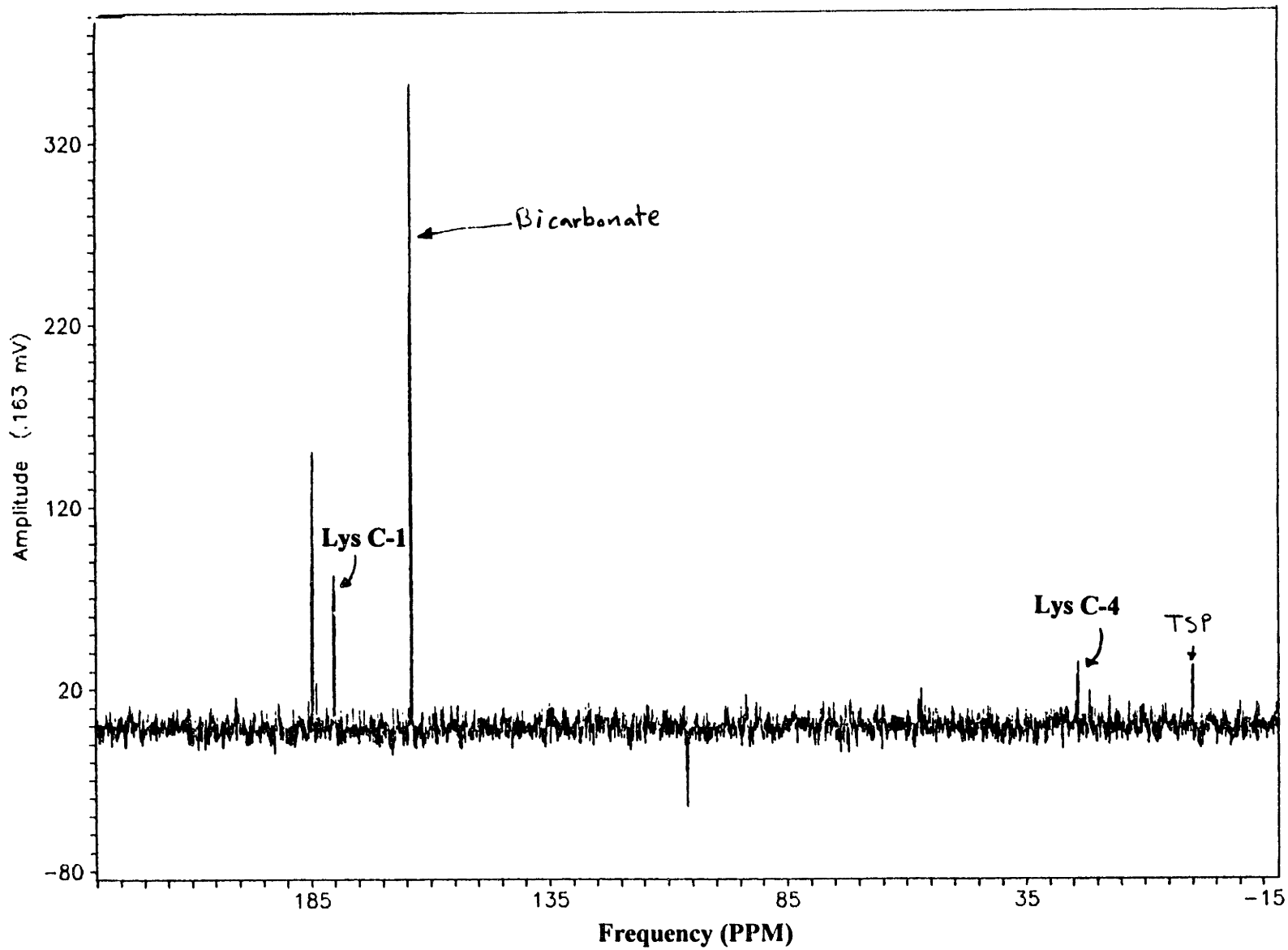

Figure 8.8 A proton-decoupled ^{13}C NMR spectrum from the supernatant of PK-deficient mutant (SM575) incubated with 10 g/l [U-^{13}C]gluconate and 10g/l unlabeled pyruvate (800 accumulation).

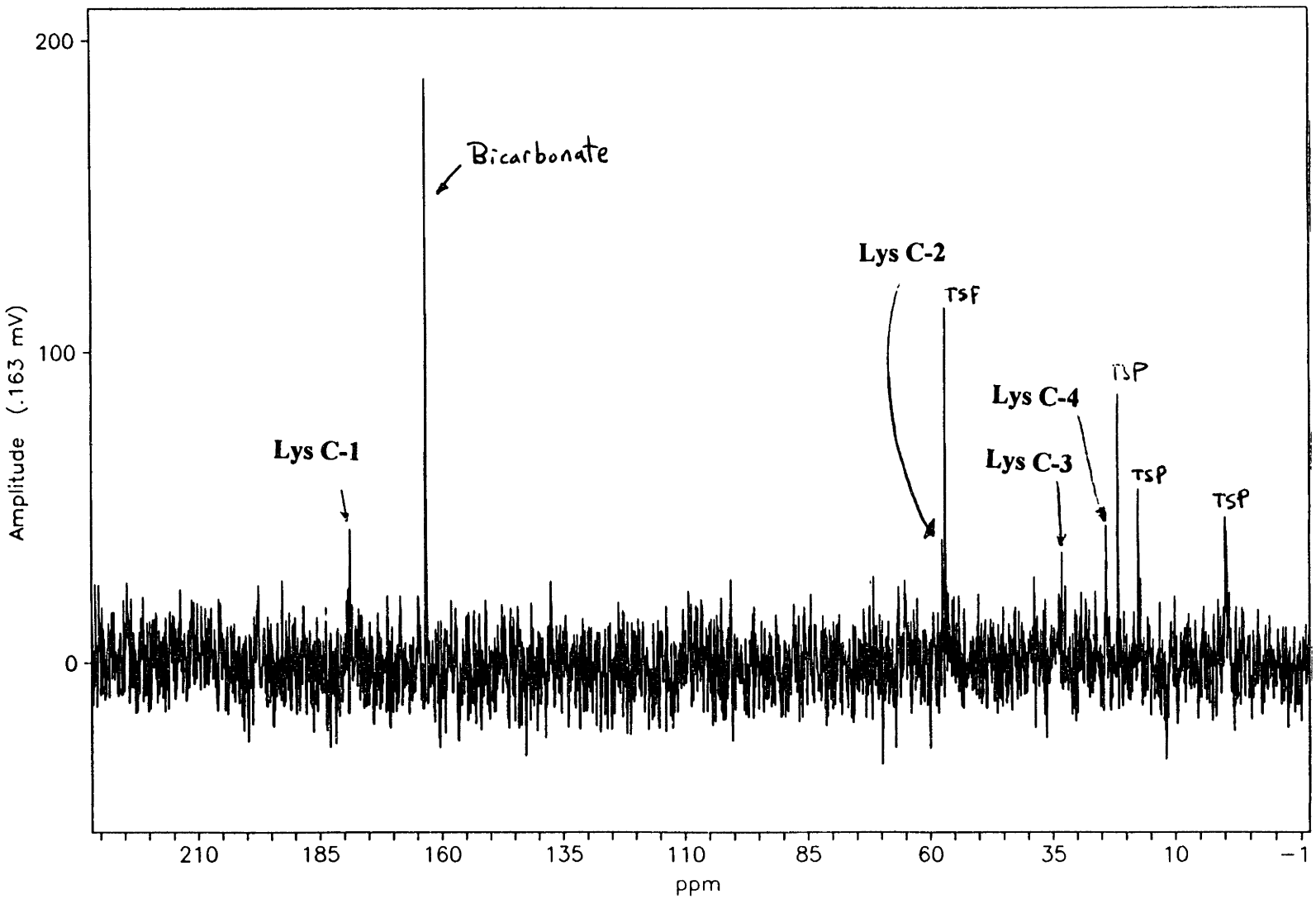

Chapter 9: Metabolic and Physiological Studies of *Corynebacterium glutamicum* Mutants

9.1 Summary

The physiology and central carbon metabolism of *Corynebacterium glutamicum* was investigated through the study of specific deletion mutants. Mutants deficient in phosphoenolpyruvate carboxylase (PPC) and/or pyruvate kinase (PK) activity were constructed by deleting the corresponding gene(s) via transconjugation. Standard batch fermentations were carried out with these mutants and results were evaluated in the context of intracellular flux analysis. It was determined that: (1) There is a significant reduction in the glycolytic pathway flux in the pyruvate kinase deficient mutants during growth on glucose as evidenced by secretion of dihydroxyacetone and glyceraldehye. The resulting overflow is accomplished by the pentose phosphate pathway (PPP) acting as mechanism of dissimilating large amounts of built-up intermediates in the form of CO_2. (2) The high activity through the PPP causes an overproduction of reducing power in the form of NADPH. The overproduction of biosynthetic reducing power, as well as the shortage of NADH produced via the tricarboxylic acid cycle (as evidenced by a reduced citrate synthase flux), are compensated by an increased activity of the transhydrogenase (THD) enzyme catalyzing the reaction $NADPH + NAD^+ \leftrightarrow NADP^+ + NADH$. The presence of active THD was also confirmed directly by enzymatic assays. (3) Specific glucose uptake rates declined during the course of fermentation and this decline was more pronounced in the case of a double mutant strain deficient in both PPC and PK. Specific ATP consumption rates similarly declined during the course of the batch. However, they were approximately the same for all strains, indicating that energetic requirements for biosynthesis and maintenance are independent of the specific genetic background of a strain. The above results underline the importance of intracellular flux analysis, not only for producing a static set of intracellular flux estimates but also for uncovering changes occurring in the course of a batch fermentation or as result of specific genetic modifications.

9.2 Introduction

Metabolic flux analysis is slowly being introduced in the repertoire of methodologies used in order to upgrade the information content of fermentation data. Aiba and Matsuoka [1979] first calculated fluxes of the metabolic pathways for citrate production in *Candida lipolytica* for the purpose of identifying the metabolic model that is most consistent with experimental data. The approach was further refined and extended by Papoutsakis and co-workers to describe fermentations of butyric acid, butanediol, mixed-acid and propionic acid bacteria [Papoutsakis; 1984, 1985a, 1985b]. Similar concepts were applied to a number of different systems for the estimation of intracellular fluxes: acetone fermentation by *Clostridium acetobutylicum* [Reardon *et al.*, 1987], effect of expression of the *pet* operon in carbon metabolism of *Escherichia coli* [Diaz-Ricci *et al.*, 1992], metabolism of hybridoma cell cultures [Savinell *et al.*, 1992; Zupke *et al.*, 1995], growth of *Saccharomyces cerevisiae* on different carbon sources [Cortassa *et al.*, 1995], fed-batch fermentation of penicillin production by *Penicillium chrysogenum* [Jorgensen *et al.*, 1995], and lysine production by *Corynebacterium glutamicum* [Vallino and Stephanopoulos, 1993, 1994; Cocaign-Bousquet and Lindley, 1995].

In the above cases, metabolic flux analysis provided quantitative information on intracellular fluxes not easily obtainable by other methods. The value of static metabolic flux data, however, is rather limited. It is rather the deviations of metabolic fluxes obtained in response to various kinds of perturbations that provide significant information about metabolic flux control. In this paper we present metabolic flux data obtained in response to two types of perturbations, namely, genetic perturbations at specific points of the metabolic network as well as changes occurring during the normal course of a batch fermentation.

Due to its importance in determining the yield and productivity of many fermentation products, central carbon metabolic pathways have been studied extensively in the past. Of particular interest are modifications of the central carbon metabolic pathway in the genus *Corynebacterium* (or *Brevibacterium*), widely used for the production of various amino acids [Yoshinaga *et al.*, 1983; Shiio *et al.*, 1982, 1984a, 1984b, 1987;

Ozaki and Shiio, 1983; Tosaka *et al.*, 1985; Sano *et al.*, 1987]. In order to further understand the control and regulation of central metabolism in *C. glutamicum*, we have analyzed carbon flux distributions following the deletion of certain enzymes in the central metabolic pathway. Specifically, we have targeted PPC and PK, as these enzymes play key roles in allocating carbon metabolites either for energy generation via the tricarboxylic acid (TCA) cycle or for biosynthesis through the synthesis of the OAA precursor. Deletion mutants of combinations of the two enzymes were constructed via transconjugation and cultured in a standard batch fermentation. Metabolite production-consumption rates were measured and the data were analyzed in the framework of metabolic flux analysis [Vallino and Stephanopoulos, 1993]. Flux distributions through key enzymatic steps in the central metabolic pathways, PEP:glucose PTS system, phosphoglucose isomerase, glucose 6-phosphate dehydrogenase, citrate synthase, anaplerotic reaction and ATP dissipation reaction, were obtained and compared for various strains.

Metabolic flux analysis with the *ppc pyk* mutant suggested the possibility of an active transhydrogenase (THD; EC 1.6.1.1; *thd* gene) in this bacterium as a mechanism of balancing the redox state between NADPH and $NADP^+$. Support for this conclusion was further provided from the measurement of substantial THD enzymatic activities in the cell-free crude extracts of all four strains. Additionally, the blockage of carbon flow at the PEP branchpoint in the *pyk* mutants increased the rate of metabolite assimilation via the pentose phosphate pathway (PPP) in the form of CO_2 and concomitant production of large quantities of NADPH.

It should be noted that the presence of THD was suggested by the failure of flux consistency tests that also pointed to NADPH accumulation as the most likely factor of the observed inconsistency. Additional observations resulting from flux analysis are the significant reduction of glycolytic fluxes and the concomitant increase of the PPP flux in the *pyk* mutants, in particular, the *ppc pyk* mutant. Fluxes through glucose-6-phosphate isomerase are in the reverse direction for the above mutants, which also exhibit reduced anaplerotic fluxes. Finally, specific glucose transport is reduced in the course of the batch following a similar trend in ATP requirements. The latter, however, were found to be

invariant for the four strains, pointing to relatively constant metabolic energy requirements with respect to varying genetic backgrounds.

9.3 Metabolic Flux Analysis for the Metabolic Reaction Network of *C. glutamicum*

Metabolic pathways known to exist in wild type *C. glutamicum* are depicted in Figure 9.1 [Vallino and Stephanopoulos, 1993]. Not all reactions described in Figure 9.1 occur in all four strains. For example, excretion of dihydroxyacetone, glyceraldehyde and propionate is observed only in *pyk* and *ppc pyk* mutants.

Intracellular fluxes x_1 through x_{34} of Figure 9.1 are determined by solving the set of linear equations:

$$\mathbf{Ax} = \mathbf{r} \qquad \textbf{(Eq. 9.1)}$$

where $\mathbf{x}$ is a $(n \times 1)$ vector of fluxes, $\mathbf{A}$ is a $(m \times n)$ stoichiometry matrix in which the *ij*th element represents the stoichiometric coefficient for the *i*th metabolite in the *j*th reaction and $\mathbf{r}$ is a $(m \times 1)$ rate vector with r_i representing the net conversion rate of the *i*th metabolite. Vector $\mathbf{r}$ can be further partitioned into two column vectors:

$$\mathbf{r} = \begin{bmatrix} \mathbf{r}_I \\ \mathbf{r}_E \end{bmatrix} \qquad \textbf{(Eq. 9.2)}$$

where subscripts I and E refer to intracellular and extracellular metabolites, respectively. The components of $\mathbf{r}_I$ are set equal to zero under the assumption that the pools of all intracellular metabolites remain constant. $\mathbf{r}_E$ is determined by monitoring the change in the concentrations of extracellular metabolites. In the case of over-determined system where the number of equations is greater than the number of unknown fluxes ($m > n$), the solution $\mathbf{x}$ can be obtained as

$$\mathbf{x} = (\mathbf{A}^T\mathbf{A})^{-1}\mathbf{A}^T\mathbf{r} \qquad \textbf{(Eq. 9.3)}$$

In this case, extra equations provide a redundancy that can be used to test the consistency of the biochemistry and measurement [Wang and Stephanopoulos, 1983].

The exact stoichiometry for each reaction in Figure 9.1 is summarized in Appendix 9.1. The constant factors appearing in Reaction 6 indicate the amount of corresponding

metabolites (in mmol) required to synthesize 1 g of DCW. These values are adapted from the stoichiometric relationship in *E. coli* [Neidhardt *et al.*, 1990].

Reactions 36, 37, 38, and 39 deserve some further discussions. Reaction 36 and 37 represent two possible routes of OAA synthesis in *C. glutamicum* by carboxylation of PEP and pyruvate, respectively. Reaction 38 is the step catalyzed by the THD and it can operate in either direction, making possible the production of NADH in the presence of excess NADPH or vice versa. The inclusion of THD into the network was considered after accumulation of NADPH was determined with the *ppc pyk* mutant. This provision greatly improved the fit and suggested a very active THD in the *pyk* and *ppc pyk* mutants.

For each fermentation depicted in Figures 9.2-9.5, the intracellular fluxes ($\mathbf{x}$) were estimated in the following manner. First, the fermentation was divided into four phases as described in the next section. The net accumulation rates ($\mathbf{r}_E$) for the extracellular metabolites were calculated by dividing the net change in the concentration by the time duration of each phase. These rates were converted into mmol/g DCW/h by dividing by the average cell concentration in the phase. The rates of change for all intracellular metabolites ($\mathbf{r}_I$) and other undetected metabolites were set equal to zero.

9.4 Results

9.4.1 Growth and Lysine Production of *ppc* Mutant (253SM1), *pyk* Mutant (SM575), and *ppc pyk* Mutant (SM607)

In order to assess the consequences of PPC and/or PK deficiency on overall growth, lysine production and glucose consumption, standard 10-liter fermentations were performed. The results for the three mutant strains as well as for the wild type *C. glutamicum* ATCC 21253 strain [from Vallino and Stephanopoulos, 1993] are presented in Figures 9.2-9.5. All fermentations exhibit four distinct phases indicated by solid lines: phase I of pure growth, phase II, a transition stage from pure growth to high lysine production, phase III of no growth but high lysine production, and phase IV of death and productivity loss. There are several points to be noted in these figures. Dihydroxyacetone and glyceraldehyde which may be derived from dihydroxyacetone phosphate and glyceraldehyde phosphate *in vivo* or *in vitro*, respectively, were detected at significant

levels in the fermentations with *pyk* and *ppc pyk* mutants. This suggests that there is a built-up of glycolytic intermediates due to the blockage of PEP conversion to pyruvate. Alanine and valine secreted by the *pyk* and *ppc pyk* mutants, both of which would be derived from pyruvate, were reduced compared to the wild type and *ppc* mutant indicating that pyruvate may be limiting in these mutants. Trehalose is continuously produced throughout the course of fermentation in all four strains. It is also interesting to note that the maximum cell concentration reached by the *ppc pyk* mutant is 15g/l, which is about 75% of the level reached by the other three strains. The production profile of other by-products is altered in the *pyk* and *ppc pyk* mutants.

The results of Figures 9.2-9.5 can be best summarized in Table 9.1 showing the yields of cell mass and lysine on glucose and the specific rates of growth, glucose uptake and lysine production for the four strains in phases I-III. The cell yield (g DCW/g glucose consumed), specific glucose uptake rate and growth rate in phase I are similar among the wild type, *ppc* mutant and *pyk* mutant but are significantly lower for the *ppc pyk* mutant. This suggests that glucose utilization is seriously impaired in the case of *ppc pyk* mutant. The specific glucose uptake rates decrease in all four strains during the course of fermentation.

9.4.2 Compensation of PPC by Pyruvate Carboxylation in *C. glutamicum*

The results of Table 9.1 should be evaluated in the light of Figure 9.6 summarizing the possible anaplerotic routes leading to the formation of OAA. The fact that the deletion of *ppc* gene leaves growth and lysine production essentially unaffected indicates that there exist additional anaplerotic pathways operational in *C. glutamicum*. Potentially, there exists two alternative pathways for the formation of OAA: (1) one via carboxylation of PEP by the action of enzyme other than PPC such as PEP carboxykinase (EC 4.1.1.32), PEP carboxytransphosphorylase (EC 4.1.1.38) or transcarboxylase (EC 2.1.3.1); and (2) via carboxylation of pyruvate by pyruvate carboxylase (EC 6.4.1.1).

The presence of an alternative PEP carboxylating pathway is not supported by the results obtained with the *pyk* and *ppc pyk* mutants. For if such alternative PEP carboxylating pathway truly existed, then blockage of PEP conversion to pyruvate in the

pyk mutant should result in PEP accumulation and increased OAA (hence lysine) synthesis. On the contrary, lysine productivity and yield are reduced by approximately 30% and 40% respectively, consistent with the viewpoint that pyruvate carboxylation is the main anaplerotic pathway: As pyruvate availability is reduced in the *pyk* mutant, anaplerotic flux and lysine productivity decline.

Similarly, if PEP carboxylation was the main anaplerotic pathway, a decline in lysine production should be observed in the case of the *ppc* mutant. This, however, is not supported by the data of Table 9.1 that, if anything, suggest an increased lysine production with the *ppc* mutant. Finally, the hypothesis that pyruvate carboxylation is the main anaplerotic route in this *C. glutamicum* strain is corroborated by the attenuation of both growth and lysine production observed with the *ppc pyk* double mutant. In this case the only route of pyruvate formation is via PEP:glucose PTS transport system which produces one molecule of pyruvate for every molecule of glucose imported. There would be less pyruvate available for the synthesis of OAA via pyruvate carboxylation as well as for acetyl-CoA synthesis via pyruvate dehydrogenase. This consequently limits the generation of both energy and biosynthetic precursors. During the lysine production phase, this effect is more severe as some pyruvate must also be drained off in the condensation step with aspartate semialdehyde to synthesize lysine. It must be also pointed out that our results are in direct contrast to the results of Shiio *et al.* [1987] who reported an improved lysine yield with a *pyk* mutant.

9.4.3 Determination of Metabolic Fluxes

There are 40 metabolites participating in a total of 39 reactions depicted in the network of Figure 9.1. Reactions and metabolites are further detailed in Appendices 9.1 and 9.2 respectively. This means that there are 39 unknown fluxes and 40 equations, sufficient, in principle, to provide a unique solution to the system along with one redundancy for testing the overall consistency of the biochemical assumption and fermentation measurements. Before, however, one attempts to invert the matrix of (Eq. 9.1), it must first be established that the matrix is nonsingular and a unique solution exists. If, for example, both a PEP and pyruvate carboxylating reaction are present in the

network, matrix A is singular implying that a PEP carboxylating reaction cannot be determined independently from a pyruvate carboxylation flux solely based on the extracellular measurements. This is true when at least one of the THD or PK activities are present. However, in the case of a strain deficient in both THD and PK activities, matrix A becomes nonsingular and PEP and pyruvate carboxylation fluxes can be determined independently.

There are, obviously, many possibilities to be considered with the wild type and three mutants considered in this study. Table 9.2 summarizes the outcome regarding the nature of matrix A for the 16 cases corresponding to all possible permutations of the four key enzymes, PPC, PC, THD and PK. Along with matrix singularity, a row for the biochemical feasibility of the particular combination is provided: Clearly, no strain can grow in the absence of both anaplerotic reactions, hence strains deficient in both PPC and PC activities are marked infeasible.

For each strain, the stoichiometric matrix A must be reconfigured to reflect the corresponding genetic background and enzymatic data. The wild type strain reflecting the presence of PK activity while allowing flexibility with respect to the exact nature of the anaplerotic reaction can be described by any of A_1, A_2, A_5, A_6, A_9, and A_{10}. A_1, A_2 and A_5 are singular, and therefore only cases A_6, A_9, and A_{10} are solved for the intracellular fluxes. Results from matrix A_9 suggest a very high THD flux similar in magnitude to that of glycolysis. As such a high flux is not supported by the measured THD activity, this case is rejected. Discrimination between the possibilities of PEP (A_6) and pyruvate (A_{10}) carboxylation pathway is not possible based on the flux analysis because both lead to the same error estimation. In fact, both solutions are identical except that the anaplerotic flux is through PPC or PC and PK respectively. This means that any linear combination of solutions based on A_6 and A_{10} are likely, namely carbon flow through both PEP carboxylation and pyruvate carboxylation is possible.

For the case of the *ppc* mutant, three possible cases were examined. Even though there is yet no concrete data for the presence of pyruvate carboxylation pathway in this bacterium, experimental results [see Chapter 8] based on ^{13}C labelling studies strongly

indicated that this pathway is operative *in vivo*. Assuming the existence of a pyruvate carboxylating pathway and no activity of THD, the solution based on A_{10} is most likely.

The case of the *pyk* mutant was analyzed assuming the stoichiometry of A_4, A_7, A_8, A_{11}, and A_{12} in which PK is absent. Cases A_8 and A_{12} were rejected for not satisfying the redundant equations and allowing NADPH accumulation. The solution of A_{11} was also rejected as it resulted in negative TCA cycle fluxes. Likewise, the solution based on A_4 is unlikely since it produced a negative flux through the pyruvate carboxylation pathway. Consequently, A_7 is the most likely stoichiometry in this mutant. A high flux via the THD step also supported by the enzymatic data should be noted.

The fermentation data of the *ppc pyk* mutant were analyzed in a similar manner as the *pyk* mutant. Similarly, the estimation based on A_7 is the most likely solution for this mutant.

The fluxes through key central carbon pathways for each strain in the three phases are compared in Figures 9.7-9.12. The fluxes are represented in mmol/g DCW/h. Certain important trends can be seen. Fluxes via PEP:glucose PTS system (Figure 9.7) decrease in all four strains during the course of fermentation, indicating a decline in metabolic activity as the cell growth rates tend to decrease. This is more pronounced in the case of *ppc pyk* mutant. Fluxes via citrate synthase (Figure 9.8) which essentially represents the activity of the TCA cycle is similar in the wild type and *ppc* mutant but lower in the *pyk* and *ppc pyk* mutants. However, total ATP generated and consumed (Figure 9.9) are comparable in all four strains despite the difference in the NADH production via the TCA cycle. The required NADH production is compensated for by the increase in the flux via glucose 6-phosphate dehydrogenase (Figure 9.10) which indicates the activity of the PPP. Excess NADPH will be generated via the high activity of the PPP and this will be converted into NADH via the action of THD. Fluxes via the phosphoglucose isomerase (Figure 9.11) which converts reversibly glucose 6-phosphate and fructose 6-phosphate is positive in the wild type, *ppc* mutant, and *pyk* mutant strains except in the phase I of the *pyk* mutant. However, these fluxes are negative in the *ppc pyk* mutant indicating that all glucose is metabolized exclusively via the PPP. Fluxes via the anaplerotic pathway

(Figure 9.12) consisting of PEP and pyruvate carboxylation pathways are significantly lower in the *ppc pyk* mutant due to the limited available sources for OAA.

9.4.4 Presence of Transhydrogenase in *C. glutamicum*

In order to experimentally corroborate the functioning of THD as suggested by the metabolic flux analysis, we measured the activity of THD in crude extracts for the four strains which were grown with PMB medium in 1-liter shake flasks and harvested at mid-exponential stage. The data are reported in column 4 of Table 9.3. Significantly higher activities were detected for the *pyk* and *ppc pyk* mutants compared to the other two strains as suggested by the increased PPP flux and NADPH synthesis rate of the intracellular flux analysis.

9.5 Discussion

9.5.1 Role of THD

One of the interesting findings is the presence of THD activity in this bacterium. THD, found in the inner membrane of mitochondria and the cytoplasm of some bacteria, catalyzes the reversible reaction $NADPH + NAD^+ \leftrightarrow NADP^+ + NADH$. The reaction direction is determined by the mass action ratio $\Gamma = \frac{[NADP^+][NADH]}{[NADPH][NAD^+]}$ which often is used as a measure of the metabolic reduction state of the cell. It is believed that under energy limiting conditions, the reaction in the forward direction is favored whereas in the presence of excess ATP, the reaction in the reverse direction is greatly enhanced. It has been suggested that the role of THD is to supply NADPH for biosynthesis or hydroxylation reactions when operating in the reverse direction or to provide NADH and therefore generate ATP via oxidative phosphorylation when operating in the forward direction [Hoek and Rydström, 1988].

Additionally, THD acts to maintain efficient recycling of $NADP^+$ from NADPH which is needed in the oxidative portion of the PPP. Potential depletion of $NADP^+$ and accumulation of NADPH can be avoided by the action of this enzyme. This role is used to explain the different properties of phosphoglucose isomerase (PGI; EC 5.3.1.9; *pgi* gene)

mutants of several species [Boles *et al.*, 1993]. PGI is the second enzyme in the glycolytic pathway catalyzing the reversible conversion of glucose 6-phosphate and fructose 6-phosphate. A *pgi* mutant of *E. coli* [Vinopal, 1975] was able to grow on glucose medium, although at a slower rate as compared to the wild type. This metabolic adaptation was explained by glucose being utilized solely via the PPP and thus bypassing the normal glycolytic pathway. However, this would lead to an oversupply of NADPH and a shortage of $NADP^+$. Cell growth is possible since THD restores the depleted level of $NADP^+$. This hypothesis was further supported by Maitra [1971] who showed that a *pgi* mutant of *S. cerevisiae* was unable to grow on the glucose medium apparently due to absence of NADPH oxidation mechanism in *S. cerevisiae*. The flow via the PPP cannot be sustained due to the depletion of $NADP^+$ required in the oxidative portion of the PPP. Boles, *et al.* [1993] also demonstrated that the addition of NADPH oxidizing agents or the overexpression of the NAD-dependent glutamate dehydrogenase, both of which lead to oxidation of NADPH to $NADP^+$, restores the growth of the *pgi* mutant on glucose. A similar result was obtained by Dickinson *et al.* [1995] who showed that a spontaneous mutation increasing the activity of the NAD- and NADP-dependent glutamate dehydrogenase also enables the *pgi* mutant to grow on glucose.

It is also possible that under certain growth conditions, THD may be dispensable. This was demonstrated by Zahl *et al.* [1978] who showed that a *thd* mutant of *E. coli* has normal growth characteristics in various carbon sources when cultured aerobically or anaerobically. This is expected since under balanced growth conditions, the cell can balance the NADPH generation and utilization rates without the action of THD. It would be interesting to observe the effect of deletion of *thd* gene in the four genetic backgrounds of *C. glutamicum*. Extrapolating from the above results, one can predict that a *thd* mutant, a *thd ppc* mutant, and a *thd pyk* mutant would behave similar to the wild type with glucose as the sole carbon source but a *thd ppc pyk* mutant would not be able to grow with glucose as the sole carbon source.

In a gluconate fermentation with the wild type strain, Vallino and Stephanopoulos [1994] also observed that excess NADPH was produced. However, due to unsuitable enzymatic assay, THD activity was not detected and assumed to be absent. Instead in

order to balance NADPH overproduction, they assumed direct NADPH oxidation as follows:

$$NADPH + \frac{1}{2}O_2 \rightarrow H_2O + NADP^+$$

The combined reactions of THD and NADH oxidative phosphorylation as follows is essentially equivalent to the above reaction except for the generation of ATP:

$$NADH + \frac{1}{2}O_2 + 2ADP \rightarrow H_2O + NAD^+ + 2ATP$$

$$NADPH + NAD^+ \rightarrow NADP^+ + NADH$$

$$NADPH + \frac{1}{2}O_2 + 2ADP \rightarrow H_2O + NADP^+ + 2ATP$$

In cases where ATP is produced in excess, the two representations are indistinguishable.

9.5.2 Proposed Mode of Glucose Assimilation in the *ppc pyk* Mutant

Based on the metabolic flux analysis and detection of a high level of THD activity, a proposed pathway of glucose assimilation in the *ppc pyk* mutant is presented in Figure 9.16. Glucose is preferentially oxidized via the PPP with the reduction of $NADP^+$ to NADPH. THD converts NADPH to $NADP^+$ so that the high level of the PPP can be maintained. Due to the blockage of metabolite flow at the PEP branchpoint, glycolytic metabolites, specifically glyceraldehyde 3-phosphate and dihydroxyacetone phosphate, will be dephosphorylated and excreted from the cell thus relieving the intracellular accumulation of glycolytic intermediates. OAA is derived solely from pyruvate which in turn is derived solely via the PEP:glucose PTS system. The activity of the TCA cycle is lower because of limited availability of acetyl-CoA and consequently generates less NADH. However, the shortage of NADH is compensated for by the activity of THD.

9.5.3 Glucose Uptake in the *ppc pyk* Mutant

It is interesting to observe that the glucose uptake rate is significantly attenuated in the *ppc pyk* mutant. Saier and Chin [1990] proposed that the glucose uptake rate in *Escherichia coli* which is mediated by the PEP:glucose PTS transport system is regulated by the $\frac{[PEP]}{[pyruvate]}$ ratio. High $\frac{[PEP]}{[pyruvate]}$ would increase the glucose uptake rate. This

hypothesis is supported by Chao and Liao [1993] who demonstrated that the overexpression of *ppc* gene, which would lower the PEP concentration and thus decrease the ratio, decreased the glucose uptake rate whereas the overexpression of PEP synthase gene, which would increase the PEP concentration, increased the glucose uptake rate. However, our results with *ppc pyk* mutant seems to be contradictory to this hypothesis. PEP concentration is probably elevated intracellularly as evidenced by the excretion of dephosphorylated glycolytic intermediates, yet the glucose uptake rate is lower.

9.5.4 Limitations of the Metabolic Flux Analysis

Metabolic flux analysis is useful for estimatomg *in vivo* reaction rates which are otherwise difficult to measure. In this way, a picture of intracellular flux distribution that is most consistent with the known biochemistry and the experimental data can be generated. Yet there are limitations with this approach. One limitation is the obvious inability to differentiate between reactions that give rise to singular stoichiometries, as in the PPC and PC cases. In such cases nonobservable reactions should be lumped and their sum estimated. Clearly the degree of reaction observability (and subsequent refinement of biochemical detail) depends directly on the number and type of measurement available. As discussed in Chapter 8, NMR spectroscopy and in particular ^{13}C enrichment, isotopomer and fine structure measurements can play a critical role in this area.

A second problem arises when the operating biochemistry is not completely known. For example, in the description of metabolic flux with the *ppc pyk* mutants, the analysis with and without THD in the network totally alters the flux estimates through the various pathways. It should be noted that even though the disagreement between the estimated and observed rates can be used to reject the proposed biochemistry, the close agreement does not necessarily guarantee the validity of the proposed biochemistry. Despite the above limitations, intracellular flux estimates, especially when obtained from very overdetermined systems, provide very valuable insights about the physiology and metabolism of strains and their variation in response to genetic and environmental perturbations. Properly handled, even the above limitations can be turned into advantages

as with the THD case whose existence was first suggested after the failure of the consistency test and NADPH violation of the steady state hypothesis.

We have introduced mutations in *C. glutamicum* that have perturbed the central carbon metabolic pathway. This in turn has resulted in secondary responses such as enhanced carbon utilization via the PPP and an active THD as the cells attempt to adapt to the perturbed metabolic conditions. This indicates that even in this relatively simple bacterium, complex regulation exists which can be induced by changes in the intracellular metabolite pools.

We have demonstrated the utility of the metabolic flux analysis for the description and comparison of fermentations with strains which are genetically or environmentally perturbed. The methodology is clearly useful for providing insight into metabolic pathways that are otherwise difficult to decipher. At the same time, the methodology can be used to reject unrealistic metabolic pathways through data consistency analysis. By applying this technique to the fermentation data of *C. glutamicum* mutants we were able to illustrate the likelihood for the existence of THD activity in this bacterium followed by experimental verification and also to postulate a peculiar glucose assimilation mechanism as a response to the introduced mutations.

9.6 Nomenclature

A	**matrix of stoichiometric coefficients from metabolic reaction network**
OAA	oxaloacetate
PC	pyruvate carboxylase
PEP	phosphoenolpyruvate
PK	pyruvate kinase
PPC	phosphoenolpyruvate carboxylase
ppc	gene encoding phosphoenolpyruvate carboxylase
PPP	pentose phosphate pathway
pyk	gene encoding pyruvate kinase
r	vector of metabolite rates of change
THD	transhydrogenase
x	vactor of metabolic fluxes

9.7 References

Aiba, S., Matsuoka, M. (1979). Identification of metabolic model: citrate production from glucose by *Candida lipolytica*. *Biotechnol. Bioeng.* **21**: 1373-1386.

Boles, E., Lehnert, W., Zimmermann, F.K. (1993). The role of the NAD-dependent dehydrogenase in restoring growth on glucose of a *Saccharomyces cerevisiae* phosphoglucose isomerase mutant. *Eur. J. Biochem.* **217**: 469-477.

Bradford, M.M. (1976). A rapid and sensitive method for the quantification of microgram quantities of protein utilizing the principle of protein-dye binding. *Anal. Biochem.* **72**: 248-254.

Clarke, D.M., Bragg, P.D. (1986). Expression of the cloned subunits of *Escherichia coli* transhydrogenase from separate replicons. *FEBS Lett.* **200**: 23-26.

Cortassa, S., Aon, J.C., Aon, M.A. (1995). Fluxes of carbon, phosphorylation, and redox intermediates during growth of *Saccharomyces cerevisiae* on different carbon sources. *Biotechnol. Bioeng.* **47**: 193-208.

Cremer, J., Eggeling, L., Sahm, H. (1991). Control of the lysine biosynthesis sequence in *Corynebacterium glutamicum* as analyzed by overexpression of the individual corresponding genes. *App. Environ. Microbiol.* **57**: 1746-1752.

Diaz-Ricci, J.C., Tsu, M., Bailey, J.E. (1992). Influence of expression of the *pet* operon on intracellular metabolic fluxes of *Escherichia coli*. *Biotechnol. Bioeng.* **39**: 59-65.

Dickinson, J.R., Sobansk, M.A., Hewlins, M.J. (1995). In *Saccharomyces cerevisiae* deletion of phosphoglucose isomerase can be suppressed by increased activities of enzymes of the hexose monophosphate pathway. *Microbiol.* **141**: 385-391.

Fellay, R., Frey, J., Krisch, H. (1987). Interposon mutagenesis of soil and water bacteria: a family of DNA fragments designed for in vitro insertional mutagenesis of gram-negative bacteria. *Gene* **52**: 147-154.

Gubler, M., Park, S.M., Jetten, M., Stephanopoulos, G., Sinskey, A.J. (1994a). Effects of phosphoenol pyruvate carboxylase deficiency on metabolism and lysine production in *Corynebacterium glutamicum*. *Appl. Microbiol. Biotechnol.* **40**: 857-863.

Gubler, M., Jetten, M., Lee, S.H., Sinskey, A.J. (1994b). Cloning of the pyruvate kinase gene (*pyk*) of *Corynebacterium glutamicum* and site-specific inactivation of *pyk* in a lysine producing *Corynebacterium lactofermentum* strain. *Appl. Microbiol. Biotechnol.* **60**: 2494-2500.

Hanahan, D. (1983). Studies on transformation of *Escherichia coli* with plasmids. *J. Mol. Biol.* **166**: 557-580.

Hoek, J.B., Rydström, J. (1988). Physiological roles of nicotinamide nucleotide transhydrogenase. *Biochem. J.* **254**: 1-10.

Humphrey, A.E. (1971). Present limitations to the control and understanding of a fermentation process. *Proc. LABEX Symp. Comput. Control Ferment. Process* **1**:

Jones, B.N., Gilligan, J.P. (1983). o-Phthalaldehyde precolumn derivatization and reversed-phase high-performance liquid chromatography of polypeptide hydrolysates and physiological fluids. *J. Chromatogr.* **266**: 471-482.

Jørgensen, H., Nielsen, J., Villadsen, J., Mollgaard, H. (1995). Metabolic flux distributions in *Penicillium chrysogenum* during fed-batch cultivations. *Biotechnol. Bioeng.* **46**: 117-131.

Kiss, R.D., Stephanopoulos, G. (1991). Metabolic activity control of the L-lysine fermentation by restrained growth fed-batch strategies. *Biotechnol. Prog.* **7**: 501-509.

Mavrovouniotis, M.L. (1993). Identification of localized and distributed bottlenecks in metabolic pathways. International Conference on Intelligent Systems in Molecular Biology. AAAI Press, Washington, D.C., **1**: 275-283

Maitra, P.K. (1971). A kinetic study of glycolytic enzyme synthesis in yeast. *J. Bacteriol.* **246**: 475-488.

Mori, M., Shiio, I. (1985). Purification and some properties of phosphoenol pyruvate carboxylase from Brevibacterium flavum and its over producing mutant. *J. Biochem.* **97**: 1119-1128.

Neidhardt, F.C., Ingraham, J.L., Schaechter, M. (1990). *Physiology of the Bacterial Cell*, Sinauer Associates, Inc., Sunderland, MA.

Ozaki, H., Shiio, I. (1983). Production of lysine by pyruvate kinase mutants of *Brevibacterium flavum*. *Agric. Biol. Chem.* **47**: 1569-1576.

Papoutsakis, E.T. (1984). Equations and calculations for fermentations of butyric acid bacteria. *Biotechnol. Bioeng.* **26**: 174-187.

Papoutsakis, E.T., Meyer, C.L. (1985a). Fermentation equations for propionic-acid bacteria and production of assorted oxychemicals from various sugars. *Biotechnol. Bioeng.* **27**: 67-80.

Papoutsakis, E.T., Meyer, C.L. (1985b). Equations and calculations of product yields and preferred pathways for butanediol and mixed-acid fermentations. *Biotechnol. Bioeng.* **27**: 50-66.

Peters-Wendisch, P.G., Eikmanns, B.J., Thierbach, G., Bachmann, B., Sahm, H. (1993). Phosphoenolpyruvate carboxylase in *Corynebacterium glutamicum* is dispensable for growth and lysine production. *FEMS Microbiol. Let.* **112**: 269-274.

Phelps, D.C., Hatefi, Y. (1981). Inhibition of the mitochondrial nicotinamide nucleotide transhydrogenase by dicyclohexylcarbodiimide and diethylpyrocarbonate. *J. Biol. Chem.* **256**: 8217-8221.

Reardon, K.F., Scheper, T.H., Bailey, J.E. (1987). Metabolic pathway rates and culture fluorescence in batch fermentations of *Clostridium acetobutylicum*. *Biotechnol. Prog.* **3**: 153-167.

Schäfer, A., Kalinowski, J., Simon, R., Seep-Feldhaus, A.-H., Pühler, A. (1990). High-frequency conjugal plasmid transfer from gram-negative *Escherichia coli* to various gram-positive coryneform bacteria. *J. Bacteriol.* **172**: 1663-1666.

Sambrook, J., Fritsch, E.F., Maniatis, T. (1989). *Molecular cloning-a laboratory manual*, Cold Spring Harbor Laboratory, Cold Spring Harbor, N.Y.

Sano, K., Ito, K., Miwa, K., Nakamori, S. (1987). Amplification of the phosphoenolpyruvate pyruvate carboxylase gene of *Brevibacterium lactofermentum* to improve amino acid production. *Agric. Biol. Chem.* **51**: 597-599.

Savinell, J.M., Palsson, B.O. (1992). Network analysis of intermediary metabolism using linear optimization: II. Interpretation of hybridoma cell metabolism. *J. Theor. Biol.* **154**: 455-473.

Shiio, I., Ozaki, H., Ujigawa-Takeda, K. (1982). Production of aspartic acid and lysine by citrate synthase mutants of *Brevibacterium flavum*. *Agric. Biol. Chem.* **46**: 101-107.

Shiio, I., Sugimoto, S.-I., Toride, Y. (1984a). Studies on the mechanisms for lysine production by pyruvate kinase-deficient mutants of *Brevibacterium flavum*. *Agric. Biol. Chem.* **48**: 1551-1558.

Shiio, I., Toride, Y., Sugimoto, S.-I. (1984b). Production of lysine by pyruvate dehydrogenase mutants of *Brevibacterium flavum*. *Agric. Biol. Chem.* **48**: 3091-3098.

Shiio, I., Yokota, A., Sugimoto, S. (1987). Effect of pyruvate kinase deficiency on L-lysine productivities of mutants with feedback-resistant aspartokinases. *Agric. Biol. Chem.* **51**: 2485-2493.

Tosaka, O., Yoshihara, Y., Ikeda, S., Takinami, K. (1985). Production of L-lysine by fluropyruvate-sensitive mutants of *Brevibacterium flavum*. *Agric. Biol. Chem.* **49**: 1305-1312.

Tozo, K., Sejalon-Delmas, N., Jerebzoff-Quintin, S., Jerebzoff, S. (1992). Pyruvate carboxylase in *Leptosphaeria michotii*. Isolation, properties, intracellular localization and cyclic variations of its activity in relation to polypeptide level. *Physiol. Plant.* **86**: 484-494.

Vallino, J.J., Stephanopoulos, G. (1994). Carbon flux distributions at the glucose-6-phosphate branch point in *Corynebacterium glutamicum* during lysine overproduction. *Biotechnol. Prog.* **10**: 327-334.

Vallino, J.J., Stephanopoulos, G. (1993). Metabolic flux distributions in *Corynebacterium glutamicum* during growth and lysine overproduction. *Biotechnol. Bioeng.* **41**: 633-646.

Vinopal, R.T., Hillman, J.D., Schulman, H., Reznikoff, W.S., Fraenkel, D.G. (1975). New phosphoglucose isomerase mutants of *Escherichia coli*. *J. Bacteriol.* **122**: 1172-1174.

Yokota, A., Shiio, I. (1988). Effects of reduced citrate synthase activity and feedback phosphoenolpyruvate carboxylase on lysine productivities of *Brevibacterium flavum*. *Agric. Biol. Chem.* **52**: 455-463.

Yoshinaga, F., Nakamori, S. (1983). *Production of Amino Acids*, Addison-Wesley, London.

Zahl, K.J., Rose, C., Hanson, R.L. (1978). Isolation and partial characterization of a mutant of *Escherichia coli* lacking pyridine nucleotide transhydrogenase. *Arch. Biochem. Biophys.* **190**: 598-602.

Zupke, C., Stephanopoulos, G. (1995). Intracellular flux analysis in hybridomas using mass balances and in vitro ^{13}C NMR. *Biotechnol. Bioeng.* **45**: 292-303.

9.8 Appendices

9.8.1 Stoichiometric relationships for each enzymatic step shown in Figure 9.1 (modified from Vallino and Stephanopoulos (1993)). Each reaction represents the element of **x** in (Eq. 9.1).

PEP: glucose phosphotransferase system

(1) GLC + PEP = GLC6P + PYR

Embden-Meyerhof-Parnas pathway

(2) GLC6P = FRU6P

(3) FRU6P + ATP = 2 GAP + ADP

(4) GAP + ADP + NAD = NADH + G3P + ATP

(5) G3P = PEP + H_2O

Biomass synthesis

(6) 0.021 GLC6P + 0.007 FRU6P + 0.09 RIB5P + 0.036 E4P + 0.013 GAP + 0.15 G3P + 0.052 PEP + 0.03 PYR + 0.332 ACCOA + 0.08 ASP +0.033 LYSI + 0.446 GLUT + 0.025 GLUM + 0.054 ALA + 0.04 VAL + 3.82 ATP + 0.476 NADPH + 0.312 NAD = BIOMASS + 0.364 AKG + 0.143 CO_2 + 3.82 ADP + 0.476 NADP + 0.312 NAD

ATP dissipation for cellular maintenance

(7) ATP = ADP

Tricarboxylic acid cycle

(8) PYR + COA + NAD = ACCOA + CO_2 + NADH

(9) ACCOA + OAA + H_2O = ISOCIT + COA

(10) ISOCIT + NADP = AKG + NADPH +CO_2

(11) AKG + COA + NAD = SUCCOA + CO_2 + NADH

(12) SUCCOA + ADP = SUC + COA + ATP

(13) SUC + H_2O + FAD = MAL + FADH

(14) MAL + NAD = OAA + NADH

Glutamate, glutamine, alanine, and valine production

(15) NH_3 + AKG + NADPH = GLUT + H_2O + NADP

(16) GLUT + NH_3 + ATP = GLUM + ADP

(17) PYR + GLUT = ALA + AKG

(18) 2 PYR + NADPH + GLUT = VAL + CO_2 + H_2O + NADP + AKG

Pentose phosphate pathway

(19) GLC6P + H_2O + 2 NADP = RIBU5P + CO_2 + 2 NADPH

(20) RIBU5P = RIB5P

(21) RIBU5P = XYL5P

(22) XYL5P + RIB5P = SED7P + GAP
(23) SED7P + GAP = FRU6P + E4P
(24) XYL5P + E4P = FRU6P + GAP

Oxidative phosphorylation: P/O = 2
(25) 2 NADH + O_2 + 4 ADP = 2 H_2O + 4 ATP + 2 NAD
(26) 2 FADH + O_2 + 4 ADP = 2 H_2O + 4 ATP + 2 FAD

Aspartate and lysine synthesis
(27) OAA + GLUT = ASP + AKG
(28) ASP + PYR + 2 NADPH + SUCCOA + GLUT + ATP
= SUC + AKG + CO_2 + LYSI + 2 NADP + COA + ADP
(29) LYSI = LYSE

Propionate, glyceraldehyde, dihydroxyacetone, acetate, and lactate production
(30) SUC = PROP + CO2
(31) G3P + ADP = GLY + ATP
(32) G3P + ADP = DHA + ATP
(33) ACCOA + ADP = AC + COA + ATP
(34) PYR + NADH = LAC + NAD

Trehalose synthesis
(35) GLC6P + 0.5 ATP = 0.5 TREHAL + 0.5 ADP

Anaplerotic reactions: PPC and PC
(36) PEP + CO_2 = OAA
(37) PYR + CO_2 + ATP = OAA + ADP

Pyruvate kinase reaction
(38) PEP + ADP = PYR + ATP

Transhydrogenase reaction
(39) NADPH + NAD = NADP + NADH

9.8.2 Mass balances were conducted only on the following metabolites. Numbers indicate the elements of **r** in (Eq. 9.2).

AC	(20)	Acetate
ACCOA	(1)	Acetyl coenzyme A
AKG	(2)	α-Ketoglutarate
ALA	(3)	Alanine
ASP	(4)	Aspartate
ATP	(5)	Adenosine 5'-triphosphate
BIOMASS	(6)	Biomass
CO_2	(7)	Carbon dioxide
DHA	(19)	Dihydroxyacetone
E4P	(8)	Erythrose-4-phosphate
FADH	(9)	Flavin adenine dinucleotide, reduced
FRU6P	(10)	Fructose-6-phosphate
G3P	(11)	3-Phosphoglycerate
GAP	(12)	Glyceraldehyde-3-phosphate
GLC	(13)	Glucose
GLC6P	(14)	Glucose-6-phosphate
GLUM	(15)	Glutamine
GLUT	(16)	Glutamate
GLY	(18)	Glyceraldehyde
ISOCIT	(21)	Isocitrate
LAC	(27)	Lactate
LYSE	(22)	Lysine, extracellular
LYSI	(23)	Lysine, intracellular
MAL	(24)	Malate
NADH	(25)	Nicotinamide adenine dinucleotide, reduced
NADPH	(26)	Nicotinamide adenine dinucleotide phosphate, reduced
O_2	(28)	Oxygen
OAA	(29)	Oxaloacetate
PEP	(30)	Phosphoenolpyruvate
PROP	(17)	Propionate
PYR	(31)	Pyruvate, intracellular
PYRE	(38)	Pyruvate, extracellular
RIB5P	(32)	Ribose-5-phosphate
RIBU5P	(33)	Ribulose-5-phosphate
SED7P	(34)	Sedoheptulose-7-phosphate
SUC	(35)	Succinate
SUCCOA	(36)	Succinyl coenzyme A
TREHAL	(37)	Trehalose
VAL	(39)	Valine
XYL5P	(40)	Xylose-5-phosphate

Table 9.1 Comparison of fermentation results of *C. glutamicum* ATCC 21253, 253SM1, SM575, and SM607 in three distinct phases. Growth rate, specific rates and yields are given in h^{-1}, g/g DCW/h and g/g glucose consumed, respectively.

Parameter	Phase I				Phase II				Phase III			
	21253	253SM1	SM575	SM607	21253	253SM1	SM575	SM607	21253	253SM1	SM575	SM607
Growth rate	0.35	0.26	0.27	0.12								
Cell yield on glucose	0.54	0.59	0.50	0.36								
Specific glucose uptake rate	0.59	0.59	0.53	0.33	0.35	0.29	0.25	0.11	0.22	0.21	0.20	0.11
Specific lysine productivity					0.08	0.11	0.04	0.02	0.04	0.06	0.05	0.005
Lysine yield on glucose					0.23	0.37	0.17	0.21	0.16	0.27	0.23	0.05

Table 9.2 Results of feasibility check. Sixteen cases are considered. Each case consists of basic reaction set (1 through 35 as described in Appendix 1) and additional reactions described below in each column. Reaction 36 represents the enzymatic step for PEP carboxylase, reaction 37 for pyruvate carboxylase, reaction 38 for pyruvate kinase, and reaction 39 for transhydrogenase. Abbreviations: +, presence of pathway; -, absence of pathway; S, singular; N, non-singular; F, biochemically feasible; I, biochemically infeasible.

Reaction	1	2	3	4	5	6	7	8	9	10	11	12	13	14	15	16
36 (PPC)	+	+	+	+	+	+	+	+	-	-	-	-	-	-	-	-
37 (PC)	+	+	+	+	-	-	-	-	+	+	+	+	-	-	-	-
38 (PK)	+	+	-	-	+	+	-	-	+	+	-	-	+	+	-	-
39 (THD)	+	-	+	-	+	-	+	-	+	-	+	-	+	-	+	-
Matrix Singularity	S	S	S	N	S	N	N	N	N	N	N	N	N	N	N	N
Biochemical Feasibility	F	F	F	F	F	F	F	F	F	F	F	F	I	I	I	I

Table 9.3 Activities of selected enzymes in *C. glutamicum* ATCC 21253, 253SM1, SM575, and SM607. Activities are given in nmol per min per mg of protein. Pyruvate kinase and PEP carboxylase assays were done with the cells grown in LB medium whereas transhydrogenase assays were done with the cells grown in PBM medium and harvested at the mid-exponential stage. N.D., not detected.

Strain	Pyruvate kinase	PEP carboxylase	Transhydrogenase
21253 (WT)	822	344	220
253SM1 (*ppc* mutant)	677	N.D.	150
SM575 (*pyk* mutant)	N.D.	279	310
SM607 (*ppc pyk* mutant)	N.D.	N.D.	490

Figure 9.1 Metabolic pathways in *C. glutamicum*. The numeral in circle indicates the reaction step whose reaction stoichiometry is shown in details in the Appendix 9.8.1. The boxed metabolite indicate extracellular components which can be monitored. Abbreviations are in the Appendix 9.8.2.

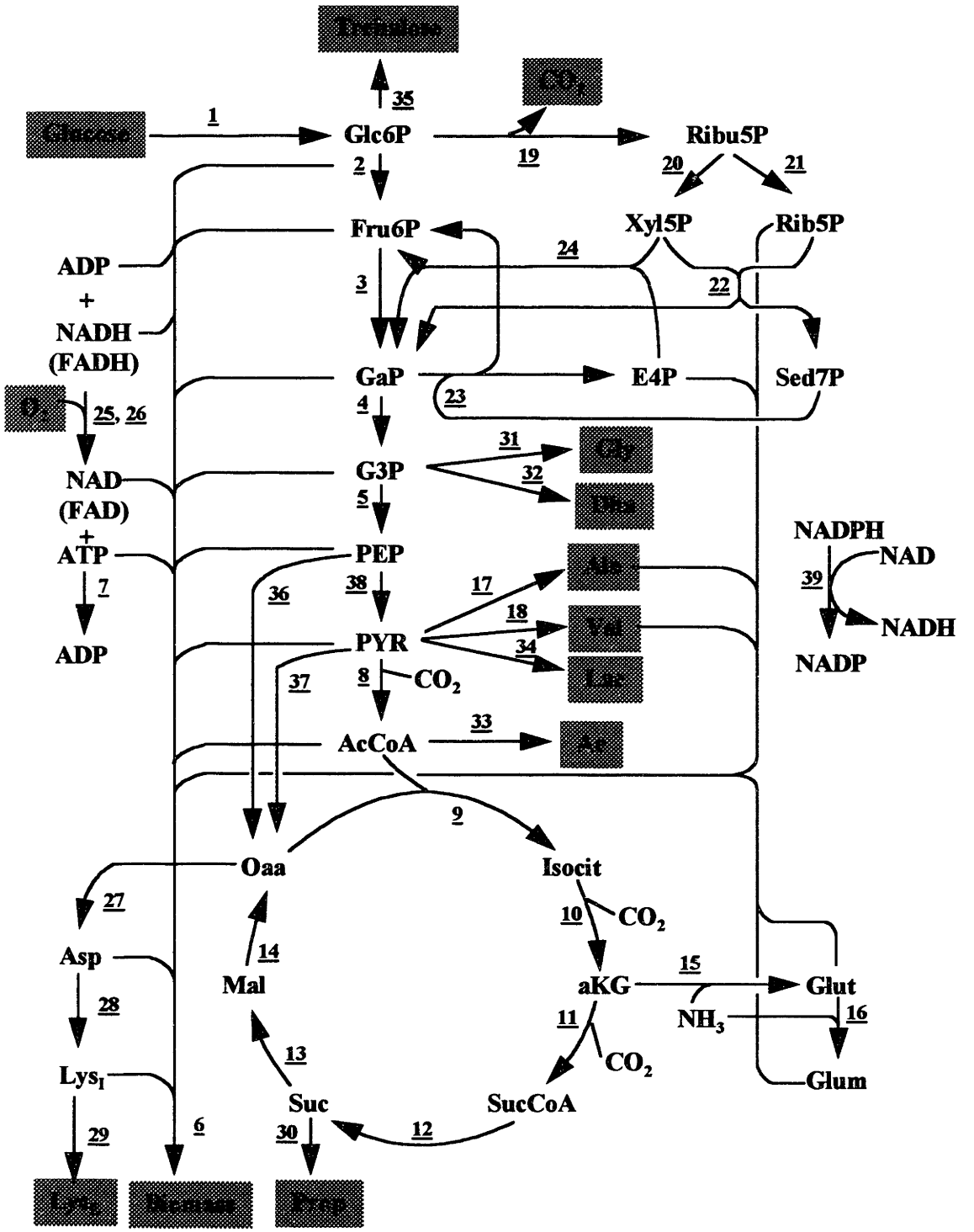

Figure 9.2 Lysine fermentation of *C. glutamicum* ATCC 21253. Top: glucose, biomass, and L-lysine. Middle: Profiles of organic acids, alcohols, and other amino acids. Bottom: culture respiration; carbon dioxide evolution rate (CER), oxygen uptake rate (OUR), cumulative values of carbon dioxide evolution and oxygen utilization. Adapted from Vallino and Stephanopoulos [1993].

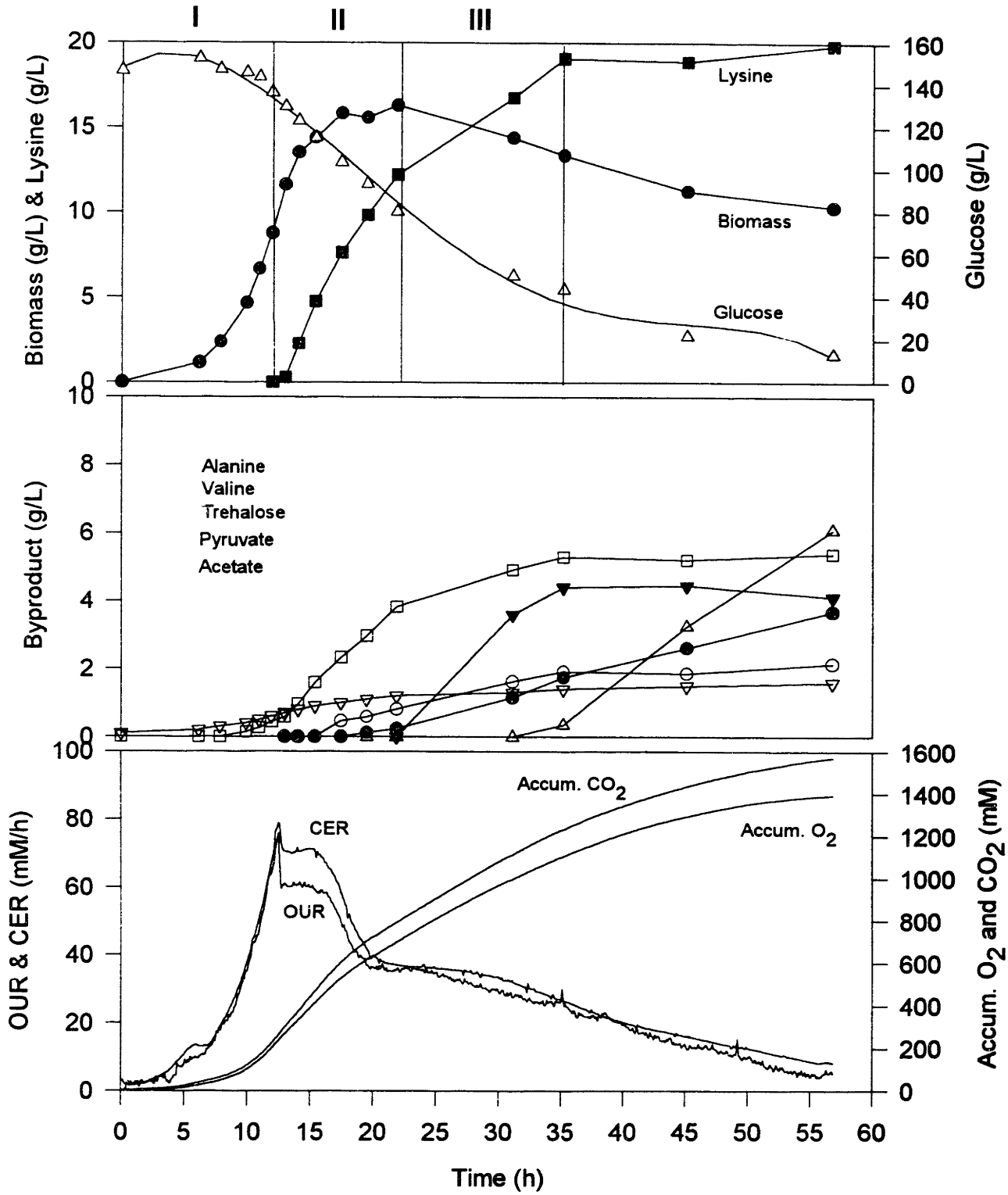

Figure 9.3 Lysine fermentation of *ppc* mutant (253SM1).

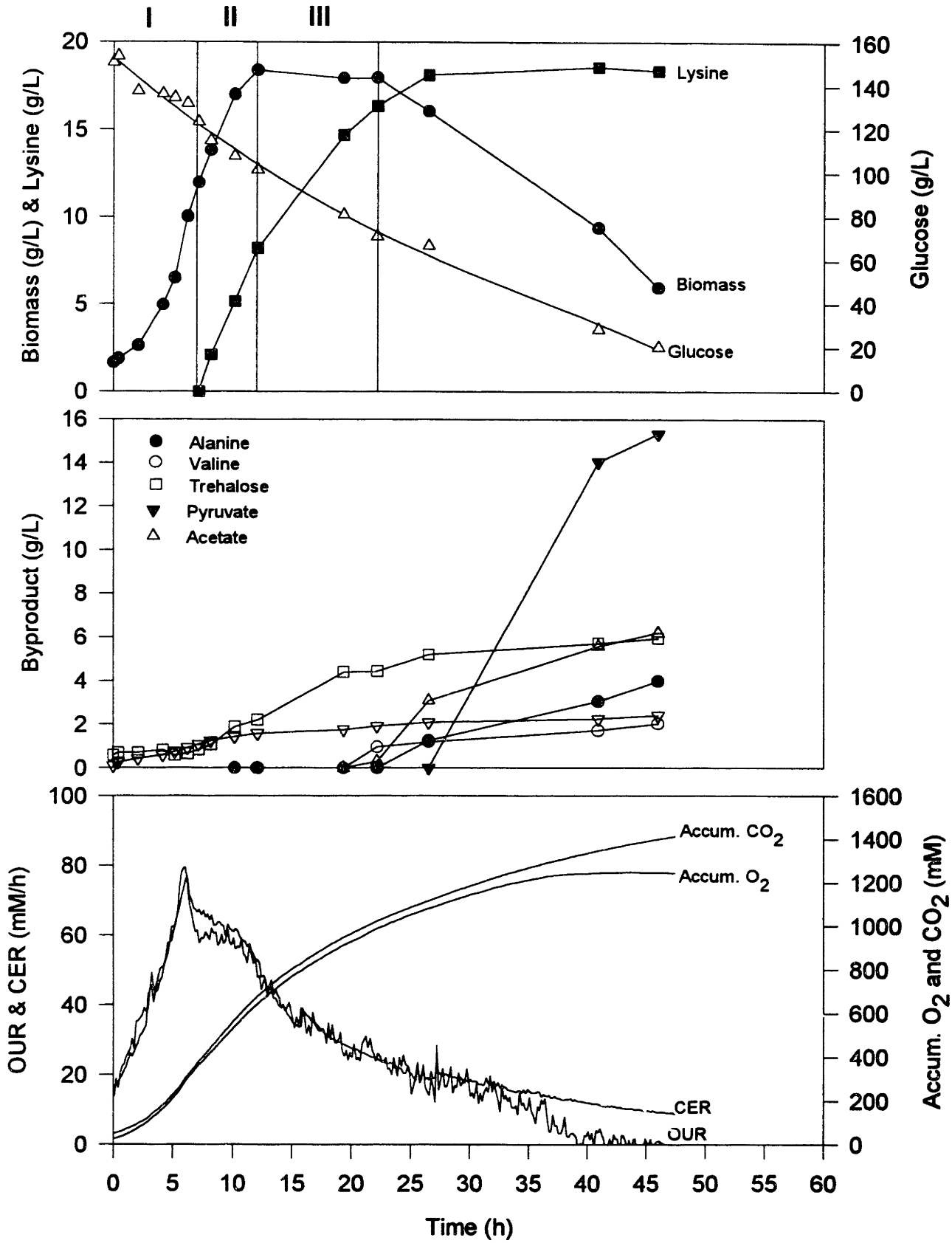

Figure 9.4 Lysine fermentation of *pyk* mutant (SM575).

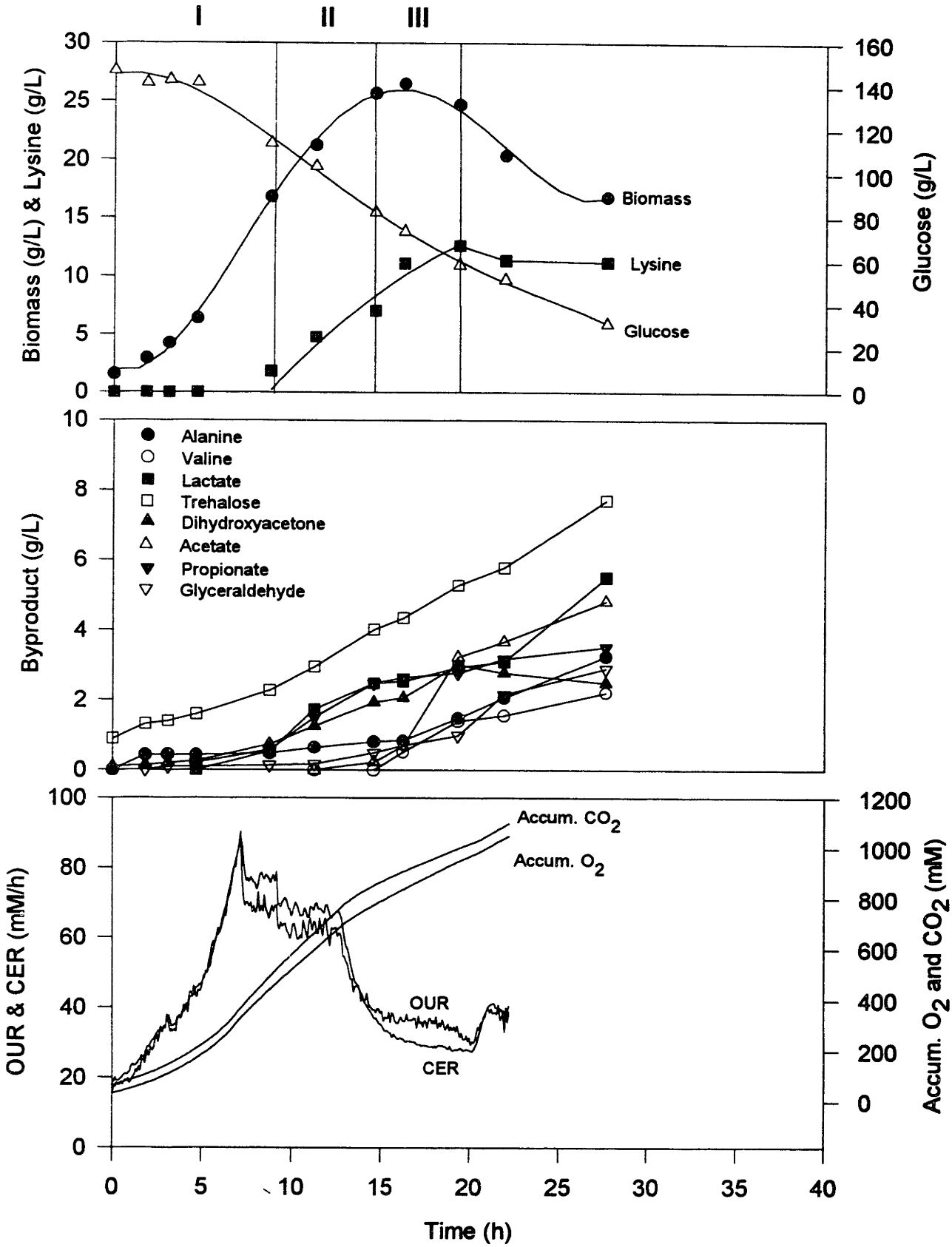

Figure 9.5 Lysine fermentation of *ppc pyk* mutant (SM607).

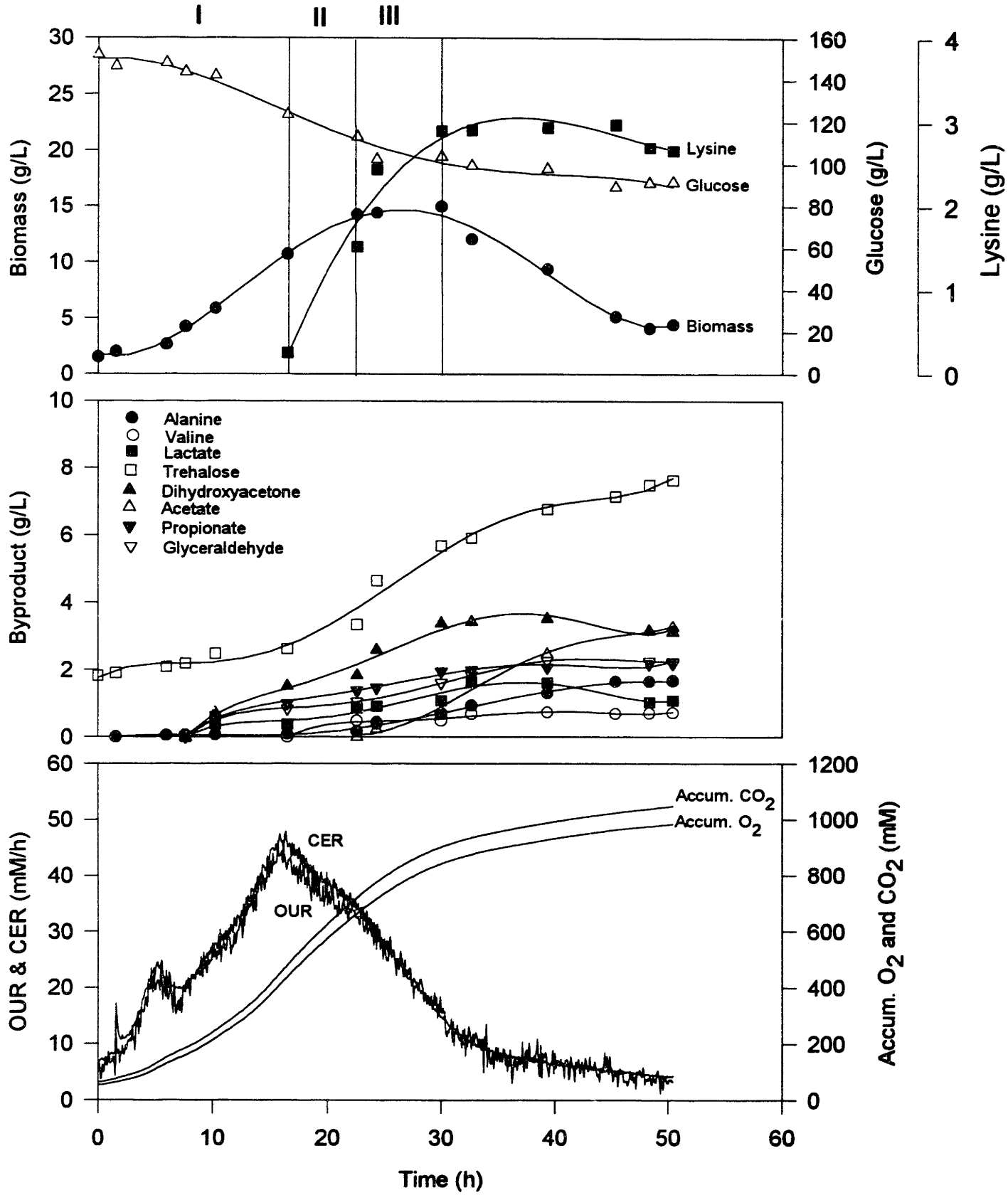

Figure 9.6 Proposed carbon flow at the PEP, pyruvate and OAA branchpoints in the four strains: (a) wild type; (b) *ppc* mutant; (c) *pyk* mutant; (d) *ppc pyk* mutant. See text for more details.

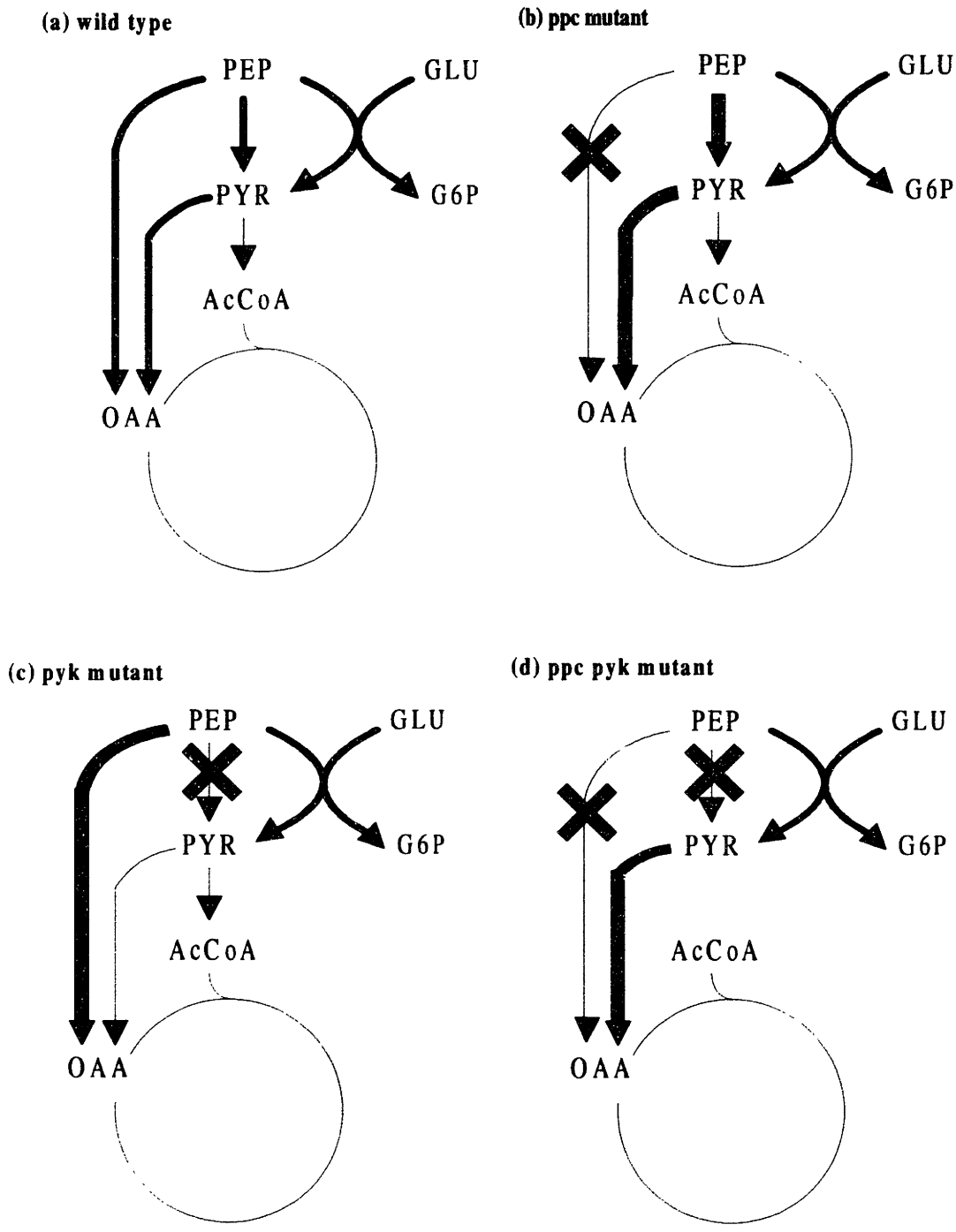

Figure 9.7 Comparison of fluxes via PEP:glucose PTS system for the four strains in the three growth phases. Fluxes are in mmol/g DCW/h.

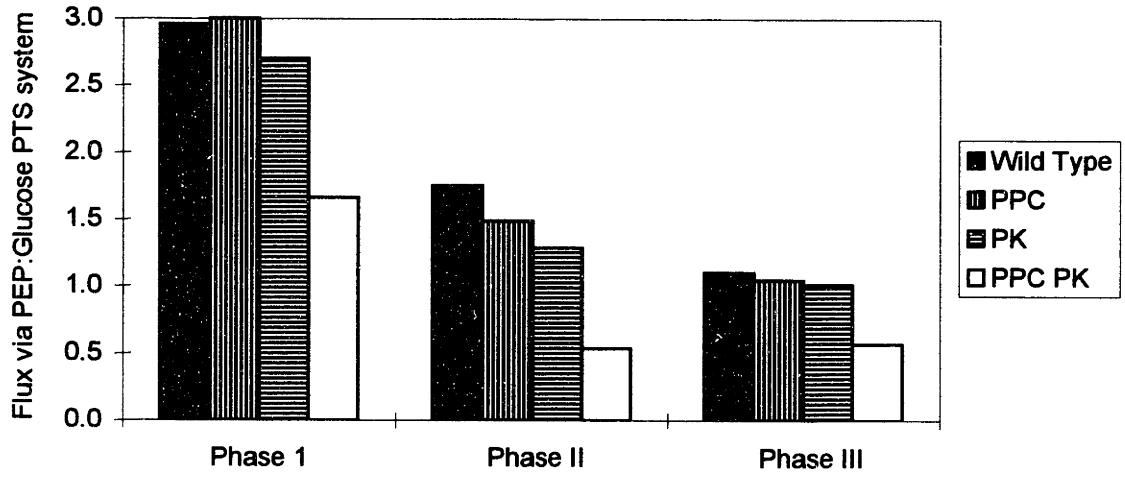

Figure 9.8 Comparison of fluxes via citrate synthase.

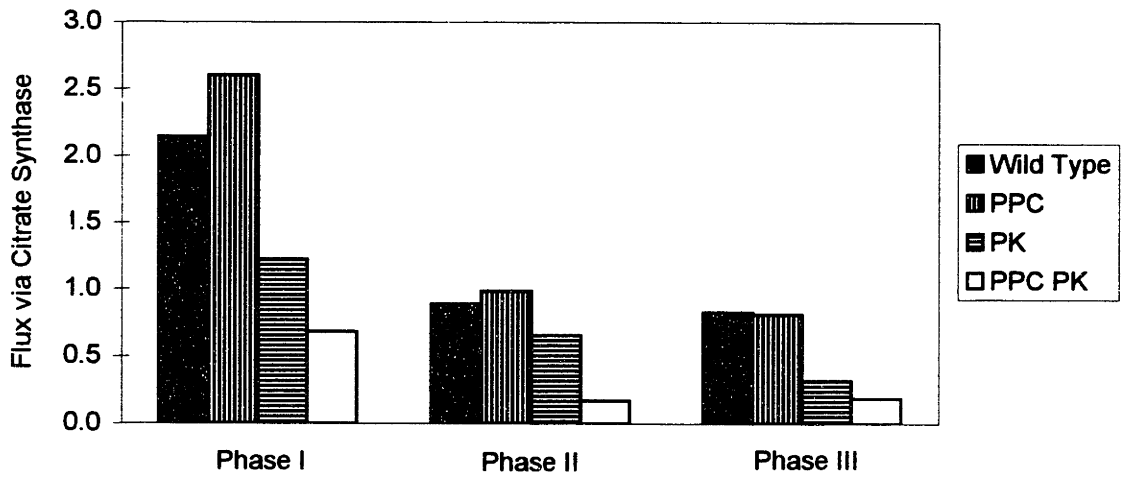

Figure 9.9 Comparison of fluxes via ATP dissipation reaction.

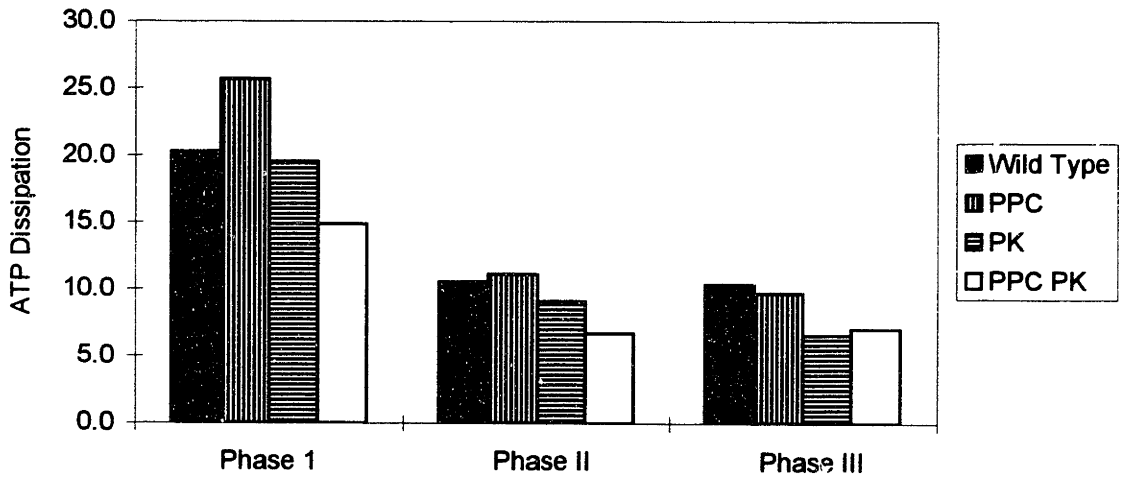

Figure 9.10 Comparison of fluxes via glucose 6-phosphate dehydrogenase.

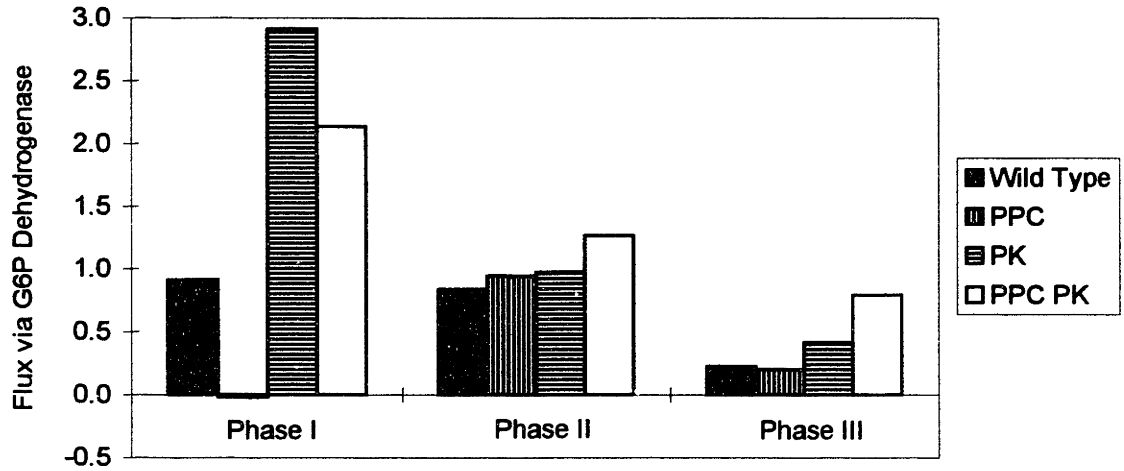

Figure 9.11 Comparison of fluxes via phosphoglucose isomerase.

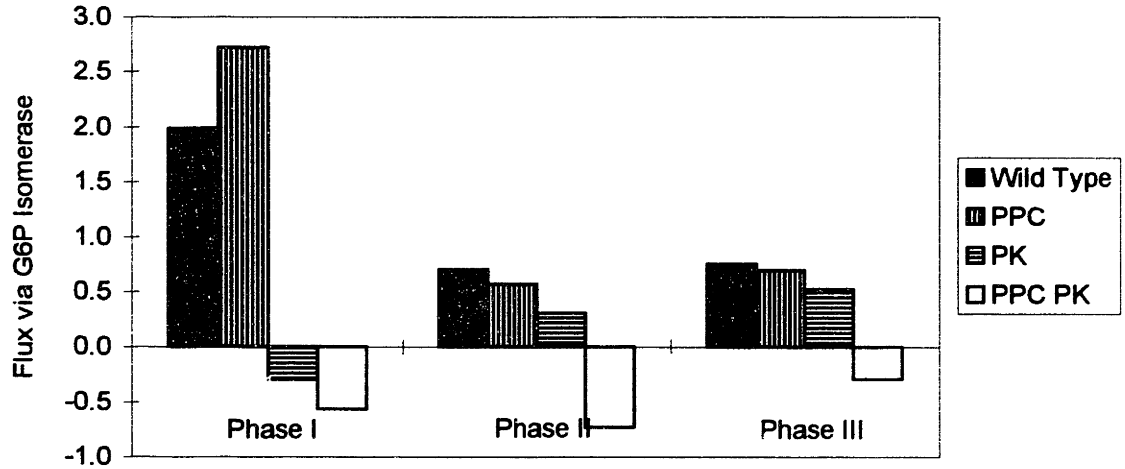

Figure 9.12 Comparison of fluxes via anaplerotic reaction (PPC and PC combined).

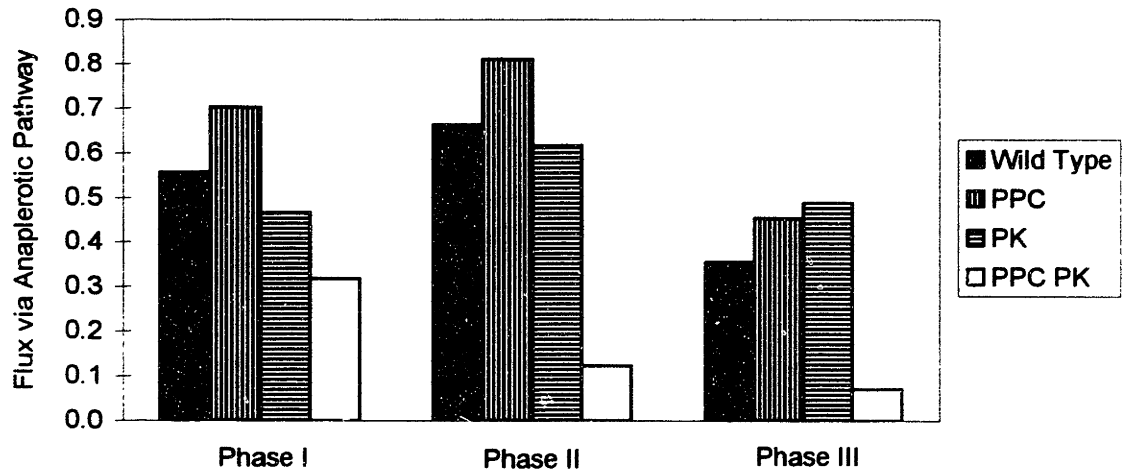

Figure 9.13 Proposed model of glucose assimilation in the *ppc pyk* mutant. Note the incorporation of the newly found THD enzyme to remove excess NADPH generated by the oxidative portion of the PPP.

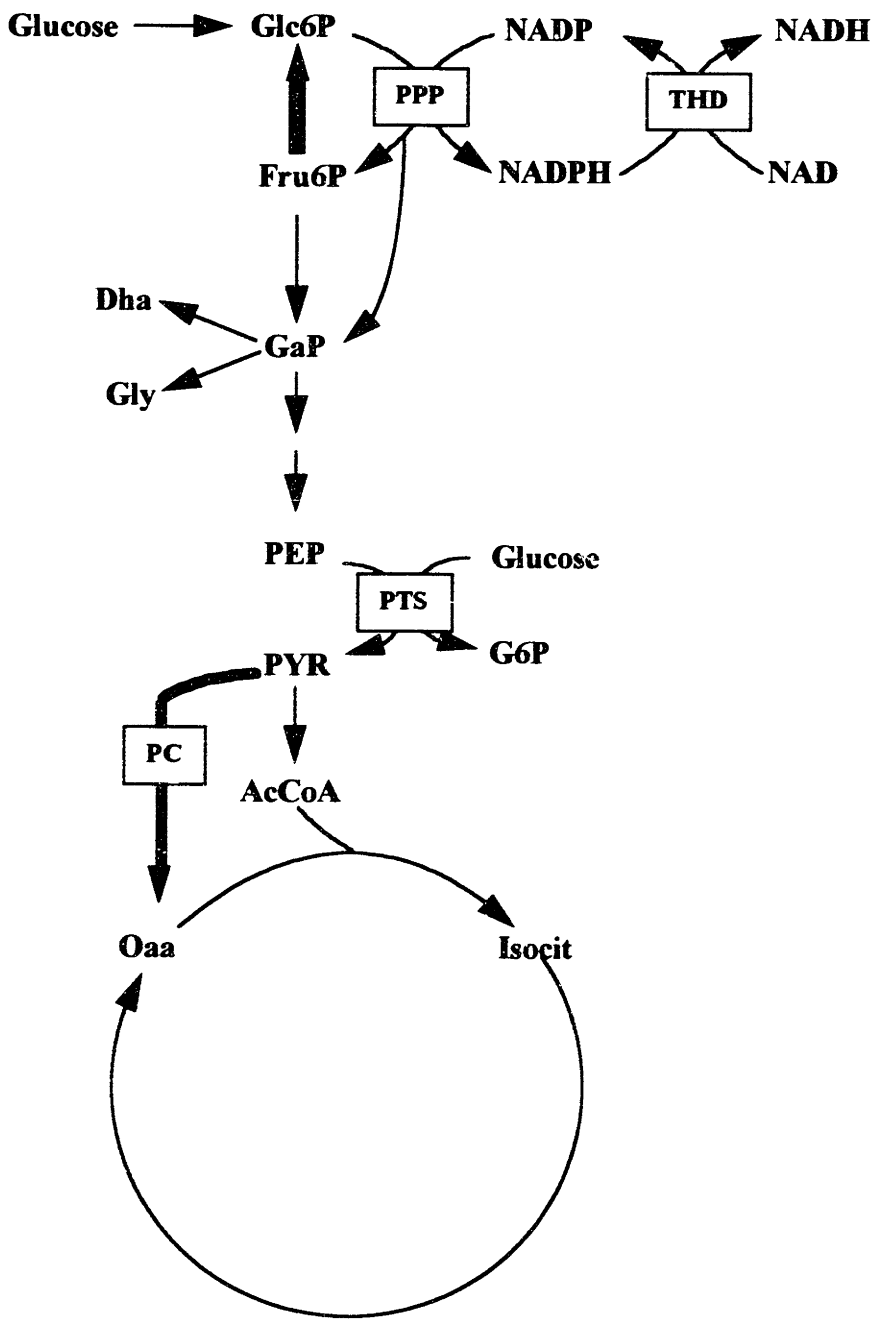

Chapter 10: Test of Reaction Pathway Feasibility in a Metabolic System

10.1 Introduction

This chapter presents a general methodology for determining the feasibility of a given set of chemical reactions to proceed simultaneously in a metabolic system. For a given set of chemical reactions to be feasible, basic thermodynamic criteria must be satisfied regardless of kinetic constraints. This chapter describes the formulation of the problem in the context of linear network and illustrates several examples to demonstrate the approach. This method will be valuable in screening proposed modifications of pathways and elucidating the reaction pathways and in designing metabolic pathways for the production chemicals and other products.

In metabolic engineering, the first step is often the proposal of modification of biochemical pathways in order to overcome the existing kinetic or thermodynamic rate limitations. In this chapter, we present a methodology to determine whether the proposed pathway is feasible from the thermodynamic standpoint. The way we approach this question is to formulate thermodynamic constraints involving chemical reactions in the context of linear network and to test if any feasible solution exists within the defined constraints.

A metabolic process is a set of many simultaneous reactions. Regardless of kinetic constraints, thermodynamic constraints derived from the chemical reaction equilibrium must be satisfied. Concentrations of metabolites permitted inside the cell impose additional physiological constraint. Several papers [Mavrouniotis *et al.*, 1992; Seressiotis *et al.*, 1988] dealt with synthesizing biochemical pathways based on the stoichiometric consideration of metabolites. However, these approaches did not consider the operability of synthesized pathways under real physiological conditions. Our procedure which is based on determining thermodynamic equilibrium consideration can be used a priori to eliminate any infeasible pathways.

10.2 Problem Formulation

10.2.1 General kinetic and thermodynamic equations

Consider a sequence of reactions taking place in m mechanistic steps involving n species denoted as S_i:

$$\{S_1, S_2, \ldots, S_N\} \Leftrightarrow \{S_1, S_2, \ldots, S_N\} \Leftrightarrow \cdots \Leftrightarrow \{S_1, S_2, \ldots, S_N\}$$

The chemical reaction at the ith step can be represented as

$$\sum_{j=1}^{N} \upsilon_{ij} S_j = 0$$

where $_{ij}$ is the stoichiometric coefficient with $_{ij} > 0$ for the product and $_{ij} < 0$ for the substrate. The energy profile such as Figure 10.1 might be expected. The role of enzymes is to lower the activation energy barriers so that the reaction can proceed rapidly. The forward reaction rates of this sequence are designated as $v_{+1}, v_{+2}, \ldots, v_{+N}$. The reverse reaction rates are $v_{-1}, v_{-2}, \ldots, v_{-N}$. The generalized statistical theory of rate [Happel, 1973] provides the expression for the forward and reverse reaction rates as

$$v_{+i} = \frac{k_{+i}}{f[T(i)]} a[I(i)], \qquad v_{-i} = \frac{k_{-i}}{f[T(i)]} a[F(i) \qquad \textbf{(Eq. 10.1)}$$

where $I(i)$, $T(i)$, and $F(i)$ denote the initial, transition, and final states of the set of reacting species involved, respectively. $f[T(i)]$ is the activity coefficient of the transition state, and $a[I(i)]$ and $a[F(i)]$ are the activity of the initial and final states. Furthermore,

$$k_{+i} = \kappa \frac{kT}{hN[T(i)]} \exp\left\{\frac{\mu[\mathrm{I(i)}] - \mu[\mathrm{T(i)}]}{RT}\right\} \qquad \textbf{(Eq. 10.2)}$$

$$k_{-i} = \kappa \frac{kT}{hN[T(i)]} \exp\left\{\frac{\mu[\mathrm{F(i)}] - \mu[\mathrm{T(i)}]}{RT}\right\} \qquad \textbf{(Eq. 10.3)}$$

where k_{+i}, k_{-i} are the rate constants, κ is the transmission coefficient, $1/N[T(i)]$ is the magnitude of the "space available for a single critical system" in the assembly. Therefore, $f[T(i)]N[T(i)] = a[T(i)]$. From (Eq. 10.1), (Eq. 10.2), and (Eq. 10.3),

$$\frac{v_{+i}}{v_{-i}} = \exp\left\{\frac{\mu[\mathrm{F(i)}] - \mu[\mathrm{T(i)}]}{RT}\right\} = \exp\left\{\frac{\Delta \mathrm{G_i}}{RT}\right\} \qquad \textbf{(Eq. 10.4)}$$

The net flux through the reaction step i is

$$v_i = v_{+i} - v_{-i} = v_{-i}\left[1 - \exp\left\{\frac{\Delta \mathrm{G_i}}{RT}\right\}\right] \qquad \textbf{(Eq. 10.5)}$$

The sign of ΔG_i determines the direction of the net reaction. If $\Delta G_i < 0$, the reaction proceeds forward. If $\Delta G_i = 0$, chemical equilibrium is reached where there is no net generation and consumption of reacting molecules. When $\Delta G_i > 0$, the reaction proceeds backward. If we require the overall reaction to proceed simultaneously, the net flux at each step must be all greater than zero, i.e.,

$$v_i > 0 \text{ or } \Delta G_i < 0 \text{ for all i.}$$

In other words, through each step, there must exist a decrease in free energy as depicted in Figure 10.1.

10.2.2 Representation of ΔG_i as a function of concentrations.

The Gibbs energy of reaction, ΔG_i, can be represented as

$$\Delta G_i = \sum_{j=1}^{N} v_{ij} \mu_j \qquad \textbf{(Eq. 10.7)}$$

where μ_j is the chemical potential of species j. Assuming all species behave ideal, the chemical potential is reduced to

$$\mu_j = \mu_j^0 + RT \ln c_j = \Delta G_f^0[j] + RT \ln c_j \qquad \textbf{(Eq. 10.8)}$$

where μ_j^0, μ_j, $\Delta G_f^0[j]$ are standard chemical potential, concentration, and standard Gibbs energy of formation of species j. Combining (Eq. 10.7) and (Eq. 10.8) leads to

$$\begin{aligned} \Delta G_i &= \sum_{j=1}^{N} v_{ij} \left\{ \Delta G_f^0[j] + RT \ln c_j \right\} \\ &= \sum_{j=1}^{N} v_{ij} \Delta G_f^0[j] + RT \sum_{j=1}^{N} v_{ij} \ln c_j \\ &= \Delta G_i^0 + RT \sum_{j=1}^{N} v_{ij} \ln c_j \end{aligned} \qquad \textbf{(Eq. 10.9)}$$

The standard Gibbs energy of reaction, ΔG_i^0, can be calculated from $\Delta G_f^0[j]$ which can be experimentally measured [Thauer *et al.*, 1977] or for many biological species where such data are not readily available, theoretically calculated using the group contribution method [Mavrouniotis, 1990]. It should be emphasized that the sign of ΔG_i^0 should be used only as a guide of reaction directionality as there exists many enzymatic reactions whose ΔG_i^0 is much greater than zero and net forward reaction can still occur. The value of ΔG_i

determined from concentrations of involved metabolites eventually determines the direction of reaction.

10.2.3 Physiological constraints on metabolite concentrations

A metabolic system faces serious problems of maintaining solubility of many macromolecular polyelectrolytes and smaller molecules of various ion charges. Such a system can exist only if the solvent capacity of water is maintained by keeping the concentrations of all the solutes at low levels [Atkinson, 1969]. This need to limit solute concentrations imposes a maximum permissible concentration limit for each species. A minimal limit exists in order to avoid the chemical potential of the reacting species reaching an infinite negative value. 10^{-9} M corresponds to a concentration of about one molecule in a cell of size *Escherichia coli*. Therefore, in a metabolic reaction network system,

$$c_j^{\min} \le c_j \le c_j^{\max} \text{ for all j}$$

where $c_j^{\min}$ and $c_j^{\max}$ are the minimum and maximum allowed concentrations of species j. This is equivalent to imposing constraints on the chemical potential on species j.

10.2.4 Linear problem formulation

The problem is to find any solution $Y=\{c_1,c_2,...,c_N\}$ which satisfies the two constraint sets (Eq. 10.9) and (Eq. 10.10). The constraint of (Eq. 10.9) is nonlinear in $\{c_j\}$ and can be transformed into a linear constraint form by introducing new variables

$$\xi_j = -\ln c_j ,$$
$$\xi_j^{\min} = -\ln c_j^{\max} ,$$
$$\xi_j^{\max} = -\ln c_j^{\min}$$

Since $c_j < 1$, $\xi_j > 0$. (Eq. 10.9) can be represented as

$$\sum_{j=1}^{N} \nu_{ij} \xi_j < g_i \qquad \textbf{(Eq. 10.11)}$$

where $g_i = \dfrac{\Delta G_i^0}{RT}$ is a dimensionless quantity. Also (Eq. 10.10) can be restated as

$$\xi_j^{min} < \xi_j < \xi_j^{max} \qquad \textbf{(Eq. 10.12)}$$

The original problem of finding Y is solvable if and only if the transformed problem of finding $Y(\xi) = \{ \xi_1, \xi_2, ..., \xi_N \}$ is solvable. The new problem is linear in variables in $\{\xi_j\}$ and feasibility of existence of solution can be easily checked by using the phase I of the simplex algorithm which is designed to find a solution set of nonnegative variables that satisfies a system of linear equations. If the problem is well poised, i.e., the set of reactions defining the pathway is feasible, then at least one solution satisfying (Eq. 10.11) and (Eq. 10.12) exists. The existence of a solution is a sufficient and necessary condition which follows directly from the definition.

10.3 Examples

We illustrate applications of our methodology to discriminate the infeasible from feasible biochemical pathways by investigating three characteristic metabolic processes: (a) glycolysis, (b) anaplerotic reactions, and (c) gluconeogenesis. Each of these pathways has been studied extensively from both theoretical and experimental point of view with many different organisms. In this section, the standard state refers to water at 55M, pH of 7.0, pressure of one atmosphere, and temperature at 298°K.

10.3.1 Glycolysis

The glycolytic pathway is the basic pathway in most bacteria and eucaryotes that catabolizes glucose to pyruvate. Through the sequence of enzyme reactions shown in Table 10.1, energy metabolites such as ATP and biosynthetic precursors are generated [Lehringer, 1973]. For simplicity of calculation, some variables are fixed: [ATP]/[ADP] = 10, [NAD]/[NADH] = 1, and P_i = 10 mM. These are typically observed values in erthrocytes under glycolysis [Lehringer, 1973]. Taking the linear constraint sets $\{r_i: i = 1$ to $10\}$ and $\{-\ln 10^{-2} < \xi_j < -\ln 10^{-8}\}$ reveals that feasible solution exists despite several reactions with a large positive ΔG_i^0. This indicates that as expected, the glycolytic pathway can proceed forward simultaneously with each metabolite concentration within 10^{-2} to 10^{-8} M ranges. Sets of $\{c_i\}$ which fulfill these constraints may not be, in general,

unique. Because of the linear nature of constraints, any linear combination of solution sets is also solution.

10.3.2 Anaplerotic reaction

Oxaloacetate is a major metabolite used for both biosynthesis and energy generation. It is constantly drained off from the primary pathway and replenished by the so-called anaplerotic pathway. Table 10.2 gives several possible choices of enzymatic pathways which can catalyze the synthesis of oxaloacetate. The constraints which will be examined consist of all of the glycolytic reactions of the previous section plus one additional pathway taken from Table 10.2.

Reaction 11 describes the common pathway found in bacterial systems for the formation of oxaloacetate via phosphoenolpyruvate carboxylase. These sets of constraints lead to a feasible solution. Reaction 12 shows an identical pathway to the reaction 11 except that phosphoenolpyruvate carboxykinase catalyzes the reaction. The maximum allowed concentration of oxaloacetate under the most favorable condition is $5x10^{-7}$ M. Though this value of oxaloacetate is within our constrained range, this is a physiologically extremely low value considering the important role of oxaloacetate in metabolism. Indeed, most organisms utilizes this enzyme only under gluconeogenic conditions where the reverse reaction is used. Reaction 13 shows a variation of reaction 11 in eucaryotic system in which pyruvate carboxylase catalyzes the conversion of pyruvate to oxaloacetate. As expected, feasible solution exists. Reaction 14 describes an identical pathway to reaction 13 with oxaloacetate decarboxylase carrying out the reaction. No feasible solution exists for these concnetration sets. By inspecting ΔG_i^0 of this step in isolation apart from the whole pathway one can readily arrive at the same conclusion. For this enzyme to catalyze the formation of oxaloacetate, it requires that

$$\Gamma = \frac{[OAA]}{[PYR][CO_2]} < K_{eq} = \ln\left(\frac{-\Delta G_i^0}{RT}\right) = 6.2x10^{-6}$$

Allowing the maximum concentrations for [PYR] and [CO_2] at 10^{-2} M means that the [OAA] is less than $6x10^{-10}$ M. It should be kept in mind that intuitive reasoning based on partial calculation works only in extreme cases like this.

The last alternative involves a set of two reactions: malic enzyme and malate dehydrogenase. The combination of two reactions results in conversion of pyruvate to oxaloacetate. This variation is identical to reaction 14 in overall net transformation and is also infeasible. Experimentally, the reverse reaction of reaction 14 and reaction 15 are also known to operate only under the gluconeogenic conditions.

Our analysis can be used qualitatively for predicting consequence of genetic modifications. Suppose that a mutant cell exists which does not have the ability to produce oxaloacetate. Such mutant would not grow on glucose as sole carbon substrate even all the glycolytic enzymes are present. This mutant can be used as a genetic background to clone anaplerotic genes by selecting cells which can now grow on glucose via standard genetic transformations. However, mutants deficient only in pyruvate carboxylase and phosphoenolpyruvate will be selected in this way. Transformants with either one of other three pathways will not be seleted. This is a clear demonstration of utility of our methodology.

10.3.3 Gluconeogenesis

The gluconeogenic pathway, occurring in many organs and tissues, provides another interesting example. The real metabolic sequence is almost identical to the reverse operation of glycolytic pathway with few notable changes. Five reaction sets described below (a) to (e) whose net reaction generates glucose from pyruvate are tested for thermodynamic feasibility.

(a) $\{-r_{10},-r_9,-r_8,-r_7,-r_6,-r_5,-r_4,-r_3,-r_2,-r_1\}$

(b) $\{r_{11},-r_{12},-r_9,-r_8,-r_7,-r_6,-r_5,-r_4,-r_3,-r_2,-r_1\}$

(c) $\{ r_{11},-r_{12},-r_9,-r_8,-r_7,-r_6,-r_5,-r_4, r_{17},-r_2,-r_1\}$

(d) $\{ r_{11},-r_{12},-r_9,-r_8,-r_7,-r_6,-r_5,-r_4,-r_3,-r_2,r_{18}\}$

(e) $\{ r_{11},-r_{12},-r_9,-r_8,-r_7,-r_6,-r_5,-r_4,r_{17},-r_2,r_{18}\}$

The negative sign indicates the reverse reaction of the enzyme and the whole proposed pathway is supposed to proceed in the order indicated. Two new enzyme reactions listed in Table 10.3 which are known to be involved in gluconeogenesis are included. Fructose 1,6-diphosphatase (r_{17}) catalyzes the same reverse reaction of phosphosfructokinase (r_3),

but has a negative ΔG_i^0. Glucose 6-phosphatase (r_{18}) can replace the hexokinase reaction (r_1). The proposed pathways (a) to (e) forms a perfectly legitimate sequence of enzymatic reactions from the stoichiometric sense. With the developed algorithm, it should be possible to reject any infeasible pathways.

The pathway (a) is simply reversing the reactions of glycolysis. This turns out to be infeasible. From the cellular regulatory standpoint, this makes sense. Cells would not have evolved the same biochemical machinery to meet two antagonistic purposes. This would be highly unsophisticated, if not uncontrollable, regulatory system. Reversing the first step of pyruvate kinase poses severe thermodynamic difficulties because of its high ΔG_i^0. This step is actually bypassed by the combination of two enzymes: carboxylation of pyruvate to oxaloacetate by pyruvate carboxylase (r_{11}) and subsequent decarboxylation of oxaloacetate to phosphoenolpyruvate by phosphoenolpyruvate carboxykinase ($-r_{12}$). The net reaction has lowered ΔG_i^0 to 0.5 kcal/mol, making the conversion of pyruvate to phosphoenolpyruvate favorable.

Table 10.4 summarizes the maximum allowed concentration levels for ten metabolities under two different energy states for four pathways (b) to (e): [ATP]/[ADP] ratio at 10 and 1. Low [ATP]/[ADP] ratio is preferred to make certain metabolite concentration above reasonable physiological level. Depending on the value, pathway (b) can be feasible only when the concentration of glucose, terminal product, is only 0.01 μM. All three pathways (c), (d), and (e) are feasible within given conditions. The last pathway (e) actually corresponds to actual gluconeogenic process observed experimentally. All biochemical steps have a small negative ΔG_i^0 except 3-phosphoglycerate kinase.

10.4 Conclusions

Several general methods have been proposed previously for the generation of pathways based on the assumption of elementary reactions. The generated pathways can be further elimininated from consideration by examining thermodynamic, kinetic, and physiological constraints. Thermodynamically, the pathway must be chosen such that along the reaction coordinates, the free energy associated with each step must decrease.

Unlike nonbiological system, most reactions in biological system are catalyzed by enzymes which require maintenance of substrate levels within certain physiological ranges. Our developed criteria must be cautiously used with respect to the precise calculation of the underlying thermodynamic quantity. Although we have not attempted yet, in principle it would be possible to include additional constraints of known kinetic information to improve the feasibility determination criteria.

It should be emphasized that in general, determination of reaction directionality should be considered as a whole, not as a single isolated step. In fact, some enzymes regardless of their ΔG_i^0 will catalyze reaction in either direction under different circumstances. For example, 3-phosphoglycerate kinase catalyzes the forward reaction in the glycolytic condition and backward reaction in the gluconeogenic condition.

10.5 References

Atkinson, D.E. (1969). Limitations of metabolite concentration and the conservation of solvent capacity in the living cell. In: *Current Topics in Cellular Regulation.* Horecker, B.L., Stadtman, E.R. (eds.), Academic Press, New York, pp. 29-43.

Lehninger, A.E. (1975). *Biochemistry*, Worth Publishers, New York.

Marvrovouniotis, M., Stephanopoulos, G., Stephanopoulos, G. (1992). Synthesis of biochemical production routes. *Computers Chem. Engng.* **16**: 605-619.

Mavrovouniotis, M.L. (1990). Group contributions for estimating standard Gibbs energies of formation of biochemical compounds in aqueous solution. *Biotechnol. Bioeng.* **36**: 1070-1082.

Seressiotis, A., Bailey, J.E. (1988). MPS: An artificially intelligent software system for the analysis and synthesis of metabolic pathways. *Biotechnol. Bioeng.* **31**: 587-602.

Thauer, R.K., Jungermann, K., Decker, K. (1977). Energy conservation in chemotropic anaerobic bacteria. *Bacteriol. Rev.* **41**: 100-180.

Figure 10.1 Schematic representation of change in free energy in a metabolic system.

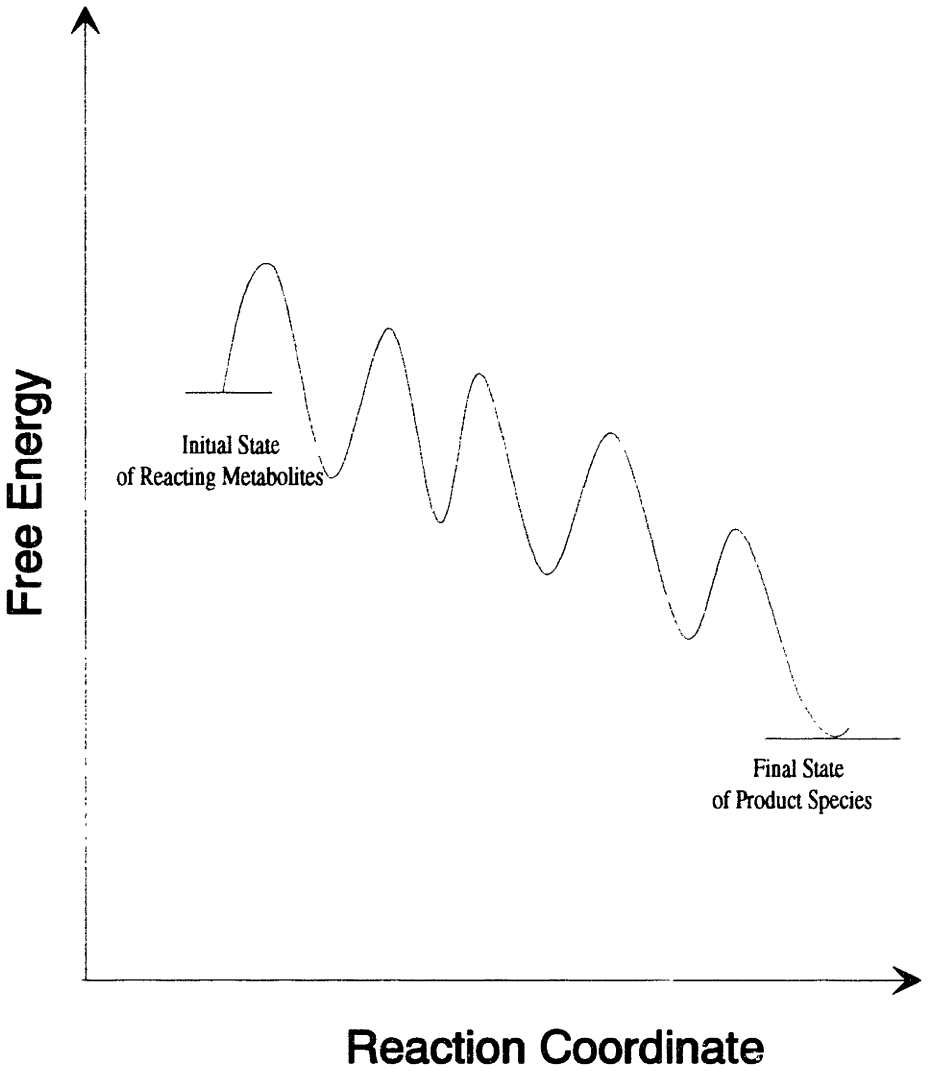

Table 10.1 Glycolytic reaction stoichiometry, ΔG^0(kcal/mol), and linearly transformed constraint at standard state of 25°C and $[H^+] = [OH^-] = 10^{-7}$ M.

Step	Catalyzing Enzyme	Reaction stoichiometry	ΔG^0	Transformed constraint
r_1	GLU hexokinae	GLU + ATP $\rightarrow$ GLU6P + ADP	-4.0	$-\xi_1-\xi_{16}+\xi_2+\xi_{17}>-6.755$
r_2	G6P isomerase	GLU6P $\rightarrow$ FRU6P	+0.40	$-\xi_2+\xi_3>0.676$
r_3	Phosphofructokinase	FRU6P + ATP $\rightarrow$ FRUDP + ADP	-3.40	$-\xi_3-\xi_{16}+\xi_4+\xi_{17}>-5.742$
r_4	FRUDP aldolase	FRUDP $\rightarrow$ DHAP + G3P	+5.73	$-\xi_4+\xi_5+\xi_6>9.677$
r_5	Triose phosphate isomerase	DHAP $\rightarrow$ G3P	+1.83	$-\xi_5+\xi_6>3.091$
r_6	G3P dehydrogenase	G3P + NAD^+ + PI $\rightarrow$ 13BPG + NADH + H^+	+1.50	$-\xi_6-\xi_{15}-\xi_{19}+\xi_7+\xi_{14}>2.533$
r_7	3PG kinase	13BPG + ADP $\rightarrow$ 3PG + ATP	-4.50	$-\xi_7-\xi_{16}+\xi_8+\xi_{17}>-7.600$
r_8	Phosphoglycerate mutase	3PG $\rightarrow$ 2PG	+1.06	$-\xi_8+\xi_9>1.790$
r_9	Enolase	2PG $\rightarrow$ PEP + H_2O	+0.44	$-\xi_9+\xi_{10}>0.743$
r_{10}	Pyruvate kinase	PEP + ADP $\rightarrow$ PYR + ATP	-7.50	$-\xi_{10}-\xi_{16}+\xi_{11}+\xi_{17}>-12.666$

Abbreviations:GLU, glucose; GLC6P, glucose 6-phosphate; FRU6P, fructose 6-phosphate; FRUDP, fructose 1,6-diphosphate; DHAP, dihydroxyacetone; G3P, glyceraldehyde 3-phosphate; 13BPG, 1,3-bisphosphate; 3PG, 3-phosphate; 2PG, 2-phosphate; PEP, phosphoenolpyruvate; PYR, pyruvate; OAA, oxaloacetate; MAL, malate; NADH, nicotinamide adenine dinucleotide; NAD, nicotinamide adenine mononucleotide; P_i, phosphate.

Table 10.2 Known anaplerotic reactions for the synthesis of oxaloacetate.

Step	Catalyzing Enzyme	Reaction stoichiometry	ΔG^0	Transformed constraint
r_{11}	PEP carboxylase	$PEP + HCO_3 \rightarrow OAA + PI$	-7.0	$-\xi_{10} - \xi_{20} + \xi_{12} + \xi_{19} > -11.822$
r_{12}	PEP carboxykinase	$PEP + HCO_3 + ADP \rightarrow OAA + ATP$	-1.0	$-\xi_{10} - \xi_{20} - \xi_{17} + \xi_{12} + \xi_{16} > -1.689$
r_{13}	PYR carboxylase	$PYR + HCO_3 + ATP + H_2O \rightarrow OAA + ADP + PI$	-0.5	$-\xi_{11} - \xi_{20} - \xi_{16} + \xi_{12} + \xi_{17} + \xi_{19} > -0.844$
r_{14}	OAA decarboxylase	$PYR + HCO_3 \rightarrow OAA$	+6.8	$-\xi_{11} - \xi_{20} + \xi_{12} > 11.484$
r_{15}	Malic enzyme	$PYR + HCO_3 + NADH + H^+ \rightarrow MAL + NAD^+$	-0.36	$-\xi_{11} - \xi_{19} - \xi_{14} + \xi_{13} + \xi_{15} > -0.608$
r_{16}	MAL dehydrogenase	$MAL + NAD^+ \rightarrow OAA + NADH + H^+$	+7.1	$-\xi_{13} - \xi_{15} + \xi_{12} + \xi_{14} > 11.991$

Table 10.3 Enzymes involved in gluconeogenesis.

Step	Catalyzing Enzyme	Reaction stoichiometry	ΔG^0	Transformed constraint
r_{17}	FRU 1,6-diphosphatase	$FRUDP + H_2O \rightarrow FRU6P + PI$	-5.2	$-\xi_4 + \xi_3 + \xi_{19} > -8.782$
r_{18}	GLU 6-phosphatase	$GLU6P + H_2O \rightarrow GLU + PI$	-4.6	$-\xi_2 + \xi_1 + \xi_{19} > -7.769$

Table 10.4 Maximum allowed concnetration (in M) of metabolites under gluconeogenic condition for four proposed pathways (b) to (e) calculated at [ATP]/[ADP] = 10 and 1 with [NAD]/[NADH} = 100.

Metabolite	[ATP]/[ADP] = 10				[ATP]/[ADP] = 1			
	(b)	(c)	(d)	(e)	(b)	(c)	(d)	(e)
GLU	1.02E-12	1.16E-06	0.01	0.01	1.02E-08	1.16E-05	0.01	0.01
GLC6P	8.79E-09	0.01	6.3E-06	0.0001	8.79E-06	0.01	6.3E-05	0.0001
FRU6P	4.47E-09	0.01	3.21E-06	0.01	4.47E-06	0.01	3.21E-05	0.01
FRUDP	1.39E-05	0.01	0.01	0.01	0.001395	0.01	0.01	0.01
DHAP	0.000139	0.000139	0.000139	0.000139	0.000139	0.000139	0.000139	0.000139
G3P	6.3E-06	6.3E-06	6.3E-06	6.3E-06	6.3E-06	6.3E-06	6.3E-06	6.3E-06
13BPG	5.01E-07	5.01E-07	5.01E-07	5.01E-07	5.01E-07	5.01E-07	5.01E-07	5.01E-07
3PG	0.01	0.01	0.01	0.01	0.01	0.01	0.01	0.01
2PG	0.01	0.01	0.01	0.01	0.01	0.01	0.01	0.01
PEP	0.01	0.01	0.01	0.01	0.01	0.01	0.01	0.01

Chapter 11: Conclusions and Recommendations

11.1 Summary

The central focus of this thesis was to investigate the carbon flux in the central metabolic pathway of *Corynebacterium glutamicum*. This thesis was initiated by attempting to express various heterologous phosphoenolpyruvate carboxylase (PPC) genes in *C. glutamicum* in order to increase the carbon flow into oxaloacetate (OAA). A clean genetic background devoid of PPC activity was necessary to detect the expression of these genes beyond the native background PPC expression level. This need necessitated the development of transconjugation technique as a means of introducing specific deletion mutation into the chromosome instead of traditional random mutagenesis. Subsequently, the *ppc* mutant of *C. glutamicum* was constructed. Even though the expressions in *C. glutamicum* of *Zea mays ppc* gene under the control of *tac* promoter and of *Anacystis nidulans ppc* gene under the control of *C. glutamicum fda* promoter were not successful, the fermentation study with the *ppc* mutant provided a surprising evidence for the presence of a new anaplerotic pathway in *C. glutamicum*.

Consequently, in order to determine the enzyme that can compensate the function of PPC in *C. glutamicum*, enzymatic activities of phosphoenolpyruvate carboxykinase (PPCK), phosphoenolpyruvate carboxytransphosphorylase (PPCTP), pyruvate carboxylase (PC), transcarboxylase (TC), malic enzyme (ME), OAA decarboxylase (OAADC), glyoxylate shunt enzymes were measured in the wild type and the *ppc* mutant strains of *C. glutamicum* under the glycolytic conditions. Only PPCK and OAADC which generally fulfills a gluconeogenic role were detected. Therefore, establishment of PPC-compensating enzyme based on enzymatic assays with the crude extracts was incomplete and inconclusive.

An alternative method utilizing ^{13}C NMR and GC-MS was investigated. The results from the ^{13}C NMR and GC-MS provided a conclusive evidence that the unknown PPC-compensating anaplerotic reaction is the carboxylation of pyruvate. Of critical importance for the application of ^{13}C substrates was the ability to deal with ^{13}C label

scrambling via the cyclic pathways such as the tricarboxylic acid (TCA) cycle or the pentose phosphate pathway (PPP). This need necessitated the rigorous analysis of carbon transfer through biochemical pathways. This provided an opportunity to study carbon label scrambling via cyclic pathways such as the TCA cycle and the PPP.

A mathematical model was constructed to describe the isotopomer distribution via the TCA cycle and was verified by comparing the modeling results to the published experimental data. Isotopomer analysis provided several ways to extract the relevant and useful information from the ^{13}C labeling studies such as the interpretation of the multiplet pattern. The modeling results were extended to question the validity of conclusions in the literature which were built upon the simplified model that does not properly account for all the possible effect of label scrambling via the citric acid cycle. These have led to conclude: (1) there exists the glyoxylate shunt pathway in *Pseudomonas* AM1 strain, (2) there is no evidence of propionate carboxylating pathway in *Escherichia coli*, and (3) acetone utilization in mammals solely via the "lactate/methylglyoxal" pathway is consistent with the labeling data.

A similar approach to that of the TCA cycle was taken to model the carbon label distribution via the PPP. The modeling results were used (1) to dispel claims of the operation of a glycolytic fructose futile cycle and (2) to uphold that the PPP is operative in all tissues. In sum, this simple mathematical model proved to be a versatile and robust tool for analyzing isotopic labeling in a variety of experimental systems.

Following the establishment of pyruvate carboxylating pathway in *C. glutamicum*, batch fermentations were performed with three deletion mutants deficient in PPC and/or pyruvate kinase (PK) and analyzed using the methodology of metabolic flux analysis. Results can be summarized as follows: (1) There is a significant back-up along the glycolytic pathway in the PK deficient mutants during growth on glucose as evidenced by secretion of dihydroxyacetone and glyceraldehye. This causes an overflow via the PPP as a mechanism of dissimilating large amount of built-up intermediates in the form of CO_2. (2) The high activity through the PPP causes an overproduction of reducing power in the form of NADPH. In order to accommodate this overproduction of reducing power as well as to compensate the shortage of production of NADH via the tricarboxylic acid

cycle, an increased activity of the transhydrogenase (THD) enzyme is necessary which catalyzes the reversible reaction NADPH + NAD^+ $\leftrightarrow$ $NADP^+$ + NADH. Experimentally, the presence of active THD is confirmed directly by the enzymatic assays. (3) Specific glucose uptake rates declined during the course of fermentation and this decline is more pronounced in the case of strains deficient in both PPC and PK. These results and approaches provide a useful framework for studying and manipulating the metabolic pathways in order to increase the yield and productivity of fermentation products.

11.2 Conclusions

The following major conclusions can be drawn from this work:

1. The fermentation of the *Corynebacterium glutamicum ppc* mutant (253SM1) on glucose showed almost identical growth and L-lysine production compared to the parental strain *C. glutamicum* ATCC 21253.

2. ^{13}C NMR and GC-MS analysis with the *C. glutamicum* possess a pyruvate carboxylating enzyme(s) in addition to PPC as an anaplerotic enzyme to synthesize OAA under the glycolytic condition.

3. ^{13}C NMR and GC-MS analysis with the *C. glutamicum pyk* mutant (SM575) indicates that under the cultivation with gluconate and pyruvate as carbon sources, about 90% of OAA is replenished by the pyruvate carboxylation pathway whereas the remaining 10% is replenished by the PEP carboxylation pathway.

4. Flux analysis based on the metabolite balances can be a useful tool to test the presence of enzymatic reactions in the biochemical network. With this analysis, the presence of THD in the *C. glutamicum ppc pyk* mutant (SM607) is suggested. By direct enzymatic assay, this enzyme is found to be present in the wild type, the *pyk* mutant and the *ppc pyk* mutant strains as well. The level of THD activity is highest in the *C. glutamicum ppc pyk* mutant.

5. Intracellular flux calculations with the *C. glutamicum ppc pyk* mutant based on the flux analysis indicates that all the glucose can be assimilated via PPP, bypassing the glycolytic pathway. Excess NADPH generated via PPP is converted back to NADP by the action of THD.

6. In ^{13}C substrate labeling studies, a rigorous treatment must be applied in order to account for ^{13}C label scrambling via the cyclic pathways such as the TCA and the PPP. A modeling based on the steady state distribution of ^{13}C isotopomer species proves to be robust for analyzing labeling pattern in a variety of experimental conditions.

7. The operation of futile cycling at fructose-6-phosphate in the glycolytic pathways in various organisms discussed in the literature can not be proved solely with the data obtained with the labeling studies with the C-1, C-2, or C-3 labeled hexose substrates. The C-4, C-5, and C-6 labeled substrates should be employed for this purpose.

8. A rigorous analysis of the carbon isotope labeling data in the literature is consistent with the operation of the classical PPP, but not the L-type.

11.3 Recommendations for Future Work

11.3.1 Investigation of Anaplerotic Pathways in *Corynebacterium*

One of the significant findings of this thesis is the elucidation of the presence of the pyruvate carboxylating pathway operative in the formation of OAA in *Corynebacterium*. Despite several attempts, enzymatic activity for this pathway has not been detected. Even though the exact nature of this enzyme has not been established, it is most likely to be pyruvate carboxylase (PC: *pc* gene). Further study on this enzyme will be valuable not only for improving the yield and productivity of the amino acids of the aspartate family with this bacterium but also for fundamentally understanding the regulation of the carbon flow in the central metabolic pathways with dual anaplerotic enzymes. With the cloning of the *pc* gene, the following three important questions can be addressed:

1. Can PPC compensate the deficiency of PC in *Corynebacterium*? It was found that PPC is dispensable for the glucose catabolism and cell growth in *Corynebacterium* due to the presence of PC which can fulfill the anaplerotic role. It would be interesting to see if the same compensating role can be performed by PPC in the absence of PC. This would help to understand the role of PPC as well as PC.

2. Will the amplification of *pc* gene lead to higher amino acid yield and productivity in *Corynebacterium*? It is observed that in organisms possessing both PPC and PC, PPC is subject to a tight regulation via feedback inhibition by L-aspartate and activation by acetyl-CoA whereas PC is not subject to any regulation. Because of the apparent lack of regulation on PC, the amplification of the *pc* gene would lead to enhanced flow from pyruvate to OAA which is the precursor for the amino acids of the aspartate family.

3. What is the role of OAADC and PEP carboxykinase (PPCK) whose activity is found high under the glycolytic condition?

Two strategies are suggested here for the cloning and characterization of this putative *pc* enzyme. First strategy is based on the assumption that the unknown enzyme is indeed pyruvate carboxylase. PC in all organisms reported is a biotin-requiring enzyme. Biotin is covalently attached to a lysine residue of the prosthetic group of this protein. This unique property allow the easy purification and isolation of such biotin-containing proteins. Biotin-containing proteins can be conveniently purified with an avidin (or streptavidin) monomer affinity column because of the high affinity of avidin for the biotin moiety ($K_d = 10^{-15}$). Initially, only the biotin-containing proteins to bind to the columns which can be subsequently recovered by elution with biotin. This technique has been successfully used to purify biotin proteins such as PC [Thampy *et al.*, 1988], propionyl-CoA carboxylase (PCC; EC 6.4.1.3) [Henrikson *et al.*, 1979; Haase *et al.*, 1982], transcarboxylase (TC) [Henrikson *et al.*, 1979], and acetyl-CoA carboxylase (ACC; EC 6.4.1.2) [Guchhait *et al.*, 1974].

The biotin-containing proteins can be easily identified by Western blotting after all the proteins in the crude extract are separated by size and shape using polyacrylamide gel electrophoresis and transferred to the proper medium (usually nitrocellulose membrane). The biotin-containing proteins can be detected using the commercially available kit based on avidin conjugated with horseradish peroxidase for chemiluminescence detection or avidin conjugated with alkaline phosphatase for colorimetric detection. This method is very sensitive and specific and bypasses the use of radioisotopes. This method can be employed to detect pyruvate carboxylase enzyme in *Corynebacterium*.

Fortunately, for the screening of biotin-containing proteins as the source of pyruvate carboxylase, there are only very few enzymes identified so far to be biotin-dependent: PC, ACC, PCC, TC and 3-methylcrotonyl-CoA carboxylase (MCC; EC 6.4.1.4). Sodium transport decarboxylases in some anaerobic prokaryotes are also biotin-dependent: OAA decarboxylase, methylmalonyl-CoA decarboxylase and glutaconyl-CoA decarboxylase [Dimroth, 1987]. It is interesting to note that all these enzymes are carboxylases that shares common catalytic mechanisms even though the substrates are different in each enzyme. However, not all carboxylases are biotin-dependent as exemplified in PPC, ribulose-1,5-bisphosphate carboxylase, and PPCK.

Second strategy is the complementation strategy using the *C. glutamicum* mutant strain SM0301 (see Section 4.5) which is deficient in the anaplerotic enzymes. This mutant requires citrate during growth on glucose minimal medium. Following the transformation of genomic library via electroporation, transformants that does not require citrate during growth on glucose minimal medium can be identified by selective replica-plating. Since two are the primary anaplerotic routes, two types of transformants are likely to be selected: one bearing a plasmid encoding the *ppc* gene and other bearing a plasmid encoding the *pc* gene. Since the sequence of the *ppc* gene is known, the genotypes of the two transformants can be simply differentiated based on the restriction analysis of the plasmids. The complementation strategy is similar to that employed by Eikmanns *et al.* [1989] and O'Regan *et al.* [1989] for the cloning of *ppc* gene in which a *ppc* mutant of *E. coli* was used as a complementation host. Even though PC can theoretically function to compensate the role of PPC, no plasmid harboring the *pc* gene was identified by both groups. O'Regan *et al.* isolated more than 100 clones which complemented the *E. coli ppc* mutant but found that all the clones contained the *ppc* gene. There are various explanations why these studies failed to isolate a *pc* gene such as the inability to express functional *Corynebacterium* PC in *E. coli*.

11.3.2 Glucose Metabolism of *C. glutamicum ppc pyk* Mutant

Flux analysis indicates that all the glucose is utilized via the PPP and the action of THD in the *C. glutamicum ppc pyk* mutant. The verification of this peculiar metabolic scheme will add further validity to the flux analysis technique. The proposed metabolic scheme can be independently verified by at least two methods. The first is the construction and subsequent characterization of a *ppc pyk thd* mutant. In the triple mutant, deletion of THD would slow down the PPP due to the lack of mechanism to regenerate NADP from NADPH and hence glucose utilization rate. However, deletion of THD in the other genetic backgrounds of the wild type, the *pyk* mutant and the *ppc* mutant would have a negligible effect on the glucose metabolism.

The second method involves the use of ^{13}C labeled hexose substrates and is based on the theoretical prediction of ^{13}C label distribution via the PPP. It was shown in Chapter

8 that if the rate of glucose oxidation via the PPP exceeds that via the glycolytic pathway, then in the steady state conditions, no ^{13}C label would be incorporated into the glycolytic and pentose phosphate intermediates. This can be experimentally verified by either ^{13}C NMR or GC-MS. For example, no ^{13}C should be present in pyruvate if the *ppc pyk* mutant is incubated with [1-^{13}C]glucose as the sole carbon source.

11.3.3 Role of Biotin

The role of biotin in *C. glutamicum* remains unclear even though it is probably involved in only carboxyl transfer reactions in other organisms. The earlier studies with *Corynebacterium*, mainly to understand the glutamate excretion under the biotin-limitation condition, claim that biotin is a cofactor in fatty acid synthesis for cell membrane and alter the phospholipid composition of the plasma membrane [Hirose and Okada, 1979]. However, based on our understanding of the role of biotin in other organisms, it is conceivable that biotin may not be directly involved in determining the phospholipid composition and rather is a cofactor of carboxylating enzymes.

It is a matter of conjecture to postulate what biotin enzymes are possibly present in *C. glutamicum*. Typically, only a limited number of biotin enzymes is present in a particular organism. For example, there is only one biotin enzyme (ACC) in *E. coli* [Shenoy *et al.*, 1993]. Four biotin enzymes (PCC, ACC, PC, and MCC) are present in human [Gravel and Robinson, **Year**] and two (PCC and ACC) are found in *S. cerevisiae*. Two are most likely to be present in *C. glutamicum*: PC and ACC. Evidence for the presence of ACC in *Corynebacterium* is provided by Nakao *et al.* [1972]. They isolated a biotin auxotroph from a glutamate overproducing *C. alkanolyticum*. This mutant required biotin for its growth in glucose but not in n-paraffins (C_{11}-C_{17}). Furthermore, the biotin auxotropic requirement can be fulfilled by oleic acid in *C. alkanolyticum*. Unsaturated fatty acids, especially oleic acid, could be directly synthesized from n-paraffins via saturated fatty acids, bypassing the action of ACC. This observation is consistent with the presence of ACC.

The similar experiment could be performed to deduce the presence of PC in *C. glutamicum*. Without biotin in the glucose minimal medium, both wild type *C.*

glutamicum and the *C. glutamicum ppc* mutant would not grow on glucose. However, when supplemented with oleic acid to compensate the absence of ACC activity for fatty acid synthesis, only the wild type *C. glutamicum* would grow. This is because of biotin requirement for PC to compensate the deficiency of PPC in the *C. glutamicum ppc* mutant.

11.3.4 Biotin Biosynthetic Pathway

It would be advantageous to allow *Corynebacterium* to be biotin self sufficient since large amounts of D-biotin are required during the fermentation production of amino acids with this bacterium. Furthermore, *Corynebacterium* with its high glucose utilization capability and ability to excrete many types of metabolites may be a suitable organism for the fermentative production of D-biotin. Biotin is currently manufactured by complex chemical synthesis methods [Sakurai *et al.*, 1993] and is used as a pharmaceutical and an animal feed supplement.

The potential of using *Corynebacterium* as the biotin producer has been demonstrated by Ogino *et al.* [1974a, 1974b] who reported a biotin conversion using n-paraffin utilizing *Corynebacterium* species from DL-*cis*-tetrahydro-2-oxo-4-*n*-pentyl-thieno-(3,4-D)-imidazoline, which is a biotin analog having a methyl group instead of a carboxyl group in the biotin molecule. Several research groups have been attempting to develop the fermentative production of D-biotin using recombinant strains of *E. coli* [Brown *et al.*, 1991], *Bacillus sphaericus* [Ohsawa *et al.*, 1992] and *Serratia marcescens* [Sakurai *et al.*, 1993]. In these cases, recombinant strains were constructed by expressing the five genes in the D-biotin biosynthetic pathway. With the recent development of cloning vectors and transformation system, the same approach can be taken with *C. glutamicum.*

11.3.5 Pathways to Allow Utilization of Wide Range of Carbon Substrates

One interesting application of the metabolic engineering of *Corynebacterium* is to widen the range of carbon substrates so that more economical raw materials can be used in production processes. For industrial fermentation processes employing *Corynebacterium*

and *Brevibacterium*, glucose or sucrose based media are predominantly used, even though the use of acetate and ethanol has been reported [Kinoshita and Nakamaya, 1978]. Undoubtedly cheaper carbohydrates are preferred and this research effort is already undertaken by Brabetz *et al.* [1991] who transformed *E. coli* lactose operon into *C. glutamicum* and therefore endowed this bacterium with the capability to utilize lactose, which is abundantly present in whey, a waste product of dairy industry. Another example of this type of research efforts is the development of *Zymonas mobilis* strains capable of fermenting xylose into ethanol. As a step toward producing fuel ethanol from hemicellulose and cellulose in lignocellulosic feedstocks such as agricultural and forestry residues, Zhang *et al.* [1995] transformed *Z. mobilis* with two *E. coli* operons encoding the xylose assimilation pathway and the PPP. The transformed *Z. mobilis* was able to produce ethanol from xylose which is commonly found in hemicellulose.

11.3.6 Dual Anaplerotic Pathways in Other Related *Corynebacterium* Species

It seems likely that the two dual pathways found in the anaplerotic pathways and L-lysine biosynthetic pathway of *C. glutamicum* may be characteristic of the genera *Corynebacterium* and *Brevibacterium*. The genetic approach of deleting one specific gene in these dual sequences via transconjugation may provide finer distinctions among the various species not only in the industrially relevant *Corynebacterium* or *Brevibacterium*, but also in the other clinically important *Corynebacterium*. Furthermore, it would be interesting to understand how widespread these dual pathways occur in the other relatives of *Corynebacterium* such as the genera *Mycobacterium*, *Nocardia* and *Rhodococcus*.

11.3.7 Mathematical Modeling of Central Carbon Metabolism of *C. glutamicum*

With the elucidation of the kinetics of PC, the mathematical model originally developed by Vallino to describe the carbon flow around the PEP branchpoint can be reexamined. The original model conceived PPC as the major anaplerotic enzyme and did not account for the flux distribution by the presence of PC, ME, and OAADC. Of particular interest would be the regulation mechanisms surrounding the partitioning of

fluxes into OAA. These types of information are hard to obtain experimentally and would demonstrate the utility and usefulness of the mathematical modeling approach.

11.4 References

Brabetz, W., Liebl, W., Schleifer, K.H. (1991). Studies on the utilization of lactose by *Corynebacterium glutamicum*, bearing the lactose operon of *Escherichia coli*. *Arch. Microbiol.* **155**: 607-612.

Brown, S.W., Speck, D., Sabatie, J., Gloeckler, R., O'Regan, M.O., Viret, J.F., Lemoine, Y. (1991). The production of biotin by recombinant strains of *Escherichia coli*. *J. Chem. Tech. Biotechnol.* **50**: 115-121.

Dimroth, P. (1987). Sodium ion transport decarboxylases and other aspects of sodium ion cycling in bacteria. *Microbiol. Rev.* **51**: 320-340.

Gravel, R.A., Lam, K.F., Mahuran, D., Kronis, A. (1980). Purification of human liver propionyl-CoA carboxylase by carbon tetrachloride extraction and monomeric avidin affinity chromatography. *Arch. Biochem. Biophys.* **201**: 669-673.

Gravel, R.A., Robinson, B.H. Biotin-dependent carboxylase deficiencies (propionyl-CoA and pyruvate carboxylases). *Ann. N.Y. Acad. Sci.* 225-234.

Guchhait, R.B., Polakis, S.E., Dimroth, P., Stoll, E., Moss, J., Lane, M.D. (1974). Acetyl-coenzyme A carboxylase system of *Escherichia coli*: Purification and properties of the biotin carboxylase, carboxyl transferase and carboxyl carrier proteins. *J. Biol. Chem.* **249**: 6633-6645.

Haase, F.C., Henrikson, K.P., Treble, D.H., Allen, S.H.G. (1982). The subunit structure and function of the propionyl coenzyme A carboxylase of *Mycobacterium smegmatis*. *J. Biol. Chem.* **257**: 11994-11999.

Henrikson, K.P., Allen, S.H.G., maloy, W.L. (1979). An avidin monomer affinity column for the purification of biotin-containing enzymes. *Anal. Biochem.* **94**: 366-370.

Hirose, Y., Okada, H. (1979). Microbial production of amino acids. pp. 211-240 In: *Microbial Technology 1*. (eds.), Academic Press, New York, NY.

Kinoshita, S., Nakayama, K. (1978). Amino Acids. pp. 209-261 In: *Primary Products of Metabolism*. Rose, A.H. (eds.), Academic Press, London.

Nakao, Y., Kikuchi, M., Suzuki, M., Doi, M. (1972). Microbial production of L-glutamic acid by glycerol auxotrophs. Part I. Induction of glycerol auxotrophs and production of L-glutamic acid from n-paraffins. *Agric. Biol. Chem.* **36**: 490-496.

O'Regan, M., Thierbach, G., Bachmann, B., Villeval, D., Lepage, P., Viret, J.-F., Lemoine, Y. (1989). Cloning and nucleotide sequence of the phosphoenolpyruvate carboxylase-coding gene of *Corynebacterium glutamicum* ATCC13032. *Gene* **77**: 237-251.

Ogino, S., Fujimoto, S., Aoki, Y. (1974a). Cooxidation of *dl-cis*-tetrahydro-2-oxo-4-*n*-pentyl-thieno-(3,4-*d*)-imidazoline (*dl*-TOPTI) by soil isolates of the genus *Corynebacterium*. *Agric. Biol. Chem.* **38**: 275-278.

Ogino, S., Fujimoto, S., Aoki, Y. (1974b). Production of biotin by microbial transformation of *dl-cis*-tetrahydro-2-oxo-4-*n*-pentyl-thieno-(3,4-*d*)-imidazoline (*dl*-TOPTI). *Agric. Biol. Chem.* **38**: 707-712.

Ohsawa, I., Kisou, T., Kodama, K., Yoneda, I., Speck, D., Gloeckler, R., Lemoine, Y., Kamogawa, K. (1992). Bioconversion of pimelic acid into biotin by *Bacillus sphaericus bioB* transformants. *J. Ferment. Bioeng.* **73**: 121-124.

Sakurai, N., Imai, Y., Masuda, M., Komatsubara, S., Tosa, T. (1993). Molecular breeding of a biotin-hyperproducing *Serratia marcescens* strain. *App. Environ. Microbiol.* **59**: 3225-3232.

Shenoy, B.C., Magner, W.J., Kumar, G.K., Phillips, N.F.B., Haase, F.C., Samols, D. (1993). The nonbiotinylated form of the 1.3 S subunit of transcarboxylase binds to avidin (monomeric)-agarose: purification and separation from the biotinylated 1.3S subunit. *Protein Expr. Purif.* **4**: 85-94.

Sundaram, T.K., Cazzulo, J.J., Kornberg, H.L. (1969). Anaplerotic CO_2 fixation in mesophilic and thermophilic bacilli. *Biochim. Biophys. Acta* **192**: 355-357.

Thampy, K.G., Huang, W.-Y., Wakil, S.J. (1988). A rapid purification method for rat liver pyruvate carboxylase and amino acid sequence analysis of NH_2-terminal and biotin peptides. *Arch. Biochem. Biophys.* **266**: 270-276.

Zhang, M., Eddy, C., Deanda, K., Finkelstein, M., Picataggio, S. (1995). Metabolic engineering of a pentose metabolism pathway in ethanologenic *Zymomonas mobilis*. *Science* **267**: 240-243.